UNIVERSIDAD DE GRANADA

FACULTAD DE CIENCIAS

DEPARTAMENTO DE MICROBIOLOGÍA

SYNTHESIS OF PALLADIUM AND RUTHENIUM NANOPARTICLES FROM METAL SOLUTIONS USING BACTERIA WITH APPLICATIONS AS NANOCATALYST

SÍNTESIS DE NANOPARTÍCULAS DE PALADIO Y RUTENIO A PARTIR DE SOLUCIONES METÁLICAS, POR MEDIO DE BACTERIAS, CON APLICACIONES EN REACCIONES DE CATÁLISIS

Programa oficial de Doctorado en Biología Fundamental y de Sistemas

Jaime Gómez Bolívar

TESIS DOCTORAL

Granada, 2019

Editor: Universidad de Granada. Tesis Doctorales
Autor: Jaime Gómez Bolívar
ISBN: 978-84-1117-762-7
URI: https://hdl.handle.net/10481/80970

Esta Tesis Doctoral ha sido realizada en el Departamento de Microbiología (Facultad de Ciencias) de la Universidad de Granada durante los años 2016-2019 dentro del grupo de investigación de Mixobacterias (BIO 103) y el grupo de investigación de "Unit of functional bionanomaterials, School of Biosciences" la Profesora Lynne Macaskie.

Para la realización de este trabajo el doctorado disfrutó de un contrato del Sistema Nacional de Garantía Juvenil grant PEJ-2014-P-00391 (Promoción de Empleo Joven e Implantación de la Garantia Juvenil 2014, MINECO). El doctorando ha participado en el proyecto de investigación *"Beyond biorecovery: environmental win-win by biorefining of metallic wastes into new functional materials"* cuya responsable de proyecto ha sido la Profesora Lynne Macaskie, del cual se han obtenido algunos de los trabajos publicados en la presente tesis doctoral.

Además, el doctorado ha disfrutado de ayudas para la realización de estancias en centros extranjeros:

- Beca de "Movilidad Internacional de Jóvenes Investigadores de Programas de Doctorado de la Universidad de Granada". Otorgada por el Vicerrectorado de Internacionalización de la Universidad de Granada en Abril de 2018 para una estancia de 3 meses en la Universidad de Birmingham (Reino Unido).

- Beca de Movilidad dentro del "Programa Europeo de Prácticas para Estudiantes Erasmus +" de la Universidad de Granada para estudiantes de doctorado.

Los resultados obtenidos durante la realización de esta Tesis Doctoral han sido publicados o están en proceso de evaluación de revistas científicas de impacto.

1) Artículos científicos publicados o bajo revisión con los resultados obtenidos durante esta Tesis Doctoral:

- Gomez-Bolivar, J., Mikheenko, I. P., Orozco, R. L., Sharma, S., Banerjee, D., Walker, M., … Macaskie, L. E. (2019). Synthesis of Pd/Ru bimetallic nanoparticles by Escherichia coli and potential as a catalyst for upgrading 5-hydroxymethyl furfural into liquid fuel precursors. *Frontiers in Microbiology*, *10*(JUN), 1–17. https://doi.org/10.3389/fmicb.2019.01276
- Mikheenko, I.P.; Gomez-Bolivar, J.; Merroun, M.L.; Macaskie, L.E.; Sharma, S.; Walker, M.; Hand, R.A.; Grail, B.; Johnson, D.B.; Orozco, R.L. (2019). Upconversion of cellulosic waste into a potential 'drop in fuel' via novel catalyst generated using *Desulfovibrio desulfuricans* and consortium of acidophilic sulfidogens. *Frontiers in Microbiology*. 10(MAY), 1-20. https://doi.org/10.3389/fmicb.2019.00970.

- Gomez-Bolivar, J., Mikheenko, I. P., Macaskie, L. E., & Merroun, M. L. (2019). Characterization of palladium nanoparticles produced by healthy and microwave-injured cells of *Desulfovibrio desulfuricans* and *Escherichia coli*. *Nanomaterials*, *9*(6), 1–16. https://doi.org/10.3390/nano9060857
- Lynne E. Macaskie, John Collins, Iryna P. Mikheenko, Jaime Gomez-Bolivar, Mohamed L. Merroun, James A. Bennett. Enhanced hydrogenation rate and selectivity of biogenic palladium catalyst synthesized by Desulfovibrio desulfuricans exposed to a radio frequency magnetic field. *Biotechnology and Bioengineering*. En revisión.

AGRADECIMIENTOS

I would like to acknowledge in first place to my supervisors Dr. Mohamed Merroun and Prof. Lynne Macaskie for encouraging me to get through many difficulties during my PhD and for giving me the opportunity to start this PhD in such an exciting field of research which is the nanothechnology. I would also like to thank to my colleagues at the University of Birmingham, Iryna and Rafa and Jacob for the constant guide, support and the interesting talks in the long days of work and their help to make this Thesis become real.

Por otro lado, me gustaría agradecer a mis compañeros y compañeras del departamento de microbiología, a Iván, el himalayista de sofá más grande de todos, por aguantarme y ayudarme en esos comienzos de laboratorio cuando no sabía ni coger una pipeta, a Fadwa sus orientaciones, a Miguel, la persona que conozco con más pesetas ahorradas y por esas largas esperas en los pasillos para usar la campana. A Pablo y a su barba, tan buen investigador como mal compañero de piso. A Wirson y por esa futura empresa conjunta, a Vicky por sus fotos épicas, a Ylenia la caudilla, a Ana la caudilla en la sombra, a Germán el eterno corredor de las dos colinas, a Cristina, a María, Marcos y tantos otros.

Agradecer también a los profesores del departamento: Mª Teresa, Inés, Pirri, Manolo, Platero, Manuel, Conchi, Juani, Jose, Mercedes… gracias por estar dispuestos a echarme una mano cuando lo he necesitado. Al personal del Centro de Instrumentación Científica, que tanto me ha ayudado: Mª del Mar, Conchi, Juande y Mª José.

A mis amigos de siempre, por esas rutas en bici y por las que están por venir, Lopezón, Borja, Matansa, Wir wir, Bigotes, Charles, Hesu, Yisus, tato y muchos más. Al consejo, que siempre resucita por navidad. A esos biólogos de toda la vida. A ti Cristina, por aguantarme tanto en los malos momentos como en los buenos, el mayor acierto que tuve fue equivocarme escogiendo mi primera carrera para empezar Biología un año más tarde.

A mi familia, a mi hermano Jose y a mis padres Mari Paz y Pepe, por enseñármelo absolutamente todo y ser la persona que soy ahora.

“El fracaso enseña, lo que el éxito oculta”

(Enrique Rojas)

RELACIÓN DE ACRÓNIMOS

5-HMF: 5-Hydroxymethylfurfural

2,5-DMF: 2,5-Dimethylfuran

AMD: Acid Mine Drainage

CAS: Consortium of Acidofilic Sufidogenic

CDP: Calcium Dipicolinate

DUBBLE: Dutch-Belgian Beamline

EDX: Energy Dispersive X-ray

EPS: Extracellular Polymeric Substance

ESRF: European Synchrotron Radiation Facility

ESEM: Environmental scanning electron microscopy

EXAFS: X-ray Absorption Fine Structure

FFT: Fast Fourier Transform

FEG-ESEM: Field Emission Gun Environmental Scanning Electron Microscopy

GC-MS: Gas Chromatography - Mass Spectrometry

HAADF-STEM: High Angle Annular Dark Field Scanning Transmission Electron Microscopy

HRSTEM: High-Resolution Scanning Transmission Electron Microscopy

HTH: Hydrothermal Hydrolysis

LB: Luria-Bertani

MGP: Metales de Grupo del Platino

MOPS-NaOH: sodium; 3-morpholino-4-propane-1-sulfonic acid; hydroxide

MOC: Menders Overlap Coefficient

MTHF: Methyltetrahydrofuran

MTQ: 1-metil-tetrahidroisoquinolina

MW: Microwave

NPs: Nanoparticles

OFN: Oxygen Free Nitrogen

PGM: Platinum Group Metals

PyMCA: Phyton Multichannel Analyser

QDs: Quantum Dots

RF: Radio Frequency

SAED: Selected-Area Electron Diffraction

SRB: Sulfate Reducing Bacteria

STEM: Scanning-Transmission Electron Microscopy

THF: Tetrahydrofuran

T-RFLP: Terminal Restriction Enzyme Fragment Length Polymorphism

XANES: X-ray Absorption Near-Edge Structure

XAS: X-ray Absorption Spectroscopy

XPS: X-ray Photoelectron Spectroscopy

XRF: X-ray fluorescence

XRD: X-ray Diffraction

ÍNDICE

RESUMEN

En la presente tesis doctoral se describe la reducción bacteriana de paladio (Pd) y rutenio (Ru) en estado iónico, procedentes de soluciones en forma de nanopartículas monometálicas y bimetálicas con una elevada actividad catalítica.

Algunas cepas bacterianas son capaces de reducir de forma enzimática el Pd(II) a Pd(0) mediante la adicción de una fuente externa donadora de electrones. Las nanopartículas (NPs) formadas son retenidas e inmovilizadas en el citoplasma, membrana y periplasma de las células bacterianas, dando como resultado la formación de pequeñas NPs con un tamaño homogéneo y elevadas propiedades catalíticas. La actividad catalítica de las NPs de Pd formadas por las células bacterianas resulta ser, en ocasiones, mayor que la de los catalizadores comerciales con la ventaja adicional de haber sido producidas de una forma mucho más económica y con metodologías no perjudiciales para el medio ambiente.

Estudios previos han demostrado la habilidad de algunas bacterias de recuperar oro (Au) y Pd procedentes de desechos mediante el uso de células bacterianas de *Escherichia coli* y *Desulfovibrio desulfuricans*, y se han identificado algunas de las principales enzimas que juegan un papel importante en la formación inicial y nucleación de las NPs de Pd. Otros estudios también han demostrado la capacidad de algunas bacterias de sintetizar NPs bimetálicas de Au y Pd y de Pd y Ru.

En el primer capítulo de la presente tesis doctoral se han empleado células de *E. coli* para la síntesis bacteriana de NPs de Pd/Ru. Una información más detallada acerca de la estructura de dichas NPs bimetálicas se obtuvo mediante el uso combinado de técnicas espectroscópicas y microscópicas; una estructura "*core/shell"* (compuesta por Ru en el interior y Pd en el exterior de la NPs bimetálica) fue obtenida por un mecanismo similar al previamente demostrado por Deplanche *et al*., (2012) con NPs bimetálicas de Pd/Au sintetizadas por *E. coli*. Además, las notorias propiedades catalíticas de las NPs bimetálicas se pusieron de manifiesto mediante la conversión catalítica del compuesto 5-hidroximetilfurfural (5-HMF) (un producto intermediario de gran interés para la industria de química fina y de biocombustibles generado por la degradación térmica de glúcidos y celulosa) al compuesto 2,5-dimetilfurano (2,5-DMF), un valioso compuesto que puede ser empleado como biocombustible con unas propiedades similares al etanol.

En el segundo capítulo de esta tesis, se comprobó la habilidad de sintetizar NPs bimetálicas de Pd/Ru empleando un desecho bacteriano de un consorcio de bacterias acidófilas sulfato-reductoras obtenidas de un biorreactor destinado a procesos de bioloxiviación. Por otro lado, también se empleó, con el mismo propósito, otra bacteria sulfato-reductora más conocida como *D. desulfuricans.* Tanto las NPs bimetálicas sintetizadas por *D. desulfuricans* como las sintetizadas por el consorcio bacteriano mostraron una elevada actividad catalítica para la conversión del compuesto 5-HMF en 2,5-DMF.

En el tercer capítulo tesis doctoral se llevó a cabo el uso de una fuente externa de radio frecuencia (RF) o energía microondas (MW) sobre células bacterianas de *E. coli* y *D. desulfuricans* en suspensión, previamente a ser expuestas a una solución de Pd(II). Esta exposición a MW, previa al proceso de síntesis de NPs de Pd, tuvo como resultado final una mayor dispersión de las NPs resultantes contenidas en la bacteria que las NPs formadas por bacterias que no habían sido expuestas a energía MW. En el capítulo cuatro, la actividad catalítica de las NPs de Pd sintetizadas por células de *D. desulfuricans* se comprobó mediante la reacción de hidrogenación del compuesto 2-pentino, demostrando una mayor actividad catalítica.

ABSTRACT

In this thesis, the bioconversion of palladium and ruthenium solutions into valuable monometallic and bimetallic nanoparticles with highly catalytic activity is described. Bacteria can enzymatically reduce Pd(II) at the expense of an exogenous electron donor to Pd(0). The resulting nanoparticles (NPs) are immobilised in the cytoplasm, membrane and periplasm of the cells resulting in small NPs with a homogeneous size and high catalytic properties. The catalytic activity of the biogenic Pd NPs is sometimes higher than the commercial catalysts with the additional advantage of being synthesized using more economic and environmentally friendly methodologies. Previous studies have shown the ability of some bacteria to recover gold and palladium from wastes using cells of *Escherichia coli* and *Desulfovibrio desulfuricans* and have elucidated some of the main enzymes involve in the initial nucleation and formation of Pd NPs. Other studies proved the ability of bacteria to synthesize bimetallic NPs of gold and palladium and palladium and ruthenium.

In this study, cells of *E. coli* were used for the synthesis of bimetallic NPs of Pd/Ru. A detailed information of the structure of the bimetallic NPs was provided using a combination of spectroscopic and microscopic techniques; a *"core/shell"* (Ru core, Pd shell) structure was reported with a similar mechanism to that reported previously by Deplanche et al., (2012) with *E. coli* Pd/Au NPs. In addition, the catalytic properties of the bio-bimetallic NPs were reported for the conversion of 5-hydroxymethylfurfural (5-HMF) (a waste compound derived from the hydrolysis of starch and cellulose for obtaining biofuel) into 2,5-dimethylfuran (2,5-DMF), a valuable compound with similar properties to ethanol, with onward application as biodiesel. The ability to synthesize Pd/Ru NPs was tested using a consortium of acidophilic sulfidogenic (CAS) waste culture recovered from an unrelated biotechnology process together with a traditional sulfidogenic bacterium (*D. desulfuricans*). *D. desulfuricans* and CAS culture showed high activity for the conversion of 5-HMF into 2,5-DMF.

Finally, an external source of radio-frequency (RF) (microwave energy (MW)) was applied to resting cells (i.e. before being exposed to Pd(II) solution) of *E. coli* and *D. desulfuricans* reporting changes in the dispersity of the resulted Pd NPs compared with untreated cells. The catalytic activity of Pd-NPs on MW-pretreated cells of *D.*

desulfuricans was tested for the hydrogenation of 2-pentyne, showing increased catalytic properties as compared to Pd-NPs on untreated cells

INTRODUCCIÓN

1. Metales del Grupo del Platino

El grupo de los metales del platino, MGP, incluye, además del propio platino (Pt), elementos como el paladio (Pd), rodio (Rh), rutenio (Ru), iridio (Ir) y osmio (Os). Estos metales, junto con el oro (Au) y la plata (Ag), son denominados metales nobles debido a sus excelentes propiedades entre las que destacan su actividad catalítica, su resistencia a la corrosión y oxidación, sus propiedades inertes y su estabilidad termoeléctrica (Dong et al., 2015). Los principales depósitos naturales de MGP son muy limitados, y las reservas de estos metales se estima que están en torno a 66.000 toneladas, repartidas por todo el mundo. Aproximadamente el 80% de estos depósitos se encuentran en Sudáfrica y el resto de los depósitos naturales se encuentran entre Estados Unidos, Canadá, Rusia y Zimbabwe (Wiseman 2015).

Estos metales suelen estar asociados con minerales de sulfuro y gangas, en una concentración que oscila entre 2 y 10 gr/ton de mineral. Además, los MGP se obtienen como subproductos derivados de la extracción de otros minerales o coproductos en función de la concentración del mineral (Kumar et al., 2013). También se pueden encontrar asociados a diferentes minerales en pequeñas cantidades en forma de trazas, por lo que, para llevar a cabo su extracción, y poder obtener cantidades en concentración suficiente, se necesitan tratamientos mecánicos complejos. En la naturaleza estos metales nobles se pueden encontrar asociados a minerales de sulfuros y arseniuros como es el caso de $PtAs_2$, PtS, $Pt(AsS)_2$, (Pt,Pd)S, (Pt,Pd,Ni)S, RuS_2, Pd_3Pb y rutenio elemental (Xiao et al., 2004). Y es normal encontrar los MGP junto a los llamados metales de transición, como son cobalto (Co), hierro (Fe), cobre (Cu) y níquel (Ni).

La escasa presencia de los MGP en los recursos minerales naturales ha despertado cierta preocupación en cuanto a la capacidad de disponer de ellos a largo plazo y poder cubrir la demanda de las futuras necesidades tecnológicas por parte de la sociedad (Gordon et al., 2006). Al mismo tiempo el proceso de extracción procedente de las minas conlleva unos impactos ambientales y sociales de importancia, como son la contaminación de las aguas subterráneas, la emisión de gases de efecto invernadero, un consumo excesivo de agua y la injusta relocalización de los pueblos o asentamientos situados donde se encuentran localizados los recursos minerales (Rajak et al., 2008).

Tabla 1. Minerales de sulfuro y gangas con contenido en MGP.

Mineral	Fórmula
Calcopirita	$CuFeS_2$
Pentlandita	$(Fe, Ni)_9 S_8$
Pirita	FeS_2
Pirrotina	$Fe_{1-x}S_x$
Cromita	$FeCr_2O_4$
Piroxeno	$(Mg, Fe)SiO_3 – Ca(Mg, Fe)Si_2O_6$
Olivino	$(Mg, Fe)_2 SiO_4$
Plagioclasa	$NaAlSi_3O_8 – CaAl_2 Si_2O_8$
Hematita	Fe_2O_3

Durante el proceso de tratamiento para la obtención de los MGP de alta pureza los minerales son sometidos a altas temperaturas con lo que se separan tanto los sulfuros como los silicatos (los llamados ganga) que contienen los MGP. Después del proceso de fundición el sulfuro de hierro es oxidado a óxido de hierro y el azufre es oxidado a dióxido de azufre (Cramer et al., 2008; Safarzadeh et al., 2018). El dióxido de azufre y el dióxido de hierro son eliminados en forma de desecho gaseoso y residuo de fayalita, respectivamente. En el proceso de eliminación de estos residuos, un contenido importante de MGP puede ser arrastrado y acabar perdiéndose. Por ello, para recuperar estas cantidades importantes, los residuos son fundidos para recuperar los MGP que pudieran contener. Finalmente, para el proceso de refinería de MGP, los metales base son separados por un proceso de lixiviación y los MGP son tratados mediante diferentes métodos de precipitación y extracción para separar cada uno de los metales (Safarzadeh et al., 2018).

El proceso de extracción de los MGP procedente de fuentes naturales consta de las siguientes etapas: a) tratamiento mecánico, b) flotación, c) fundición, d) conversión, e) refinería de los minerales, f) refinería de MGP. Este proceso queda ejemplificado en el siguiente esquema:

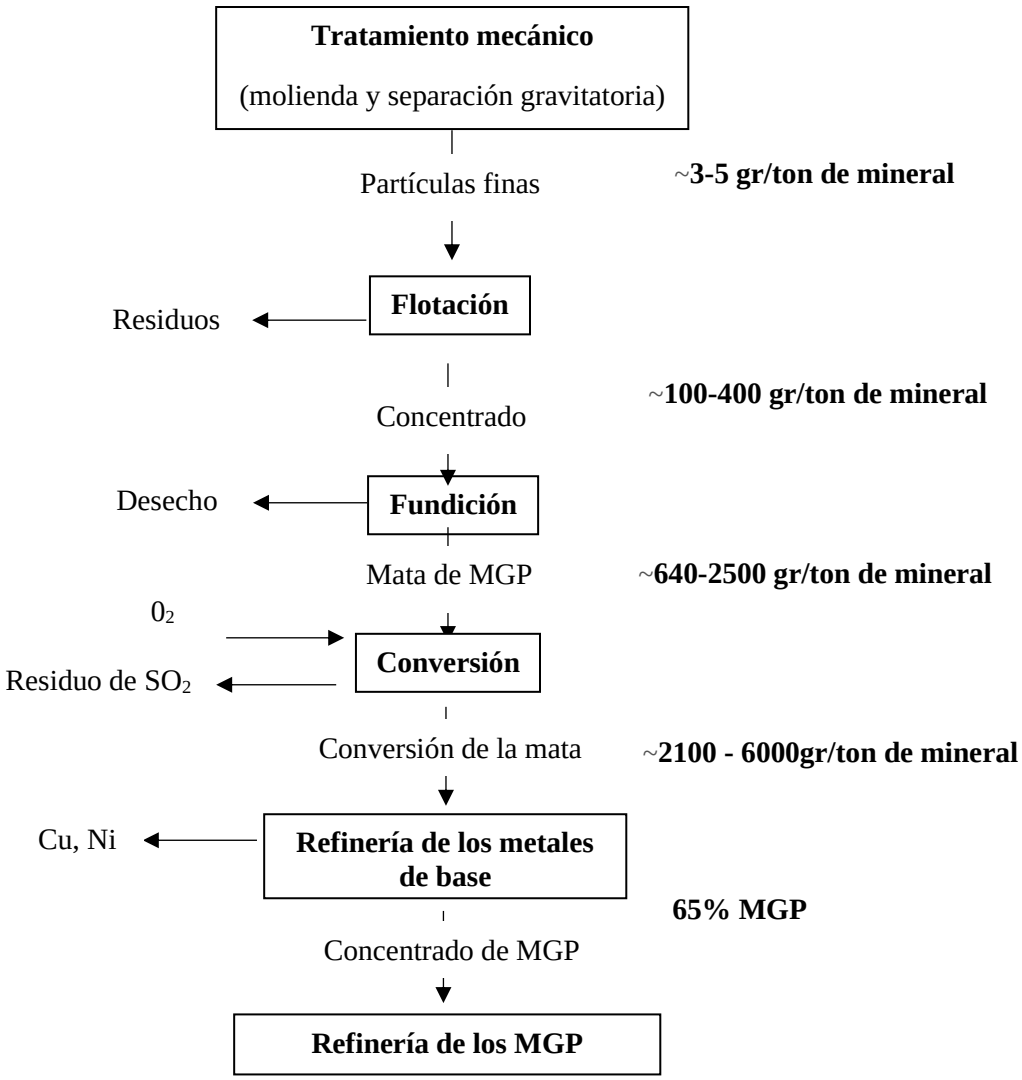

Figura 1. Esquema básico del proceso de tratamiento y extracción de los MGP adaptado de Cramer *et al*., 2008.

2. Recuperación de metales del grupo del platino

A pesar de los altos costes de producción y complejos procesos de tratamiento que conlleva la refinería de los MGP procedente de las extracciones mineras (Figura 1), así como la escasez de estos en la naturaleza, únicamente el 28% de la producción mundial de metales del grupo del platino procede del reciclaje (Figura 2). La producción anual de MGP procedente de la minería se ha mantenido constante durante los últimos 10 años, en torno a las ~450 toneladas (US geological Survey 2019). De esa cantidad, más de la mitad corresponde a paladio (Pd) ~250 toneladas, acorde a los últimos datos obtenidos de 2018

(Thomson Reuters, GFMS 2019). Aproximadamente el 83,83% del paladio producido va destinado a su uso en la industria automovilística (Cowley 2019) con el fin de cumplir con la estricta legislación por parte de los diferentes organismos internacionales para reducir la emisión de gases dañinos para el medio ambiente y el ser humano. De las ~200 toneladas que se destinan a la industria automovilística solamente ~40 toneladas son recicladas para poder ser reutilizadas nuevamente. Esto quiere decir que anualmente unas 160 toneladas de paladio se acumulan como parte de desechos sin reciclar o en automóviles que aún se encuentran en uso.

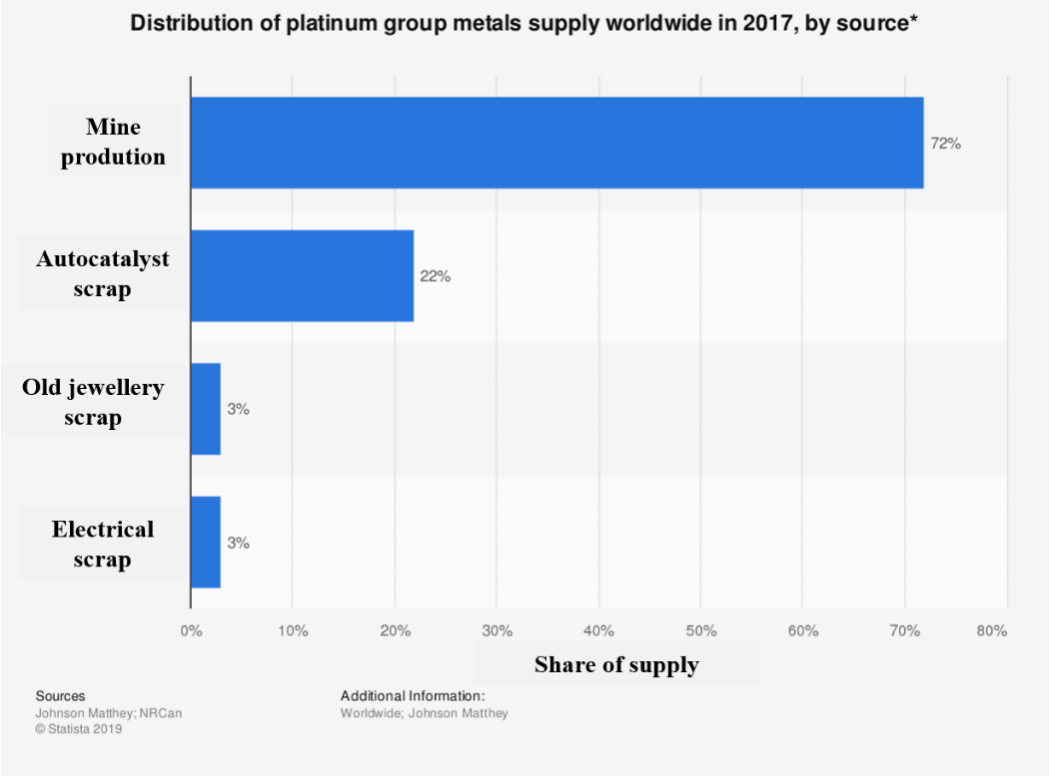

Figura 2. Gráfico de la distribución de los metales del grupo del platino en función de la fuente de procedencia. Fuente https://www.statista.com/statistics/602766/distribution-of-the-supply-of-platinum-group-metals-worldwide-by-source/.

Otra de las ventajas que ofrece la recuperación de MGP procedente de catalizadores de automóviles gastados es que presentan una mayor concentración en MGP que los minerales en su estado natural (Deng *et al*., 2018). Por otro lado, un almacenamiento inapropiado de estos residuos puede tener efectos dañinos para el medio ambiente y la salud pública (Wei *et al*., 2019).

Con el objetivo de llevar a cabo una transición energética hacia energías más limpias se ha producido un aumento de la demanda de coches híbridos frente a la de automóviles tradicionales. Estos coches híbridos están compuestos de motores eléctricos y también de motores de gasoil, los cuales contienen conversores catalíticos. Por ello está previsto un continuo aumento de la demanda de paladio en los próximos años. Desde 2008 la demanda de MGP destinada a conversores catalíticos para automóviles no ha parado de crecer, pasando de las 323 toneladas en 2008 (Platinum 2008) a 357 toneladas en 2018 (Matthey 2018). Por lo tanto, esta mayor demanda va a traer como consecuencia una mayor producción de residuos y es necesario, desde un punto de vista económico y medioambiental, aprovechar estas fuentes secundarias de MGP procedente de desechos para reutilizarlos. Cabe destacar que, aun siendo los conversores catalíticos la principal fuente secundaria de MPG, hay desechos procedentes de otros sectores que también tienen importancia como son: catalizadores procedentes de la industria petrolífera, joyería e industria odontológica.

2.1. Recuperación basada en métodos pirometalúrgicos

Este proceso está basado en la fundición del material que contiene los MGP en presencia de una corriente y un metal recolector. A menudo, los metales que se emplean para recuperar los MGP son Ce, Zr y Al, que son de cierto valor económico (Saguru *et al.*, 2018). Pero este tipo de tratamientos presenta una serie de inconvenientes como es la dificultad para recuperar el metal recolector. Por otro lado, se requiere de maquinaria especializada que, a menudo, puede ser difícil de manejar cuando se pretenden reciclar pequeñas cantidades del metal como las que se encuentran en los catalizadores. Estos equipos suelen trabajar bajo temperaturas muy elevadas y, como resultado de la combustión, se emiten sustancias tóxicas al medio ambiente. Por ello es necesario el uso de otras técnicas que permitan una recuperación de MGP más eficiente y menos perjudicial para el medio ambiente.

Figura 3. Imagen de una planta de refinería para el reciclaje de metales preciosos mediante métodos de fundición. Fuente https://www.trovaweb.net/images/recupero-affinazione-metalli-preziosi-smaltimento-rifiuti-industriali-chimet-arezzo/recupero-affinazione-metalli-preziosi-smaltimento-rifiuti-industriali-chimet-arezzo-05.png.

2.2. Recuperación basada en métodos hidrometalúrgicos

El proceso de recuperación basado en métodos hidrometalúrgicos se ha empleado en mayor medida que los procesos pirometalúrgicos. Este proceso engloba diferentes etapas como son la adsorción mediante intercambio iónico con resinas y la extracción por solvente. Siendo, además, comúnmente empleado en este método el uso de agentes reductores tóxicos para la reducción de metales (Das *et al*., 2010).

2.3. Recuperación basada en métodos biológicos

Este proceso de recuperación de metales ha atraído gran atención durante los últimos años debido al potencial que han demostrado ciertos organismos y componentes biológicos. Estos procesos permiten recuperar metales de una forma económica, abaratando los costes de operación que supone el uso de los grandes equipos de las plantas de tratamiento y, al mismo tiempo, reduciendo enormemente la generación de desechos químicos derivados del proceso de recuperación de metales (Mabbett *et al*., 2006). Además, el uso

de componentes biológicos se ha presentado como una gran alternativa para la biorremediación de ambientes contaminados con metales pesados (Sanchez-Castro *et al*., 2017). Destacan numerosos microorganismos capaces de acumular metales pesados y metales preciosos como son las algas (Das *et al*., 2016; Zeraatkar *et al*., 2016), las bacterias (Yong *et al*., 2002; de Vargas *et al*., 2004; Merroun *et al*., 2011), las levaduras (Wang y Chen 2007) y los hongos (Povedano-Priego *et al*., 2017). De hecho, en los últimos años se ha puesto el foco en el uso de microorganismos para la recuperación de metales debido, en gran medida, a la resistencia que estos presentan frente a altas concentraciones de una gran variedad de metales que pudieran resultar tóxicas para otros organismos vivos (Ruiz-Fresneda *et al*., 2018; Krawczyk-Bärsch *et al*., 2018). Por otro lado, la gran facilidad con que estos microorganismos se multiplican hace que su escalado a nivel industrial sea más fácil. Esto permite obtener grandes cantidades de biomasa de una forma mucho más rápida y sencilla de lo que sería con otros organismos biológicos más complejos, como las algas o las plantas.

Los microorganismos interaccionan con los metales a través de 5 mecanismos posibles: bioadsorción, bioacumulación, quelación, biomineralización y biotransformación (reducción/oxidación) (Figura 4).

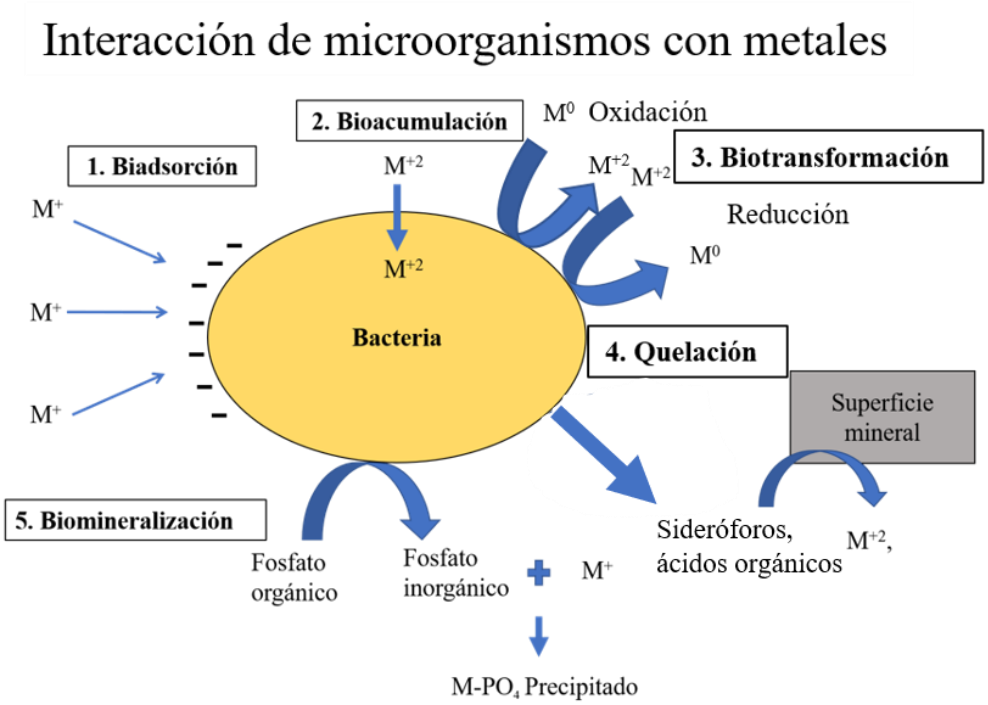

Figura 4. Esquema representativo de los diferentes mecanismos de interacción de bacterias con metales pesados.

- **Bioadsorción**

El proceso de bioadsorción consiste en la interacción fisicoquímica entre iones metálicos y la superficie celular de los microorganismos en la que se produce un "secuestro o inmovilización del metal". Para ello pueden ser utilizados tanto organismos vivos como muertos, por lo que se trata de un proceso pasivo (Abselbasir *et al*., 2018). Generalmente esta interacción se produce por una diferencia de cargas entre la superficie bacteriana, cargada negativamente, y los metales en estado iónico, cargados positivamente. Estas uniones pueden producirse de forma directa donde los metales se unen a grupos funcionales de la bacteria como grupos carboxilo, grupos aminos o grupos fosfatos. Entre los componentes celulares con los que pueden interaccionar los metales está la pared celular, la membrana celular, proteínas de la capa-S y los materiales extracelulares producidos por las bacterias, como son las sustancias poliméricas extracelulares (EPS) y la capa S (Merroun *et al*., 2005).

- **Bioacumulación**

El proceso de bioacumulación puede ser tanto un proceso activo como pasivo, por el que se produce una internalización de metales dentro de la bacteria. En el proceso activo los microorganismos introducen un metal pesado mediante un sistema de transporte específico para el metal que requiere un gasto metabólico por parte de la bacteria. Estos metales pueden ser acumulados en el interior de las células bacterianas envueltos en membranas lipídicas o vesículas y proteínas. Debido al gasto metabólico que este proceso supone para las células su aplicación, para usos industriales en la recuperación de metales, puede ser limitada ya que se trata de un proceso lento (Mishra y Malik, 2013). Este proceso, puede estar en estrecha relación con la bioadsorción ya que para una acumulación interna se requiere una rápida interacción con los componentes de la superficie celular. De hecho, el proceso pasivo requiere de menor consumo de energía por parte de las bacterias y estas pueden llevarlo a cabo incluso en ambientes con escasos nutrientes (Haferburg y Kothe, 2007). En este caso, la bioacumulación intracelular puede ser atribuida a la alteración de la permeabilidad de la propia membrana celular mediante la formación de poros (Merroun y Selenska Pobell, 2008).

- **Quelación**

La quelación es un proceso llevado a cabo por algunas bacterias en el que intervienen moléculas de bajo peso molecular, péptidos y otras sustancias que tienen una alta afinidad por ciertos metales capaces de solubilizarlos (Aguado-Santacruz *et al*., 2012). Un ejemplo

de estas sustancias son los sideróforos, sustancias que presentan una elevada afinidad por el hierro y actúan como agentes quelantes para secuestrar el hierro en presencia de otros metales y reducirlo a Fe(II), llevándolo así a una forma más soluble y aprovechable para la nutrición bacteriana (Hider *et al*., 2009).

- **Biomineralización**

La biomineralización consiste en la precipitación de metales en forma de carbonatos, sulfuros, fosfatos e hidróxidos como resultado de la interacción de los ligandos liberados por bacterias y los metales en solución (Barnes *et al*., 1991; Macaskie *et al.*, 1992; Lopez-Fernandez *et al*., 2018).

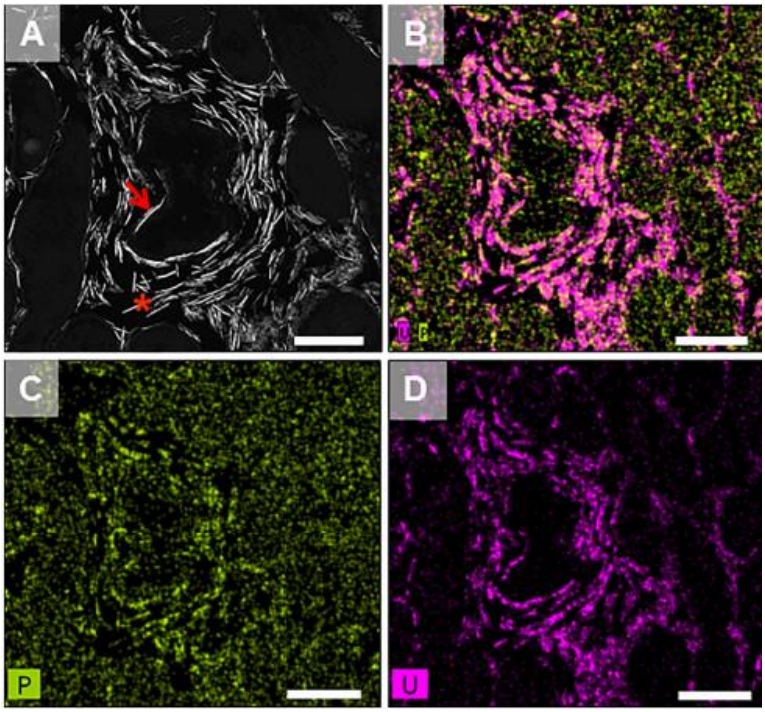

Figura 5. Imagen de microscopia STEM/HAADF de una muestra de cortes finos de cepas bacterianas tratadas con U donde se observan precipitados de uranio extracelulares asociados a fósforo. (Tomado de Povedano-Priego *et al*., 2019).

La eficiencia del proceso de biomineralización es proporcional a la cantidad de ligandos liberados por el microorganismo. Una de las ventajas que ofrecen las bacterias es la capacidad de generar elevadas concentraciones de ligandos adyacentes a la superficie celular, proporcionando sitios de nucleación donde los metales se unen formando el mineral (Tabak *et al.*, 2005). La liberación de estos ligandos es catalizada por la actividad de una amplia variedad de enzimas (fosfatasa, etc.) (Beazley *et al*., 2011). Entre ellas, las fosfatasas juegan un papel importante en la biomineralización de metales pesados tales

como plomo (Povedano-Priego *et al*., 2017), uranio (Merroun *et al*., 2011), etc. Algunas bacterias del género *Sphingomonas*, *Bacillus* o *Serratia*, son capaces de hidrolizar fosfatos orgánicos mediante la actividad fosfatasa liberando fosfatos inorgánicos (Pi) que al contactar con U(VI) forman fosfatos insolubles (Newsome *et al*., 2015).

Otro de los mecanismos más conocidos es el proceso llevado a cabo por bacterias sulfato reductoras mediante la actividad de enzimas tipo APS reductasa (Agostino *et al*., 2018). Uno de los primeros estudios llevados a cabo en este sentido es el uso de estas bacterias para el tratamiento de aguas contaminadas con Zinc (Barnes *et al.*, 1991). En este caso se le proporciona una fuente donadora de electrones, como el etanol, para la reducción de sulfatos (SO_4^{-2}) a sulfuro de hidrógeno (H_2S), de modo que, estos sulfuros al entrar en contacto con el metal en solución forman minerales de sulfuro, que precipitan, eliminando los metales tóxicos de la solución. Este proceso también se ha llevado a cabo para la producción de materiales de interés tecnológico como es la síntesis de *quantum dots* (QDs) mediante la síntesis de nanopartículas de sulfuro de zinc (ZnS) (con aplicaciones para su uso en paneles de energía solar y diodos). En este caso, se aprovechó el excedente de hidrógeno de azufre (H_2S) producido por la bacteria *Desulfovibrio desulfuricans* como producto de su metabolismo, para la síntesis de nanopartículas de sulfuro de zinc (ZnS) (Murray *et al*., 2017).

En este proceso cabe destacar que los metales no sufren ningún cambio en su estado de oxidación a diferencia de lo que ocurre en los procesos de biotransformación que se describen a continuación.

- **Biotransformación**

En este proceso se produce un cambio en el estado de oxidación del metal como resultado de la actividad microbiana. La actividad enzimática de los microorganismos puede promover la reducción o la oxidación del metal bajo condiciones dependientes o independientemente del metabolismo de la bacteria.

- **Oxidación**

La oxidación puede darse como resultado de la actividad metabólica de la bacteria donde en ciertos casos como producto de dicha oxidación, se solubilizan determinados metales procedentes de materiales sólidos (minerales, menas o residuos) liberando el metal de interés en solución. Un ejemplo es el caso de la oxidación del hierro, donde organismos como *Thiobacillus ferrooxidans* han sido capaces de llevar a cabo este proceso de forma natural (Zhang *et al*., 2018). En última instancia, el metal puede ser recuperado mediante

reacciones de oxidación/reducción formándose compuestos orgánicos o inorgánicos mediante el uso de métodos biológicos (proceso que se conoce como biolixiviación) o por métodos electroquímicos.

El proceso de biolixiviación presenta la ventaja de ser un método mucho menos perjudicial para el medio ambiente que los métodos de extracción tradicionales. La biolixiviación se lleva a cabo a temperaturas mucho más bajas (y por lo tanto reduciendo los costes de energía) y con una menor huella de carbono (Johnson *et al*., 2014). Esto se debe a que se emplean microorganismos autótrofos para llevar a cabo el proceso de biolixiviación, los cuales fijan el dióxido de carbono para emplearlo como fuente de carbono. De ellos, los comúnmente más empleados para este tipo de procesos son los acidófilos entre los que destacan: *Acidithiobacillus ferrooxidans*, *A. thiooxidans* y *Leptospirilum ferrooxidans* (Abdelbasir *et al*., 2018). También destacan algunos organismos heterótrofos como *Sulfolobus* y hongos como *Penicillium* y *Aspergillus niger* (Cui y Zhang, 2008)

- **Reducción**

En otros casos, como resultado de la actividad metabólica, muchas bacterias pueden utilizar determinados metales como aceptor final de electrones, reduciéndolo como en el caso del tecnecio (Tc) (Marshall *et al*., 2008). Este proceso ha adquirido gran importancia para tratamientos de biorremediación en los que las bacterias son capaces de utilizar como último aceptor de electrones el U(VI) reduciéndolo a U(IV), siendo esta última una forma insoluble de uranio y, por lo tanto, menos tóxica. Este proceso fue descrito por primera vez por Lovley y sus colaboradores en 1991.

En el caso de metales como el selenio (Se), que pueden resultar tóxicos en elevadas concentraciones, también se han llevado a cabo procesos de reducción en las que Se(IV) puede ser reducido a Se(0). Este proceso es llevado a cabo por diferentes géneros bacterianos como *Stenotrophomonas* o *Bacillus* (Ruiz-Fresneda *et al.*, 2018; Kora *et al.*, 2018).

Con el creciente interés de las técnicas de recuperación de MGP, el proceso de bioreducción por medio de bacterias ha adquirido mayor protagonismo. Muchas bacterias han demostrado la capacidad de reducir MGP, como son los casos del Pd (Lloyd *et al.*, 1998), del Pt (Yong *et al.*, 2002) y de otros metales nobles de gran interés como la Ag (Fu *et al.*, 2000) y el Au (Konishi *et al.*, 2006).

3. Reducción microbiana de Paladio

El trabajo de Lloyd *et al.* (1998) demostró por primera vez la capacidad de células de *D. desulfuricans* de reducir Pd(II). En este proceso las células eran expuestas a una solución de Pd(II) y, mediante la adición de un donador de electrones tal como el piruvato, el formiato o el H_2, el paladio en solución precipitaba en forma de Pd(0). Mediante el uso de microscopía electrónica de transmisión se pudieron observar depósitos en la superficie celular en los que, mediante su análisis utilizando el método de energía dispersiva de rayos-X (EDX), se confirmó la presencia de paladio. Estudios posteriores se llevaron a cabo para investigar el papel enzimático de las bacterias en la reducción del paladio. Para ello se emplearon cepas mutantes de *D. fructosovorans* que carecían de enzimas hidrogenasas tanto a nivel del periplasma como en el citoplasma reduciendo el Pd(II) sólo en aquellas regiones donde permanecían las enzimas hidrogenasas de membrana. De esta forma se confirmó el papel importante que juegan estas enzimas en el proceso de reducción del paladio (Mikheenko *et al*., 2008).

Figura 4. Imagen representativa del cambio de color como consecuencia de la reducción de Pd(II) (izquierda) a Pd(0) (derecha). (Tomado de Foulkes *et al*., 2016).

El proceso de reducción del paladio no solamente se ve afectado por los parámetros más comunes en los procesos de bioadsorción (como son el pH, la concentración del metal o la sal con la que se suministra el metal) sino que, además, el donador de electrones juega un papel fundamental. Yong *et al.,* (2002) descubrieron que la reducción era más lenta cuando se empleaba H_2 que cuando se añadía formiato. Esto era debido a la dificultad por

parte de las bacterias de acceder al hidrógeno gaseoso y a la lenta disolución de éste en el medio líquido. Por otro lado, estos autores determinaron también la importancia de la concentración del agente reductor empleado en la velocidad de reducción del paladio. El proceso inicial de formación de nanopartículas de paladio es mediado por las enzimas, posteriormente el crecimiento de estos depósitos es llevado a cabo por medio de un proceso autocatalítico del propio paladio. El Pd(0) formado inicialmente como resultado de la actividad enzimática de las células, acumula el H_2 liberado procedente de la degradación bacteriana del formiato. Este Pd (sintetizado por actividad enzimática), es capaz actuar como catalizador para la degradación química de más formiato, liberando más H_2 que es empleado para la reducción de Pd(II) a Pd(0) (Yong *et al*., 2002). Por lo tanto, podemos decir que el proceso de formación de nanopartículas de paladio consta de una etapa inicial de formación mediada por bacterias (formando los sitios de nucleación) y una etapa posterior química que permite el crecimiento de la nanopartícula.

Otros muchos microorganismos han demostrado la capacidad de reducir Pd, desde bacterias Gram positivas como *B. benzoevorans* (Omajali *et al*., 2015) hasta bacterias Gram negativas como *Shewanella oneidensis* y *Escherichia coli* (Deplanche *et al*., 2010, Foulkes *et al*., 2016, De Windt *et al*., 2005). En este trabajo, y gracias al avance tecnológico de los equipos de análisis como es la microscopía de transmisión de alta resolución (HRTEM), se ha podido observar que los acúmulos de paladio no solamente se forman a nivel de la superficie celular, sino también a nivel intracelular. Se ha llevado a cabo un estudio comparativo entre *B. benzoevora*ns y *D. desulfuricans* en el que se han observado nanopartículas de Pd de tamaños que oscilan entre 1-5 nm. Además, un estudio más detallado del tamaño y la estructura de las nanopartículas mediante alta resolución llevó a la conclusión de que el donador de electrones empleado para llevar a cabo el proceso de bioreducción del paladio jugaba un papel importante en cuanto al tamaño de las NPs de Pd y su estructura cristalina, confirmando los estudios iniciales llevados a cabo previamente por Young *et al*. (2002).

Otras bacterias como *E. coli* han demostrado la capacidad de reducir Pd(II) a Pd(0) formando NPs, tanto a nivel intracelular como a nivel de la membrana, destacando el papel fundamental de las enzimas hidrogenasas en la formación de las NPs de Pd (Deplanche *et al.*, 2010). Con *E. coli* también se evidenció el papel fundamental que juega el donador de electrones, de modo que las NPs de Pd formadas cuando se había empleado

formiato como agente reductor eran más pequeñas y dispersas que cuando se empleaba H_2, y esto influía en la actividad electroquímica de las NPs (Courtney *et al*., 2016). El uso de *E. coli* para la síntesis de NPs de Pd ofrece muchas ventajas ya que, al tratarse de un organismo "modelo" y haber sido estudiado ampliamente, permite conocer con mayor facilidad los mecanismos implicados en la síntesis de NPs de Pd. Al tratarse de un organismo anaerobio facultativo permite conocer tanto los mecanismos empleados bajo condiciones aerobias, demostrados recientemente por Foulkes *et al*., (2016), como bajo condiciones anaerobias (Mabbett *et al*., 2006). Trabajar bajo condiciones aerobias ofrece la ventaja de la reducción de costes en el laboratorio ya que el crecimiento bacteriano bajo condiciones anaerobias requiere de mayor tiempo y de disponer de un equipamiento específico.

4. Interacciones microbianas con rutenio

La interacción microbiana con rutenio (Ru) ha sido, hasta la fecha, objeto de pocos estudios. El motivo principal es que el Ru es uno de los elementos más raros de la tierra y, al igual que el resto de los MGP, suele encontrarse asociado a otros elementos y en muy escasa cantidad. Los usos más comunes del Ru se encuentran en electrónica, para la fabricación de chips de resistencia y conectores eléctricos. Otras formas de rutenio, como los óxidos de rutenio, son empleados para recubrimiento de ánodos en pilas eléctricas y en paneles solares para la producción de electricidad. Una de las aplicaciones más importantes y recientes del rutenio es su uso en la industria clínica, como agente antitumoral. En este sentido, determinados complejos de rutenio resultan menos tóxicos que el platino pero, sin embargo, siguen manteniendo una gran actividad antitumoral. No obstante, una de sus aplicaciones más importantes es su uso como catalizador de reacciones químicas. Por ejemplo, el rutenio se emplea como catalizador para la oxidación de ácido acético y ello conduce a que los complejos de rutenio sean desechados, lo que conlleva el poder causar problemas en el medio ambiente al mismo tiempo que se desperdicia el preciado metal (Gallezot *et al.,* 1997).

La recuperación de rutenio procedente de residuos industriales que presentan ácido acético ha sido objeto de algunos estudios. Un ejemplo es el uso de fibras bacterianas modificadas con polietilenimina para la recuperación de rutenio procedente de residuos industriales con unos niveles de adsorción de rutenio 16,5 veces superior que con el uso

de resinas químicas (Kwak *et al*., 2013). Precisamente, un estudio llevado a cabo utilizando la bacteria *Rhodopseudomonas palustris* demostró la capacidad de recuperar, de forma selectiva, rutenio procedente de residuos industriales, reduciendo así los costes de electrodeposición y el impacto medioambiental (Colica *et al.,* 2013). En este trabajo se demostró que la bacteria era capaz de absorber unos 40 mg/ g (biomasa seca) de rutenio procedente de los residuos, obteniendo unos porcentajes de eliminación que oscilaban entre el 42% y el 72%.

5. Síntesis de NPs bimetálicas por medio de bacterias

Muchos trabajos se han publicado describiendo las ventajas que ofrece el uso de NPs bimetálicas y las diferentes rutas de síntesis que se pueden llevar a cabo mediante métodos químicos (Zaleska-Medynska *et al.,* 2016). Las NPs bimetálicas presentan ventajas frente a las monometálicas desde el punto de vista electrónico, óptico, catalítico o fotocatalítico. Esto es debido a que presentan las propiedades no solo de cada elemento que la conforma sino nuevas propiedades debido a la sinergia entre los dos elementos combinados que conforman las NPs bimetálicas.

El estudio de la síntesis de NPs monometálicas por medio de bacterias ha sido ampliamente estudiado, como se ha mencionado en apartados anteriores. Pero la síntesis de NPs bimetálicas por medio de bacterias se ha desarrollado escasamente. Unos de los pocos estudios realizados en este campo es el caso de la síntesis de NPs de Pd/Au por *E. coli* y *D. desulfuricans* (Deplanche *et al.,* 2012). Mediante el uso combinado de técnicas de espectroscopía y microscopía se pudo confirmar que las NPs bimetálicas presentaban una estructura de "*core/shell*". Las NPs bimetálicas con este tipo de estructura han demostrado tener una mayor actividad catalítica con respecto a otras NPs en diferentes reacciones (Zhao *et al.,* 2006). En este caso el Pd estaba localizado en la parte más externa de la NP bimetálica, "*shell*", y el Au en el centro, "*core*". Para llevar a cabo el proceso de síntesis de estas NPs las bacterias se exponen, en primer lugar, a una solución de Pd(II) en la que se forman las NPs de Pd con H_2 como donador de electrones. Posteriormente, las células con las NPs de Pd ya formadas, se ponen en contacto con una solución de Au(III) que, mediante un flujo constante de H_2, da lugar a Au(0). La hipótesis planteada por Deplanche *et al*., (2012) para la formación de este tipo de estructura es una reducción galvánica del Au(III), asistida por las NPs de Pd, debido a la diferencia del potencial

redox entre ambos elementos y a la capacidad del Pd para almacenar H_2, lo que lleva a la reducción de Au(III) a Au(0) y la oxidación de Pd(0) a Pd(II) que, ocasionalmente, provoca la migración de los estados oxidados de Pd a la parte más externa de la NP que posteriormente vuelve a reducirse por el flujo de H_2 formando el "*shell*" de la NPs bimetálica.

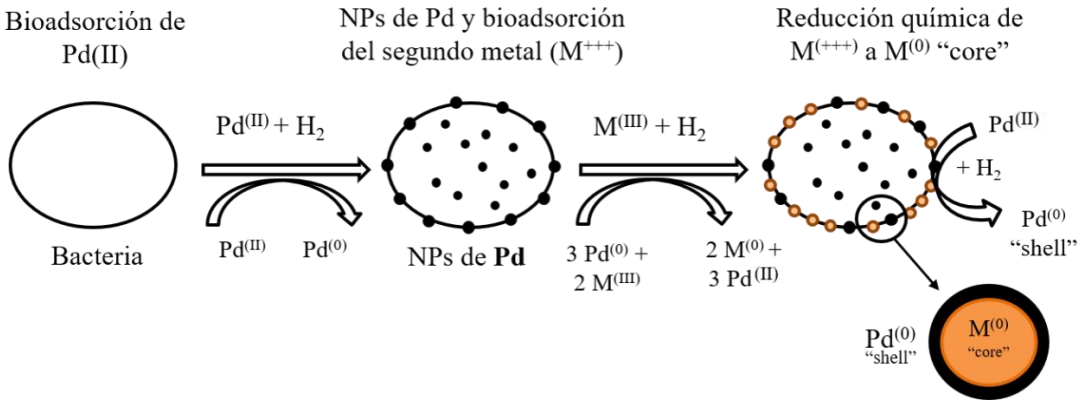

Figura 6. Resumen esquemático de la formación de NPs bimetálicas con estructura "*core/shell*"

Por otro lado, en este proceso se evidenció una reducción más rápida de las formas de Au(III) a Au(0) en presencia de las NPs de Pd que cuando las bacterias solas eran expuestas a una solución de Au(III), poniendo así de manifiesto el papel de la actividad autocatalítica de las NPs Pd sintetizadas inicialmente por las bacterias.

Recientemente Stephen et al., (2019) han descrito un método de síntesis microbiana de NPs bimetálicas de Pd/Pt por *E. coli*. La metodología empleada para la síntesis de estas NPs fue similar a la publicada previamente por Deplanche et al., (2012), de modo que una vez que las células han formado las NPs de Pd son puestas en contacto con una solución de Pt(II). Mediante el análisis por difracción de rayos-X (XRD) evidenciaron un ligero desplazamiento en los picos de las NPs bimetálicas con respecto a los picos de Pd y Pt lo que puede deberse a la formación de una aleación de ambos elementos.

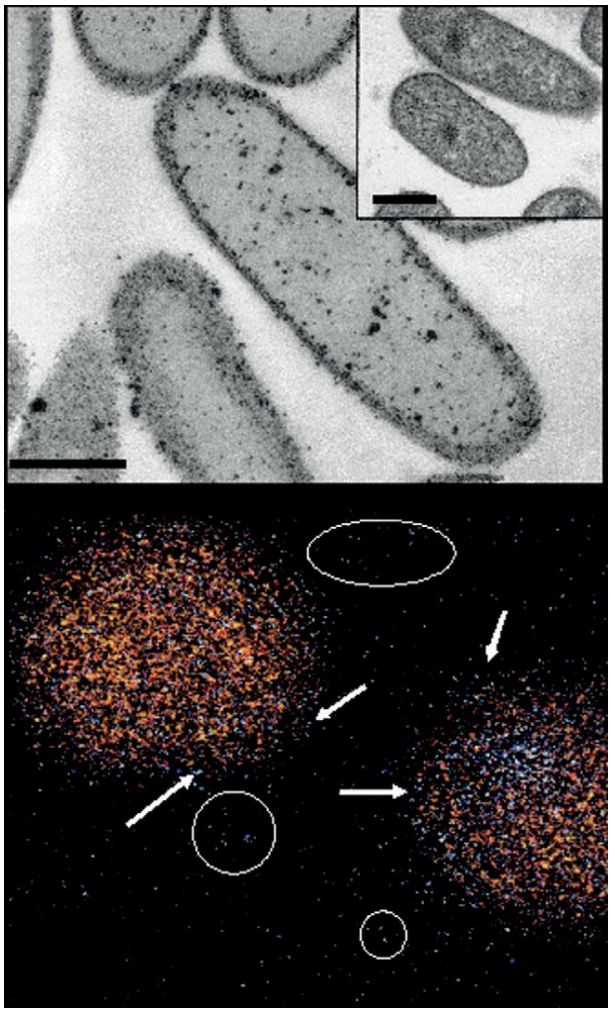

Figura 6. Imagen de microscopía electrónica de transmisión TEM (parte superior) y mapeo mediante energía dispersiva de rayos-X de las NPs bimetálicas de Pd/Au sintetizadas por *E. coli* (Tomado de Deplanche *et al*., 2012).

5.1.Síntesis de NPs bimetálicas de Pd/Ru

Estudios recientes llevados a cabo por Omajali *et al*., (2019) han demostrado la capacidad de *B. benzoevorans* de formar NPs de Ru y de paladio/rutenio (Pd/Ru NPs) mediante la adición de H_2 como donador de electrones. Los análisis mediante microscopía electrónica de transmisión de alta resolución y barrido determinaron la presencia de dos poblaciones de NPs (1-2 nm y 5-8 nm) que, mediante EDX, confirmaron la presencia de rutenio y paladio en los acúmulos. Los estudios de adsorción de rayos-X determinaron el carácter metálico de las NPs de paladio y la formación de óxidos de rutenio (RuO_2 y RuOH). Por

otro lado, mediante el estudio combinado de técnicas espectroscópicas y microscópicas se evidenció la presencia de algunas NPs con estructura "*core/shell*".

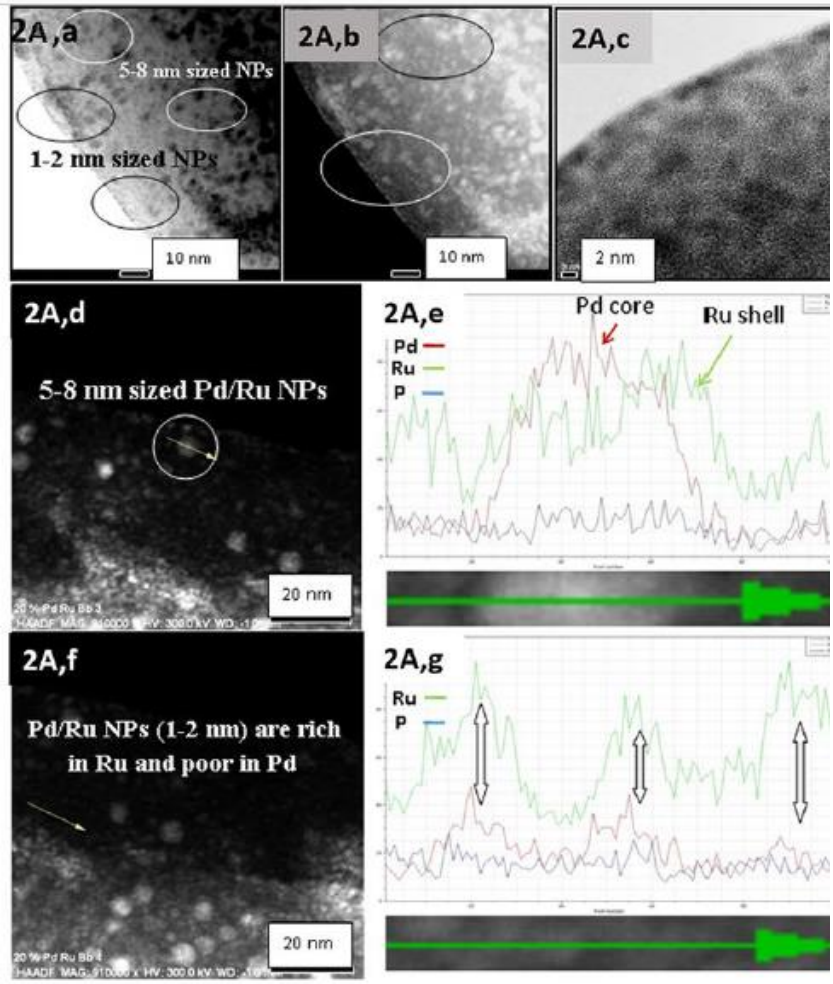

Figura 7. Imágenes de microscopía y análisis por energía dispersiva de rayos X de las NPs bimetálicas sintetizadas por la cepa *Bacillus benzoevorans* mostrando una estructura de "*core/shell*" (Tomado de Omajali *et al*., 2019).

6. Uso de las NPs sintetizadas por bacterias como catalizadores

El hecho de que las NPs formadas por las bacterias se encuentren confinadas en diferentes compartimentos de la bacteria, ya sea en el periplasma, citoplasma o membrana celular, hace que presenten un tamaño nanométrico homogéneo. Esto las convierte en un material ideal para su uso en diferentes reacciones de catálisis. Y fue poco después de que Lloyd *et al*., (1998) descubrieran el mecanismo de reducción de Pd por bacterias formando NPs cuando se llevaron a cabo los primeros ensayos de la actividad catalítica de las NPs de Pd

sintetizadas por *D. desulfuricans* que demostraron una actividad catalítica superior a la de los catalizadores químicos comerciales para la reacción de liberación de H_2 a partir de fosfinatos (Young *et al.,* 2002). También se han empleado las NPs de Pd formadas por bacterias para la descontaminación de compuestos aromáticos, con una actividad catalítica superior a la de los catalizadores comerciales empleados (Baxter plant *et al.*, 2003).

Sin embargo, en este campo, existen una serie de obstáculos debido al recelo por parte de las industrias tradicionales de síntesis de catalizadores comerciales de apostar por unas técnicas nuevas de recuperación de metales y síntesis de catalizadores que solo presentan mejoras poco significativas. Con el objetivo de llamar la atención por parte de los diferentes sectores industriales para una apuesta por esta metodología menos perjudicial para el medio ambiente, y menos costosa, es necesario destacar aquellos casos en los que el catalizador formado por bacterias presente una actividad muy superior a los métodos tradicionales usados. Un ejemplo es el descrito por Foulkes *et al*., (2011) donde las NPs de Pd presentaban una excelente actividad catalítica para la conversión del compuesto racémico 1-metil-tetrahidroisoquinolina (MTQ) en su forma R-MTQ con gran interés en industria médica y farmacéutica. Por otra parte, el hecho de que las bacterias puedan ser modificadas genéticamente permite la opción de llevar a cabo una "síntesis a la carta" de los catalizadores para la obtención de NPs con un tamaño deseado. En el caso de los mutantes de *D. fructosovorans* se demostró que con el uso de mutantes que tenían eliminados genes que expresaban enzimas que intervenían en los procesos de síntesis de NPs se obtenía un tamaño diferente de NPs y en regiones diferentes de la bacteria (Mikheenko *et al.,* 2008).

Otro ejemplo de las diferentes aplicaciones de las NPs de Pd sintetizadas por bacterias para eliminación de compuestos tóxicos es el caso de la reducción del Cr(VI) a Cr(III) mediante el uso de *D. desulfuricans* y *D. vulgaris* (Humphries *et al.,* 2004; Mabbett *et al.,* 2004)

Con la aparición de las NPs bimetálicas sintetizadas por bacterias se ha abierto un abanico de nuevas aplicaciones en la industria catalítica. Recientemente se han empleado las NPs bimetálicas de Pd/Pt para la extracción de petróleo, lo que produce una reducción de la viscosidad del petróleo facilitando así su extracción (Omajali et al., 2017). En el caso de las NPs bimetálicas de Pd/Au, estas han mostrado una notable actividad catalítica para la

oxidación de alcohol bencílico en condiciones de bajas temperaturas (Deplanche *et al.*, 2012). En el caso de NPs bimetálicas de Pd/Ru, hasta la fecha se han realizado pocos estudios, pero recientemente se ha destacado su importancia en determinadas reacciones de hidrogenación en las que se pueden obtener biocombustibles a partir de desechos de otros procesos industriales como, por ejemplo, obtención del compuesto 2,5-dimetilfurano a partir del compuesto 5-hidroximetilfurfural mediante el uso de NPs bimetálicas de Pd/Ru sintetizadas por la cepa bacteriana *B. benzoevorans* (Omajali *et al.*, 2019).

Referencias

Abdelbasir, S. M., Hassan, S. S. M., Kamel, A. H., & El-Nasr, R. S. (2018). Status of electronic waste recycling techniques: a review. *Environmental Science and Pollution Research, 25(17)*, 16533–16547. https://doi.org/10.1007/s11356-018-2136-6

Agostino, V., & Rosenbaum, M. A. (2018). Sulfate-reducing electroautotrophs and their applications in bioelectrochemical systems. *Frontiers in Energy Research, 6(JUN)*, 1–10. https://doi.org/10.3389/fenrg.2018.00055

Aguado-Santacruz, G. A., Moreno-Gómez, B., Jiménez-Francisco, B., García-Moya, E., & Preciado-Ortiz, R. E. (2012). Impacto de los sideróforos microbianos y fitosideróforos en la asimilación de hierro por las plantas: Una síntesis. *Revista Fitotecnia Mexicana, 35(1)*, 9–21.

Barnes LJ, Janssen FJ, Sherren J, Versteegh JH, Koch RO & Scheeren PJH (1991) A new process for the microbial removal of sulphate and heavy metal from contaminated waters extracted by a geohydrological control system. *Chem. Eng. Res. Des. 69* 184–186

Baxter-Plant, V. S., Mikheenko, I. P., & Macaskie, L. E. (2003). Sulphate-reducing bacteria, palladium and the reductive dehalogenation of chlorinated aromatic compounds.*Biodegradation*, *14*(2), 83–90. https://doi.org/10.1023/A:1024084611555

Beazley, M. J., Martinez, R. J., Webb, S. M., Sobecky, P. A., & Taillefert, M. (2011). The effect of pH and natural microbial phosphatase activity on the speciation of uranium in subsurface soils. *Geochimica et Cosmochimica Acta, 75(19)*, 5648–5663. https://doi.org/10.1016/j.gca.2011.07.006

Cramer, L. a. (2008). What is your PGM concentrate worth? Third International Platinum Conference ‘Platinum in Transformation,’ 387–394.

Cowley, A. (2019). *JM PGM Market Report*.

Chen, C., & Wang, J. (2007). Influence of metal ionic characteristics on their biosorption capacity by Saccharomyces cerevisiae. *Applied Microbiology and Biotechnology*, *74*(4), 911–917. https://doi.org/10.1007/s00253-006-0739-1

Cui, J., & Zhang, L. (2008). Metallurgical recovery of metals from electronic waste: A review. *Journal of Hazardous Materials, 158(2–3)*, 228–256. https://doi.org/10.1016/j.jhazmat.2008.02.001

Courtney, J., Deplanche, K., Rees, N. V., & Macaskie, L. E. (2016). Biomanufacture of nano-Pd(0) by *Escherichia coli* and electrochemical activity of bio-Pd(0) made at the expense of H_2 and formate as electron donors. *Biotechnology Letters*, *38(11)*, 1903–1910. https://doi.org/10.1007/s10529-016-2183-3

Colica, G., Caparrotta, S., & De Philippis, R. (2012). Selective biosorption and recovery of Ruthenium from industrial effluents with *Rhodopseudomonas palustris* strains. *Applied Microbiology and Biotechnology*, *95(2)*, 381–387. https://doi.org/10.1007/s00253-012-4053-9

Das, N. (2010). Recovery of precious metals through biosorption - A review. *Hydrometallurgy*, *103*(1–4), 180–189. https://doi.org/10.1016/j.hydromet.2010.03.016

Das, D., Chakraborty, S., Bhattacharjee, C., & Chowdhury, R. (2016). Biosorption of lead ions (Pb2+) from simulated wastewater using residual biomass of microalgae. *Desalination and Water Treatment*, *57*(10), 4576–4586. https://doi.org/10.1080/19443994.2014.994105

Deng, J., Zhou, Y., Li, S., Xiong, L., Wang, J., Yuan, S., & Chen, Y. (2018). Designed synthesis and characterization of nanostructured ceria-zirconia based material with enhanced thermal stability and its application in three-way catalysis. *Journal of Industrial and Engineering Chemistry*, *64*, 219–229. https://doi.org/10.1016/j.jiec.2018.03.018

De Vargas, I., Macaskie, L. E., & Guibal, E. (2004). Biosorption of palladium and platinum by sulfate-reducing bacteria. *Journal of Chemical Technology and Biotechnology*, *79*(1), 49–56. https://doi.org/10.1002/jctb.928

Dong, H., Zhao, J., Chen, J., Wu, Y., & Li, B. (2015). Recovery of platinum group metals from spent catalysts: A review. *International Journal of Mineral Processing*, *145*, 108–113. https://doi.org/10.1016/j.minpro.2015.06.009

De Windt, W., Aelterman, P., & Verstraete, W. (2005). Bioreductive deposition of palladium (0) nanoparticles on *Shewanella oneidensis* with catalytic activity towards reductive dechlorination of polychlorinated biphenyls. *Environmental Microbiology*, *7*(3), 314–325. https://doi.org/10.1111/j.1462-2920.2004.00696.x

Deplanche, K., Caldelari, I., Mikheenko, I. P., Sargent, F., & Macaskie, L. E. (2010). Involvement of hydrogenases in the formation of highly catalytic Pd(0) nanoparticles by bioreduction of Pd(II) using Escherichia coli mutant strains. *Microbiology*, *156*(9), 2630–2640. https://doi.org/10.1099/mic.0.036681-0

Deplanche, K., Merroun, M. L., Casadesus, M., Tran, D. T., Mikheenko, I. P., Bennett, J. A., … Macaskie, L. E. (2012). Microbial synthesis of core/shell gold/palladium nanoparticles for applications in green chemistry. *Journal of the Royal Society Interface*, *9*(72), 1705–1712. https://doi.org/10.1098/rsif.2012.0003

Fu, J. Z., Liu, Y. Y., Gu, P. Y., Shang, D. L., Lin, Z. Y., Yao, B. X., & Weng, S. Z. (2000). Spectroscopic charcterization on the biosorption and bioreduction of Ag (I) by *lactobacillus sp*. A09. *Acta Physico-Chimica Sinica*, *16*(09), 779-782. https://doi.org/10.3866/PKU.WHXB20000904

Foulkes, J. M., Deplanche, K., Sargent, F., Macaskie, L. E., & Lloyd, J. R. (2016). A novel aerobic mechanism for reductive palladium biomineralization and recovery by *Escherichia coli*. *Geomicrobiology Journal*, *33*(3–4), 230–236. https://doi.org/10.1080/01490451.2015.1069911

Foulkes, J. M., Malone, K. J., Coker, V. S., Turner, N. J., & Lloyd, J. R. (2011). Engineering a biometallic whole cell catalyst for enantioselective deracemization reactions. *ACS Catalysis*, *1*(11), 1589–1594. https://doi.org/10.1021/cs200400t

Gordon, R. B., Bertram, M., & Graedel, T. E. (2006). From the Cover: Metal stocks and sustainability. *PNAS, 103*, 1209–1214. https://doi.org/10.1073/pnas.0509498103

Gallezot, P., Perrard, A., & Isnard, P. (1997). Catalytic Wet Air Oxidation of Acetic Acid on Carbon-Supported Ruthenium Catalysts. *109(1)*, 104–109.

Haferburg, G., & Kothe, E. (2007). Microbes and metals: Interactions in the environment. *Journal of Basic Microbiology*, *47*(6), 453–467. https://doi.org/10.1002/jobm.200700275

Hider, R. C., & Kong, X. (2010). Chemistry and biology of siderophores. *Natural Product Reports*, *27*(5), 637–657. https://doi.org/10.1039/b906679a

Humphries, A. C., Nott, K. P., Hall, L. D., & Macaskie, L. E. (2004). Continuous removal of Cr(VI) from aqueous solution catalysed by palladised biomass of *Desulfovibrio vulgaris*. *Biotechnology Letters*, *26*(19), 1529–1532. https://doi.org/10.1023/B:BILE.0000044457.80314.4d

Johnson Matthey. (2018). *PGM MARKET REPORT FEBRUARY 2018 Summary of Platinum SUPPLY & DEMAND IN 2017*. Retrieved from http://www.platinum.matthey.com/documents/new-item/pgm market reports/pgm_market_report_february_2018.pdf

Johnson, D. B. (2014). ScienceDirect Biomining — biotechnologies for extracting and recovering metals from ores and waste materials. *Current Opinion in Biotechnology*, *30*, 24–31. https://doi.org/10.1016/j.copbio.2014.04.008

Kora, A. J. (2018). Bacillus cereus, selenite-reducing bacterium from contaminated lake of an industrial area: a renewable nanofactory for the synthesis of selenium nanoparticles. *Bioresources and Bioprocessing*, *5*(1). https://doi.org/10.1186/s40643-018-0217-5

Konishi, Y., Tsukiyama, T., Ohno, K., Saitoh, N., Nomura, T., & Nagamine, S. (2006). Intracellular recovery of gold by microbial reduction of AuCl 4- ions using the anaerobic bacterium *Shewanella algae*. *Hydrometallurgy, 81*(1), 24–29. https://doi.org/10.1016/j.hydromet.2005.09.006

Krawczyk-Bärsch, E., Gerber, U., Müller, K., Moll, H., Rossberg, A., Steudtner, R., & Merroun, M. L. (2018). Multidisciplinary characterization of U(VI) sequestration by *Acidovorax facilis* for bioremediation purposes. *Journal of Hazardous Materials*, *347*, 233–241. https://doi.org/10.1016/j.jhazmat.2017.12.030

Kumar, M., Lee, J., Kim, M., Jeong, J., Kim, B., & Kumar, V. (2013). Hydrometallurgy Hydrometallurgical recovery / recycling of platinum by the leaching of spent catalysts : A review. *Hydrometallurgy*, *133*, 23–32. https://doi.org/10.1016/j.hydromet.2012.11.012

Kwak, I. S., Won, S. W., Chung, Y. S., & Yun, Y. S. (2013). Ruthenium recovery from acetic acid waste water through sorption with bacterial biosorbent fibers. *Bioresource Technology*, *128*, 30–35. https://doi.org/10.1016/j.biortech.2012.10.146

Lopez-Fernandez, M., Romero-González, M., Günther, A., Solari, P. L., & Merroun, M. L. (2018). Effect of U(VI) aqueous speciation on the binding of uranium by the cell surface of *Rhodotorula mucilaginosa*, a natural yeast isolate from bentonites. *Chemosphere*, *199*, 351–360. https://doi.org/10.1016/j.chemosphere.2018.02.055

Lovley, D. R., Phillips, E. J. P., Gorby, Y. A., & Landa, E. R. (1991). Microbial reduction of uranium. *Nature*, *350*(6317), 413–416. https://doi.org/10.1038/350413a0

Lloyd, J. R., Yong, P., & Macaskie, L. E. (1998). Enzymatic recovery of elemental palladium by using sulfate-reducing bacteria. *Applied and Environmental Microbiology*, *64*(11), 4607–4609.

Mabbett, A. N., Yong, P., Farr, J. P. G., & Macaskie, L. E. (2004). Reduction of Cr(VI) by “palladized” biomass of *Desulfovibrio desulfuricans* ATCC 29577.

Biotechnology and Bioengineering, *87*(1), 104–109. https://doi.org/10.1002/bit.20105

Mabbett, A. N., Sanyahumbi, D., Yong, P., & Macaskie, L. E. (2006). Biorecovered precious metals from industrial wastes: Single-step conversion of a mixed metal liquid waste to a bioinorganic catalyst with environmental application. *Environmental Science and Technology*, *40*(3), 1015–1021. https://doi.org/10.1021/es0509836

Macaskie, L. E. (1991). The application of biotechnology to the treatment of wastes produced from the nuclear fuel cycle: Biodegradation and bioaccumulation as a means of treating radionuclide-containing streams. *Critical Reviews in Biotechnology*, *11*(1), 41–112. https://doi.org/10.3109/07388559109069183

Marshall, M. J., Plymale, A. E., Kennedy, D. W., Shi, L., Wang, Z., Reed, S. B., … Fredrickson, J. K. (2008). Hydrogenase- and outer membrane c-type cytochrome-facilitated reduction of technetium(VII) by *Shewanella oneidensis* MR-1. *Environmental Microbiology*, *10*(1), 125–136. https://doi.org/10.1111/j.1462-2920.2007.01438.x

Merroun, M. L., Raff, J., Rossberg, A., Hennig, C., Reich, T., & Selenska-Pobell, S. (2005). Complexation of uranium by cells and S-layer sheets of Bacillus sphaericus JG-A12. *Applied and Environmental Microbiology*, *71*(9), 5532–5543. https://doi.org/10.1128/AEM.71.9.5532-5543.2005

Merroun, M. L., & Selenska-Pobell, S. (2008). Bacterial interactions with uranium: An environmental perspective. Journal of Contaminant Hydrology, 102(3–4), 285–295. https://doi.org/10.1016/j.jconhyd.2008.09.019

Merroun, M. L., Nedelkova, M., Ojeda, J. J., Reitz, T., Fernández, M. L., Arias, J. M., … Selenska-Pobell, S. (2011). Bio-precipitation of uranium by two bacterial isolates recovered from extreme environments as estimated by potentiometric titration, TEM and X-ray absorption spectroscopic analyses. Journal of Hazardous Materials, 197, 1–10. https://doi.org/10.1016/j.jhazmat.2011.09.049

Mishra, A., & Malik, A. (2013). Recent advances in microbial metal bioaccumulation. Critical Reviews in Environmental Science and Technology, 43(11), 1162–1222. https://doi.org/10.1080/10934529.2011.627044

Mikheenko, I. P., Rousset, M., Dementin, S., & Macaskie, L. E. (2008). Bioaccumulation of palladium by Desulfovibrio fructosivorans wild-type and hydrogenase-deficient strains. *Applied and Environmental Microbiology, 74*(19), 6144–6146. https://doi.org/10.1128/AEM.02538-07

Murray, J.A., Roussel, J., Rolley, J., Woodhall, F., Mikheenko, I.P., Johnson, D.B., Gomez-Bolivar J., Merroun. M.L. & Macaskie L.E. (2017). Biosynthesis of zinc sulfide quantum dots using waste off-gas from a metal bioremediation process. *RSC Advances, 7*, 21484. https://doi.org/10.1039/c6ra17236a

NRCan. "Distribution of platinum group metals supply worldwide in 2017, by source*." Chart. August 9, 2019. Statista. Accessed October 02, 2019. https://static2.statista.com/statistics/602766/distribution-of-the-supply-of-platinum-group-metals-worldwide-by-source/

Newsome, L., Morris, K., & Lloyd, J. R. (2015). Uranium biominerals precipitated by an environmental isolate of Serratia under anaerobic conditions. *PLoS ONE, 10*(7), 1–14. https://doi.org/10.1371/journal.pone.0132392

Omajali, J. B., Mikheenko, I. P., Merroun, M. L., Wood, J., & Macaskie, L. E. (2015). Characterization of intracellular palladium nanoparticles synthesized by Desulfovibrio desulfuricans and Bacillus benzeovorans. *Journal of Nanoparticle Research, 17*(6), 264. https://doi.org/10.1007/s11051-015-3067-5

Omajali, J. B., Hart, A., Walker, M., Wood, J., & Macaskie, L. E. (2017). In-situ catalytic upgrading of heavy oil using dispersed bionanoparticles supported on gram-positive and gram-negative bacteria. *Applied Catalysis B: Environmental, 203*, 807–819. https://doi.org/10.1016/j.apcatb.2016.10.074

Omajali, J. B., Gomez-Bolivar, J., Mikheenko, I. P., Sharma, S., Kayode, B., Al-Duri, B., … Macaskie, L. E. (2019). Novel catalytically active Pd/Ru bimetallic nanoparticles

synthesized by Bacillus benzeovorans. *Scientific Reports, 9(1)*. https://doi.org/10.1038/s41598-019-40312-3

Platinum 2008, 2008 [WWW Document], Johnson Matthey, URL http://www.platinum.matthey.com/documents/market-review/2008/full-review/english.pdf

Povedano-Priego, C., Martín-Sánchez, I., Jroundi, F., Sánchez-Castro, I., & Merroun, M. L. (2017). Fungal biomineralization of lead phosphates on the surface of lead metal. *Minerals Engineering*, *106*, 46–54. https://doi.org/10.1016/j.mineng.2016.11.007

Povedano-Priego, C., Jroundi, F., Lopez-Fernandez, M., Sánchez-Castro, I., Martin-Sánchez, I., Huertas, F. J., & Merroun, M. L. (2019). Shifts in bentonite bacterial community and mineralogy in response to uranium and glycerol-2-phosphate exposure. *Science of The Total Environment*, *692*, 219–232. https://doi.org/10.1016/j.scitotenv.2019.07.228

Rajak, D. (2008). "Uplift and empower": The market, morality and corporate responsibility on South Africa's platinum belt. *Research in Economic Anthropology*, Vol. 28, pp. 297–324. https://doi.org/10.1016/S0190-1281(08)28013-3

Ruiz Fresneda, M. A., Delgado Martín, J., Gómez Bolívar, J., Fernández Cantos, M. V., Bosch-Estévez, G., Martínez Moreno, M. F., & Merroun, M. L. (2018). Green synthesis and biotransformation of amorphous Se nanospheres to trigonal 1D Se nanostructures: Impact on Se mobility within the concept of radioactive waste disposal. *Environmental Science: Nano, 5(9)*, 2103–2116. https://doi.org/10.1039/c8en00221e

Safarzadeh MS, Horton M, Van Rythoven AD. (2018). Review of recovery of platinum group metals from copper leach residues and other resources. *Mineral Processing and Extractive Metallurgy Review*, *39*(1), 1-17

Saguru, C., Ndlovu, S., & Moropeng, D. (2018). A review of recent studies into hydrometallurgical methods for recovering PGMs from used catalytic converters.

Hydrometallurgy, *182*(October), 44–56. https://doi.org/10.1016/j.hydromet.2018.10.012

Sánchez-Castro, I., Amador-García, A., Moreno-Romero, C., López-Fernández, M., Phrommavanh, V., Nos, J., … Merroun, M. L. (2017). Screening of bacterial strains isolated from uranium mill tailings porewaters for bioremediation purposes. *Journal of Environmental Radioactivity*, *166*, 130–141. https://doi.org/10.1016/j.jenvrad.2016.03.016

Stephen, A. J., Rees, N. V., Mikheenko, I., & Macaskie, L. E. (2019). Platinum and Palladium Bio-Synthesized Nanoparticles as Sustainable Fuel Cell Catalysts. *Frontiers in Energy Research*, *7*(July), 1–13. https://doi.org/10.3389/fenrg.2019.00066

Thomson Reuters, GFMS. (2019). Total global palladium supply from 2005 to 2018 (in 1,000 ounces). Statista. Statista Inc. Accessed: September 03, 2019. https://www.statista.com/statistics/418218/global-palladium-supply/

Tabak, H. H., Lens, P., Van Hullebusch, E. D., & Dejonghe, W. (2005). Developments in bioremediation of soils and sediments polluted with metals and radionuclides - 1. Microbial processes and mechanisms affecting bioremediation of metal contamination and influencing metal toxicity and transport. *Reviews in Environmental Science and Biotechnology*, *4*(3), 115–156. https://doi.org/10.1007/s11157-005-2169-4

US Geological Survey. (2019) *Major countries in global mine production of platinum from 2014 to 2018 (in metric tons). Statista* Inc. Accessed: September 02, 2019. https://www.statista.com/statistics/273645/global-mine-production-of-platinum/

Wei, X., Liu, C., Cao, H., Ning, P., Jin, W., Yang, Z., … Sun, Z. (2019). Understanding the features of PGMs in spent ternary automobile catalysts for development of cleaner recovery technology. Journal of Cleaner Production, 239, 118031. https://doi.org/10.1016/j.jclepro.2019.118031

Wiseman, C. L. S. (n.d.). *Platinum Metals in the Environment*. 2015.

Xiao, Z., & Laplante, A. R. (2004). Characterizing and recovering the platinum group minerals - A review. *Minerals Engineering*, *17*(9–10), 961–979. https://doi.org/10.1016/j.mineng.2004.04.001

Yong, P., Rowson, N. A., Farr, J. P. G., Harris, I. R., & Macaskie, L. E. (2002). Bioreduction and biocrystallization of palladium by Desulfovibrio desulfuricans NCIMB 8307. *Biotechnology and Bioengineering*, *80*(4), 369–379. https://doi.org/10.1002/bit.10369

Yong, P., Rowson, N. A., Farr, J. P. G., Harris, I. R., & Macaskie, L. E. (2002). Bioaccumulation of palladium by Desulfovibrio desulfuricans. *Journal of Chemical Technology and Biotechnology*, *77*(5), 593–601. https://doi.org/10.1002/jctb.606

Zaleska-Medynska, A., Marchelek, M., Diak, M., & Grabowska, E. (2016). Noble metal-based bimetallic nanoparticles: The effect of the structure on the optical, catalytic and photocatalytic properties. *Advances in Colloid and Interface Science*, *229*, 80–107. https://doi.org/10.1016/j.cis.2015.12.008

Zeraatkar, A. K., Ahmadzadeh, H., Talebi, A. F., Moheimani, N. R., & McHenry, M. P. (2016). Potential use of algae for heavy metal bioremediation, a critical review. *Journal of Environmental Management*, *181*, 817–831. https://doi.org/10.1016/j.jenvman.2016.06.059

Zhang, S., Yan, L., Xing, W., Chen, P., Zhang, Y., & Wang, W. (2018). Acidithiobacillus ferrooxidans and its potential application. *Extremophiles*, *22*(4), 563–579. https://doi.org/10.1007/s00792-018-1024-9

Zhao, D. & Xu, B.-Q. (2006). Enhancement of Pt utilization in electrocatalysts by using gold nanoparticles. *Angewite. Chemistry. 118*, 5077–5081. https://doi.org/10.1002/ange.200600155

OBJECTIVES

The objectives of this doctoral Thesis are as follows:

1. To demonstrate the microbial manufacture of bimetallic Pd/Ru NPs by *E. coli* as a model microorganism and their potential as a catalyst

2. Demonstrate the ability of a Consortium of Acidophilic sulfidogenic (CAS) waste bacteria from an unrelated biotechnology process to synthesize Pd/Ru NPs

3. To compare the catalytic activity of the NPs synthesized by CAS culture, *D. desulfuricans* and *E. coli* for the conversion of 2, 5-DMF from real hydrolyzates of 5-HMF from cellulose and starch

4. To investigate the response to microwave energy of *D. desulfuricans* and *E. coli* in the synthesis of Pd NPs

5. To demonstrate the increased catalytic activity of the Pd NPs in microwaved cells of *D. desulfuricans*

MATERIALS AND METHODS

1. Bacterial strains, growth conditions and media preparation

The bacterial strains used in this study were *Escherichia coli* MC4100 (from laboratory stock) *Desulfovibrio desulfuricans* NCIMB 8307 and a consortium of acidophilic sulfidogenic (CAS) bacteria recovered as the side-stream from an industrial treatment process (waste culture) which had produced H_2S off-gas for the recovery of metal wastes from minewater (Mikheenko *et al*., 2019).

Two different culture media were used for the growth of these strains, Postgate medium C for *D. desulfuricans* and Nutrient Broth (Sigma Aldrich) medium for *E. coli*. CAS bacteria were used as obtained from Bangor University, UK

1.1. Postgate medium C for growth of D. desulfuricans

Chemical	**g/L**
KH_2PO_4	0.5
NH_4Cl	1
#Na_2SO_4	4.5
$CaCl_2 . 6H_2O$	0.06
$MgSO_4 . 7H_2O$	0.06
Sodium lactate	1% v/v
Yeast extract	1
$FeSO_4 . 7H_2O$	0.004
*Trisodium citrate . $2H_2O$	0.3

Electron acceptor for sulfidogenic growth *Citrate was added to avoid precipitation of the iron salt

The pH was adjusted to 7.5 ± 0.2 using 5 M NaOH.

The medium was prepared into 200 ml, 1000 ml and 2000 ml anaerobic bottles sealed with rubber stoppers with needles for access to add gases (and ingredients via syringe) as required. In order to remove the oxygen from the solution the bottles were degassed for

30 minutes by displacement with oxygen free N_2 gas (OFN) and autoclaved for 15 minutes at 121ºC. The cells were grown anaerobically at 30ºC, inoculated from a 24h preculture (10% v/v). Cells were grown to mid-exponential phase in a 2000 ml anaerobic bottle to increase the amount of biomass for the catalyst preparation and harvested (Beckman Coulter Avati J-25 Centrifuge, U.S.A) by centrifugation at 12,000 x g for 15 minutes. In order to remove the residual salts from the growth medium, the biomass was washed 3 times with sodium; 3-morpholino-4-propane-1-sulfonic acid; hydroxide (MOPS-NaOH) buffer. After the washing step, cells were concentrated in a small volume of MOPS-NaOH buffer (concentration of 20-30 mg dry weight per ml; dry wt calculated from OD_{600} by reference to a pre-determined calibration) and stored under OFN at 4ºC until next day (Mikheenko *et al*., 2016).

1.2. Nutrient Broth medium for E. coli

Chemical	**g/L**
Beef extract	1
Yeast extract	2
Peptone	5
Sodium chloride	5

*The medium was supplemented with 0.5% glycerol (v/v) and 0.4% fumarate (w/v) to enhance the hydrogenase expression under anaerobic conditions.

Medium was prepared into 200 ml and 1000 ml anaerobic bottles sealed with rubber bungs as in 1.1; oxygen was removed by bubbling the solution with oxygen-free nitrogen (OFN) gas (30 min) and medium was autoclaved for 15 minutes at 121ºC. Cells were grown anaerobically at 37ºC inoculated from a 24h preculture (10% v/v). Cells were centrifuged and washed as for *D. desulfuricans* cells.

1.3. Consortium of acidophilic sulfidogenic bacteria (CAS)

Two different batches of CAS of an approximate volume of 15 L each were provided by Professor D. B. Johnson's group (Bangor University, UK) The CAS comprises 66% *Desulfosporosinus acididurans*, 7% Firmicute strain CEB3, 10% *Acidocella aromatica* strain PFBC, 10% *Actinobacterium* AR3 and 7% *Acidithiobacillus ferroxidans*. The

information about CAS bacterial composition was provided by (Santos and Johnson, 2017) and was obtained by these authors using terminal restriction enzyme fragment length polymorphism (T-RFLP) analysis. Cells were harvested and washed as for *D. desulfuricans* and left under N_2.

2. Interaction of bacteria with palladium and ruthenium.

2.1. Preparation of palladium solution

For experiments with palladium a Pd(II) solution of 2 mM Na_2PdCl_4 (Sigma-Aldrich) at pH 2 in 0.01 M HNO_3 and degassed with OFN was prepared.

2.2. Preparation of ruthenium solution

To study the interactions of bacteria with ruthenium a 1 mM solution of $RuCl_3$ (Sigma-Aldrich) at pH 2 was prepared in 0.01 M HNO_3 and degassed with OFN.

2.3. Preparation of monometallic and bimetallic bionanoparticles

For the preparation of Pd nanoparticles, a specific amount of a cell suspension in 20 mM MOPS-NaOH buffer was diluted to the required biomass/metal ratio into a OFN-outgassed Pd(II) solution (Na_2PdCl_4 solution, pH 2) at 30ºC for 30 min for the biosorption step. After biosorption of Pd(II), hydrogen was added as electron donor by bubbling H_2 gas through the suspension in the sealed bottles and left for 24h until complete reduction of Pd(II) into Pd(0) (as confirmed by assay of the residual solution). The same procedure was carried out for the preparation of Ru nanoparticles onto bacterial cells, with determination of Ru(III) in the residual solution by assay.

For bimetallic preparations cells were first contacted with Pd(II) solution and bio-Pd nanoparticles were formed according to the previous paragraph. The resulting bio-Pd was washed twice in distilled water and the resulting pellet was added as a concentrated suspension into 1 mM $RuCl_3$ solution adjusted to give the required final nominal metal loading on cells (5wt% Pd/loading of Ru as noted in individual experiments). The mixture of bio-Pd cells plus the Ru(III) was left for 30 min to stand for biosorption of Ru(III) and then bubbled with H_2. The bottle containing the mixture was pressurized with H_2 and

transferred to a shaker (30ºC, 180 rpm). After 3 days the suspension was harvested by centrifugation (12,000 x g, 10 min) and residual Ru in solution was determined by assay.

To prepare the samples for TEM analysis an aliquot was taken and washed with distilled water and fixed in glutaraldehyde ($C_5H_8O_2$). For the catalyst preparation the cells were washed 3 times with distilled water and once with acetone (9,000 x g, 15 min, 4ºC) air-dried and ground manually in a pestle and mortar.

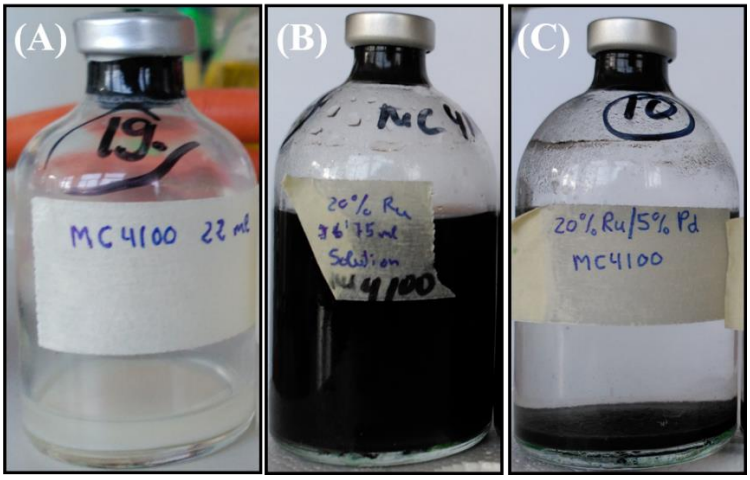

Figure 8. Image of the different steps of preparation of monometallic and bimetallic bio-NPs in sealed bottles. Cell suspension in 20 mM MOPS-NaOH (A). Bio-Pd cells and Ru(III) solution mixture prior to H_2 bubbling (B). Formation of bio-Pd/Ru cells after 3 days pressurised in H_2 (C).

3. Calibration assay for Pd(II) and Ru(III) (tin chloride method)

In order to confirm the complete removal of Pd(II) and Ru(III) ions in the solution after contacting cells, the spectrophotometric tin (II) chloride-based method was used. For the preparation of $SnCl_2$ solution 29.9 g of $SnCl_2$ was dissolved in 500 ml of concentrated HCl. The measurement of the remaining ions in solution was done using a spectrophotometer reading the absorbance at 463 nm for Pd(II) assay and 400 nm for Ru(III) assay. The method is non-specific (i.e. both metals are determined) but since, for making the bimetallic, all Pd(II) was removed in the first step (forming bio-Pd) the analysis of the metal in the second step (Ru-loading) gave the residual concentration of Ru(III).

Method:

1. Add 0.2 ml of sample (supernatant) to 0.8 ml of tin chloride solution in 1.5 ml cuvette.
2. Mix well and incubate for 30 min at 30ºC
3. Read the absorbance at 463 nm for Pd(II) and 400 nm for Ru(III). For blank use 0.2 ml of distilled water and mix with 0.8 ml of tin chloride solution

- **Pd(II) calibration curve**

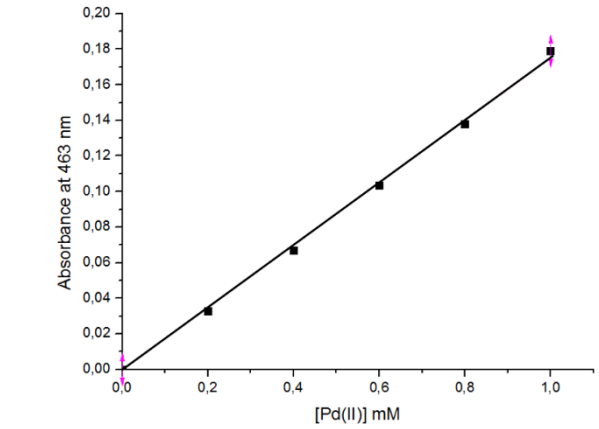

Figure 1. Calibration curve for Pd(II) assay. Errors bars are negligible.

Equation for the linear regression:

$Y = 0.17498\ X$; $R^2 = 0.99938$

Y: Absorbance a 463 nm

X: Concentration of Pd(II) in mM

[Pd(II)] = A463/0.17498.

- **Ru(III) calibration curve**

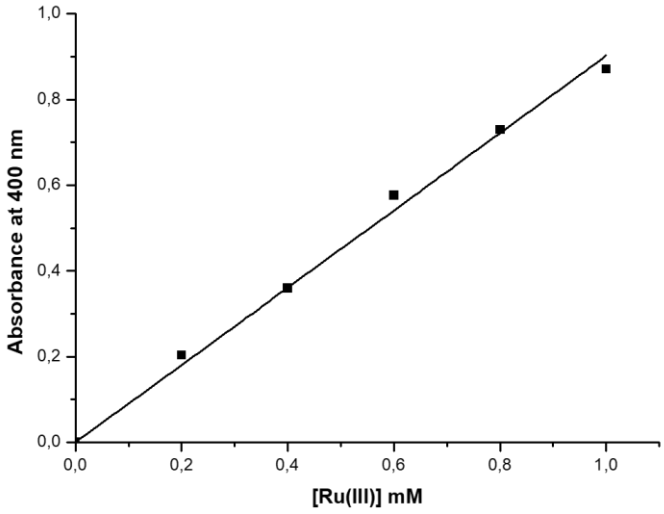

Figure 2. Calibration curve for Ru(III) assay. Errors bars are negligible.

Equation for the linear regression:

$Y = 0.9024\ X$; $R^2 = 0.998$

Y: Absorbance a 400 nm

X: Concentration of Ru(III) in mM

[Ru(II)] = A400/0.9024.

4. Examination of cells and microscopic characterization of bio-NPs and naked cells

4.1. STEM-HAADF analysis

Cells samples were fixed (2.5% (w/v) glutaraldehyde fixative in 0.1 M cacodylate buffer, pH 7.2; 2 h at 4 ºC), washed three times with the same buffer and stained (1% aq. osmium tetraoxide). The samples were thin sectioned (0.25 µm) using a diamond knife on a Reichert Ultracut S ultramicrotome, and the sections were supported on copper grids and coated with carbon. Characterisation of the monometallic and bimetallic NPs of Pd and Ru used a Scanning-Transmission Electron Microscope (STEM; FEI TITAN G2 80-300)

equipped with energy dispersive X-ray analysis (EDX; FEI). The conditions used for the EDX analysis were accelerating voltage of 300 kV using a spot size of 4 Å and a live counting time of 50 s. The structural characterization of the NPs was investigated using high-resolution transmission electron microscopy (HR-TEM) combined with Fast Fourier Transform (FFT) and selected-area electron diffraction (SAED). To study the location of the NPs alongside the cell, the samples were examined under High-Angle Annular Dark Field Scanning Transmission Electron Microscope (HAADF-STEM) FEI TITAN G2 80-300. The microscope was available from Centro de Instrumentación Científica at Granada University (Granada, Spain). These techniques have been widely used in the characterization of metallic nanoparticles produced by biological systems for Pd NPs (Omajali *et al*., 2015), Au NPs (Deplanche *et al*., 2012) etc.

Figure 9. High-Angle Annular Dark Field Scanning Transmission Electron Microscope FEI TITAN G2 80-300 available at Centro de Instrumentación Científica (Universidad de Granada) (https://cic.ugr.es/servicios-y-unidades/ficha.php?codServicio=6&unidad=28).

4.2. FEI-ESEM analysis

To study the morphology of the CAS culture, Environmental Scanning Electron Microscopy (FEI-ESEM) Quanta 400 was used. The microscope can operate in three different modes (high vacuum, low vacuum and ESEM), with an accelerated voltage 200

V – 30 kV. For this purpose, microscope was operating at an accelerating voltage of 5 kV Samples were washed three times in MOPS buffer. The biomass was fixed with 1% osmium tetroxide solution (OsO_4) in cacodylate buffer before dehydration in graded ethanol solutions in water. The critical point drying method was used to dehydrate the samples. Finally, samples were mounted on aluminum stubs using carbon adhesive tape and coated with carbon (EMITECH K975X coater).

5. Spectroscopic characterisation of palladium and ruthenium NPs

5.1. X-ray photoelectron spectroscopy (XPS)

XPS is a surface chemistry technique that under a vacuum environment, can analyse the energy of the photoelectrons when the surface is bombarded with X-rays. Each atom emits a specific energy when it is bombarded with X-rays providing detailed information about the elemental composition, chemical state and electronic state of the elements and molecules within the sample (Mattox, 2010). This technique, accessing the outermost ~10 of the sample (i.e. bacterial cell surfaces) can be useful in many different fields such as physics, chemistry and biology. It can provide useful information about the chemistry of metals associated with organic molecules such as or functional groups in the membrane of some bacteria (Gomez-Bolivar *et al*., 2019)

In the present work, this technique was employed to study the chemical composition and the oxidation state of metals in the Pd/Ru NPs. A few mg of samples were retained and air-dried. Data about the sample were collected using a Kratos Axis Ultra DLD spectrometer (Kratos Analytical), with the core levels recorded using a pass energy of 160 eV, with a pass energy reduced to 20 eV (resolution about 0.4 eV) at the University of Warwick (Coventry, United Kingdom). In order to prevent surface charging, a charge neutralizer was used during XPS data acquisition with low energy electron beam directed to the sample. Measurements were done at room temperature and at a take-off angle of 90º to get a maximum depth of 5-10 nm for the analysis of the surface-bond NPs of the cells (Omajali *et al*., 2017). The data were converted into VAMAS format and analysed using the CasaXPS package (Farley *et al*., 2013).

5.2. X-ray absorption spectroscopy (XAS)

In order to obtain complementary information about the chemical structure(s) within the (bulk) samples and the oxidation state in the deepest regions of the cells, (which by using XPS was not possible) this synchrotron radiation-based technique was used. The XAS spectrum is divided into two different sections, the extended x-ray absorption fine structure (EXAFS) and the x-ray absorption near-edge structure (XANES) region (Figure 10). The EXAFS region provides structural information about the local, short-range coordination environment and chemical structure of specific sites within materials. Meanwhile the XANES region provides information about the oxidation state of the atoms.

Samples containing Pd and Ru were analysed at the Dutch-Belgian Beamline (DUBBLE) at the European Synchrotron Radiation Facility (ESRF), Grenoble (France) with a Si(111) monochromator operating in fixed-exit mode. Data were acquired using Ar/He filled ionization chambers. XAS is commonly used for characterization of chemical structure of different materials and different state such as semiconductors, solid, liquid, crystalline structure, amorphous structure and nanoscale or bulk materials. For this technique, the sample is bombarded with x-rays of specific energy, some of this energy is absorbed by the atoms in the sample inducing the excitation of a core electron (Schnohr and Ridgway, 2015). The specific X-ray energy used for the samples were calibrated by measuring the Pd and Ru k-edge transmission spectra of Pd and Ru foils and were calibrated to 24350 and 22117 eV, respectively.

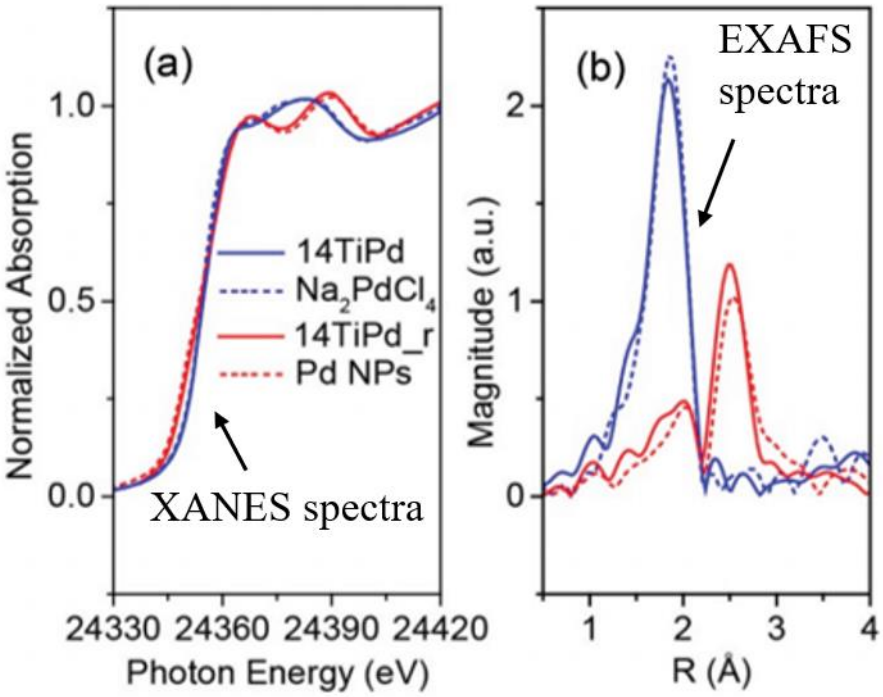

Figure 10. Example of Pd-K XANES spectra (a), and EXAFS Fourier Transform of Pd catalyst and reference samples (b) (adapted from Piernavieja-Hermida *et al.*, 2016).

Figure 11. European Syncrotron Radiation Facility in Grenoble (France). (http://www.ciencia.gob.es/stfls/MICINN/Investigacion/IMAGENES/ESRF.jpg).

6. Image processing, lattice spacing, particle size and statistical analysis

For determination of the average of the NPs, images from HAADF-STEM from different experiments were imported and processed to the software ImageJ (National Institute of Health, Maryland, United Stated) (Schneider *et al*., 2012) according to Omajali *et al*., (2015) (mean SEM from at least 3 different areas of samples; total NPs analyzed was > 100). The information about lattice spacing from the different samples was obtained and compared with bulk palladium and ruthenium from database using Powder cell 2400 software. Determination of distribution and mean size was done using Origin C software and polydispersity index or coefficient of variation was calculated dividing the standard deviation od means by the means. The co-localization analysis was done using Menders overlap coefficient (MOC) (Manders *et al*., 1993) implemented in ImageJ via JACoP (Bolte *et al*., 2008).

7. Microwave (MW) irradiation conditions

Microwave frequencies range from 300 MGz to 300 GHz and wavelengths between 1 cm and 1 m. Materials can be heated by applying electromagnetic energy, the origin of the heating lies in the ability of the electric field to induce polarization of charges within the heated product (Stuerga *et al*., 2008). Two different sets of equipment were used to study how MW energy applied onto the cells can affect the synthesis of Pd-NPs. The two sets of equipment delivered different power outputs to the samples and hence the exposure time was set to give a comparable [power] x [time] dose (arbitrary units) in each case.

7.1. CEM Discover SP microwave digestion system

The commercial apparatus (CEM Corporation, North Carolina, United States) operated in a single mode energy source at 300 W magnetron. The samples were prepared in 6 ml vials and microwave energy was applied in short burst of 10 seconds with periods of 30 seconds of cooling in ice cold acetone after exposure with concentrations according to (Gomez-Bolivar *et al*., 2019). In order to avoid samples becoming over-heated, during the microwave exposure samples were kept in cooled hexane.

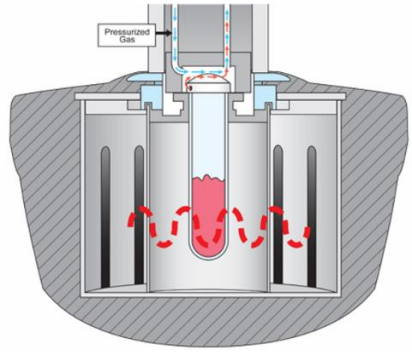

Figure 12. Schematic illustration of CEM Discover SP Microwave digestion system. (https://www.johnmorrisgroup.com/AU/Product/126928/DISCOVER-SP-D---MICROWAVE-DIGESTION-SYSTEM).

7.2. 27 MHz Radio Frequency generator

The system (10P Plasma Product Inc.), comprised a Faraday cage to separate the magnetic field from the electrical heating components. The 27 MHz RF Generator was connected to the Faraday cage by using a matching network to tune the circuit. As the electric component of the electromagnetic radiation produces heating in dielectric materials, the magnetic component was isolated to exclude heating from the sample. Inside the Faraday cage, an applicator circuit of a capacitor plate and a solenoid induction coil was placed. The glass vial sample (working volume 12 ml, 51 mm x 22 mm diameter) was located immersed the coil and stood on a ceramic holder.

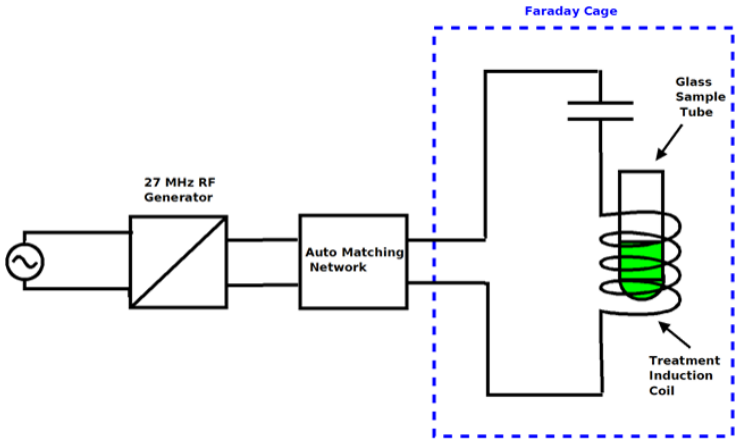

Figure 13. Schematic illustration of 27 MHz Radio Frequency Generator (Bennett et al., manuscript in submission).

8. Thermochemical hydrolysis of cellulose and starch for the upgrading of 5-hydroxymethyl furfural

According to Orozco *et al*., (2012), for starch/cellulose hydrolysis the batch reactor system comprised a bench top reactor (100 ml; Parr series 4590; pressure 200 bar; temperature 350ºC) of Type 316 stainless steel equipped with a heat/agitation controller (Parr 4848). Temperature and pressure were maintained within 1 bar and 0.1 K, respectively and for the hydrolysis, the material (starch (7.2 g, from potato powder; Sigma-Aldrich) or cellulose (5.1 g, Sigma-Aldrich)) was suspended in de-ionized water (final volume of 60 ml for starch; 120 g/l and 70 ml for cellulose; 72.9 g/l) and added into the reactor for the reaction (head space 120 ml). After sealing, the reactor was purged with N_2 three times, pressurized (30 bar), heated to the set-point temperature (220ºC for starch, 260ºC for cellulose; agitation 300 rpm), held for 15 min and cooled by submersion in cold water. The solid residue and the hydrolyzate were separated (after depressurization and vacuum filtration; filter paper Fisherbrand QL100) or by centrifugation (10,000 rpm; 10 min). Hydrolyzates and samples were kept at 4ºC until the analysis. The reactions were repeated several times until having enough pooled starch and cellulose-derived 5-HMF for the upconversion tests.

Figure 14. Image of a reactor Type 316 stainless steel equipped with a heat/agitation controller (Parr 4848). (Adapted from R.L. Orozco PhD Thesis 2011).

9. Solvent extraction of 5-HMF using 2-Methyltetrahydrofuran (2-MTHF)

The methodology of 5-HMF separation from the other products generated from cellulose and starch hydrolysis was based in previous experiments done by Blumenthal *et al*., (2016). When the range of 5-HMF concentration is between 1-5% the mass transfer of 5-HMF from the aqueous phase to the organic phase is faster at 60ºC. Products from starch or cellulose were mixed with the same volume of 2-MTHF (organic extraction solvent) in an Erlenmeyer flask at 200 rpm and 60ºC for 25 min using a magnetic stirrer. Subsequently, aqueous and organic phases were separated using a separation funnel. Both phases were sampled and kept at -20ºC before analysis using gas chromatography (GC).

10. Catalytic reaction tests using monometallic and bimetallic bio-NPs

For the catalyst tests of the bio-NPs two different hydrogenation reactions were tested. The hydrogenation reaction of 2-pentyne used bio-Pd NPs made during or following exposure of the cells to the RF field and the hydrogenation reaction of 5-hydroxymethyl furfural used bio-Ru NPs and bio-Pd/Ru NPs

10.1. Hydrogenation of 2-pentyne

The reaction was done using a 500 ml Baskerville autoclave reactor. Pd catalyst mixed with propanol was added in a proportion of 1:100 (i.e 1.5 mg Pd(0) and 150 ml 2-propanol) added to the reactor, purged with N_2 and stirred (500 rpm, 40ºC) with hydrogen bubbled through (0.1litres/min). After that the reactor was purged with N_2 and 2-pentyne (4ml) was added.

10.2. Hydrogenation of 5-Hydroxymethyl furfural

The hydrogenation reactions of 5-HMF were carried out in a stainless-steel Parr reactor series 4590. Three different sets of reactions were prepared: set 1 using commercially obtained 5-HMF, set 2 using starch-derived 5-HMF and set 3 using cellulose-derived 5-HMF, obtained as described above. For set 1 the reactor was charged with 250 mg of commercial 5-HMF in 25 mL of MTHF (80 mM 5-HMF solution); sets 2 and 3 used appropriate volumes of 5-HMF in MTHF extracted from starch and cellulose hydrolyzates, respectively, to the same final concentration of 5-HMF. In all sets a weight

ratio of 2.5:1 of 5-HMF: catalyst was added to the reactor. The reactor was sealed, purged three times with H_2 (50 bar), pressurized with H_2 (50 bar), and heated (260 ºC; 2 h; 500 rpm).

Figure 15. Image of the stainless-steel Parr reactor series 4590 used for the experiments

11. Analysis of co-products in the catalytic conversion reaction

Samples were analyzed using a GC-FID for quantification and a GCMS-QP2010s for compound identification. All GC-FID analysis was performed on a Shimadzu GC2014 equipped with a Shimadzu AOC-20i autosampler. The carrier gas was hydrogen, supplied by an external hydrogen generator (Parker). The GC was fitted with a Restek Stabilwax-DA column (30 m length, 0.32 mm ID, and 0.25 mm film thickness). The injection volume was 1 mL with a 39 split ratio. The inlet temperature was 250 ºC. The detector was a flame ionization detector (FID) with a flame temperature of 300 ºC, and a sampling rate of 40 ms. The heating profile was 60 ºC for 2 min then heated to 200 ºC at 5ºC/min followed by further heating to 240 ºC at 15 ºC/min where it remained for a further 3 min. Analysis was carried out using Shimadzu GC solutions software. Calibration curves were third order between 80 and 0.4 mM. All GC-MS analysis was performed on a Shimadzu GCMSQP2010s equipped with a Shimadzu AOC-20i autosampler. The carrier gas was

helium. The GC was fitted with a Restek Rxi-1ms column (15 m length, 0.25 mm ID, and 0.25 mm film thickness). The injection volume was 1 mL with a -1 split ratio. The inlet temperature was 250 ºC. The detector was a single quadrupole mass spectrometer in electron ionization mode. The detector and interface temperatures were 250 ºC. The detector acquisition mode was scanning between 40 and 400 m/z, with a scan every 300 ms. The solvent cut time was 1 min. The heating profile was 60 ºC for 2 min then heated to 200 ºC at 5 ºC/min followed by further heating to 240 ºC at 15 ºC/min where it remained for a further 3 min. Analysis was carried out using Shimadzu GCMS Real Time Analysis and Shimadzu GCMS Post Run Analysis software.

References

Blumenthal, L. C., Jens, C. M., Ulbrich, J., Schwering, F., Langrehr, V., Turek, T., … Palkovits, R. (2016). Systematic Identification of Solvents Optimal for the Extraction of 5-Hydroxymethylfurfural from Aqueous Reactive Solutions. *ACS Sustainable Chemistry and Engineering*, *4*(1), 228–235. https://doi.org/10.1021/acssuschemeng.5b01036

Bolte, S., Cordelières, F. P., (2006). A guided tour into subcellular colocalization analysis in light microscopy. *Journal of Microscopy*, *224*(3), 213–232. Retrieved from http://dx.doi.org/10.1111/j.1365-2818.2006.01706.x

Deplanche, K., Merroun, M. L., Casadesus, M., Tran, D. T., Mikheenko, I. P., Bennett, J. A., … Macaskie, L. E. (2012). Microbial synthesis of core/shell gold/palladium nanoparticles for applications in green chemistry. *Journal of the Royal Society Interface*, *9*(72), 1705–1712. https://doi.org/10.1098/rsif.2012.0003

Gomez-Bolivar, J., Mikheenko, I. P., Orozco, R. L., Sharma, S., Banerjee, D., Walker, M., … Macaskie, L. E. (2019). Synthesis of Pd/Ru bimetallic nanoparticles by Escherichia coli and potential as a catalyst for upgrading 5-hydroxymethyl furfural into liquid fuel precursors. *Frontiers in Microbiology*, *10*(JUN), 1–17. https://doi.org/10.3389/fmicb.2019.01276

Gomez-Bolivar, J., Mikheenko, I. P., Macaskie, L. E., & Merroun, M. L. (2019). Characterization of palladium nanoparticles produced by healthy and microwave-injured cells of *Desulfovibrio desulfuricans* and *Escherichia coli*. *Nanomaterials*, *9*(6), 1–16. https://doi.org/10.3390/nano9060857

Mikheenko, I. P., Gomez-Bolivar, J., Merroun, M., Sharma, S., & Macaskie, L. E. (2016). High resolution electron microscopy study of biologically derived ruthenium and palladium/ruthenium nanoparticles. *Proceedings of the 6th International Conference Nanomaterials: Applications and Properties, NAP 2016*. https://doi.org/10.1109/NAP.2016.7757229

Mattox, D.M., 2010. Substrate (“Real”) surfaces and surface modification, in: handbook of Physical Vapor Deposition (PVD) processing. Oxford, Elsevier, pp. 25-72. https://doi.org/10.1016/B978-0-8155-2037-5.00002-2

Manders, E. M. M., Verbeek, F. J., & Aten, J. A. (1993). Measurement of co-localization of objects in dual-colour confocal images. *Journal of Microscopy, 169*(3), 375–382. https://doi.org/10.1111/j.1365-2818.1993.tb03313.x

N. Fairley, CasaXPS. Casa Software Ltd. www.casaxps.com. 2013.

Omajali, J. B., Mikheenko, I. P., Merroun, M. L., Wood, J., & Macaskie, L. E. (2015). Characterization of intracellular palladium nanoparticles synthesized by Desulfovibrio desulfuricans and Bacillus benzeovorans. *Journal of Nanoparticle Research, 17*(6), 264. https://doi.org/10.1007/s11051-015-3067-5

Omajali, J. B., Hart, A., Walker, M., Wood, J., & Macaskie, L. E. (2017). In-situ catalytic upgrading of heavy oil using dispersed bionanoparticles supported on gram-positive and gram-negative bacteria. *Applied Catalysis B: Environmental, 203*, 807–819. https://doi.org/10.1016/j.apcatb.2016.10.074

Orozco-pulido, R. (2012). *Hydrogen Production From Biomass By Integrating Thermo-Chemical and Biological Processes*. PhD Thesis 2012

Piernavieja-Hermida, M., Lu, Z., White, A., Low, K. Bin, Wu, T., Elam, J. W., … Lei, Y. (2016). Towards ALD thin film stabilized single-atom Pd1catalysts. *Nanoscale, 8*(33), 15348–15356. https://doi.org/10.1039/c6nr04403d

Schnohr, C.S., Ridgway, M.C., 2015. Introduction to X-Ray Absorption Spectroscopy, in: Schnohr, C.S., Ridgway, M.C. (Eds.). X-Ray Absorption Spectroscopy of Semiconductors. Heildelberg, Springer, Series in Optical Sciences, 355p. https://doi.org/10.1007/978-3-662-44362-0

Schneider, C. A., Rasband, W. S., & Eliceiri, K. W. (2012). NIH Image to ImageJ: 25 years of image analysis. *Nature Methods, 9*(7), 671–675. https://doi.org/10.1038/nmeth.2089

Stuerga, D. (2008). Microwave-Material Interactions and Dielectric Properties, Key Ingredients for Mastery of Chemical Microwave Processes. In *Microwaves in Organic Synthesis: Second Edition* (Vol. 1). https://doi.org/10.1002/9783527619559.ch1

CHAPTER I

Synthesis of Pd/Ru bimetallic nanoparticles by *Escherichia coli* and potential as a catalyst for upgrading 5-hydroxymethyl furfural into liquid fuel precursors

Jaime Gomez-Bolivar[1*], Iryna P. Mikheenko[2], Rafael L. Orozco[2], Surbhi Sharma[2], Dipanjan Banerjee[3], Marc Walker[4], R. A. Hand[5], Mohamed L. Merroun[1] and L.E. Macaskie[2#]

[1]Department of Microbiology, Faculty of Sciences, University of Granada, Campus Fuentenueva, 18071, Granada, Spain

[2]School of Biosciences, University of Birmingham, Edgbaston, Birmingham B15 2TT, UK

[3]Dutch-Belgian Beamline (DUBBLE), European Synchrotron Radiation Facility (ESRF), 71 avenue des Martyrs, CS 40220, 38043 Grenoble Cedex 9, France and Department of Chemistry, Katholieke Universiteit Leuven, Celestijnenlaan 200F box 2404, 3001 Leuven, Belgium

[4]Department of Physics, University of Warwick, Coventry, CV4 7AL, United Kingdom

[5]Department of Chemistry, University of Warwick, Coventry, CV4 7AL, United Kingdom

Corresponding author: Prof Lynne Macaskie L.E.Macaskie@bham.ac.uk

frontiers in Microbiology

ORIGINAL RESEARCH
published: 20 June 2019
doi: 10.3389/fmicb.2019.01276

Check for updates

Synthesis of Pd/Ru Bimetallic Nanoparticles by *Escherichia coli* and Potential as a Catalyst for Upgrading 5-Hydroxymethyl Furfural Into Liquid Fuel Precursors

Jaime Gomez-Bolivar[1], Iryna P. Mikheenko[2], Rafael L. Orozco[2], Surbhi Sharma[2], Dipanjan Banerjee[3,4], Marc Walker[5], Rachel A. Hand[6], Mohamed L. Merroun[1] and Lynne E. Macaskie[2]*

OPEN ACCESS

Abstract

Escherichia coli cells support the nucleation and growth of ruthenium and ruthenium-palladium nanoparticles (Bio-Ru and Bio-Pd/Ru NPs). We report a method for the synthesis of these monometallic and bimetallic NPs and their application in the catalytic upgrading of 5-hydroxymethyl furfural (5-HMF) to 2,5 dimethylfuran (DMF). Examination using high resolution transmission electron microscopy with energy dispersive X-ray microanalysis (EDX) and high angle annular dark field (HAADF) showed Ru NPs located mainly at the cell surface using Ru(III) alone but small intracellular Ru-NPs (size ~ 1-2 nm) were visible only in cells that had been pre-'seeded' with Pd(0) (5 wt%) and loaded with equimolar Ru. Pd(0) NPs were distributed between the cytoplasm and cell surface. Cells bearing 5%Pd/5%Ru showed some co-localization of Pd and Ru but chance associations were not ruled out. Cells loaded to 5 wt% Pd/20wt% Ru showed evidence of core-shell structures (Ru core, Pd shell). Examination of this cell surface material using X-ray photoelectron spectroscopy (XPS) showed Pd(0) and Pd(II) and Ru(IV) and Ru(III), with confirmation by analysis of bulk material using X-ray absorption near edge structure (XANES) and extended X-ray absorption fine structure (EXAFS) analyses. Both Bio-Ru NPs and Bio-Pd/Ru NPs were active in the conversion of 5-HMF into 2,5-DMF but commercial Ru on carbon catalyst outperformed 5 wt% bio-Ru by 4-fold. While 5wt%Pd/20wt%Ru achieved 20% yield of DMF the performance of the 5wt%Pd/5wt%Ru bio-catalyst was higher and comparable to the commercial 5wt% Ru/C catalyst in a test reaction using commercial 5-HMF (> 50% selectivity). 5-HMF was prepared by thermochemical hydrolysis of starch and cellulose with solvent extraction of 5-HMF into methyltetrahydrofuran (MTHF). Here, with MTHF as the reaction solvent the commercial Ru/C catalyst had little activity (100% conversion, negligible selectivity to DMF) whereas the 5wt%Pd/5wt%Ru bio-bimetallic gave 100% conversion and 14% selectivity to DMF from material extracted from hydrolyzates. The results indicate a potential green method for realizing increased energy potential from biomass wastes as well as showing a bio-based pathway to manufacturing a scarcely-described bimetallic material.

Keywords: ruthenium bionanoparticles, Pd/Ru core-shells, 5-hydroxymethyl furfural conversion, 2,5-dimethyl furan synthesis, cellulose conversion

1. Introduction

Many types of living cells have the ability to template and form metallic nanoparticles (NPs) by reduction of soluble metal species. This has formed the subject of numerous studies and reviews (e.g. de Corte et al., 2012; Castro et al., 2014; Kulkarni and Maddapur, 2014; Singh, 2015; Singh et al., 2016). The goal is to develop alternative, facile, routes to the synthesis of industrially relevant catalysts using biomaterial scaffolds for catalytically active nanoparticles while preventing NP agglomeration and consequent loss of activity. Recent focus has moved towards the biosynthesis of bimetallic nanoparticles since these can have unique properties due to synergy of the metallic components. For example, in Pd/Au the formation of $Pd^{\delta+}/Au^{\delta-}$ was suggested to underlie the superior catalytic activity of the bimetallic (Gao and Goodman 2012). However, synthesis of bimetallic NPs by chemical routes is more difficult than for monometallic counterparts. Various preparation methods of bimetallic nanostructures have been reviewed (e.g. Zaleska-Medynska et al., 2016) and a variety of shapes, properties and catalytic activities has been obtained. However, biosynthetic routes are relatively unexplored, despite the potential for applying the tools of synthetic biology to obtain targeted NP manipulation (Torgeman, 2017).

An early example of bio-Pd/Au NPs was reported by Deplanche (2008) and this bio-catalyst, made on *Escherichia coli* and *Cupriavidus necator*, was applied in two respective catalyses: partial oxidation of benzyl alcohol to benzaldehyde (Deplanche et al., 2011) and reduction of *p*-nitrophenol (Hosseinkhani et al., 2012). The former, together with bio-Pd/Au made by *D. desulfuricans* (Tran et al., 2012) had a core-shell structure (Au core/Pd shell). This structure is formed by initially depositing 'seeds' of Pd(0) nanoparticles with enzymatic assistance involving hydrogenases (Mikheenko et al., 2008; Deplanche et al., 2010). The resulting Pd(0) reduces Au(III) galvanically and oxidized Pd species migrate outwards from the core of neo-Au(0) followed by their chemical reduction under hydrogen to form a shell of Pd(0) (Deplanche et al., 2012). Bio-Pd/Au core shells form inside the bacterial cytoplasm (Supplementary information Figure S1), which implies uptake and processing mechanisms for these heavy metals, that have no known biological function. Although the bacteria remain metabolically competent during Pd(0) 'seeding', as shown by the use of flow cytometry (Omajali et al., 2018), the routes by which the Pd(0) 'seeds'

are localized and then develop from initial Pd-nuclei is still unknown, despite that these are key to the patterning of the subsequent bimetallic.

Following formation of the Pd 'seeds' cell viability is lost rapidly, although hydrogenase activity persists for several hours (Mikheenko, et al., 2008). The use of dead cells (and retention of the NPs upon them (Bennett et al., 2013)) ensures acceptability of the nanomaterial while mitigating against NP release into the environment. The need to supply Pd(II) in acidic solution (10 mM HNO_3), was shown by previous optimization studies; the function of the acid is to protonate the polyanionic cell surface to permit access of the $PdCl_3^-$ ion that predominates in solution. Importantly, deposition of the second metal is an abiotic process, which enables metal recovery from highly acidic solutions following 'seeding' with Pd(0) under physiologically-compatible conditions (Murray et al., 2018).

Using a similar approach, the formation of bimetallic bio-Pd/Pt NPs was recently reported (Murray et al., 2018). These were active in the catalytic reduction of Cr(VI) (Murray et al., 2018) and in the selective hydrogenation of soybean oil (Murray et al., 2018) and 2-pentyne (Murray et al., 2017) as well as in in the catalytic upgrading of heavy oils from Canadian oilsands (Omajali et al., 2017), and oils produced by thermochemical processing of wet biomass (Kunwar et al., 2017). However, the arrangement of the metallic components in the NPs (e.g. alloys or core-shell structures) was not reported.

With a developing global focus on sustainable energy and green chemistry Pd/Ru bimetallics have been highlighted in these areas but study of Pd/Ru is neglected in comparison with Pd/Au. Raja et al. (1999) showed that the hydrogenation of hex-1-ene to *n*-hexane was several orders of magnitude higher via use of Pd_6Ru_6 clusters than with Pd alone. Later, Qui et al. (2006) showed higher conversion and selectivity in hydrogenation of cinnamyl alcohol using Pd/Ru catalyst compared to that obtained by using single metals. Luo et al. (2015) reported catalytic hydrogenation of levulinic acid by a Pd/Ru bimetallic alloy; here, the metals were randomly dispersed and the high catalytic activity was attributed to dilution and isolation of Ru by Pd (Kyriakou et al. (2012). Boucher et al. (2013) and Sykes and Stephanopoulos (2014) had previously attributed highly selective hydrogenations to isolated Pd atoms. On the other hand, oxidation of formic acid (Liu et al., 2012) was reported, and also oxidation of ethanol, the latter using Pd-Ru

bimetallic-NPs on carbon; this catalyst comprised a mix of Pd metal, Ru oxides and Pd oxides (Monyoncho et al., 2015). A Pd-overlayer enhanced the activity of Ru-nanotubes in hydrogen oxidation (John et al., 2015). Clearly, the activity for a certain reaction relates to the metal arrangement in the NPs but production of Pd/Ru core-shell structures is neglected. Modulating fcc and hcp ruthenium on the surface of a Pd-Cu alloy produced a core-shell (Yao et al., 2016) but the catalytic activities of hcp-dominated Ru-Cu NPs and fcc-dominated Ru showed opposing results in hydrogenations of 4-nitrochlorobenzene and styrene according to the predominant type of Ru. This highlights the potential to moderate selectivity according to the bimetallic fine structure but also cautions that the outcome of a reaction may be difficult to achieve if the metal arrangement is not controlled. Biomanufacture of Pd/Ru NPs is not yet reported in the literature. An initial study (Omajli et al., 2015) suggested this route for making bimetallic NPs for the catalytic conversion of 5-hydroxymethyl furfural (5-HMF) to 2,5 dimethyl furan (DMF) but no NP characterization was performed.

5-HMF is a derivative of glucose, fructose (Van Putten et al., 2013) or cellulose under thermochemical degradation (Román-Leshkov et al., 2007). The product, DMF (Lei et al., 2014; Nagpure et al., 2015), is a 'platform' precursor of plastics and also of 'drop in' fuels (Lei et al., 2014; Nagpure et al., 2015). 'Drop-in' biofuels are defined as 'liquid bio-hydrocarbons that are functionally equivalent to petroleum fuels and are fully compatible with existing petroleum infrastructure' (Karatzos et al., 2014). Working towards higher yields and selectivity towards DMF, studies have focused on 'classical' mono and bimetallic catalysts including Pd and Ru (Hansen et al., 2012; Zu et al., 2014; Nishimura et al., 2014; Luo et al., 2015). Study of bacterially derived Pd/Ru NPs is a new development. Omajali et al., (2015) showed the potential of cells of the Gram-positive bacterium *Bacillus benzeovorans* to make bio-Pd/Ru bimetallic structures using the same approaches as described above for bio-Pd/Au and bio-Pd/Pt. Most of the work on bio-NP catalysts has used Gram-negative bacteria. Deplanche et al., (2014) and Zhu et al., (2014) noted that bio-Pd catalysts supported on typical Gram-positive cells were less active catalytically than those on Gram negative bacteria. Hence the primary aim of this work was to evaluate the potential for the use of the paradigm Gram negative *Escherichia coli* to synthesise NPs of bio-Ru and bio-Pd/Ru and evaluate their potential for the catalytic upgrading of 5 HMF to DMF. In order to move towards real-life application, the

upconversion of 5-HMF derived from thermochemical hydrolysis of starch and cellulose was also evaluated.

The use of *E. coli* is attractive as this ubiquitous organism is readily grown at scale and waste *E. coli* cells grown for another primary process (biohydrogen production) were successfully used in 'second life' to make bio-Pd catalyst for hydrogenation (Zhu et al., 2016) and in fuel cells (Orozco et al., 2010), while the ability to fabricate the metallic catalyst from liquid wastes (Yong et al., 2010; 2015; Murray et al., 2017) has positive implications for both economy and sustainability.

2. Materials and methods

2.1.Bacteria, growth conditions, and chemicals used

Escherichia coli strain MC4100, grown as described by Deplanche et al., (2012), was harvested in mid-logarithmic phase (OD_{600} of 0.7-1.0) by centrifugation (9,000 x g, 15 min, 4^{o}C), washed three times (20 mM MOPS-NaOH buffer, pH 7.0) and routinely stored as a concentrated suspension overnight (4^{o}C). The cell dry weight was estimated from a previously determined OD/dry weight conversion.

Commercial metal salts (Na_2PdCl_4 and $RuCl_3$) were from Sigma-Aldrich, as were 5wt% Pd and 5wt% Ru on carbon catalysts and commercial 5-HMF (≥ 99%) and 2,5-DMF (99%).

2.2.Preparation of monometallic and bimetallic bionanoparticles (bio-NPs)

For monometallic bio-Ru cell suspension was diluted into 2 mM Ru (III) $RuCl_3.2H_2O$ solution (pH 2, in 10 mM HNO_3) to the required biomass/metal ratio for the desired loading (5wt%) and left for 30 min (30 ^{o}C) for metal uptake by the cells. H_2 was bubbled through the suspension for 1h and left for 96 h (sealed bottle; 180 rpm agitation; 30^{o}C). Monometallic bio-Pd (5 wt%) was made similarly, according to Deplanche et al. (2012).

Synthesis of bimetallic Pd/Ru used, sequentially, a 2mM Pd (II) and then a 1 mM Ru (III) solution (in 10 mM HNO_3) by the method of Deplanche et al., (2012) with modifications:

2 mM Pd (II) solution was reduced to Pd(0) on the cells under H_2 (30 min; complete removal (by assay) of residual soluble metal) to give 5wt% bio-Pd(0). The bio-Pd(0) was washed twice (distilled water, DW), and added as a concentrated suspension into 1 mM Ru (III) solution (final concentration; volume was adjusted to give the required final metal loading on cells) to give a final loading of (nominally) 5 wt% Pd/5wt% Ru or 5wt% Pd/20 wt% Ru. The bio-Pd/Ru mixture was left to stand then saturated with H_2 (as above; 180 rpm, 30^{o}C; 96h). The presumptive bio-NPs were washed three times (DW) and once with acetone (9,000 x g, 15 min, 4^{o}C), air-dried and ground manually. The actual Ru loadings were determined by difference via assay of residual soluble Ru(III) by the stannous chloride method (Charlot, 1978); Pd was completely removed in the first step and was retained on the cells (as determined by assay of wash solutions).

2.2.High resolution scanning-transmission electron microscopy (STEM) with HAADF (high-angle annular dark field) detector, energy dispersive X-ray analysis (EDX) and determination of lattice spacing.

Where cell sections were to be examined, fresh preparations were fixed (2.5% (w/v) glutaraldehyde fixative in 0.1 M cacodylate buffer, pH 7.2; 2h at 4^{o}C), washed three times with the same buffer and stained (1% aq. osmium tetraoxide). For TEM thin samples were prepared as described previously (Deplanche et al., 2012). Electron opaque deposits were examined by EDX with peaks sought corresponding to X-ray emission energies of Ru and Pd. STEM and EDX were done using a FEI image Cs-corrector configuration Titan^{TM} G2 60-300 STEM microscope equipped with HAADF detector, accelerating voltage of 300 kV. Lattice spacings were determined using "ImageJ" (Abramoff et al., 2004) through profiling of high resolution HAADF-STEM images.

2.3.X-Ray photoelectron spectroscopy (XPS) of cell surfaces

Subsamples (a few mg) were retained and air-dried. Surface chemical composition and oxidation state analyses were done by XPS via published methods (Omajali et al., 2017) using a Kratos Axis Ultra DLD spectrometer (Kratos Analytical). The samples were illuminated using an Al Kα x-ray source and the photoelectrons were collected using a

hemispherical electron analyser. Survey spectra were recorded using a pass energy of 160 eV, with the pass energy reduced to 20 eV for acquisition of the core level spectra (resolution approx. 0.4 eV). The samples were insulating, therefore a charge neutralizer was used to prevent surface charging with a low energy electron beam directed onto the sample during XPS data acquisition. Measurements were made at room temperature and at a take-off angle of 90°, to probe a depth of approx. 5-10 nm to examine bio-NPs bound to the outermost cell surfaces. Generated data were converted into VAMAS format and analysed using the CasaXPS package (Fairley, 2013) employing Shirley backgrounds, mixed Gaussian-Lorentzian (Voigt) lineshapes and asymmetry parameters where appropriate. All binding energies were calibrated to the C 1s peak originating from C-H or C-C groups at 284.8 eV.

2.4.X-ray Absorption Spectroscopy (XAS) analysis.

This synchrotron radiation based technique was used to determine the local coordination of Pd and Ru in the biogenic Pd/Ru NPs samples. Pd and Ru K–edge XAS spectra were acquired at the Dutch-Belgian Beamline (DUBBLE) beamline at the European Synchrotron Radiation Facility (ESRF), Grenoble (France), using a Si(111) monochromator operating in fixed-exit mode. Data were acquired using Ar/He filled ionization chambers (transmission mode). The energies were calibrated by measuring the Pd and Ru K-edge transmission spectra of Pd and Ru foils and were calibrated to 24350 and 22117 eV, respectively. Samples (Ru and Pd/Ru-loaded cells) were examined as dry samples (powder, a few mg). Data were processed using the ATHENA code (Ravel et al., 2005) with subtraction of background via a pre-edge linear function. Atomic absorption was simulated with a square-spline function. The amplitude reduction factor was held constant at 1.0 for the FEFF8 calculation and extended X-ray absorption fine structure (EXAFS) fits, with the shift in threshold energy, $\Delta E0$, varied as a global parameter. The theoretical scattering phase and amplitude functions used in data analysis were calculated using FEFF8 (Ankudinov et al., 1998). For the Pd edge EXAFS spectra, data for phase-shifts and backscattering amplitudes were obtained from reference materials of PdO (Pd–O scattering) and Pd foil (Pd–Pd scatterings). For the Ru edge EXAFS spectra, data for

phase-shifts and backscattering amplitudes were obtained from RuO_2 (Ru–O scattering), Ru foil (Ru–Ru scatterings) and $RuCl_3$ (Ru-Cl scattering) reference compounds.

2.5.Preparation of 5-HMF via thermochemical hydrolysis of starch and cellulose

Methods for thermal hydrolysis were as reported previously (Orozco et al., 2012). For starch/cellulose hydrolysis the batch reactor system comprised a bench top reactor (100 ml; Parr series 4590; pressure 200 bar; temperature 350 °C) of Type 316 stainless steel equipped with a heat/agitation controller **(**Parr 4848**).** Temperature and pressure were measured from inside the reactor and maintained within 1 bar and 0.1 K respectively.

For hydrolysis the material (starch (7.2 g, from potato powder; Sigma-Aldrich) or cellulose (5.1 g, Sigma-Aldrich)) was suspended in de-ionized water (final reactant volume of 60 ml for starch; 120 g/l and 70 ml for cellulose; 72.9 g/l) or as otherwise stated) and charged into the reactor for hydrolysis (head space ~ 120 ml). The reactor was sealed, purged with N_2 three times, pressurized (30 bar), heated to the set-point temperature (220 ^oC for starch, 260 ^oC for cellulose; agitation 300 rpm), held for 15 min and cooled by submersion in cold water. The hydrolyzate was separated (after depressurization) from solid residue (vacuum filtration; filter paper Fisherbrand QL100) or by centrifugation (10,000 rpm; 10 min). Hydrolyzates and samples were kept at 4°C prior to analysis. The reactions were repeated as required to produce sufficient pooled starch and cellulose-derived 5-HMF for the upconversion tests.

Hydrolyzates were analyzed using a GC (Shimadzu 2010 equipped with an autosampler AOC-20S, a FID detector and ZB-Wax column (30m x 0.25mm × 0.25µm); injection volume 1 µl; inlet temperature 260°C; injector temperature 300 ^oC; detector temperature; 300 ^oC, inlet pressure 100 KPa; split ratio of 100:1 with H_2 carrier gas at a flow rate of 1 ml/min). The heating gradient was 0 min GC temp 100°C; 10 min GC temp 200°C; 22 min GC temp 200°C and 25 min GC temp 250°C. Reaction residues were not quantified nor analyzed.

2.6.Solvent extraction of 5-HMF using 2-methyltetrahydrofuran (2-MTHF)

The method for 5-HMF extraction was based from the experimental determination of partition coefficients under batch and continuous conditions according to Blumenthal et al. (2016). The mass transfer of 5-HMF from the aqueous to the organic phase is faster at 60°C and concentrations of 5-HMF in the range between 1-5wt% in the aqueous feed has little effect on the partition coefficients. Therefore, the produced starch and cellulose hydrolyzates respectively were mixed in equal volumetric proportions with 2-MTHF (organic extraction solvent) in an Erlenmeyer flask at 200 rpm and 60°C using a magnetic stirrer and a temperature-controlled water bath (25 min). After extraction aqueous and organic phases were separated using a separation funnel: the top organic phase was 'supernatant' and the bottom aqueous phase was 'filtrate'. Both phases were sampled and kept at -20°C before analysis by GC.

Solvent extraction efficiency was calculated using the following formula:

$$\text{Extraction efficiency } (\%) = \frac{\text{moles of HMF in supernatant}}{\text{moles of HMF in hydrolyzate}} * 100$$

2.7.Catalytic conversion of 5-hydroxymethyl furfural to 2,5-dimethyl furan

Starch and cellulose derived 5-HMF were obtained via hot compressed water treatment (Orozco 2012; Orozco et al., 2012) followed by solvent extraction of 5-HMF using MTHF (as above). The catalytic transfer hydrogenation reactions used a 100 ml Parr series 4590 bench top reactor of Type 316 stainless steel equipped with a heat/agitation controller **(**Parr 4848). Three sets of experiments were carried out: set 1 (commercial 5-HMF); set 2 (starch-derived 5-HMF) and set 3 (cellulose- derived 5-HMF). For set 1 the reactor was charged with 250 mg of 5-HMF in 25 ml of MTHF (80 mM 5-HMF solution); for sets 2 and 3 volumes of 28 and 50 ml of 5-HMF in MTHF were extracted from starch and cellulose hydrolyzates, respectively. In all sets a weight ratio of 2.5:1 of 5-HMF: catalyst was added to the reactor. The reactor was sealed, purged 3 times with H_2 (50 bar), pressurized with H_2 (50 bar) and heated (260 ^oC; 2 h; 500 rpm). After the reaction (time as determined by prior tests), the reactor was quenched to 35-40°C in a water bath and the reaction mixture was filtered (Fisherbrand QL100 filter paper). Samples were stored at -20°C before analysis using a GC-FID for quantification and a GCMS-QP2010s for

compound identification. All GC-FID analysis was performed on a Shimadzu GC2014 GC equipped with a Shimadzu AOC-20i autosampler. The carrier gas was hydrogen, supplied by an external hydrogen generator (Parker). The GC was fitted with a Restek Stabilwax-DA column (30 m length, 0.32 mm ID and 0.25 µm film thickness). The injection volume was 1 µl with a 39 split ratio. The inlet temperature was 250 °C. The detector was a flame ionization detector (FID) with a flame temperature of 300 °C, and a sampling rate of 40 ms. The heating profile was 60 °C for 2 minutes then heated to 200 °C at 5 °C/min min followed by further heating to 240 °C at 15 °C /min where it remained for a further 3 minutes. Analysis was carried out using Shimadzu GC solutions software. Calibration curves were third order between 80 mM and 0.4 mM.

All GC-MS analysis was performed on a Shimadzu GCMS-QP2010s equipped with a Shimadzu AOC-20i autosampler. The carrier gas was helium. The GC was fitted with a Restek Rxi-1ms column (15 m length, 0.25 mm ID and 0.25 µm film thickness). The injection volume was 1 µl with a -1 split ratio. The inlet temperature was 250 °C. The detector was a single quadrupole mass spectrometer in electron ionisation mode. The detector and interface temperatures were 250 °C. The detector acquisition mode was scanning between 40-400 m/z, with a scan every 300 msec. The solvent cut time was 1 minute. The heating profile was 60 °C for 2 minutes then heated to 200 °C at 5 °C/min followed by further heating to 240 °C at 15 °C /min where it remained for a further 3 minutes. Analysis was carried out using Shimadzu GCMS Real Time Analysis and Shimadzu GCMS Post Run Analysis software.

Conversion of 5-HMF and yields of DMF were calculated as follows:

$$\text{5HMF conversion in (\%)} = \left(1 - \frac{\text{moles of 5HMF in products}}{\text{starting moles of 5HMF}}\right) \text{x } 100$$

$$\text{2, 5DMF yield (\%)} = \left(\frac{\text{moles of 2, 5DMF in products}}{\text{starting moles of 5HMF}}\right) \text{x } 100$$

$$\text{2, 5 DMF selectivity (\%)} \left(\frac{\text{moles of 2,5DMF in products)}}{\text{starting moles of 5HMF} - \text{final moles of 5HMF}}\right) x\ 100$$

Other products were not identified or quantified.

3. Results and discussion,

3.1. Uptake of Pd (II) and Ru(III) by the cells and formation of bio-Pd and bio-Ru NPs

Initial studies using Pd(II) showed its rapid, complete removal from solution by *E. coli* (Deplanche et al., 2010) and conversion into Pd(0)-NPs, both at the cell surface and intracellularly, within 30 min. (Supplementary information Fig S2). In contrast, with Ru(III), only ~ 50% of the Ru(III) was removed, even after 96 h (Table 1); hence, the nominally 5wt% Ru was actually 2.6% of the cell dry weight. Thermogravimetric analysis of *D. desulfuricans* biomass (Omajali et al., 2017) showed that typically more than 50% of the material remains at above 600 ^{o}C, comprising residual carbon and mineral components. Hence, for the purpose of this comparison, the 2.6wt% bio-Ru (on air dried cells) and commercial 5wt% Ru/C catalysts are assumed to be broadly comparable in terms of metal/carbon but the dosing of catalyst metal into the catalytic tests (see later) would be ~ half in terms of metallic component of the biomaterial on a comparable weight basis. However, the two catalysts are probably not comparable in terms of available catalyst surface; attempts to establish the surface area of bio-Pd by standard sorption methods were unsuccessful (J.A. Bennett and L.E. Macaskie, unpublished).

Examination of 5wt% bio-Pd (the 'seeds' to promote Ru deposition) showed that Pd-free cells had no nanoparticles. The deposition of Pd(0) on/in the challenged cells was very similar to that reported for bio-Pd made on *Desulfovibrio desulfuricans* (Omajali et al., 2015) (Supplementary Information Figure S2). A full characterization of the bio-Pd on *E. coli* will be reported in full in a later publication.

In contrast, cells challenged with Ru(III) alone showed localization of electron opaque NPs detectable only at the cell surface (Figure 1A-E) and also in material extruded from the cell surface both at 2.6wt% Ru (not shown) and in cells loaded with Ru to (nominally) 20wt% Ru (the actual loading here was not determined) (Supplementary Information, Figure S3). Analysis of the cell surface (Figure 1C) and exuded material (Figure S3) using EDX confirmed the presence of Ru, while HR TEM (Figure 1F, G) showed discrete NPs of size ~ 2-3 nm, with lattice spacings of 0.210 nm, which may be assigned to the {101}

face of Ru metal (0.205 nm: Ghosh and Chen, 2008). However other studies (Kim et al., 2001) concluded that RuO_2 forms as a surface layer by epitaxial growth on the surface of Ru in a lattice-matched manner; indeed, Leng et al. (2014) attributed a lattice fringe of 0.205 Å to the {210} face of RuO_2 synthesised on graphene. In situ synchrotron X-ray diffraction showed the direct transition of amorphous $Ru(OH)_3.H_2O$ to crystalline RuO_2 NPs, i.e. the evolution of Ru(IV) from (Ru(III) (Park et al., 2015). The hydrolysis behaviour of the Ru^{3+} ion in the current study would be suppressed at the acidic pH used for metal uptake (as described by Deplanche et al., 2012) but following metal exposure (under H_2) the cells were washed in water and left in air prior to analysis and hence oxidation of any residual Ru(III) in air cannot be precluded. As some of the X-ray emission energies of Ru and Cl overlap (respectively keV 2.56 (Lα) 2.68 (Lβ) and 2.62 (KαY); 2.81 (Kβ)) keV) elemental mapping cannot preclude deposition of $RuCl_3$. (In contrast the emission lines of Pd are (keV) 2.84 (Lα1), 2.99 (Lβ1), 3.17 (Lβ2) and 3.33 (Lγ)). Hence, XPS analysis of metal and chloride speciation at the cell surface was performed (see later).

Ru was not apparently taken up into the cytoplasm (Figure 1, Figure S3) and the extruded material is suggested to be of cell surface origin, since outer membrane vesicles containing Ru were visible (see later). The Ru-deposition extended through the thickness of the cell wall layer (Figure 1E). There is little information on the interactions of Ru(III) with living cells but Ru-complexes are very common, e.g. ruthenium-amine complexes are reported to have antitumor activity (e.g. Lima et al., 2014) while a recent report (Luo et al., 2018) describes the formation of Ru(III) complexes with collagen, a structural protein. In bacteria it seems likely that incoming Ru(III) is intercepted by amine groups of the periplasmic peptidoglycan, while outer membrane proteins would also form binding sites for Ru(III); we surmise that the incoming Ru(III) is intercepted and held by ligands in the cell surface layers.

3.2.Deposition of Ru and Pd/Ru by cells of *E. coli*

In contrast to the above, when loading the cells with 5 wt%Pd/5wt% Ru or 5wt%Pd/20wt%Ru the Ru(III) was removed from the solution by 94% and 88%

respectively (Table 1). Clearly ‘seeding’ with 5 wt% Pd(0) promotes deposition of Ru as compared to challenge with Ru(III) alone. The nominal and actual loadings of Ru on the cells are shown in Table 1; for convenience the bimetallic samples will be described as ‘low-Ru’ (5wt%Pd/5wt%Ru) and ‘high Ru’ (5wt%Pd/20wt%Ru) respectively, a key difference being the greater proportion of Pd atoms in the samples with less Ru.

3.3.Examination of low-Ru bimetallic by HRTEM and HAADF and elemental mapping

Challenge of the cells with Pd(II) and Ru(III) individually suggested that, while the former entered the cells and formed intracellular deposits, Ru deposition was confined to the surface layers (above) and hence it was implied that only surface-located Pd(0) would be able to ‘seed’ the formation of structured bimetallics. However, intracellular NPs were visible (Figure 2A, B); these, and also the surface-located NPs, contained both Pd and Ru (Figure 2C, D), with an enrichment of Ru in the latter region (Figure 2C). Elemental mapping (Figure 2 E-H) confirmed the uniform distribution of Pd (Figure 2G), surface-enrichment of Ru, the presence of small intracellular Ru-NPs and putative membrane vesicles containing Ru-NPs. (Figure 2H, Supplementary information Figure S4). Intracellularly, Pd-NPs predominated (Figure 2F). While some areas of the cell contained Pd-NPs only, the Ru-NPs were located mainly alongside Pd-NPs (Supplementary Information Figure S4) although an association between them was not proved.

To prove an association between Pd and Ru a cell surface NP transect (arrowed in Figure 2I) was analyzed (Figure 2J), showing an asymmetric hybrid structure with Pd/Ru at one side and Pd-enriched at the other, corresponding to a sparse region of Ru. The predominance of Pd in the NPs was confirmed by the lattice fringes (0.24 nm: Figure 2K and L) assigned to Pd{111} facets (Omajali et al., 2015) in both the cell surface and intracellular NPs. The size of the NPs was ~3 nm but a NP size distribution analysis was not attempted due to the difficulty of setting the NP boundary due to the indistinct nature of the NPs. Some size heterogeneity is apparent (Supplementary Information Figure S4) but it is not certain if the larger NPs are simply agglomerations of smaller ones. The mean NP size (for bio-Pd) was reported as 1.4 nm in *D. desulfuricans* (Omajali et al., 2015),

while that for *E. coli* was similar, at 1.3 nm (J. Gomez-Bolivar, unpublished) and will be detailed in a subsequent publication.

3.4.Examination of high-Ru bimetallic by HRTEM and HAADF and elemental mapping

Figure 3 shows the NPs produced at the higher loading of Ru. In contrast to the low-Ru samples (above) no intracellular Ru NPs were apparent by electron microscopy (Figure 3 G; Supplementary information Figure S5) although some Ru was detected intracellularly by EDX (Supplementary information Figure S6). Small and larger intracellular NPs were visible; the latter contained more Pd (Figure S6). The reason for the apparently low cellular uptake of Ru and lack of Ru-NPs was not investigated but the higher dose of Ru was probably lethal to the cells. The observation of intracellular Ru (Figure S6) but not NPs (Figure 3E) also raises the question as to the actual role of Pd(0) seeds in the reduction of Ru(III) (assumed on the basis of earlier work using bio-Pd/Au: Deplanche et al., 2012) as a similar result to the low-Ru preparation (above) would be expected.

For catalysis the surface bound material would be more relevant and this was examined further. Lattice fringes (0.236 nm; Figure 3C) would correspond to Pd(0) {111}. Other images (not shown) confirmed lattice fringes of 0.240 nm, attributed to Pd {111} facets (Omajali et al., 2015) or possibly to the {110} plane of RuO_2 (0.231 nm: Soin et al., 2012), while the 0.201 nm lattice fringe (Figure 3D) could be Ru(0){101}/RuO_2 {210} (see above discussion).

In contrast to the low-Ru sample, regions of elemental overlap were clearly visible in the high-Ru sample (Figure 3E). An enlarged image (Supplementary Information, Figure S5) shows numerous apparent core-shell structures as well as several ‘twinned’ structures of the two metals alongside each other. In addition, a triplet structure (‘dumbbell’) is apparent that comprises a pivotal bimetallic region abutting onto separate nanostructures of both Pd and Ru (Figure S5). These features contrast with the low-Ru preparation that shows no evident hybrid structures (Figure S4).

The electron microscopy data would indicate that, with excess Ru, the material comprises mostly a random deposition of Pd and Ru/RuO_2 NPs but with some core-shell structures apparent visually. Examination of an area with a small undefined NP shows a largely random distribution of Pd and Ru with metal levels barely detectable above the background at the edge of the NP transect (Figure 3I). In contrast the patterning of a well-defined NP confirms a core-shell structure (Ru core/Pd shell) as described previously for Pd/Au (Au core/Pd shell: Deplanche et al., 2012). The previous studies on Pd/Au NPs also used Z-imaging, where the image intensity reflects the Z dependence on atomic number (Nellist and Pennycook, 2000); this can be used to localize atoms in NPs where elements of higher atomic number appear brighter. In bio-Pd/Au core-shells the Au-core was evident (Tran et al., 2012; Z Pd= 46; Z Au = 79) and, similarly, the Pt in Pd/Pt alloy (Z Pt = 78: Esparza et al., 2017). However, since Z for Ru = 44 (i.e. very close to Pd) the difference in contrast between the metals would be too small to detect. However Figure 3H provides evidence for the occurrence of a similar structure in bio-Pd/Ru; the mechanism was assigned previously to re-oxidation of the Pd(0) 'seeds' via galvanic reduction of the incoming Au(III) and migration of nascent Pd(II) around the NP, to be re-reduced under H_2 to form the shell around the Au(0) core (Deplanche et al., 2012). In contrast to bio-Pd/Au, the Pd/Ru core-shell structures occurred only occasionally and the occurrence (and persistence) of Ru(0) in the material is not proved (see above and later). Indeed, formation of Ru(IV) as RuO_2 is suggested (i.e. oxidation of Ru(III) see later) which requires an electron sink. Petkov et al. (2017) attribute electronic interactions at surface metal interfaces ($Au^{\delta+}$; $Pd^{\delta-}$) as being responsible for high catalytic activity. It would seem possible that, in this case under H_2 a core-shell may form, followed by (in air) oxidation of the Ru(0) component. It is known that a negatively charged Pd(0) can be formed by accepting electrons (i.e. behaving as a capacitor). Indeed, the capacitance (ability to store charge) of bio-Pd on *E. coli* was measured at 0.5–0.6 microamps in an electrochemical test system (at 20wt% Pd: Courtney et al., 2016).

However RuO_2 can evolve in air from Ru(III) (see above) without addition of a specific oxidant. No precaution was taken to exclude air following harvest of the NPs. It would seem that while Ru(III) may be reduced to Ru(0) into an occasional bimetallic core-shell (as for Pd/Au) it can also become oxidized to Ru(IV) and form RuO_2 in air. While the core-shell may be stabilized by its Pd-overlay, the side by side NPs would leave Ru with

an available surface for evolution into RuO_2 while having Pd(0) nearby as a possible electron acceptor, a possible benefit of co-localization (Figure S4, Figure S5) without actual integration of the two metals.

3.5.Analysis of bulk material using EXAFS: XANES Analysis.

X-ray absorption near edge structure (XANES) is an element-specific and local bonding-sensitive spectroscopic technique applied in this study to determine the oxidation state of Ru and Pd in the experimental samples. The analysis is based on relating small shifts (a few eV) in XANES absorption edge energies with the average oxidation state of the central element. Spectra of Pd-foil and Ru-foil are shown in supplementary information, Figure S7.

Figure 4A shows the XANES spectra of Pd reference compounds; palladium foil (metallic Pd) and PdO (Pd(II)), and biogenic Pd/Ru NPs (low-Ru and high-Ru). The results obtained indicate that Pd is present as a mixture of Pd(0) and Pd(II) in the two Pd/Ru samples. Linear combination fitting mode of ATHENA code was used to determine the relative amounts of Pd(0) and Pd(II) present in the bio-derived samples, revealing a mixture of 60% metallic palladium and 40% Pd(II) for both bulk biogenic Pd/Ru nanoparticles samples.

In the case of the Ru edge (Figure 4B), the XANES spectra of both biogenic NPs samples are different from that of Ru foil. In these samples, Ru is present as a mixture of Ru(III) and Ru(IV). However, linear combination fitting mode of ATHENA code showed the presence of low amounts of Ru(0) ranging between 6 and 10%.

3.6.EXAFS: Pd K-edge

The Pd K-edge EXAFS spectra of a palladium foil, and of low-Ru and high-Ru samples, along with their corresponding Fourier transforms (FT), are shown in Figure 5A. The fit parameters of the calculated spectra are summarized in Table 2a.

In the case of the Pd foil, the FT peaks of metallic Pd were attributed to four Pd-Pd shells with distances of 2.74, 3.86, 4.78, 5.40 Å. The major peak corresponds to about twelve Pd atoms at a Pd-Pd interatomic distance of 2.74 ± 0.02 Å as reported by Polizzi et al. (2001).

The EXAFS spectra of both low-Ru and high-Ru biogenic NPs samples are characterized by the presence of two Pd species: one metallic (Pd-Pd) and two complexed (Pd-O) via oxygen atoms to the cell matrix functional groups. For the Pd-O_1 and PdO_2 phases, the distances found are comparable to the ones of palladium oxide (Pd(II)O) with a simple tetragonal structure (Borowsky, 1997) with Pd-O_1 contributions at 2.1 ± 0.02 Å and 2.04 ± 0.02 Å for high-Ru and low-Ru samples, respectively, and to Pd-O_2 bond distance at 2.55 ± 0.02 Å. The distances were calculated using the Pd–O backscattering phase and amplitude functions obtained from PdO crystal structure using the FEFF8 program. The oxygen atoms could have originated from the carboxyl groups of (e.g.) aspartic and glutamic acids of the bacterial cells as reported by Fahmy et al., 2006. The interatomic distances obtained for metallic phase contribution were very close to the ones of the metallic foil.

3.7.EXAFS: Ru K-edge

Figure 5B show the Ru K-edge EXAFS spectra of a ruthenium foil, RuO_2, $RuCl_3$, low-Ru, high-Ru and Ru-only samples along with their corresponding Fourier transforms (FT). The structural parameters of the calculated spectra are summarized in Table 2b.

The FT of the three experimental samples was well fitted by the use of two Ru-O bonds with interatomic distances of 1.96-2.04 and 2.1-2.16 ± 0.02 Å, and a single Ru-Ru shell with a bond distance of 2.77-2.85 ± 0.02 Å. The distances of the shortest Ru-O bond (1.96-2.04 ± 0.02 Å) can be assigned to Ru=O of RuO_2 (McKeown et al., 1999) while the shell at bond distance of 2.1-2.16 Å is assigned to the Ru–$O_{hydroxo}$ (Ru–OH) bond as observed in $RuNi(OH)_2$ composite (Venkatesan et al., 2009). The EXAFS spectra include also a Ru-Ru shell with a bond distance of about 2.77-2.85 ± 0.02 Å. The higher Debye-Waller factor of this shell (0.01-0.019 $Å^2$) indicates that there is probably a wide spread of Ru-Ru distances with an averaged value of 2.77-2.85 ± 0.02 Å. This implies the possible contribution of Ru-Ru arising from two different ligands (Ru metal and RuO_2).

This assumption is supported by two features: 1) the bond distance value of 2.77-2.85 ± 0.02 Å could correspond to the average distance of Ru-Ru from Ru metal (2.66 ± 0.02 Å) and from RuO_2 (3.09 ± 0.02 Å) obtained for reference compounds (Table 2b). These two shells were not represented as separate shells in the FT spectra since their distances span an *R* range that was not large enough to be differentiated as individual peaks in an EXAFS spectra for which $\Delta k = 7$ Å^{-1} in agreement with $\Delta R \geq \pi/(2\Delta k)$ (Merroun et al., 2005); 2) the linear combination fitting results of the XANES spectra suggested the presence of low amounts of Ru metal in addition to Ru(III) and Ru(IV) species (see above).

However, since catalysis would be largely confined to the surfaces of the cells the bulk signal could mask the contributions of the cell surface components, placing minor surface-located species below the level of detection. Hence, the metal composition of the cell surface was investigated using XPS. This surface method probes only the outermost ~ 10nm of the structure, i.e. the depth of the outer membrane and outermost region of the periplasmic space.

3.8. Examination of cell surface bio-Ru and bio-Pd/Ru by X ray photoelectron spectroscopy

The surface-bound NPs of whole cells (the outermost ~10 nm of the cell wall) were examined by XPS, where the reduction of Pd(II) to Pd(0) in the 'seeding' step was confirmed previously (Omajali et al., 2015; Omajali et al., 2017). The wide energy spectrum for all samples is shown in Figure 6A. All samples clearly evidenced the presence of the C 1s + Ru 3d peak along with the oxygen O 1s signal centred at ~285 and ~530 eV, respectively. Apart from these, the nitrogen N 1s, Ru 3p and, where applicable, low intensity signals of Pd 3d signals were also identified. The spectrum for commercial $RuCl_3$ salt (the starting material) is shown in supplementary information, Figure S8 for reference, evidencing Ru(III) as $RuCl_3$ and $Ru(OH)_3$ species.

Figure 6B shows a comparison of the high resolution Pd 3d spectra for low-Ru and high-Ru bimetallic samples. Resolved and fitted components for the two samples are shown in Figure 6C and Figure 6D, respectively. The spectra were fitted using Gaussian peaks to identify the oxidation states of Pd. In low-Ru samples, Pd was found in its native Pd(0)

and oxidized Pd(II) and also Pd(IV) states; Table 3 lists the respective binding energies (Liu et al., 2015; Priestley et al., 2015). However, high-Ru samples revealed a very noisy Pd signal (Figure 7D), which has not been resolved into components. However, it can be stated with confidence that at least two components Pd(0) and oxidized Pd(II) are present in these samples. The weak Pd 3d signals could be suggestive of the relatively large amount of Pd internalized by the cells (Figures 2 and 3) resulting in minimal Pd nanoparticle formation near the bacterial outer membrane and outermost wall layers which are within the sampling depth of XPS.

Figure 7A shows the comparison of C 1s + Ru 3d high-resolution spectra for all three bio-NP samples. Figs. 7b -7d show, respectively, low-Ru and high-Ru samples, and Figure 7B the Ru-only sample. The high-resolution C1s spectra for *E.coli* has been previously resolved into four components identified as C-C (284.5 eV), C-OH/amine (286 eV), C=O/amide (288 eV) and COOH (290 eV), respectively (Priestley et al., 2015). The introduction and growth of metal NPs in the bacterial biomass (Figure 7B-7D) revealed a significant change in the spectra, suggesting some loss of C=O/amide and C-OH/amine groups along with the introduction of various Ru components. The amount of Ru contribution to the C 1s+Ru 3d spectra appears to increase as the metal loading increases (from only 5% Ru to 5%Ru and 5%Pd to 5%Pd and 20%Ru loading, as seen in Figure 7B-7D). This could suggest an interactive behaviour enabling a greater amount of Ru to stay near the outer bacterial membrane (or limited/reduced uptake of Ru with increasing Ru loading), in the presence of Pd in the system. Specifically, four C1s components, namely, C-C/C-OH, C-O/amine, C=O/amide and COOH were identified/resolved in all three types of metal loaded *E.coli* samples. Three to four types of Ru doublet components were also resolved in all three metal NPs -bacterial biomass samples (Figure 7B-7D). These were attributed to RuO_2, (Morgan, 2015) $RuCl_3$ and $Ru(OH)_3$. Further analysis of Ru 3p spectra (supplementary information, Figure S9) suggested the possibilities of Ru-ligand complexes forming with aromatic carbon structures and Ru-nitrogen oxide (Ru-NOx) like structures being formed within the biological system. Ru complexes are known to be formed within cellular structures, as discussed earlier. These components were, therefore, identified in the Ru 3d spectra, which led to dual attributions, given the minor shifts in the binding energies (Table 3) in comparison to the literature (Morgan, 2015). The presence of Ru-NOx components corroborated with the N 1s spectra (not shown). It

is worth mentioning that the $RuCl_3$ component could not be distinctly identified in the Ru-only sample. Since this sample has only small quantity of metal added (5% Ru only) it is possible to have minimal or no $RuCl_3$ residues and maximum uptake and internalisation of Ru into cellular layers beneath the XPS-accessible depth. The slight shift of $Ru(OH)_3$ towards higher binding energy may be due to small residues of $RuCl_3$ which could not be resolved into a distinct peak given the complexity of the C 1s + Ru 3d spectra.

The high-resolution O 1s spectra for all samples can be seen in Figure 8A. Specifically, the deconvolution of O 1s spectrum into the various components for all three samples revealed a small component peak at ~529.5 eV, suggesting the presence of metal oxides, which is in agreement with the Pd 3d and Ru 3d spectra, with the EXAFS analysis (PdO) and with RuO_2 evolving from $Ru(OH)_3$ (see earlier). Another observation was the decrease in the C-O component and a relative increase in C=O/sulfate components as the metallic content increased in the form of Ru-alone and low-Ru and high-Ru bimetallics. This could be due to singly bonded oxygen being sacrificed for metal (Ru/Pd) oxide formation. A similar trend was also observed for the adsorbed water content peak denoted by the component peak near 534.7 eV. The slight loss of adsorbed water content and its possible implication is not very clear. Perhaps it can be suggested that with an increase in the metallic component, the formation of various Ru oxides and complexes was promoted and contributed to by the adsorbed/loosely bound water molecules within the cellular structures. However, the exact nature of such interactions in such a complex system would be difficult to predict within the limitations of this study.

None of the spectra provide sufficient evidence for the occurrence of Ru(0) as no peaks are visible at 280 eV.

3.9 Catalytic activity of the metallized cells in the conversion of 5-HMF to 2,5-DMF.

Most published work has used commercially-available substrates but, since one of the goals of this work is to realise resources from wastes, 5-HMF was extracted from hydrolyzates of starch and cellulose made by thermochemical hydrolysis methods, previously developed to yield parallel fermentable and added-value side-streams (see

Introduction). The catalysts were therefore tested against commercial 5-HMF and 5-HMF from hydrolyzate extracts in a common solvent (MTHF) for extraction and catalytic upgrading. Preliminary work established that this solvent extracted between 60% and 65% of the 5-HMF (R.L. Orozco, unpublished) but the extraction method was not optimized.

First, commercial 5wt% Ru/C and 5wt% Pd/C catalysts were compared in MTHF using commercial 5-HMF. The Ru catalyst gave 100% conversion of 5-HMF with 57.1% selectivity to 2,5 DMF with respective values of 100% and 3.3% for the Pd/C equivalent. Therefore, Pd-only catalysts were not considered further. All catalysts tested (data are shown in Supplementary Information Table 1) gave close to 100% conversion of 5-HMF (Figure 9A) but the high-Ru biomaterial showed a low yield (21%) and selectivity to 2,5-DMF and this, too, was not considered further. It would seem that the presence of the core-shells in the high-Ru sample confers no benefit but these were few in number as compared to the remainder of the metal NPs (Figure S5). Lei et al. (2014) noted an adverse effect of an excess of Ru, attributing this to excessive Ru accelerating the occurrence of side reactions. Hence further tests compared the low-Ru samples and 5wt% bio-Ru.

Using pure 5-HMF the bio-Ru was less effective than the commercial 5wt% Ru/C catalyst (~ 10% selectivity) whereas the low-Ru bimetallic and commercial catalyst gave similar results (> 50% selectivity: Figure 9A). However, notably the commercial Ru/C catalyst had little activity against 5-HMF made from the starch or cellulose (Figure 9B, C). It is possible that residual polymeric components fouled the commercial catalyst (co-extracted into the MTHF), or that catalyst poisons were made via the thermochemical hydrolysis reactions, but this was not tested and assumes that these adverse components were co-extracted into MTHF. An alternative explanation is that the chemical catalyst was overactive in this reaction, proceeding into additional by-products. An example of the product mix is shown in Supplementary Information (Figure S10). In each case (Figure 9B, C) the 5wt%Pd/5wt%Ru bio-catalyst achieved significant production of 2,5-DMF and, in the case of cellulose hydrolysate, the Ru-only bio-catalyst became comparable to the low-Ru bimetallic. (c.f. Figure 9A). A detailed investigation of the reaction pathway was beyond this scoping study and is in progress but clearly the bio-derived catalyst is

able to compete effectively with commercial catalyst against pure 5-HMF and outperforms the latter in conversion of 5-HMF from actual hydrolyzates.

4. Conclusions

This study shows clearly that bio-Pd/Ru catalyst (5wt% of each metal) has potential in the production of 2,5 DMF from 5-HMF from biomass hydrolyzate, which is not achieved using a commercial counterpart. This study reports the formation of Pd/Ru core shell structures in an analogous way to those of Pd/Au reported previously but these may contribute little overall to the outcome since the dominance of the non core-shell excess Ru in the high-Ru material is counterproductive to 2,5 DMF selectivity. It is far from clear what metal species (or combination of them) actually catalyzes the reaction; evidence was found for various valences of both metals but not, equivocally for Ru(0) whereas Ru(IV) was evident (as RuO_2) (along with Pd(O) and Pd(0) and also Pd(IV)). The metal speciation is important, e.g. the degree of Ru oxidation was found to influence the catalytic activity in bimetallic Pt/Ru nanoparticles (Wang et al., 2016). It is likely that heterogeneous NPs are produced since the bacterial cell surface offers a variety of ligands to initiate the nucleation of Pd(II) (and also sites that would complex with incoming Ru(III)) and NP evolution may also be influenced by the surrounding biochemical matrix as well as oxygen ingress during catalyst storage in air. Future work would use systems biology approaches to 'dissect' the microbial features that contribute to, and steer, metallic NP development. Initial steps have been taken in the case of monometallic Pd-NPs (Torgeman, 2017) that would underpin understanding of bimetallic systems following Pd(0) nucleation.

Acknowledgements, author contributions and declaration.

The project was funded by NERC grant NE/L014076/1 to LEM (Program: '*Resource Recovery from Wastes*'). The Science City Photoemission Facility used in this research was funded through the Science Cities Advanced Materials Project 1: '*Creating and Characterizing Next Generation of Advanced Materials*' with support from AWM and ERDF funds. The microscopy work was conducted at 'Centro de Instrumentación Cientifica' at the University of Granada, Spain. The Authors acknowledge with thanks

use of GC-FID / GC-MS supplied by Dr Daniel Lester within the Polymer Characterization Research Technology Platform, University of Warwick. Biomaterials were made and characterized by JGB and IPM; RLO developed the method for 5-HMF extraction from hyrolyzates; RLO and JGB did catalytic testing, with analysis of products by RAH; High resolution SEM/TEM/elemental mapping were by JGB and MM; XPS data acquisition was by MW with XPS interpretations by MW and SS; EXAFS measurements were done by DB with interpretation by MM; The paper was lead-authored by LEM with contributions from all authors. All authors declare no competing financial interests or other conflicts of interest.

References

Abramoff, M.D., Magalhaes, P.J. and Ram, S. J. (2004) Image processing with ImageJ. *Biophotonics Int* 11, 36–42

Ankudinov, A.L., Ravel, B., Rehr, J.J., and Conradson, S.D. (1998). Real-space multiple-scattering calculation and interpretation of X-ray absorption near-edge spectra. *Phys. Rev. B* 58, 7565-7575 doi: 10.1103/PhysRevB.58,7565.

Bennett, A.J., Mikheenko, I.P., Deplanche, K., Shannon, I.J., Wood, J. and Macaskie, L.E. (2013) Nanoparticles of palladium supported on bacterial biomass: New re-usable heterogeneous catalyst with comparable activity to homogeneous colloidal Pd in the Heck reaction (2013) *Appl. Catal. B Environ*. 140-141, 700-707 doi: dx.doi.org/10.1016/j.apcatb.2013.04.02.2

Blumenthal, L.C., Jens, C.M., Ulbrich, J., Schwering, J.F., Langrehr, V., Turek, T., Kunz. T.U., Leonhard, K., and Palkovits, R. (2016). Systematic identification of solvents optimal for the extraction of 5-hydroxymethylfurfural from aqueous reactive solutions. *ACS Sust. Chem. Eng*. 4, 228−235. doi: 10.1021/acssuschemeng.5601036

Borowski, M. (1997). Size Determination of Small Cu-Clusters by EXAFS. *J. Phys. IV France* **7,** C2-259-C2-260

Boucher, M.B., Zugic, B., Cladaras, G., Kammert, J., Marcinkowski, M.D., Lawton, T.J., et al. (2013). Single atom alloy surface analogs in $Pd_{0.18}Cu_{15}$ nanoparticles for selective hydrogenation reactions. *Phys. Chem. Chem. Phys*. 15, 12187-12196. doi: 10.1039/C3CP51538A

Castro, L., Blazquez, M, Munoz, J.A., Gonzalez, F.G., and Ballester, A. (2014). Mechanism and applications of metal nanoparticles prepared by bio-mediated process. *Rev. Adv. Sci. Eng.*2014, 3, 1-18. doi: 10.1166/rase.2014.1064

Charlot, G. (1978) Dosages Absorptiométriques des Eléments Mineraux, 2nd Edn. Paris, France, Masson.

Courtney, J., Deplanche, K., Rees, N., Macaskie, L.E. (2016). Biomanufacture of nano-Pd(0) by *Escherichia coli* and electrochemical activity of bio-Pd(0) made at the expense of H_2 and formate as electron donors *Biotechnol. Lett.* 38, 1903–1910. doi: 10.1007/s10529-016-2183-3

De Corte, S., Hennebel. T., De Gusseme, B., Verstraete, W., Boon, N. (2012). Bio-palladium: from metal recovery to catalytic applications. *Microb. Biotechnol*. 5, 5-17. doi: 10.1111/j.1751-7915.2011.00265.

Deplanche, K. (2008). New nanocatalysts made by bacteria from metal solutions and recycling of Metal Wastes. *PhD Thesis* University of Birmingham, UK.

Deplanche, K., Caldelari, I., Mikheenko, I.P., Sargent, F., and Macaskie, L,E. (2010). Involvement of hydrogenases in the formation of highly catalytic Pd(0) nanoparticles by bioreduction of Pd(II) using *Escherichia coli* mutant strains. *Microbiol*. 156, 2630–2640. doi: 10.1099/mic.0.036681-0

Deplanche, K., Mikheenko, I.P., Bennett, J.A., Merroun, M.L., Mounzer, H., Wood, J., et al. (2011). Selective oxidation of benzyl-alcohol over biomass-supported Au/Pd bioinorganic catalysts. *Topics Catal*. 54, 1110–1114. doi:10.1007/s11244-011-9691-0

Deplanche, K., Merroun, M.L., Casadesus, M., Tran, D.T., Mikheenko, I.P., Bennett, J.A., et al. (2012). Microbial synthesis of core/shell gold/palladium nanoparticles for applications in green chemistry. *J. Roy. Soc. Interface* 9, 1705-1712. doi: 10.1098/rsif.2012.0003

Deplanche, K., Bennett, J., Mikheenko, I., Omajali, J., Wells, A., Meadows, R., et al. (2014) Catalytic activity of biomass-supported Pd nanoparticles: influence of the biological component in catalytic efficacy and potential application in 'green' synthesis of fine chemicals and pharmaceuticals. *Appl. Catal. B Environ*. 147, 651-665. doi:10.1016/j.apcatb.2013.09.045

Esparza, R., Santoveña, A., Ruíz-Baltazr, A., Angeles-Pascual, A., Bahena, D., Maya-Cornejo, J., et l. (2017). Study of PtPd bimetallic nanoparticles for fuel cell applications. *Mat. Res.* 20, 1193-1200. doi: 10.1590/1980-5373-mr-2016-0934

Fahmy, K., Merroun, M., Pollmann, K., Raff, J., Savchuk, O., Hennig, C., & Selenska-Pobell, S. (2006).Secondary structure and Pd(II) coordination in S-layer proteins from *Bacillus sphaericus* studied by infrared and X-ray absorption spectroscopy. *Biophys. J.* 91, 996-1007. doi: 10.1529/biophysj.105.079137

Fairley, N. CasaXPS. Casa Software Ltd. www.casaxps.com. (2013)

Gao, F., and Goodman, D.W. (2012). Pd–Au bimetallic catalysts: understanding alloy effects from planar models and (supported) nanoparticles. *Chem. Soc. Rev*. 41, 8009-8020. doi: 10.1039/C2CS35160A

Ghosh, D., Chen, S. (2008). Solid-state electronic conductivity of ruthenium nanoparticles passivated by metal–carbon covalent bonds. *Chem. Phys. Lett*. 465, 115-119. doi: 10.1016/j.cplett.2008.09.066

Hansen, T.S., Barta, K., Anastas, P.T., Ford, P.C., and Riisager, A. (2012). One-pot reduction of 5-hydroxymethylfurfural via hydrogen transfer from supercritical methanol. *Green Chem.* 14, 2457-2461. doi: 10.1039/C2GC35667H

Hosseinkhani, B., Søbjerg, L.S.,Rotaru, A.E., Emtiazi, G., Skrydstrup, T., and Meyer, R.L. (2012). Microbially supported synthesis of catalytically active bimetallic Pd-Au nanoparticles. *Biotechnol. Bioeng.* 109, 45-52. doi: 10.1002/bit.23293.

John, S.St., Atkinson, R.W., Unocic, K.A., Unocic, R.R., Zawodzinski, T.A.Jr., and Papandrew, A.B. (2015). Platinum and palladium overlayers dramatically enhance the activity of ruthenium nanotubes for alkaline hydrogen oxidation. *ACS Catal.* 5, 7015-7023. doi: 10.1021/acscatal.5b01432

Karatzos, S., McMillan, J.D. and Saddler, J.N. (2014) The potential and challenges of drop-in biofuels. Report T39, ISBN 978-1-910154-07-6. Published by IEA: Bioenergy Energy Technology Network

Kim, Y.D., Schwegmann, S., Seitsonen, A.P. and Over, H. (2001). Epitaxial growth of RuO_2 (100) on Ru (0101): surface structure and other properties. *J Phys. Chem. B.* 105, 2205-2211.

Kulkarni M. and Maddapur, U. (2014). Biosynthesis of metal nanoparticles: a review. *J Nanotechnol*, 2014 Article No D 510246.doi.org/10.1155/2014/510246

Kunwar, B., Deilami, S.D., Macaskie, L.E., Wood J., Biller P., and Sharma, B. K. (2017). Nanoparticles of palladium supported on bacterial biomass for hydroprocessing bio oil from continuous hydrothermal liquefaction (NTL) of algae. *Fuel* 209**,** 449-456. doi: 10.1016/j.fuel.2017.08.007

Kyriakou, G.K., Boucher, M.B., Jewell, A.D., Lewis, E.A., Lawton, T.J., Baber, A.E., Tierney, H.L., Stephanopoulos, M and Sykes,,E.C.H. (2012). Isolated metal atom geometries as a strategy for selective heterogeneous hydrogenations. *Science* 335, 1209-1212 doi: 10.1126/science.1215864

Lei, H., Tang, X., Xu, J., Wu, Z., Lu, L., and Liu, S. (2014). Selective transformation of 5-hydroxymethylfurfural into the liquid fuel 2,5-dimethylfuran over carbon-supported ruthenium. *Ind. Eng. Chem. Res*. 53, 3056-3064. doi: 10.1021/ie404441a

Leng, X., Zou, J., Xiong, X and He, H. (2014). Hydrothermal synthesis and pseudo capacitance behavior of a highly homogeneous dispersed graphene sheets/ruthenium oxide nanocomposite *RSC Adv*. 4, 61596 doi: 10.1039/C4RA10321A

Lima, A.P., Pereira, F.C., Almeida, M.A.P., Mello, F.M.S., Pires, W.C., Pinto, T.M., et al. (2014). Cytoxicity and apoptotic mechanism of ruthenium(II) amino acid complexes in sarcoma-180 tumor cells. *PLoS ONE* doi: 10.1371/journal.pone.0105865.

Liu, X., Yu, H., and Scott, K. (2015). Preparation and evaluation of a highly stable palladium yttrium platinum core–shell–shell structure catalyst for oxygen reduction reactions. *Appl. Catal. B. Environ*. 162, 593-601. doi: 10.1016/j.apcatb.2014.07.038

Liu, Z., Zhang, X. and Tay, SW. (2012). Nanostructured PdRu/C catalysts for formic acid oxidation. *J. Solid State Electrochem*. 16, 545-550. doi: 10.1007/s10008-011-1378-8

Luo, W., Sankar, M., Beale, A.M., He, Q., Kiely, C.J., Bruijnincx, P.C.A. et al. (2015). High performing and stable supported nano-alloys for the catalytic hydrogenation of levulinic acid to γ-valerolactone. *Nature Commun*. 6, 6549. doi: 10.1038/ncomms7540

Luo, D., Zhou, B., Li, Zh., Qin, X., Wen, Y., Shi, D., et al. (2018). Biomimetic organization of a ruthenium-doped collagen-based carbon scaffold for hydrogen evolution. *J. Mater. Chem. A*. 6, 2311-2317. doi: 10.1039/C7TA09493K

Luo, J., Arroyo-Ramirez, L., Gorte, R.J., Tzoulaki, D., and Vlachos, D.G. (2015). Hydrodeoxygenation of HMF Over Pt/C in a Continuous Flow Reactor. *AICHE J*. 61, 590-597. doi: 10.1002/aic.14660

McKeown, D. A., Hagans, P. L., Carette, L. P. L., Russell, A. E., Swider, K. E. and Rolison, D. R. (1999). Structure of hydrous ruthenium oxides: Implications for charge storage. *J. Phys. Chem. B*. 103, 4825–4832. doi: 10.1021/jp990096n

Merroun, M.L., Raff, J., Rossberg, A., Hennig, C., Reich, T., Selenska-Pobell, S. (2005). Complexation of uranium by cells and S-layer sheets of *Bacillus sphaericus* JG-A12. *App. Environ. Microbiol*. 71, 5542-5553. doi: 10.1128/AEM.71.9.5532-5543.2005

Mikheenko, I.P., Rousset, M., Dementin, S., and Macaskie, L.E. (2008). Bioaccumulation of palladium by *Desulfovibrio fructosivorans* wild-type and hydrogenase-deficient strains. *Appl. Environ. Microbiol*. 74, 6144-6146. doi: 10.1128/AEM.02538-07

Monyoncho, E.A., Ntais, S., Soares, F., Woo, T.K., and Baranova, E.A. (2015). Synergetic effect of palladium-ruthenium nanostructures for ethanol electrooxidation

in alkaline media. *J. Power Sources* 287, 139-149. doi: 10.1016/j.jpowsour.2015.03.186

Morgan, D. J. (2015). Resolving ruthenium: XPS studies of common ruthenium materials *Surf. Interf. Anal.* 47, 1072-1079. doi: 10.1002/sia.5852

Murray, A.J., Zhu, J., Wood, J., and Macaskie, L.E. (2017) A novel biorefinery: biorecovery of precious metals from spent automotive catalyst leachates into new catalysts effective in metal reduction and in the hydrogenation of 2-pentyne. *Mins. Eng*. 113, 102-108. doi: dx.doi.org/10.1016/j.mineng.2017.08.011

Murray, A.J., Zhu, J., Wood, J and Macaskie, L.E. (2018). Biorefining of platinum group metals from model waste solutions into catalytically active bimetallic nanoparticles *Microbial. Biotechnol*. 11, 359-368. doi: 10.1111/1751-7915.13030

Nagpure, A.S., Venugopal, A.K., Lucas, N., Manikandan, M., Thirumalaiswamy, R., and Chilukuri, S. (2015). Renewable fuels from biomass-derived compounds: Ru-containing hydrotalcites as catalysts for conversion of HMF to 2,5-dimethylfuran. *Catal. Sci. Technol.* 3, 1463-1472. doi: 10.1039/C4CY01376J

Nellist, P.D., and Pennycook, S.J. (2000). The principles and interpretation of annular dark field Z-contrast imaging. *Adv. Imag. Elect. Phys*. 113, 147-203. doi: 10.1016/S1076-5670(00)80013-0.

Nishimura S., Ikeda N. and Ebitani K. (2014) Selective hydrogenation of biomass-derived 5-hydroxymethylfurfural (HMF) to 2, 5-dimethylfuran (DMF) under atmospheric hydrogen pressure over carbon supported PdAu bimetallic catalyst. *Catal. Today*. 232, 89-98. doiI: https://doi.org/10.1016/j.cattod.2013.10.01

Omajali, J.B. (2015) Novel Bionanocatalysts for Green Chemistry Applications. *PhD Thesis* University of Birmingham, UK.

Omajali J.B., Mikheenko, I.P., Merroun, M.L. and Macaskie, L.E. (2015). Characterization of intracellular palladium nanoparticles synthesized by *Desulfovibrio desulfuricans* and *Bacillus benzeovorans J. Nanopart. Res*. 17, 264-281. doi: 10.1007/s11051-015-3067-5

Omajali, J.B., Hart, A., Walker, M., Wood J., and Macaskie, L.E. (2017). *In-situ* catalytic upgrading of heavy oil using dispersed bionanoparticles supported on gram-positive and gram-negative bacteria. *Appl. Catal. B: Environ.* 203, 807-819. doi: 10.1016/j.apcatb.2016.10.074

Omajali, J.B., Mikheenko, I.P., Overton, T.W., Merroun, M.L., and Macaskie, L,M, (2018). Probing the viability of palladium-challenged bacterial cells using flow cytometry. *J. Chem. Technol. Biotechnol.* https://doi.org/10.1002/jctb.5775

Orozco R.L. (2012) Hydrogen production from biomass by integrating thermochemical and biological processes' PhD Thesis University of Birmingham, UK

Orozco, R.L., Redwood, M.D., Yong, P., Caldelari, I., Sargent, F., Macaskie, L.E. (2010). Towards an integrated system for bio-energy: hydrogen production by *Escherichia coli* and use of palladium-coated waste cells for electricity generation in a fuel cell. *Biotechnol. Lett.* 32, 1837–1845. doi: 10.1007/s10529-010-0383-9

Orozco, R.L., Redwood, M.D., Leeke, G.A., Bahari, A., Santos, R.C.D., and Macaskie, L.E. (2012). Hydrothermal hydrolysis of starch with CO_2 and detoxification of the hydrolysates with activated carbon for bio-hydrogen fermentation. *Int. J. Hyd. Energy* 37, 6545-6553. doi: 10.1016/j.ijhydene.2012.01.047

Park, J., Lee, J.W., Ye, B.U., Chun, S.H., Joo, S.H., Park, H., Lee, H., Jeong, H.Y., Kim, M.H. Baik, J.M. (2015). Structural Evolution of Chemically- Driven RuO_2 Nanowires and 3-Dimensional Design for Photo- Catalytic Applications *Sci. Reports*, 5, 11933. doi: 10.1038/srep11933

Petkov V., Prasai, B., Shastri, S., Kim, J-W., Shan, S., Kareem, H., Luo, J and Zhong, C.J. (2017) Surface atomic structure and functionality of metallic nanoparticles: a case study of Au-Pd nanoalloy catalysts . *J Phys Chem C* 121,7854-7866. . doi: 10.1021/acs.jpcc.7b00139

Polizzi, S., Riello, P., Balerma, A. & Benedetti, A. (2001). Nanostructure of Pd/SiO_2 supported catalysts. *Phys. Chem. Chem. Phys.* 3, 4614-4619. doi: 10.1039/b105607g

Priestley, R. L., Mansfield, A. Bye, J., Deplanche, K., Jorge, A. B., Brett, D., Macaskie, L. E. and Sharma S. (2015). Pd nanoparticles supported on reduced graphene- *E. coli* hybrid with enhanced crystallinity in bacterial biomass RSC Adv. 5, 84093-84103 (2015). doi: 10.1039/C5RA12552A

Qui, J., Zhang, H., Wang, X., Han, H., Liang, C., and Li, C. (2006). Selective hydrogenation of cinnamaldehyde over carbon nanotube supported Pd-Ru catalyst. *React. Kinet. Catal. Letts.* 88, 269-276. doi: 10.1007/s11144-006-0061

Raja, R., Sankar, G., Hermans, S., Shephard, D.S., Bromley, S., Thomas, J.M., et. al. (1999). Preparation and characterisation of a highly active bimetallic (Pd-Ru) nanoparticle heterogeneous catalyst. *Chem. Commun*. 1999, 1571–1572. doi: 10.1039/A901263J

Ravel, B. and Newville, M. (2005). ATHENA, ARTEMIS, HEPHAESTUS: data analysis for X-ray absorption spectroscopy using IFEFFIT. *J. Synchrotron Rad.* 12, 537-541. doi: 10.1107/S0909049505012719

Román-Leshkov, Y., Barrett, C.J., Liu, Z.Y., and Dumesic, J.A. (2007). Production of dimethylfuran for liquid fuels from biomass-derived carbohydrates. *Nature* 447, 982–985. doi: 10.1038/nature05923

Singh O.V. Ed. (2015). *Bio-nanoparticles Biosynthesis and Sustainable Biotechnological Implications.* Hoboken: John Wiley and Sons.

Singh, S.P., Kim, Y-J., Zhang, D. and Yang, D.C. (2016). Biological synthesis of nanoparticles from plants and microorganisms *Trends Biotechnol*. **3**4, 588-599. doi: 10.1016/j.tibtech.2016.02.006

Soin, N., Roy, S.S., Mitra, S.K., Thubdat, T. and McLaughlin, J.A. (2012). Nanocrystalline ruthenium oxide dispersed few layered graphene (FLG) nanoflakes as supercapacitor electrodes *J. Mat. Chem.* 22, 14944-14950. doi: 10.1039/C2JM31226C

Sykes, C. and Stephanopoulos, M. F. (2014) Isolated Pd atoms allow highly selective catalysis of hydrogenation reactions US Dept of Energy science.energy.gov/bes/highlights/2014/bes-2014-06-d/.

Torgeman, E (2017) Biosynthesis of Gold and Palladium Nanoparticles via Bacteria. *M. Chem Thesis* University of Oslo, Norway.

Tran, D.T., Jones, I.P., Preece, J.A., Johnston, R.L., Deplanche, K., and Macaskie L.E. (2012). Configuration of microbially synthesized Pd-Au nanoparticles studied by STEM-based techniques. *Nanotechnol.* 23, 055701. doi:10.1088/0957-4484/23/5/055701

Wang, H., Chen, S., Wang, C., Zhang, K., Liu, D., Haleem, Y.A., Zheng, X., Ge, B. and Song, L. (2016). Role of Ru oxidation degree for catalytic activity in bimetallic Pt/Ru nanoparticles. *J. Phys. Chem. C*, 120, 6569–6576. doi: 10.1021/acs.jpcc.5b12267

Yao, Y., He, D.S., Lin, Y., Feng, X., Wang, Z., Yin, P., et al. (2016). Modulating fcc and hcp ruthenium on the surface of palladium-copper alloy through tunable lattice mismatch. *Angew. Chem. Int. Ed. Engl*. 55, 5501-5505. doi: 10.1002/anie.201601016

van Putten, R.J., van der Waal, J.C., de Jong, E., Rasrendra, C.B., Heeres, H.J., and de Vries, J.G. (2013). Hydroxymethylfurfural, a versatile platform chemical made from renewable resources. *Chem. Rev.* 113, 1499-1597. doi: 10.1021/cr300182k

Venkatesan, S., Kumar, A.S, Jyh-Fu Lee, J-F., Chan, T-S and Zen, J-M (2009) Ruthenium-functionalized nickel hydroxide catalyst for highly efficient alcohol oxidations in the presence of molecular oxygen. *Chem. Comm*. 2009, 1912–1914. doi: 10.1039/B900636B

Yong, P., Mikheenko, I.P., Deplanche, K., Redwood, M.D. and Macaskie, L.E. (2010) Biorefining of precious metals from wastes: an answer to manufacturing of cheap nanocatalysts for fuel cells and power generation via an integrated biorefinery? *Biotechnol Lett*. 32, 1821–1828 doi: 10.1007/s10529-010-0378-6

Yong, P., Liu. W., Zhang. Z., Beauregard, D., .Johns, M.L. and Macaskie, L.E. (2015) One step bioconversion of waste precious metals into *Serratia* biofilm-immobilized catalyst for Cr(VI) reduction *Biotechnol Lett*. 37, 2181-2191 doi: 10.1007/s10529-015-1894-1

Zaleska-Medynska, A., Marchelek, M., Diak M., and Grabowska, E. (2016). Noble metal-based bimetallic nanoparticles: the effect of the structure on the optical, catalytic and photocatalytic properties. *Adv. Colloid. Interface Sci*. 229, 80-107. doi: 10.1016/j.cis.2015.12.008

Zhu, Ju. (2014). Synthesis of Precious Metal Nanoparticles Supported on Bacterial Biomass for Catalytic Applications in Chemical Transformations. *PhD. Thesis*, University of Birmingham, UK.

Zhu, J., Wood, J., Deplanche, K., Mikheenko, I.P., and Macaskie, L. E. (2016). Selective hydrogenation using palladium bioinorganic catalyst. *Appl. Catal. B. Environ.* 199, 108–122. doi: 10.1016/j.apcatb.2016.05.060

Zu, Y.H., Yang, P.P., Wang, J.J., Liu, X.H., Ren, J.W., Lu G.Z., et al. (2014). Efficient production of the liquid fuel 2, 5-dimethylfuran from 5-hydroxymethylfurfural over Ru/Co_3O_4 catalyst. *Appl. Catal. B. Environ.* 146, 244-248. doi: 10.1016/j.apcatb.2013.04.026

Table 1. Materials examined in this study prepared on cells of *Escherichia coli*

		Nominal wt%		Actual wt%		Metal loading per
		Pd	Ru	Pd	Ru	catalyst (actual, wt%)
I	5% bio-Ru	0	5.0%	0	2.6%	2.6%
II	5%/5% bio-Pd/Ru	5.0%	5.0%	5.0%	4.7%	9.7%
III	5%/20% bio-Pd/Ru	5.0%	20%	5.0%	17.5%	22.5%

*The actual metal loading was determined by difference from the Ru(III) provided and that found in the spent solution by assay of the spent solution by assay (see text). Ru(III) sample (0.2 ml, aq.) was added to 0.8 ml of stannous chloride (29.9g $SnCl_2$ in 500 ml conc. HCl) and incubated at 30 ^oC (30 min). Ru(III) was estimated at A_{400} with reference to a Ru(III)-calibration similarly determined and was linear in the region of interest. Note that atomic weights of Pd and Ru are 106.4 and 101.1 respectively; hence sample II was near-equimolar.

Table 2a EXAFS structural parameters of the palladium foil and biogenic Pd-Ru NPs

Sample	Shell	N[a]	R[Å][b]	σ^2 [Å^2][c]	ΔE[eV]
Pd foil*	$Pd\text{-}Pd_1$	12[d]	2.74	0.0047	-0.66
	$Pd\text{-}Pd_2$	6[e]	3.86	0.0086	
	$Pd\text{-}Pd_3$	24[e]	4.78	0.0083	
	$Pd\text{-}Pd_4$	12[e]	5.40	0.0055	
5%Pd20%Ru	$Pd\text{-}O_1$	1.8 ± 0.3	2.10	0.0076	23.2
	$Pd\text{-}O_2$	1.2± 0.1	2.55	0.0076[e]	
	$Pd\text{-}Pd_1$	3.2 ± 0.4	2.75	0.0084	2.62
	$Pd\text{-}Pd_2$	1.6[e]	3.85	0.013	
5%Pd5%Ru	$Pd\text{-}O_1$	1.5 ± 0.2	2.04	0.0059	14.5
	$Pd\text{-}O_2$	1.0 ± 0.1	2.55	0.0059[e]	
	$Pd\text{-}Pd_1$	3.2 ± 0.3	2.75	0.011	-1.56
	$Pd\text{-}Pd_2$	1.6[e]	3.83	0.014	

[a] Errors in coordination numbers are ±25% and standard deviations as estimated by EXAFSPAK;

[b] errors in distance are ±0.02 Å ; [c] Debye-Waller factor; [d] fixed for calculation; [e] Coordination number (N) linked to the N of $Pd\text{-}Pd_1$ path or to $Pd\text{-}O_1$.*Supplementary information Fig S7.

Table 2b EXAFS structural parameters of the ruthenium foil, RuO_2, $RuCl_3$ and biogenic Ru and Pd-Ru NPs samples

Sample	Shell	N[a]	R[Å][b]	σ^2 [Å^2][c]	ΔE[eV]
Ru foil*	Ru-Ru_1	12[d]	2.67	0.004	-1.81
	Ru-Ru_2	6[d]	3.78	0.0028	
	Ru-Ru_3	24[d]	4.68	0.0084	
	Ru-Ru_4	12[d]	5.35	0.0031	
$RuCl_3$	Ru-Cl	5.3 ± 0.3	2.35	0.0059	-2.7
RuO_2	Ru-O_1	2[d]	1.87	0.002	1.80
	Ru-O_2	4[d]	1.99	0.002	
	Ru-Ru_1	2[d]	3.09	0.0068	
	Ru-Ru_2	8[d]	3.56	0.016	
5%Ru	Ru-O_1	1.1 ± 0.1	1.96	0.001	7.5
	Ru-O_2	2.5 ± 0.2	2.1	0.001[d]	
	Ru-Ru	0.5 ± 0.1	2.85	0.01	
5%Pd20%Ru	Ru-O_1	1.8 ± 0.4	2.04	0.001	8.6
	Ru-O_2	1.4 ± 0.3	2.16	0.001[d]	
	Ru-Ru	1.0 ± 0.2	2.77	0.0012	
5%Pd5%Ru	Ru-O_1	1.8 ± 0.1	1.98	0.002	7.4
	Ru-O_2	1.8 ± 0.2	2.15	0.002	
	Ru-Ru	2.0 ± 0.5	2.77	0.019	

[a] Errors in coordination numbers are ±25% and standard deviations as estimated by EXAFSPAK;

[b] errors in distance are ±0.02 Å ; [c] Debye-Waller factor; [d] Coordination number (N) linked to the N of Ru-O_1 path. *Supplementary information Figure S7.

Table 3: XPS peak positions for the various components identified in the high resolution elemental spectra

	Binding Energies as recorded for different samples, eV		
	5%Ru	**5%Pd5%Ru**	**5%Pd20%Ru**
C1s			
C-C/C-H	284.8	284.8	284.8
C-OH/amine	285.7	286.0	286.1
C=O/amide	287.5	287.5	288.0
COOH	288.8	288.7	288.8
Ru3d			
RuO_2/Ru-ligand	281.0, 286.3	280.7, 285.2	280.9, 285.6
$Ru(OH)_3$	281.9, 286.7	281.7, 286.3	281.7, 286.5
$RuCl_3$	--	282.3, 286.7	282.6, 287.0
Ru-NO	283.3, 287	283.3, 287.1	283.2, 287.5
Pd3d			
Pd(0)	--	335.3, 340.8	--
Pd(II)	--	336.7, 342.2	--
P(IV)	--	338.7, 344.1	--
O1s			
Me-Ox	529.6	529.8	529.8
O=C/sulfates	531.0	531.2	531.3
O-C/O-N	532.2	532.1	532.4

O-C(phenolic)/SiO2	533.2	533.2	533.3
H2O ads.	534.4	534.4	534.5

Legends to Figures

Figure 1. EM study of *E. coli* MC4100 cells loaded to 2.6wt% of Ru. A,B: STEM/HAADF images of cell sections. For comparison cells with no added metal are shown in Supplementary Information Fig S2. Magnification of the circled section (inset) shows the presence of nanoparticles located in the membrane (C, inset.) EDX analysis confirmed the presence of Ru in the cell surface NPs (C). Cu is from the EM grid and Os from the stain. Bars are 500 nm (A and B). HAADF image is shown enlarged (D,E) revealing heterogeneity of Ru- NP sizes (E) and NP localization only in the periplasm (width of periplasm ~ 35 nm). HR-TEM analysis of the circled area in E revealed consistent lattice spacing of 0.21 nm (F,G) which can be attributed to either Ru metal or RuO_2 (see text).

Figure 2. HAADF/STEM micrographs of cell sections (A) and magnified view (B) of 5wt%Pd/5wt%Ru NPs. Bars are 500 nm. EDX is shown of the cell surface (C) and intracellular (D) regions. A single cell (E) is shown mapped for areas of Pd (G) and Ru (H) localization and co-mapped to show distribution of the two elements (F). Bars are 200 nm. An enlarged image of F is shown in supplementary information Figure S4 to show overall lack of co-mapping of the two elements on visual inspection but also that intracellular Ru is very evident. An example NP in the cell surface region (I, arrowed; scale bar is 9 nm) was analyzed by transect (J) to show association between Pd (green) and Ru (magenta), especially evident one side of the NP as a skewed distribution. The green arrow (bottom) shows distance across the transect (as a percentage 0-100%) and the Y axis is counts (arbitrary). K and L: HRTEM Images of single NPs from membrane-bound (K) and cytoplasmic (L) NPs showing lattice fringes. Scale bar is 7 nm.

Figure 3. HAADF/STEM micrographs of cell sections showing Pd/Ru NPs (5wt%Pd/20wt%Ru). (A). A higher magnification (B) shows NPs located in the cell surface layers (B inset right) and in the bulk region (B inset left). Lattice spacing of

example NPs in cell wall layers and intracellularly are shown in respectively (C) and (D). Elemental maps (by EDX) of cells show co-localization of Pd and Ru (E) and individually Pd (F) and Ru (G). Figure3 HAADF/STEM micrographs of cell sections showing Pd/Ru NPs (5 wt%Pd/20wt%Ru). (A). A higher magnification (B) shows NPs located in the cell surface layers (B inset right) and in the bulk region (B inset left). Lattice spacing of example NPs in cell wall layers and intracellularly are shown in respectively (C) and (D). Elemental maps (by EDX) of cells show localization of Pd and Ru (E) and individually Pd (F) and Ru (G).

Figure 4a. XANES region of EXAFS spectra of the Pd K-edge in reference compounds (Pd foil and PdO) and for Pd-Ru biogenic NPs samples. **4b**. XANES spectra of ruthenium foil, RuO_2, $RuCl_3$, 5% Ru and for Pd-Ru biogenic NPs samples

Figure 5a: EXAFS spectra of Pd foil and Pd-Ru biogenic NPs samples as well as their corresponding FT. **5b.** EXAFS spectra of Ru foil, $RuCl_3$ and Pd-Ru biogenic NPs samples as well as their corresponding FT.

Figure 6. XPS spectra of (a) Wide Energy Survey Spectra (WESS) for all three samples, (b) high resolution Pd 3d spectra, and fitted components for (c) Low Pd and Ru loading sample and (d) low Pd high Ru loading sample.

Figure 7. Carbon and Ruthenium XPS spectra showing (a) comparison of high resolution C 1s + Ru 3d region for all three samples, (b) C 1s + Ru 3d peak fitting for low Ru only sample, (c) C 1s + Ru 3d peak fitting for low Pd and low Ru loading sample, (d) C 1s + Ru 3d peak fitting for low Pd and high Ru loading sample

Figure 8. Oxygen XPS spectra showing (a) comparison of high resolution O 1s region for all three samples, (b) O 1s peak fitting for low Ru only sample, (c) O 1s peak fitting for low Pd and low Ru loading sample, (d) O 1s peak fitting for low Pd and high Ru loading sample

Figure 9. 5-HMF conversion, DMF yield and selectivity to DMF of the catalyst preparations using (A) synthetic 5-HMF (commercial source), (B) starch and (C) cellulose hydrolysates with 5-HMF extracted into MTHF which was also the solvent for the reaction.

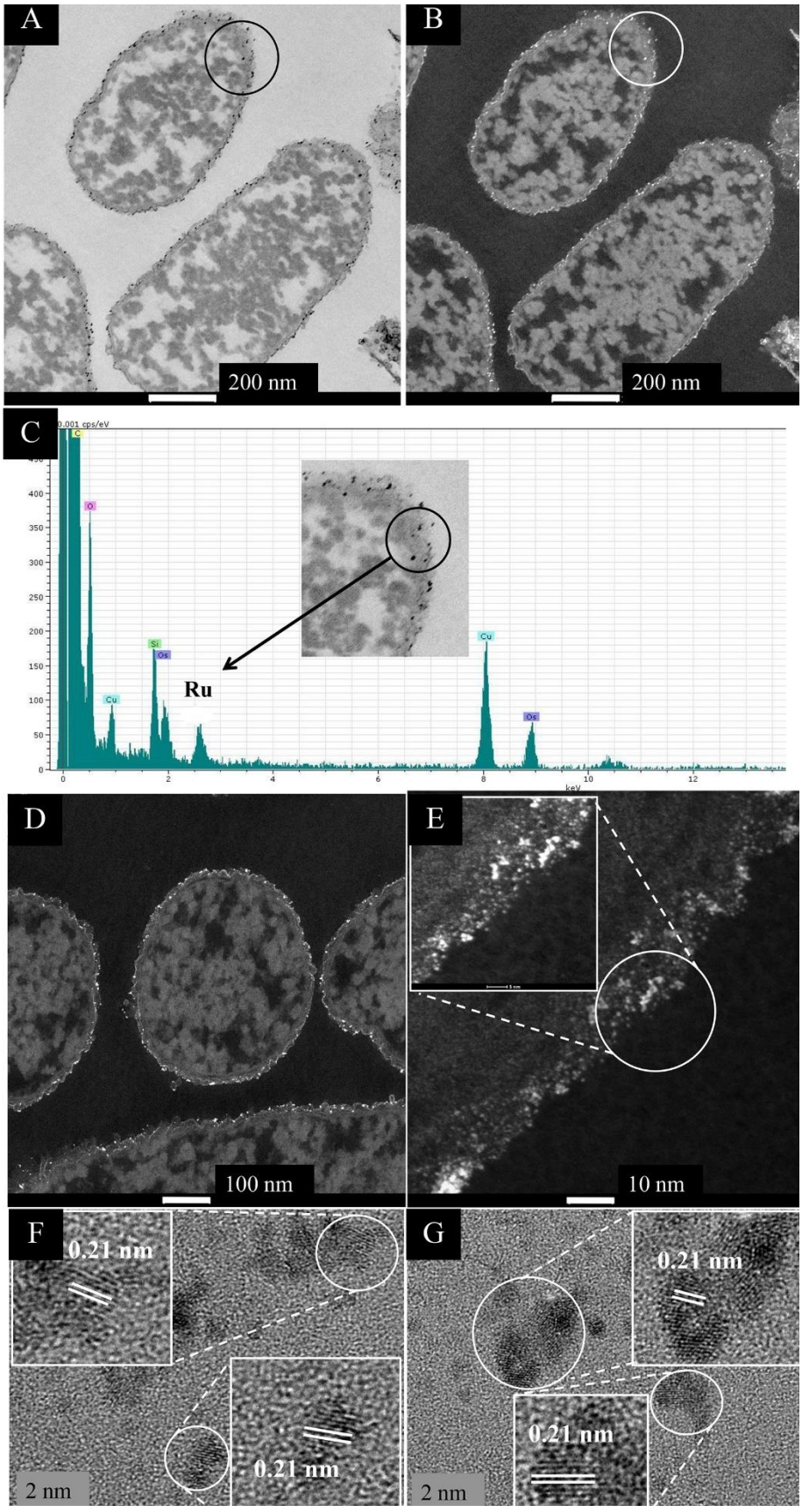
A
200 nm
B
200 nm
C
0.001 cps/eV
C
O
Si
Os
Cu
Ru
Cu
Os
keV
D
100 nm
E
10 nm
F
0.21 nm
0.21 nm
2 nm
G
0.21 nm
0.21 nm
2 nm

Figure 1.

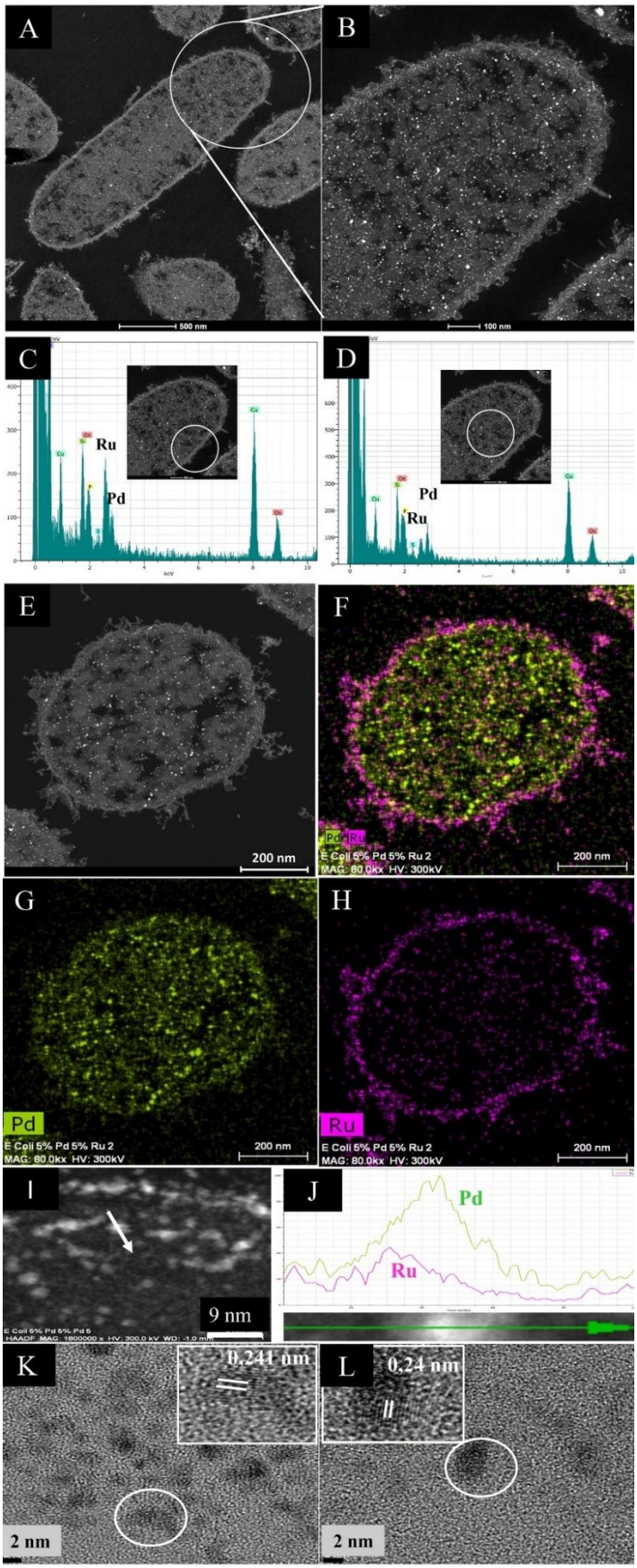
A
B
500 nm
100 nm
C
D
Ru
Pd
Pd
Ru
E
F
200 nm
Pd Ru
E Coli 5% Pd 5% Ru 2
MAG: 80.0kx HV: 300kV
200 nm
G
H
Pd
E Coli 5% Pd 5% Ru 2
MAG: 80.0kx HV: 300kV
200 nm
Ru
E Coli 5% Pd 5% Ru 2
MAG: 80.0kx HV: 300kV
200 nm
I
J
9 nm
Pd
Ru
K
0,241 nm
L
0,24 nm
2 nm
2 nm

Figure 2.

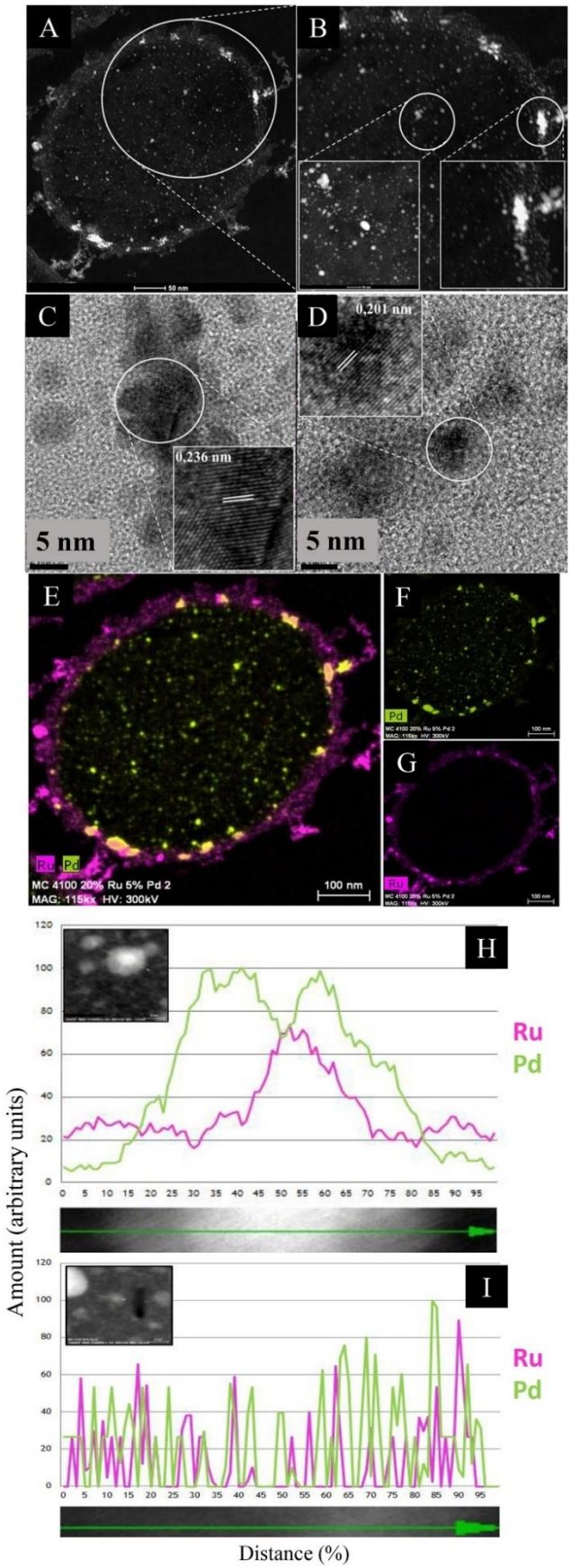
A
B
C
D
0,201 nm
0,236 nm
5 nm
5 nm
E
F
G
Ru Pd
MC 4100 20% Ru 5% Pd 2
MAG: 115kx HV: 300kV
100 nm
Pd
Ru
H
I
Ru
Pd
Amount (arbitrary units)
Distance (%)

Figure 3.

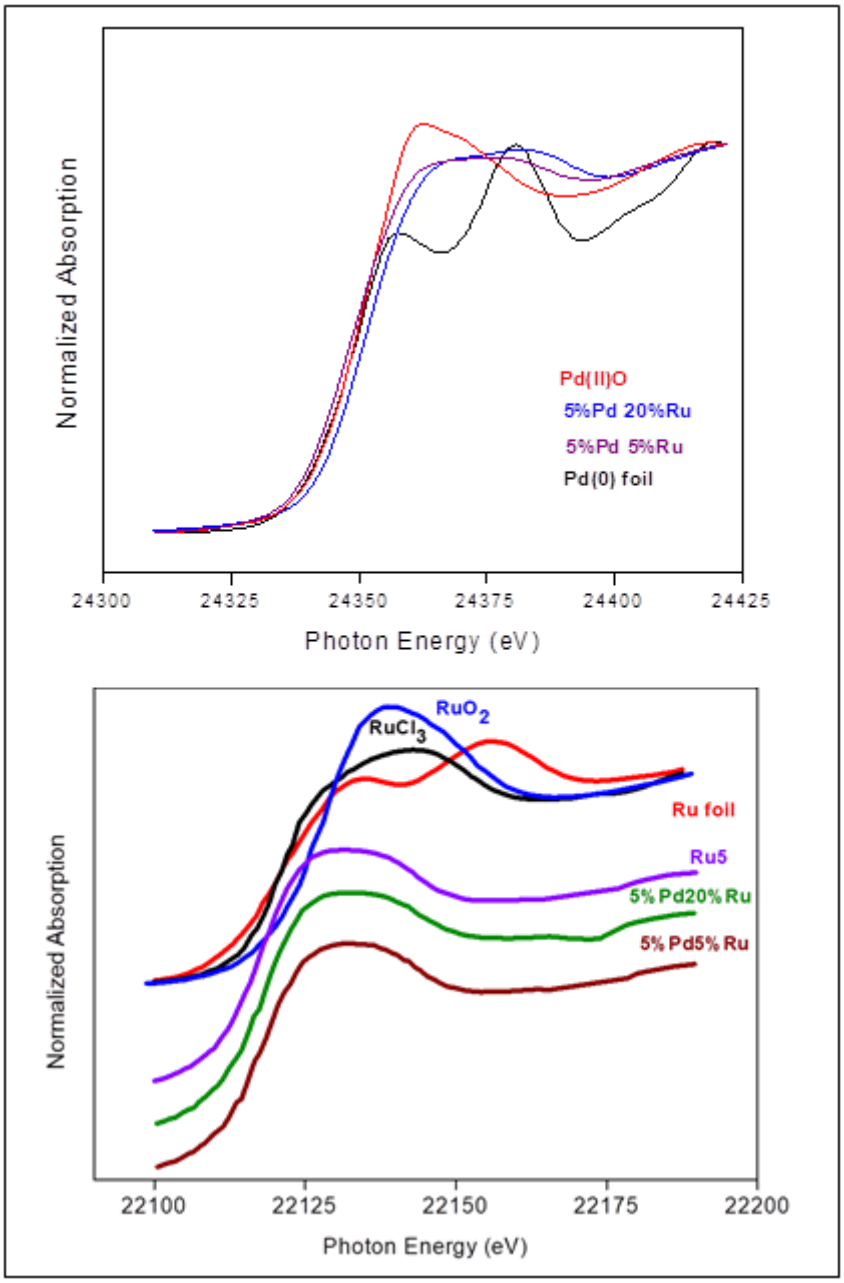
Normalized Absorption
Pd(II)O
5%Pd 20%Ru
5%Pd 5%Ru
Pd(0) foil
24300
24325
24350
24375
24400
24425
Photon Energy (eV)
RuO2
RuCl3
Ru foil
Ru5
5% Pd20% Ru
5% Pd5% Ru
Normalized Absorption
22100
22125
22150
22175
22200
Photon Energy (eV)

Figure 4.

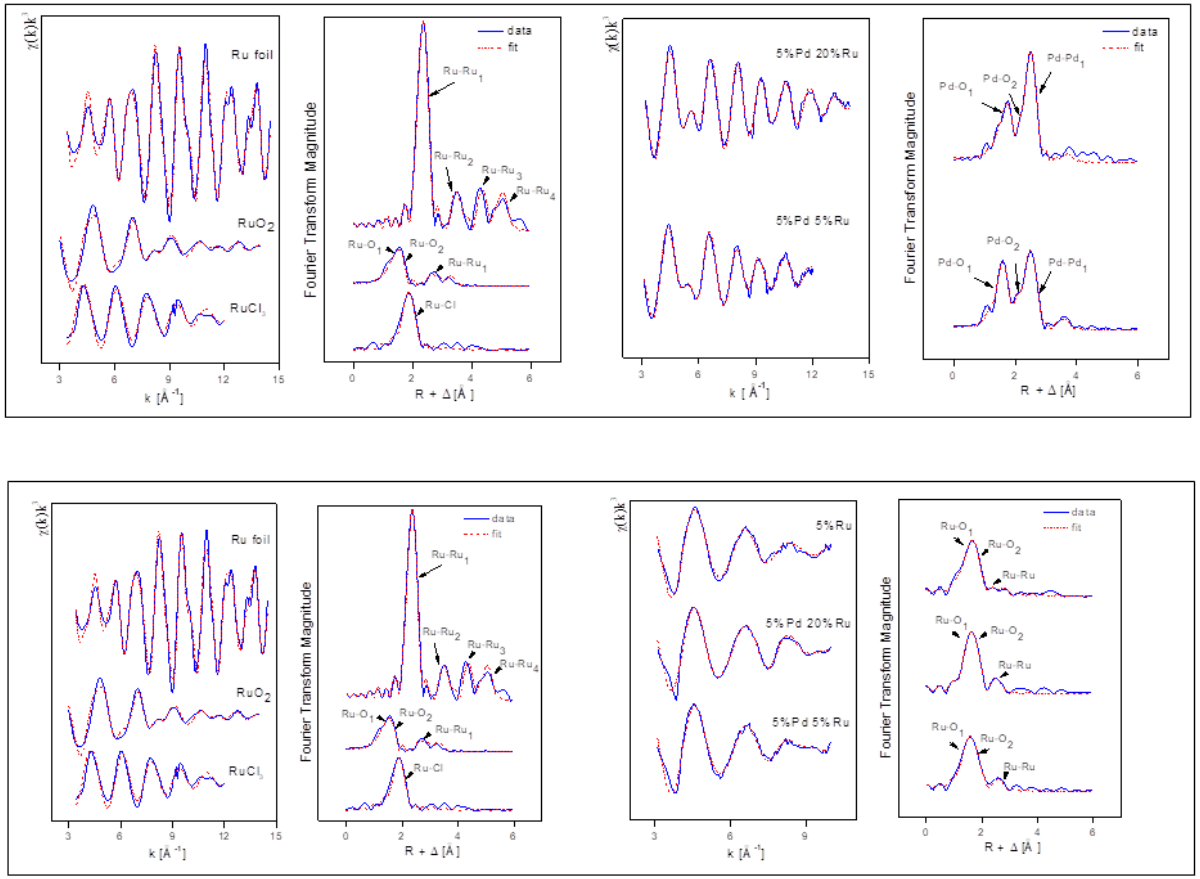
Ru foil
RuO2
RuCl3
k [Å-1]
Fourier Transform Magnitude
data
fit
Ru-Ru1
Ru-Ru2
Ru-Ru3
Ru-Ru4
Ru-O1
Ru-O2
Ru-Cl
R + Δ [Å]
5%Pd 20%Ru
5%Pd 5%Ru
Pd-O1
Pd-O2
Pd-Pd1
5%Ru
Ru-Ru

Figure 5.

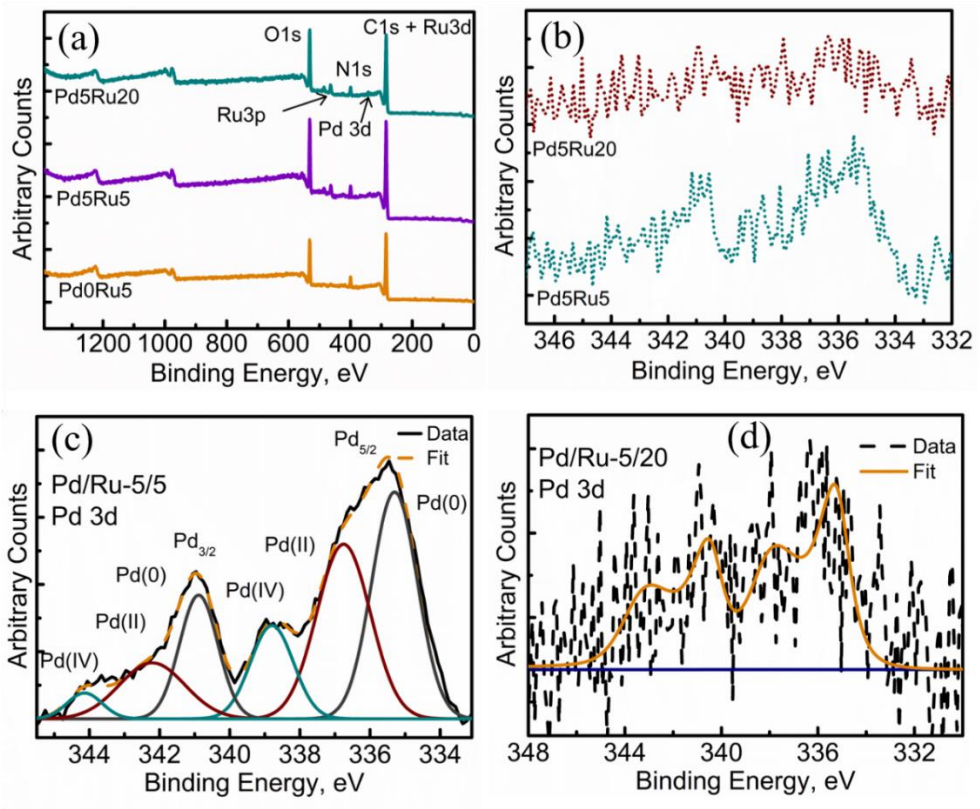

Figure 6.

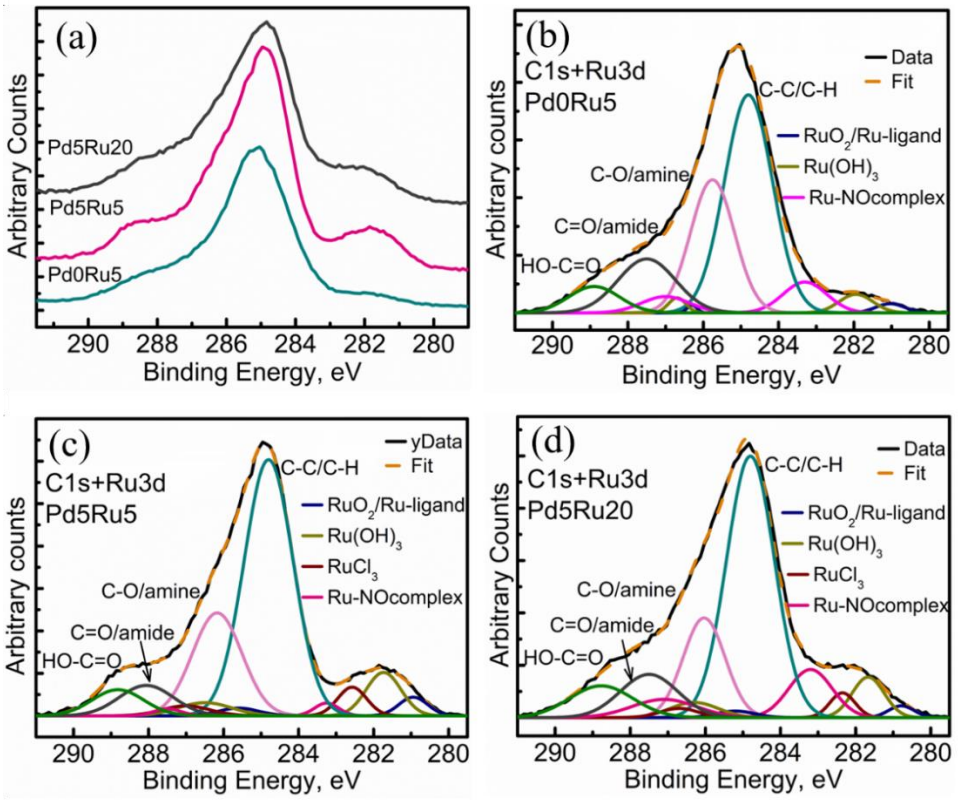

Figure 7.

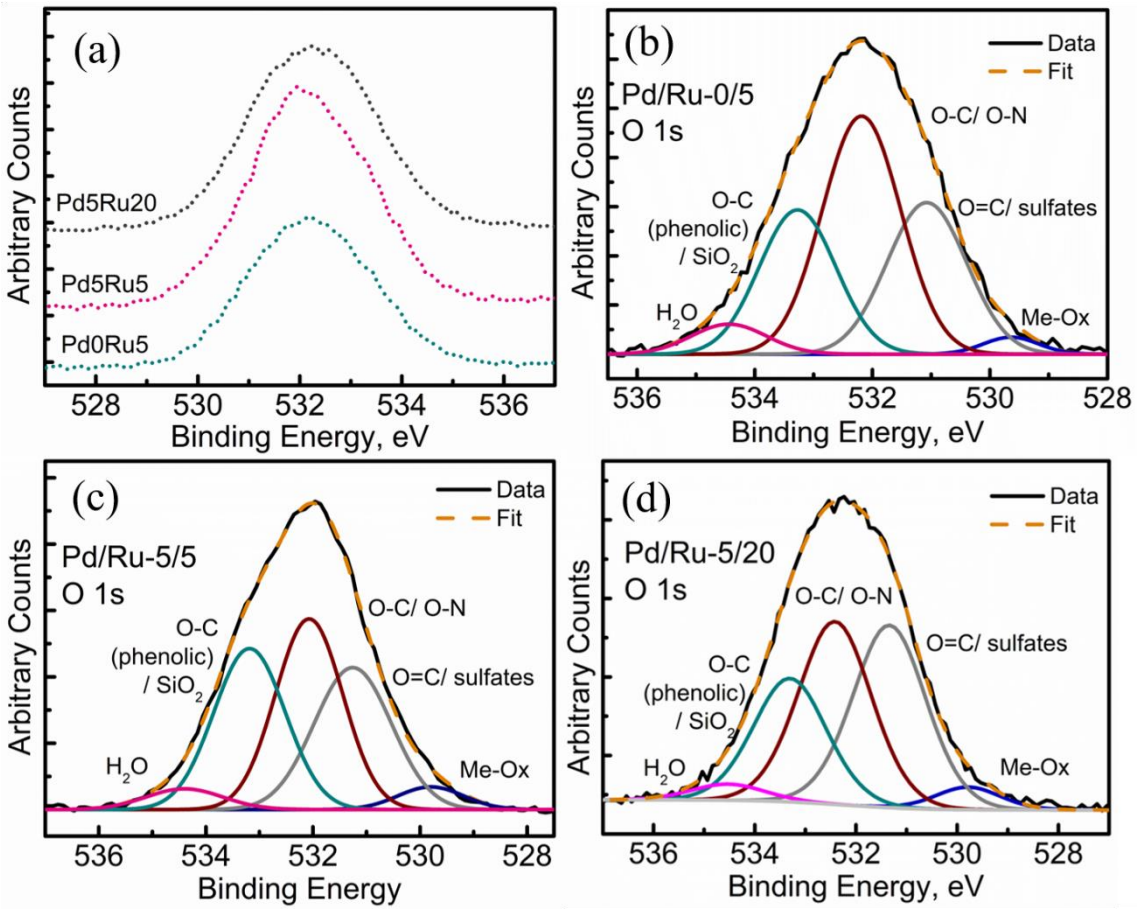
(a)
Arbitrary Counts
Pd5Ru20
Pd5Ru5
Pd0Ru5
528
530
532
534
536
Binding Energy, eV
(b)
Pd/Ru-0/5
O 1s
Data
Fit
O-C/ O-N
O-C
(phenolic)
/ SiO2
O=C/ sulfates
H2O
Me-Ox
536
534
532
530
528
Binding Energy, eV
(c)
Pd/Ru-5/5
O 1s
Data
Fit
O-C/ O-N
O-C
(phenolic)
/ SiO2
O=C/ sulfates
H2O
Me-Ox
536
534
532
530
528
Binding Energy
(d)
Pd/Ru-5/20
O 1s
Data
Fit
O-C/ O-N
O-C
(phenolic)
/ SiO2
O=C/ sulfates
H2O
Me-Ox
536
534
532
530
528
Binding Energy, eV

Figure 8.

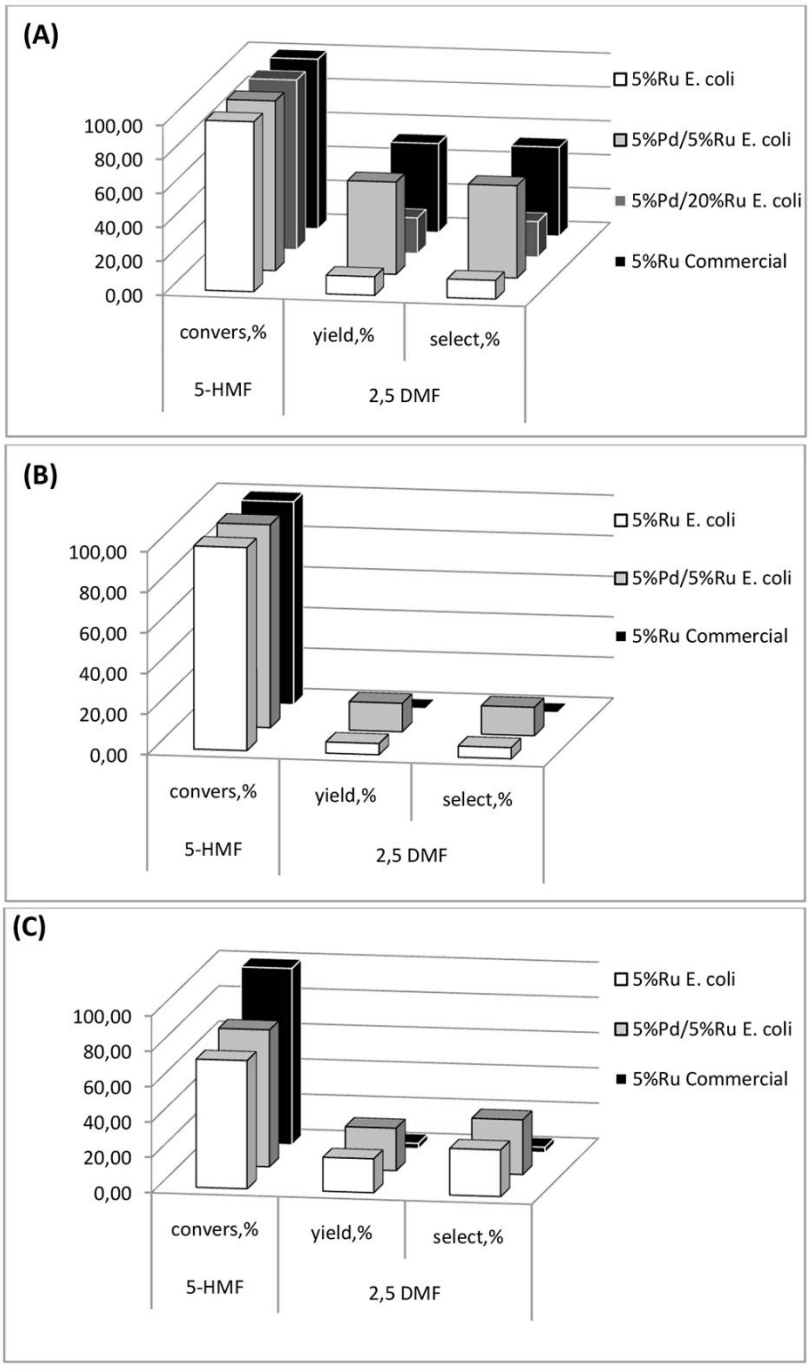
(A)
100,00
80,00
60,00
40,00
20,00
0,00
convers,%
yield,%
select,%
5-HMF
2,5 DMF
5%Ru E. coli
5%Pd/5%Ru E. coli
5%Pd/20%Ru E. coli
5%Ru Commercial
(B)
100,00
80,00
60,00
40,00
20,00
0,00
convers,%
yield,%
select,%
5-HMF
2,5 DMF
5%Ru E. coli
5%Pd/5%Ru E. coli
5%Ru Commercial
(C)
100,00
80,00
60,00
40,00
20,00
0,00
convers,%
yield,%
select,%
5-HMF
2,5 DMF
5%Ru E. coli
5%Pd/5%Ru E. coli
5%Ru Commercial

Figure 9.

Supplementary information

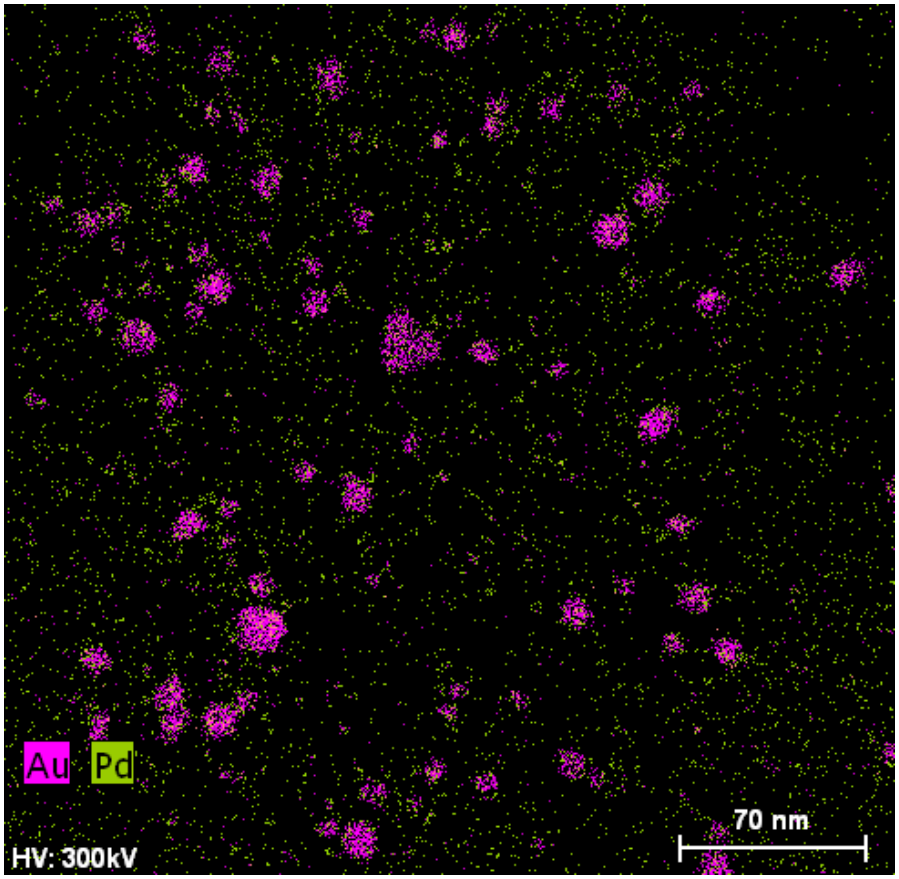

Figure S1. Pd/Au nanoparticles were made according to Deplanche et al (2012). Elemental mapping by EDX (see text) shows atom-arrangements of Pd and Au. Note the Au-core and some intermixing of Au and Pd in the surface layers of the NPs. Loading was 2.5wt%Pd/2.5wt%.

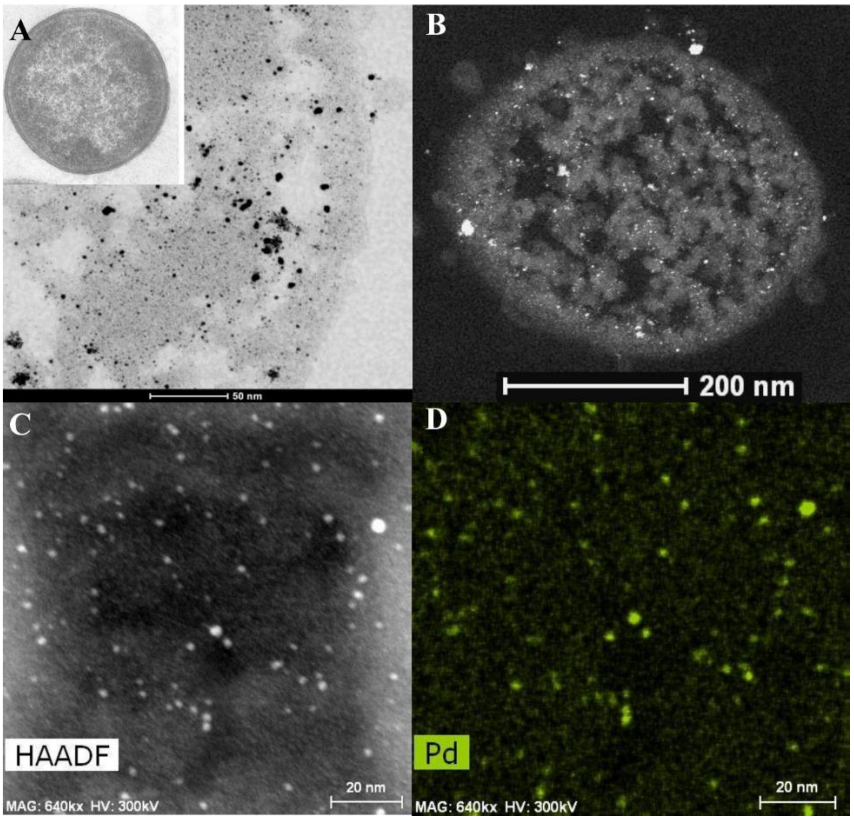

Figure S2. High-resolution HAADF-STEM (High-Angle Annular Dark Field-Scanning Transmission Electron Microscopy) micrographs of *E. coli* (sections). TEM image naked cell (panel A top left) *E. coli* loaded to 5wt%Pd (B). Dark field image. C:,D: high resolution image with elemental mapping of Pd by EDX.

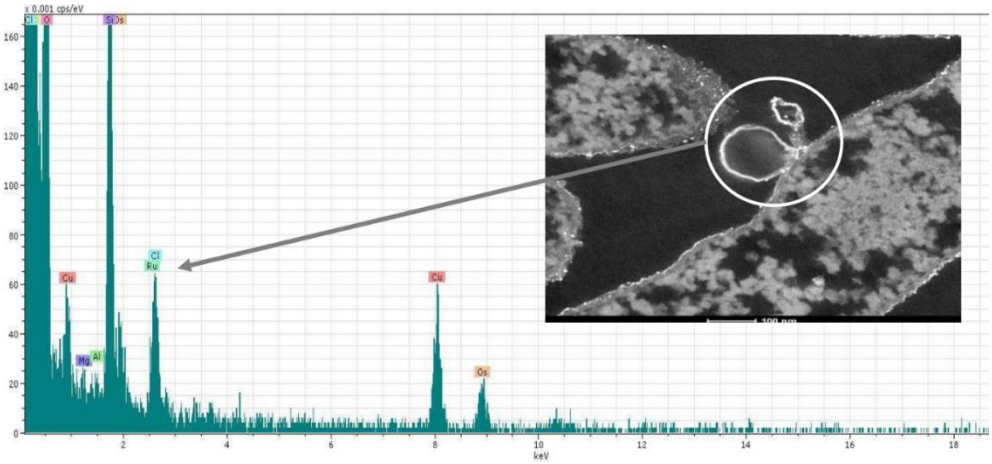

Figure S3. Extruded membrane vesicle from *E. coli* MC4100 loaded with 20wt% Ru (as RuCl3). Note that the X-ray energies of Ru and Cl overlap and hence it is not

possible to differentiate easily between sorbed RuCl3 and other species of Ru. However, XPS data rule out Cl interference in the Ru peak (see text).

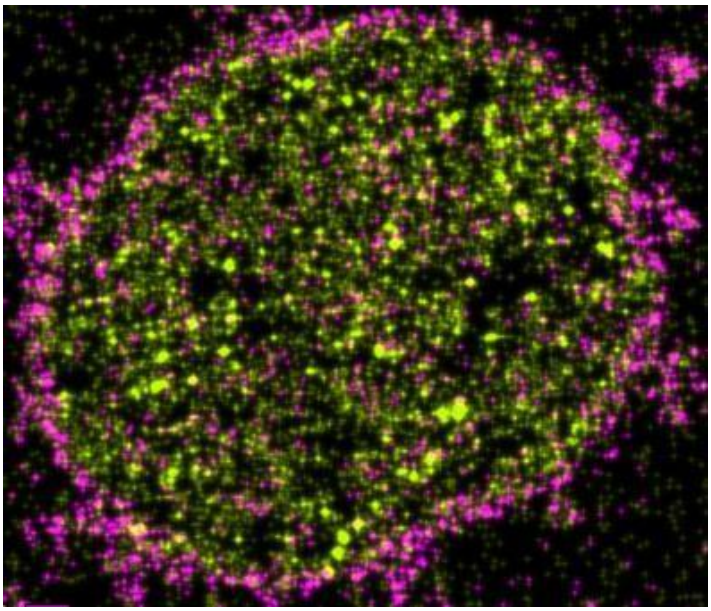

Figure S4. Legend Cross section of single cell loaded to 5wt%Pd/5wt%Ru. Cell diameter is ~ 500 nm.

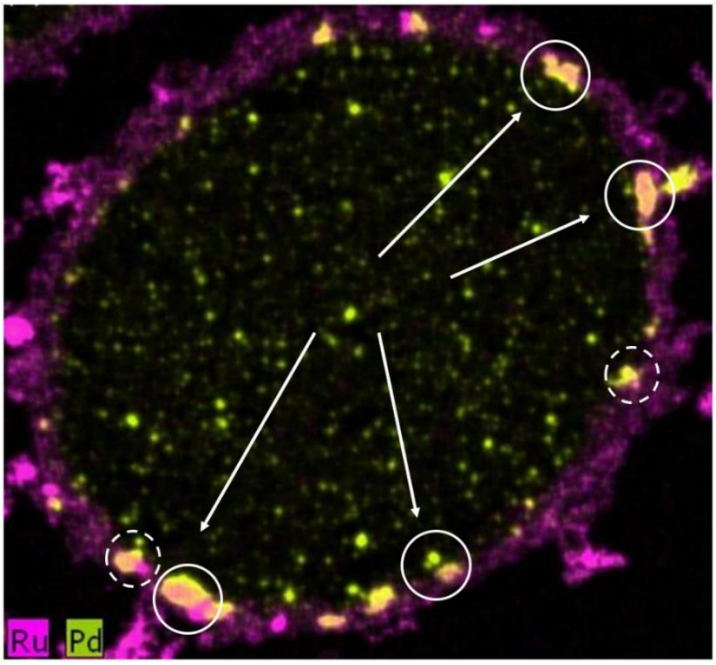

Figure S5. Cross section of single cell loaded to 5wt%Pd/20wt%Ru. Cell diameter is ~ 500 nm. Several core-shell structures are visible (Ru core, Pd shell) (solid circles) as well as 'twined' structures (dashed circle).

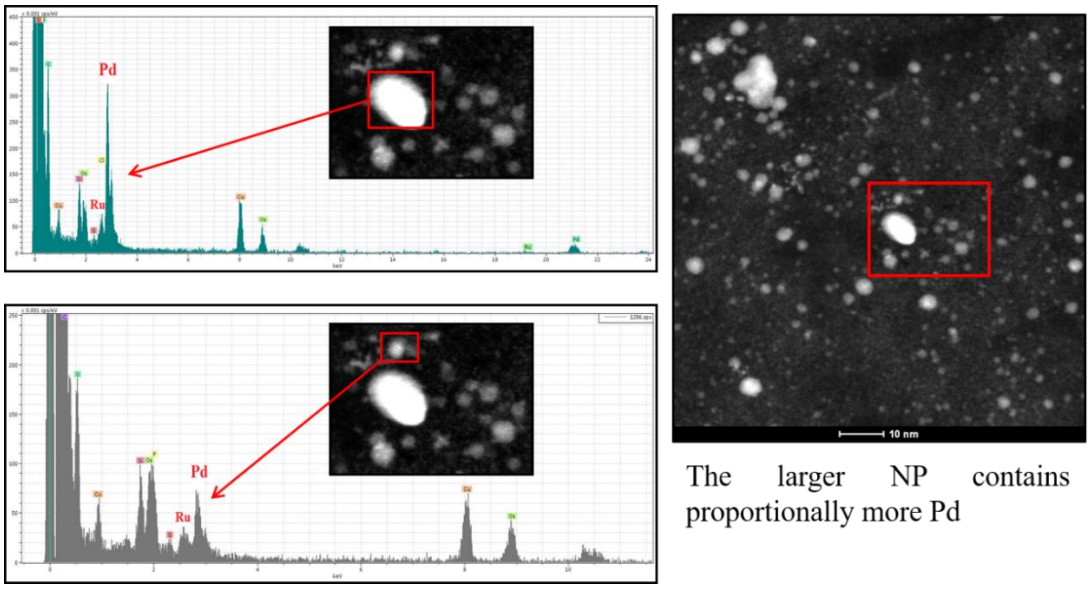

Figure S6. Note presence of Pd and Ru in both large and small NPs.

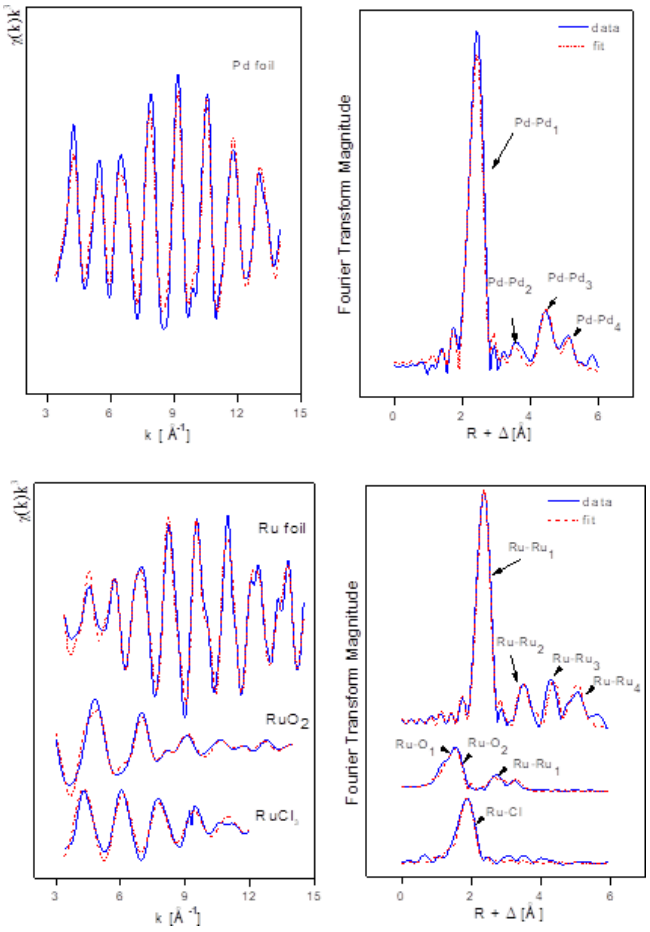

Figure. S7. EXAFS analysis of Pd-foil

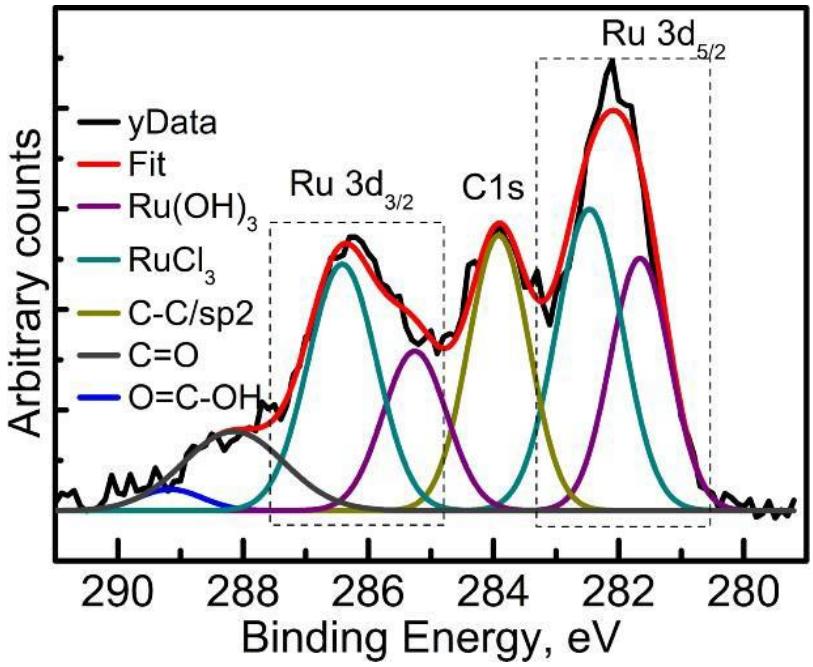

Figure S8. XPS spectra for reference $RuCl_3$ powder used for sample preparation. (Omajali et al. 2019)

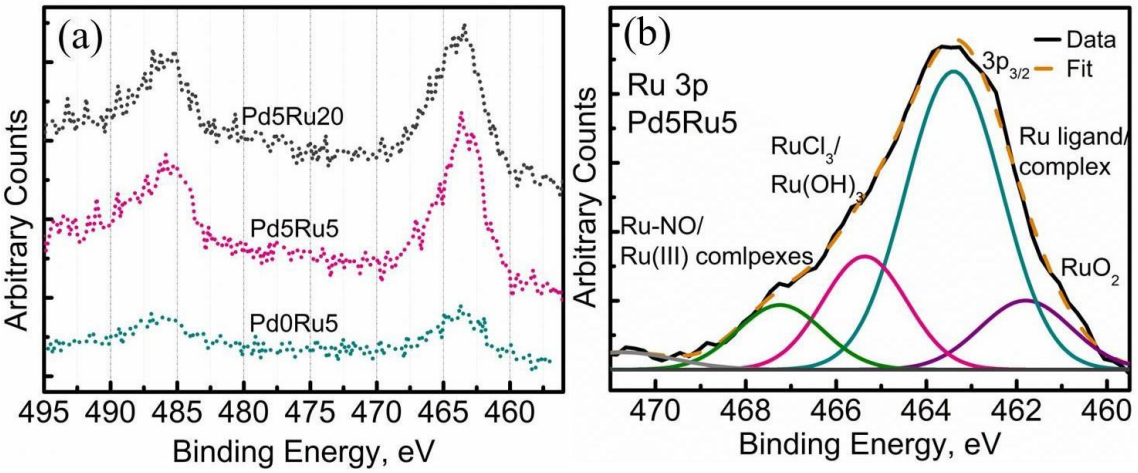

Figure S9: (a) Comparison of the high resolution Ru 3p region for all three samples, (b) Ru 3p3/2 spectra of low Pd and low Ru loading sample deconvoluted into its various component peaks.

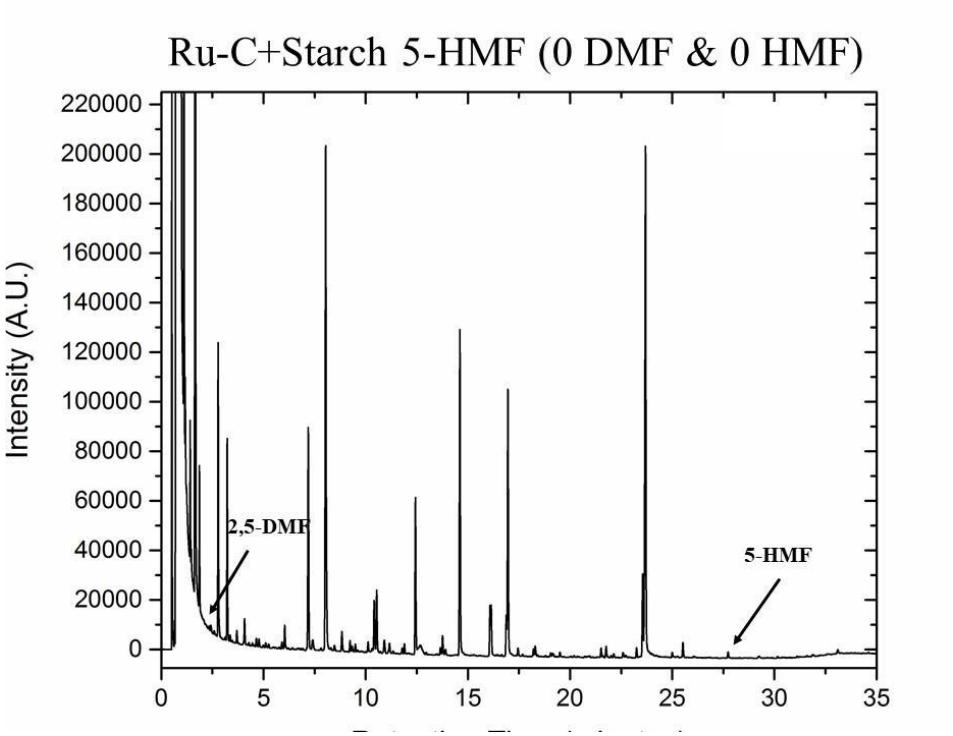

Figure. S10. Example chromatogram showing products of catalytic upgrading of 5-HMF extracted from thermochemical hydrolysis of starch

Table 1. Hydrogenation of synthetic 5-HMF, starch and cellulose into 2,5-DMF over different metal loadings of *E.coli* MC4100.

	5-HMF commercial (Set 1)			5-HMF starch (Set 2)			5-HMF cellulose (Set 3)		
Catalyst	5-HMF conversion (%)	2,5-DMF yield (%)	2,5-DMF Selectivity (%)	5-HMF conversion (%)	2,5-DMF yield (%)	2,5-DMF Selectivity (%)	5-HMF conversion (%)	2,5-DMF yield (%)	2,5-DMF Selectivity (%)
MC4100 5% Ru	100	10.95	10.95	100.00	5.49	5.49	72.57	19.14	26.38
MC4100 5%Pd/5% Ru	100	54.38	54.38	100.00	14.00	14.00	77.57	24.05	31.00
MC4100 5%Pd/20 %Ru	100	20.9	20.9	NOT DONE					
5% Ru on Carbon	100	52.38	52.38	100.00	0.00	0.00	100.00	3.00	3.00

CHAPTER II

Upconversion of cellulosic waste into a potential 'drop in fuel' via novel catalyst generated using *Desulfovibrio desulfuricans* and a consortium of acidophilic sulfidogens

Iryna P. Mikheenko[1#], Jaime Gomez-Bolivar[2#], Mohamed L. Merroun[2], Lynne E. Macaskie[1*], Surbhi Sharma[1], Marc Walker[3], Rachel A. Hand[4], Barry M. Grail[5],D. Barrie Johnson[5], Rafael L. Orozco[1]

[1]School of Biosciences, University of Birmingham, Edgbaston, Birmingham UK.

[2]Department of Microbiology, Faculty of Sciences, University of Granada, Campus Fuentenueva, Granada, Spain.

[3]Department of Physics, University of Warwick, Library Road, Coventry UK

[4]Department of Chemistry, University of Warwick, Library Road, Coventry UK

[5]School of Natural Sciences, Bangor University, Deinol Road, Bangor, Gwynedd, UK

*Correspondence: Prof L.E. Macaskie

L.E.Macaskie@bham.ac.uk

[#] Joint first authors

frontiers in Microbiology

ORIGINAL RESEARCH
published: 10 May 2019
doi: 10.3389/fmicb.2019.00970

Upconversion of Cellulosic Waste Into a Potential "Drop in Fuel" via Novel Catalyst Generated Using *Desulfovibrio desulfuricans* and a Consortium of Acidophilic Sulfidogens

OPEN ACCESS

Edited by:

Iryna P. Mikheenko[1†], Jaime Gomez-Bolivar[2†], Mohamed L. Merroun[2], Lynne E. Macaskie[1], Surbhi Sharma[1], Marc Walker[3], Rachel A. Hand[4], Barry M. Grail[5], David Barrie Johnson[5] and Rafael L. Orozco[1]*

Abstract

Biogas-energy is marginally profitable against the 'parasitic' energy demands of processing biomass. Biogas involves microbial fermentation of feedstock hydrolyzate generated enzymatically or thermochemically. The latter also produces 5-hydroxymethyl furfural (5-HMF) which can be catalytically upgraded to 2, 5-dimethyl furan (DMF), a 'drop in fuel'. An integrated process is proposed with side-stream upgrading into DMF to mitigate the 'parasitic' energy demand. 5-HMF was upgraded using bacterially supported Pd/Ru catalysts. Purpose-growth of bacteria adds additional process costs; Pd/Ru catalysts biofabricated using the sulfate-reducing bacterium *Desulfovibrio desulfuricans* were compared to those generated from a waste consortium of acidophilic sulfidogens (CAS).

Methyl tetrahydrofuran (MTHF) was used as the extraction-reaction solvent to compare the use of bio-metallic Pd/Ru catalysts to upgrade 5-HMF to DMF from starch and cellulose hydrolyzates. MTHF extracted up to 65% of the 5-HMF, delivering solutions respectively containing 8.8 and 2.2 g 5-HMF/L MTHF. Commercial 5% (wt/wt) Ru-carbon catalyst upgraded 5-HMF from pure solution but it was ineffective against the hydrolyzates. Both types of bacterial catalyst (5wt%Pd/3-5wt% Ru) achieved this, bio-Pd/Ru on the CAS delivering the highest conversion yields. The yield of 5-HMF from starch-cellulose thermal treatment to 2,5 DMF was 224 and 127 g DMF/kg extracted 5-HMF respectively for CAS and *D. desulfuricans* catalysts, which would provide additional energy of 2.1 and 1.2 kWh/kg extracted 5-HMF.

The CAS comprised a mixed population with three patterns of metallic nanoparticle (NP) deposition. Types I and II showed cell surface-localization of the Pd/Ru while type III localized NPs throughout the cell surface and cytoplasm. No metallic patterning in the NPs was shown via elemental mapping using energy dispersive X-ray microanalysis but co-localization with sulfur was observed. Analysis of the cell surfaces of the bulk populations by X-ray photoelectron spectroscopy confirmed the higher S content of the CAS bacteria as compared to *D. desulfuricans* and also the presence of Pd-S as well as Ru-S compounds and hence a mixed deposit of PdS, Pd(0) and Ru in the form of various

+3, +4 and +6 oxidation states. The results are discussed in the context of recently reported controlled palladium sulfide ensembles for an improved hydrogenation catalyst.

Keywords: 5-hydroxymethylfurfural upgrade, 5-HMF upgrade, PdRu catalyst, *Desulfovibrio desulfuricans*, waste sulfidogenic bacteria

1 Introduction

The climatic impact of atmospheric CO_2, a legacy of the use of fossil fuels, is now accepted and stricter worldwide environmental legislation has promoted global interest in developing carbon-neutral fuels from biomass (Cadez and Czerny, 2016; Al-Amin et al., 2015; Chu & Majumdar, 2012), consistent with increasing value creation from natural resources (e.g. renewable biomass) within the concept of a circular economy (Govindan and Hasanagic, 2018).

Biomass sources include wood, plants, agricultural and energy crops, aquatic plants and food processing wastes, e.g. stems and husks. Although biomass-derived fuels offer a renewable and sustainable potential alternative to fossil fuels biomass conversion technologies are usually needed. These are generally grouped into two categories: biochemical and thermochemical. The former depends on the relatively slow action of microorganisms and/or enzymatic catalysts at moderate temperatures (e.g. up to ~ 60 ^{o}C) which usually follow a mechanical, thermal or chemical pre-treatment of the native biomass (Modenbach and Nokes, 2013; Haldar et al., 2016). The latter require high temperatures and pressures (e.g. 200 - 375°C and 40 – 220 bar respectively) with or without the presence of metallic/inorganic-catalysts to obtain products from different biomass sources (Gollakota et al., 2018) in a matter of hours. Less aggressive methods such as the Hydrothermal Hydrolysis (HTH) processes (e.g. Dogaris et al., 2009; Vardon et al., 2012) provide a route for wet biomass (e.g. algae (Kunwar et al., 2017)) conversion, forestalling the energy demand of drying. The process uses water as the reaction solvent, this being compatible with downstream fermentation of the product.

Starch and cellulose are the predominant polymeric materials in biomass. Depending on the reaction conditions their HTH generates hydrolyzates containing mainly sugars (e.g. glucose, fructose) for onward fermentation into gaseous fuels, significant amounts of 5-hydroxymethylfurfural (5-HMF; a fermentation inhibitor) and smaller amounts of other sub-products resulting from further degradation of 5-HMF during the reaction (Palmquivst and Hahn-Hägerdal, 2000).The sugars are readily fermented (e.g. to make biohydrogen) following toxic 5-HMF removal (Orozco 2012; Redwood et al., 2012);

however, at the same time the latter co-product can provide a potential resource in parallel to the primary fermentation process.

5-HMF is a versatile platform chemical that offers potential pathways to the synthesis of valuable products including polymers, fine chemicals and biofuels (Yang et al., 2017). Hence it is important to explore and evaluate these routes to mitigate the shortfall of the HTH process economics mainly attributed to the high-heat requirement (Gollakota et al., 2018) for the thermochemical biomass processing, as well as the high-power demand of biomass comminution upstream. For example, the energy consumption to mill *Miscanthus* (moisture content of 15%) to 4 mm was determined at 184 kJ/kg of dry matter (Maio et al., 2011). Gollakota et al. (2018) noted that an efficient algal feedstock-HTH process (@ 280°C, 15 min) consumed ~15% of the energy contained in the feedstock thereby yielding a potential energy efficiency of ~85% (Gollakota et al., 2018). By using algal biomass comminution is not required. Other studies calculated an energy efficiency of 63.9% for thermal hydrolysis (300 ^{o}C) in a cornstalk-HTH (Shi et al., 2013).

Among the possibilities for 5-HMF conversion into valuable products2,5 dimethylfuran (DMF) is a biofuel of particular importance due to its high energy density (30 MJ/L) (similar to gasoline: 31.9 MJ/L), its high octane number, low oxygen content (O/C 0.17), its immiscibility with water and its affinity to blend with fossil-derived fuels and ethanol (Thananatthanachon et al., 2010, Zhang et al., 2017, Roman-Leshkov et al., 2007) as well as its proven use in a direct-injection spark-ignition engine (Dang et al., 2016). DMF is not water soluble, has a boiling point of 92-96^{o}C and its evaporation requires approximately one-third less energy than the evaporation of ethanol (Silva and Aznar, 2014) which is widely used as a biofuel despite the energy demand of distillation.

The catalytic upgrading of 5-HMF to DMF, proposed as a route to making liquid fuel from carbohydrates (Roman-Leshkov et al., 2007) proceeds in the absence of water as the latter negatively impacts in the hydrogenation reactions, decreasing yields and selectivity (Liu et al., 2015). HTH is performed in an aqueous system, hence an ideal method would both separate the 5-HMF from the fermentable aqueous phase (detoxifying it) and maximise its catalytic upgrading to DMF. The separation of 5-HMF from the hydrolysis products in the aqueous phase is a challenge that must be overcome in order to detoxify

the fermentation stream and valorize the 5-HMF component into local power, with the extraction and catalytic upgrading steps in a common solvent. The selection and evaluation of solvent for this dual role was the first aim of the study, considering two main factors: The 5-HMF-solvent partition coefficient (P_{HMF} [$wt\%_{org}/wt\%_{aq}$]and the solvent compatibility with the catalytic upgrading reactions. Partition coefficient (P_{HMF}) quantifies the equilibrium distribution of a solute between 2 immiscible phases and is a measure for solvent extraction efficiency. The higher the P_{HMF} value the higher the extraction efficiency.

Tetrahydrofuran (THF) is an efficient solvent for the catalytic transformation of 5-HMF to DMF in the presence of ruthenium catalysts, delivering DMF yields up to 95% (Hu et al., 2014). However, its miscibility with water limits its application here. Methyl tetrahydrofuran (MTHF) is a solvent produced from renewable resources (Aycock, 2007) with similar properties to THF (relatively high partition coefficient (P_{HMF} of 2.1)) and low water solubility (4g/100mL)). MTHF has replaced THF in several organometallic-catalyzed reactions (Blumenthal et al., 2016; Aycock, 2007). Moreover, the presence of sugars (glucose and fructose) in the hydrolyzate can enhance the extraction capacity of the MTHF and induce phase separation. For example, with the addition of 10, 30 or 50 wt% of fructose the partition coefficient increased by > 40 to 50% for MTHF (Blumenthal et al., 2016). MTHF delivers clean organic−water phase separations and, unlike THF, it can be used to dry the product for a subsequent reaction or isolation step (Aycock, 2007). The second focus of this study is the catalytic upgrading of 5-HMF to DMF and the scope for using novel biogenic metal catalysts for this reaction. Other work reports that ruthenium catalyst can achieve this conversion; (Lei et al., 2014; Hu et al., 2014; Nagpure et al., 2015). Hu et al. (2014) reported DMF yields of 95% while Nagpure et al. (2015) showed that a catalyst containing < 0.6 wt% Ru converted 5-HMF to 58 % yield of DMF in propanol. In parallel, Lei et al. (2014) obtained 95% yield of DMF (in THF; 200 ^{o}C in 2h) while the direct hydrogenation of carbohydrate-derived HMF into DMF was also achieved, with DMF separation from the reaction mixture by distillation (Lei et al., 2014).

Other studies focused on high yields and selectivity towards DMF using ‘classical’ mono and also bimetallic catalysts, including Pd and Ru (Hansen et al., 2012; Zu et al., 2014; Nishimura et al., 2014; Luo et al., 2015; Mitra et al., 2015) as well as less conventional

catalysts (Gawade et al., 2016), which include biologically-derived materials. A preliminary study using cells of *Bacillus benzeovorans* as the catalyst support noted that, while classical 5 wt% Pd on carbon catalysts achieved 95% conversion of commercial 5-HMF (yield was 25% DMF in formic acid/trimethylamine), a bimetallic bio-catalyst of 2.5wt%Pd/2.5wt%Ru achieved 97% conversion with 50% selectivity (Omajali, 2015). In propanol the respective DMF yields (at 94% conversion) for the chemical Pd/C and bio-Pd/Ru were 33% and 42% respectively (Omajali 2015) but detailed studies using THF as the solvent were not undertaken. As far as the authors are aware, most studies have focused on up-conversion of commercially-obtained 5-HMF whereas this study focuses on 5-HMF within the product mix obtained from starch/cellulose thermochemical hydrolysis. A single stage reaction hydrolysis and up-conversion reaction formed the second aim of the study.

A commissioned consultancy report (Catalytic Management Technology Ltd, unpublished) noted that for a new catalyst to achieve market acceptance it must be better than commercially available comparators or be cheaper to produce. For the latter, biogenic catalyst can be biorefined from metallic wastes into active neo-catalysts (Yong et al., 2010; Murray et al, 2017; 2019). However, growing cultures of bacteria solely for this purpose lowers the cost-effectiveness, and using 'second life' bacterial cells left over from another biotechnology process has therefore been used to make active bio-metallic catalyst for a fuel cell (Orozco et al., 2010) and as a hydrogenation catalyst (Zhu et al., 2016).Therefore, the third aim of the study was to evaluate the potential using a consortium of acidophilic, sulfidogenic (CAS) bacteria left over from an unrelated biotechnology process for its ability to make bio-Pd/Ru catalyst for upgrading of 5-HMF, and to compare this with using a pure culture of the sulfate-reducing bacterium *Desulfovibrio desulfuricans*, which was purpose-grown for the application.

The primary biotechnology process for the CAS uses H_2S generated in a low pH sulfidogenic bioreactor to selectively remove and to recover metal resources (as sulfide precipitates) from metal-rich mine water wastes (Nancucheo and Johnson, 2012; Santos and Johnson, 2017; Santos and Johnson, 2018). The bioreactors are operated in continuous flow mode and generate an effluent liquor that contains both bacterial cells and some residual sulfide A full-scale system has been estimated to generate several

hundred litres of waste liquor/day (Murray et al., 2019). The bacteria, like *D. desulfuricans*, would contain residual biogenic sulfide, usually considered as a potent catalyst poison (Dunleavy, 2006). Against this, classical sulfidogenic *Desulfovibrio*(washed) cells produced a bio-Pd(0) catalyst that was as effective as that made by (non-sulfidogenic) *E. coli* (Deplanche et al., 2014) and also produced a better fuel cell electrocatalyst (Yong et al., 2007). A recent studyhas highlighted the role of palladium sulfide modifier to a Pd catalyst which was superior in the semi hydrogenation of alkynes (Alabani et al., 2018). Analysis of bio-Pd(0) on *D.desulfuricans* confirmed the presence of sulfur by energy dispersive X-ray microanalysis, while the outermost ~ 10nm layer of washed cells was shown to comprise 1.3% atomic concentration of sulfur as determined by X-ray photoelectron spectroscopy (Omajali 2015); the binding energy (eV) of peak positions for S2p was shifted from 165.39 to the lower binding energy of 163.97 after addition of PdII) (Omajali 2015), which suggests the formation of a Pd-S bond (Gotterbarm et al 2012). Hence this study sought to compare bio-Pd/Ru from the two types of sulfidogenic culture, placing the findings in the context of what is known about the 5-HMF upgrading reaction and the potential for 'in process' energy generation within an integrated biorefinery and in the context of current developments in 'classical' hydrogenation catalysts.

2 Materials and methods

2.1 Thermo-hydrolysis reactions

The method for thermal hydrolysis was as described previously (Orozco et al., 2012). The batch reactor system for starch/cellulose hydrolysis comprised a bench top reactor (100 mL; Parr series 4590 pressure; maximum operating conditions: 200 bar;350 °C) of Type 316 Stainless Steel equipped with a heat/agitation controller **(**Parr 4848). All chemicals in the study were analytical grade from Sigma-Aldrich (potato starch, cellulose powder, 5-HMF and 2 methyl-tetra-hydro-furan).

For hydrolysis, starch (7.2 g) or cellulose (5.1 g) was suspended in de-ionized water (final reactant volume of 60 mL for starch; 120 g/L and 70 ml for cellulose; 72.9 g/L or as otherwise stated) and charged into the reactor for hydrolysis. The reactor was sealed and

purged with N_2 three times before pressurising to 30 bar (N_2) and heating to the set-point temperature (220°C for starch; 260° for cellulose) with agitation (300 rpm). Reaction conditions were held for 15 min before cooling to 35°C by submersion in cold water. The hydrolyzate was separated (after depressurization) from the solid residue (vacuum filtration; filter paper Fisher brand QL100) or by centrifugation (10,000 rpm; 10 min). The reactions were repeated as required and pooled to produce sufficient quantities of starch and cellulose-derived 5-HMF. Hydrolyzates were kept at 4°Cbefore analysis using a GC (Shimadzu 2010 with an autosampler AOC-20S, a FID detector and ZB-Wax column (30m x 0.25mm × 0.25µm); injection volume 1 µL; inlet temperature 260°C; injector temperature 300°C; detector temperature; 300 °C, inlet pressure 100 KPa; split ratio of 100:1 with H_2 carrier gas at a flow rate of 1 mL/min). The heating regime was 0 min GC temp 100°C; 10 min GC temp 200°C; 22 min GC temp 200°C and 25 min GC temp 250°C.Reaction solid residues were not quantified nor analyzed.

2.2 Solvent extraction of 5-HMF

The method for 5-HMF extraction was based on the experimental determination of partition coefficients at batch and continuous conditions according to Blumenthal et al. (2016). In this study the mass transfer of 5-HMF from the aqueous to the organic phase was faster at 60°C and concentrations of 5-HMF in the range between 1-5wt% in the aqueous feed had little effect on the partition coefficients (not shown). The produced starch and cellulose hydrolyzates respectively were mixed in equal volumetric proportions with 2-MTHF (organic extraction solvent) in an Erlenmeyer flask (magnetic stirrer, 200 rpm, 60°C (temperature-controlled water bath); 20 min). After extraction aqueous and organic phases were separated into: the top organic phase ‘supernatant’ and the bottom aqueous phase ‘filtrate’. Both phases were sampled and kept at -20°C before analysis by GC. Solvent extraction efficiency was calculated according to equation 1:

$$\text{Extraction efficiency (\%)} = \frac{\text{moles of HMF in supernatant}}{\text{moles of HMF in hydrolysate}} * 100 \qquad (1)$$

2.3 Catalyst preparation

2.3.1 Bacterial cultures

Desulfovibrio desulfuricans NCIMB 8307 was grown sulfidogenically as described previously (Omajali et al., 2015). Following harvest and washing (9,000 x g; 4 ^{o}C; washed three times in 20 mM MOPS-NaOH buffer, pH 7.0) the cells were left at 4 ^{o}C under nitrogen until use. The consortium of acidophilic sulfidogenic (CAS) bacteria (waste culture) was taken from a continuous metal waste treatment process as described previously (Murray et al., 2016) with the H_2S off-gas diverted into metal sulfide recovery from minewater. Two batches of CAS ~15 litres each, were collected independently over several days, harvested, washed as for *D. desulfuricans* and stored as a concentrated suspension at 4^{o}C under air, routinely overnight, before metallization. Using terminal restriction enzyme fragment length polymorphism (T-RFLP) analysis, as previously reported for this microbial consortium (Santos and Johnson, 2017), the CAS was found to comprise 66% *Desulfosporosinus acididurans* (Sánchez-Andrea et al., 2015) 7% Firmicute strain CEB3, 10% *Acidocella aromatica* strain PFBC, 10% *Actinobacterium* AR3 and 7% *Acidithiobacillus ferrooxidans*. Cells were harvested and washed as for *D.desulfuricans* and left under N_2 before metallization.

2.3.2 Preparation of monometallic and bimetallic bionanoparticles

Commercial metal salts ($NaPdCl_4$ and $RuCl_3$) were from Sigma-Aldrich, as were 5wt% Pd and 5wt% Ru on carbon catalysts and commercial 5-HMF (≥ 99%) and 2,5-DMF (99%).For monometallic bio-Ru catalysts cell suspensions were suspended in 1 mM Ru (III) ($RuCl_3.2H_2O$ solution; pH 2, in 10 mM HNO_3) to the required biomass/metal ratio for the desired loading (wt%) and left for 30 min (30 ^{O}C) for metal uptake by the cells. $H_2$was bubbled for ~ 1h through the Ru(III)-cells suspension then was left under H_2 (sealed bottle; 180 rpm agitation; 30^{O}C) for 96h, with residual Ru(III) in solution analysed by the tin chloride method (Charlot, 1978; Deplanche et al., 2010) to estimate the actual wt% loading on the cells (all of the Pd was removed onto the cells in the first step).

Synthesis of bimetallic Pd/Ru used, sequentially, a 2 mM Pd (II) and a 1 mM Ru (III) solution by the method of Deplanche et al. (2012) with modifications: 2 mM Pd (II) solution was reduced to Pd(0) on the cells under H_2 (30 min; complete removal (by assay) of residual soluble Pd(II)) to give 5wt% bio-Pd. The bio-Pd was washed twice (distilled water) and then added to the required volume of 1 mM $RuCl_3$ solution to give a final loading of (nominally) 5 wt% Pd/5wt% Ru. The Bio-Pd/Ru mixture was left to stand (1 h) then saturated with H_2 (as above; 180 rpm agitation, 30^{o}C; 96h). Residual Ru(III) was estimated by assay (above). The presumptive bimetallic bio-NPs were washed three times (distilled water) and once with acetone (9,000 x g, 15 min, 4^{o}C) air- dried and ground manually in a pestle and mortar.

2.4 Scanning electron microscopy (SEM), high resolution scanning-transmission electron microscopy (STEM) with HAADF (high-angle annular dark field) detector, energy dispersive X-ray analysis (EDX) and determination of lattice spacing.

For STEM samples were fixed in glutaraldehyde (2h; 4 ^{o}C; 2.5% (w/v) in 0.1 M cacodylate buffer, pH 7.2), and, after washing (three times with the cacodylate buffer), were stained (1% aq. osmium tetraoxide). Thin sections were prepared for TEM as described previously (Deplanche et al., 2012), and electron opaque regions were examined by STEM and EDX using a FEI image Cs-corrector configuration Titan^{TM} G2 60-300 STEM microscope equipped with HAADF detector, (accelerating voltage of 300 kV), with lattice spacings determined using "ImageJ" through profiling of high resolution HAADF-STEM images. For examination of the CAS mixed population by scanning electron microscopy (SEM) samples were mounted on aluminium stubs using carbon adhesive tape and coated with carbon (EMITECH K975Xcoater). The coated samples were observed using a Quanta 400 FEI ESEM operating at an accelerating voltage of 5 kV.

2.5 X-ray photoelectron spectroscopy (XPS) of material at cell surfaces

A few mg of samples were air-dried. XPS was used for analysis of surface chemical composition and determination of metal oxidation state (Kratos Axis Ultra DLD

spectrometer; Kratos Analytical),as described by Omajali (2015), at room temperature. Illumination of samples used an Al Kα x-ray source, with emitted photoelectrons collected using a hemispherical electron analyser. Survey spectra were acquired at a pass energy of 160 eV (resolution approx 2.0 eV), with the pass energy being reduced to 20 eV (resolution 0.4 eV) for the acquisition of high resolution core level spectra. As the samples were insulating, a charge neutralizer was used to prevent surface charging with a low energy electron beam directed on to the sample during XPS data acquisition. A take-off angle of 90° was used, to probe a depth of approx. 5-10 nm to examine bio-NPs located at the outermost cell surfaces. Generated data were converted into VAMAS format and analyzed (CasaXPS package: Fairley, 2013) employing Shirley backgrounds, mixed Gaussian-Lorentzian (Voigt) line-shapes and asymmetry parameters where appropriate. All binding energies were calibrated to the C 1s peak originating from C-H or C-C groups at 284.8 eV. References were commercial 5 wt% Pd on carbon and commercial $RuCl_3$.

2.6 Synchrotron-based radiation-scanning X-ray microscopy (SRSXM) study of elemental Pd, Ru and light elements in bio-Pd/Ru

Samples prepared as for TEM, thin-sectioned (0.25 μm) using a diamond knife on a Reichert Ultracut S ultramicrotome and stained as above, were examined using scanning X-ray microscopy (beamline IO8, Diamond Light Source (UK); typically operating at 3GeV energy of the storage ring with top-up injection mode at 300 mA current. The IO8 beamline at Diamond uses radiation in the 0.25 to 4.4 keV photon energy range, generated by an Apple II-type-undulator. X-ray fluorescence (XRF) elemental mapping data were acquired for the light elements using the K absorption edges and acquired from L edges for the metallic elements. X-ray fluorescence data analysis was performed using the PyMCA (Phyton Multichannel Analyser) software, a multiplatform code for the analysis of the ED-XRF spectra.

2.7 Catalytic upgrading of 5-HMF to 2,5-DMF

The catalytic transfer hydrogenation reactions were carried out in a stainless steel Parr reactor series 4590 as described above. Three sets of experiments were carried out: set 1

(commercially obtained 5-HMF); set 2 (starch-derived 5-HMF) and set 3 (cellulose derived 5-HMF) each using *D. desulfuricans* and CAS bio-catalysts. For set 1 the reactor was charged with 250 mg of commercial 5-HMF in 25 mL of MTHF (80 mM 5-HMF solution); sets 2 and 3 used appropriate volumes of 5-HMF in MTHF extracted from starch and cellulose hydrolyzates, respectively, to the same final concentration of 5-HMF.In all sets a weight ratio of 5-HMF: catalyst of 2.5:1 was added to the reactor. The catalysts tested were commercial Ru-C (5wt% Ru on charcoal: Johnson Matthey), biorecovered Ru (bio-Ru; 5wt% on CAS) and bimetallic preparations: 5wt% Pd/5wt% Ru bio-Pd/Ru (nominally) on *D. desulfuricans* and CAS cells. The reactor was sealed, purged 3 times with H_2 (50 bar), pressurized with H_2 (50 bar) and heated (260 ^oC; 2 h; 500 rpm). After the reaction, the reactor was quenched to 35-40°C in a water bath and the reaction mixture was filtered (Fisherbrand QL100 filter paper). Samples were stored at -20°C before analysis.

2.8 Analysis of residual 5-HMF, 2,5 DMF and co products in the catalytic conversion reaction

Samples were analyzed using a GC-FID for quantification and a GCMS-QP2010s for compound identification. All GC-FID analysis was performed on a Shimadzu GC2014 equipped with a Shimadzu AOC-20i autosampler. The carrier gas was hydrogen, supplied by an external hydrogen generator (Parker). The GC was fitted with a Restek Stabilwax-DA column (30 m length, 0.32 mm ID and 0.25 µm film thickness). The injection volume was 1 µL with a 39 split ratio. The inlet temperature was 250 °C. The detector was a flame ionization detector (FID) with a flame temperature of 300 °C, and a sampling rate of 40 ms. The heating profile was 60 °C for 2 minutes then heated to 200 °C at 5 °C/min followed by further heating to 240 °C at 15 °C/min where it remained for a further 3 minutes. Analysis was carried out using Shimadzu GC solutions software. Calibration curves were third order between 80 mM and 0.4 mM.

All GC-MS analysis was performed on a Shimadzu GCMS-QP2010s equipped with a Shimadzu AOC-20i autosampler. The carrier gas was helium. The GC was fitted with a Restek Rxi-1ms column (15 m length, 0.25 mm ID and 0.25 µm film thickness). The injection volume was 1 µL with a -1 split ratio. The inlet temperature was 250 °C. The

detector was a single quadrupole mass spectrometer in electron ionization mode. The detector and interface temperatures were 250 °C. The detector acquisition mode was scanning between 40-400 m/z, with a scan every 300 msec. The solvent cut time was 1 min. The heating profile was 60 °C for 2 min then heated to 200 °C at 5 °C/min followed by further heating to 240 °C at 15 °C/min where it remained for a further 3 min. Analysis was carried out using Shimadzu GCMS Real Time Analysis and Shimadzu GCMS Post Run Analysis software. 5-HMF conversions and 2,5 DMF yields were calculated as follows (equation 2-5):

$$\text{HMF conversion (\%)} = 1 - \left(\frac{\text{moles of HMF in products}}{\text{Starting moles HMF}}\right) * 100 \quad (2)$$

$$\text{DMF yiels (\%)} = \frac{\text{moles of DMF in products}}{\text{Starting moles HMF}}) * 100 \quad (3)$$

$$2,5\ \text{DMF selectivity(\%)} = \left(1 - \frac{\text{moles of } 2,5 - \text{DMF in products})}{\text{starting moles of } 5 - \text{HMF} - \text{final moles of } 5 - \text{HMF}}\right) \text{x } 100 \quad (4)$$

$$\text{DMF energy } \left(\frac{\text{MJ}}{\text{kg S. M.}}\right) = \left(\frac{\text{kg of DMF in products}}{\text{kg S. M.}}\right) * \left(\frac{\text{MJ}}{\text{kg DMF}}\right) \quad (5)$$

3 Results and discussion

3.1 Conversion of starch and cellulose to 5-HMF and HMF-MTHF extraction

The yields of 5-HMF from thermal hydrolysis of starch and cellulose were 130 and 40 mg 5-HMF/g starting material (aq.) respectively. MTHF extraction efficiency of 5-HMF from the aqueous phase was between 59 to 63% (from several preparations) resulting in 5-HMF concentrations in MTHF of 70 and 21 mM for starch and cellulose respectively when pooled (Table 1). Example extraction efficiencies from two independent preparations were 59.3% and 62.8%, however the actual efficiency is of relatively low importance for proof of principle since this specific method would require further development for scale up and final application. For example, a cost-benefit analysis would consider a raft of solvents for efficiency and economy at scale although the potential benefits of MTHF are already apparent (see Introduction).

The yield of 5-HMF obtained from starch hydrolysis was consistent with previous work (Miyazawa, 2005; Orozco, 2012) but the yield from cellulose was markedly lower (Table 1). This could be expected as the crystalline structure of cellulose makes it more difficult to hydrolyze, requiring higher temperatures; however, this also enhances reaction degradation pathways of 5-HMF to simpler structures such as formic and levulinic acids (Minowa et al., 1998; Palmqvist and Hahn-Hägerdal, 2000). This additional complexity was confirmed by examination of example product mixtures by GC (Supplementary information Figure S1A) but the actual amounts of products (other than DMF) were not determined.

The yield from cellulose was ~2.5 times lower than values reported from hot compressed water hydrolysis of cellulose (e.g. ~110 mg 5-HMF/g cellulose @ 260°C) (Kamio et al., 2006; Minowa et al., 1998; Orozco, 2012). Minowa et al. (1998) studied the decomposition of cellulose in hot compressed water with alkali or nickel catalysts; the positive effect of these on the cellulose degradation pathway to products was significant as compared to catalyst-unsupplemented conditions. The reactor vessel used by Kamio et al. (2006) and Orozco (2012) was made of Hastelloy C-22 and C-276 respectively, both containing a nickel (~ 55 %)-molybdenum-chromium alloy. Unpublished work (R.L. Orozco, 2012) attributed an improvement in cellulose conversion to possible leaching of catalytic metals from the reactor body. These materials, when corroded, are known to leach metals to the reaction medium thereby possibly affecting cellulose decomposition and product distribution (Yu et al., 1993; Lu et al., 2006). Possible benefits of catalyst-enhanced hydrolysis may be suggested; however, the presence of heavy metals in the hydrolyzate is likely to inhibit its downstream fermentation due to metal toxicity. The use of added catalyst (and its removal from the product mixture) was beyond the scope of this study although immobilized biofilm-catalyst has been used in other applications, e.g. of removal of toxic Cr(VI) via bio-Pd-mediated reduction (Yong et al., 2015). The reactor used in the present work comprised stainless steel 316 containing Fe (~65%), Ni (~12%) and Cr (17%) alloy; metal leaching was not determined but successful biohydrogen fermentations of the hydrolyzate were reported following removal of toxic 5-HMF (Orozco, 2012). The lower yields of 5-HMF and the presence of more degradation products in the cellulose hydrolysate (Figure S1A) would have an adverse effect on the delivery of additional energy. Ideally the continuous extraction of 5-HMF during the

biomass hydrolysis reaction would be desirable to avoid further degradation of this compound which occurs at high temperatures (Saha and Abu-Omar, 2014), e.g. by addition of a solvent extraction loop with organic phase removal. This would be particularly important for 5-HMF derived from hydrolysis of cellulose, which typically requires a higher reaction temperature.

The MTHF extraction efficiency of 5-HMF from the aqueous phase was comparable, at ~60% and 63% from starch and cellulose hydrolyzates respectively, delivering organic supernatants containing 8.8 and 2.2 g/l (70 and 21 mM) of 5-HMF (Table 1). The initial concentrations of 5-HMF in the aqueous phase and the effect of sugars present in the hydrolyzate will have an influence on the partition coefficient of 5-HMF which can be significantly higher with increasing concentrations. For example, the presence of 30% wt/vol fructose in MTHF increased the partition coefficient of 5-HMF from 2.1up to 36% (Blumenthal et al, 2016). The goal is separation and catalytic upgrading to DMF in the same solvent, hence the5-HMF partition coefficient must be maximized while minimizing the glucose partition coefficient. These studies were beyond the scope of this investigation; however, a lack of solubility of glucose in MTHF suggests it would be unlikely that glucose was removed from the hydrolyzate during the 5-HMF extraction process.

Other approaches for 5-HMF removal such as over-liming, activated carbon, zeolites and ion exchange resins selectively removed up to 85% of 5-HMF (Jin et al., 2015, Ma et al., 2017, Hodge et al., 2009 & Ezeji et al., 2007). However, the recovery of 5-HMF from these extraction substrates is either difficult or unfavourable for downstream processing into 2,5-DMF due to high intramolecular attraction between 5-HMF and the extraction substrates or the regenerant/eluting agents containing water or water miscible organic solvents (Liu et al., 2015).

The efficiency of MTFH in the hydrogenation reactions compared to THF was evaluated in a set of reactions as shown in Supplementary information Table S1A. In all cases MTHF proved to be a better solvent than THF, delivering higher conversion and yields of DMF. It is concluded that MTHF is able to both extract 5-HMF from the hydrolyzate and serve as the solvent for its upgrading, facilitating a one-stage reaction.

3.2 Hydrogenation of 5-HMF into 2,5 DMF using Ru and Pd catalysts

The Pd was removed onto the bacteria in the first step to give 5wt% loading of Pd.In the second step all of the Ru(III) was removed by the CAS cells (loading was 5wt%Pd/5 wt% Ru) whereas the *D. desulfuricans* only loaded Ru (III) to 3 wt% (actual catalyst composition was 5%Pd/3%Ru). The reason for this was not investigated further (see later discussion).

The hydrogenation tests for the three 5-HMF substrates are summarized in Figure 1 (with the data and errors shown in Supplementary information Table S1B) For set 1 (pure 5-HMF) and set 2 (5-HMF from starch) the conversion of 5-HMF to products was generally between 95-100% (Figure 1). In contrast using 5-HMF from cellulose (set 3) the conversion was between 61 to 81% reaching 100% only with 5%Ru commercial catalyst but delivering a very poor yield of DMF (3%: Figure 1C).It is concluded that, while commercial Ru catalyst is useful for DMF production from pure 5-HMF, it is virtually ineffective in producing DMF from the hydrolyzates (Figure 1B, C). The reason for this was not investigated but may be due to fouling of the commercial catalyst by reaction components or products or to over-reaction yielding other products which were neither identified nor quantified. Example chromatograms showing reaction products are shown in Supplementary information (Figure S1B). Notably, both types of bio-Pd/Ru gave significant DMF product from the hydrolyzates where the commercial counterpart was ineffective (Fig 1 A, B, C; Supplementary information Table S1B). In addition, using cellulose hydrolyzate, both types of bio-Pd/Ru bimetallic performed comparably (Figure 1C) whereas the DMF yield and selectivity in starch hydrolyzate using CAS was ~ double that yielded via catalyst made using bio-Pd/Ru on *D.desulfuricans*. (Figure 1B). This difference was not attributable to an effect of any component of the hydrolyzate since the effect was clear also with pure 5-HMF substrate (Figure 1A).

The highest yields of DMF obtained corresponded to 5%Pd/5%Ru on CAS using commercial 5-HMF (63.13%) and 5% Ru on CAS cells using 5-HMF from starch (29.3%) this being ~46% lower; in both cases almost 100% 5-HMF conversion was achieved. This difference using the starch hydrolyzate could be attributed to the occurrence of side reactions caused by the presence of other by products in the starch derived 5-HMF (see

GC chromatograms; supplementary information, Figure S1B). The commercial Ru-catalyst gave 57% yield of DMF using pure 5-HMF (set 1) but when reacted on starch-derived 5-HMF (set 2) the yield was negligible which has negative implications for the application of the commercial catalyst in biomass product upgrading.

In terms of potential energy to be gained from the produced DMF: set 2 (5%Pd/5%Ru CAS) would give 2.1 kWh/kg starch-derived 5-HMF and set 1 (5%Pd/5%Ru CAS) 4.6 kWh/kg commercial 5-HMF. These energy yields would contribute to mitigate by ~ 28 and 63% respectively of the 'parasitic' energy needed for the hydrolysis and catalytic reactions (7.3 kWh/kg 5-HMF) assuming 80% heat recovery from the reactions. The equivalent potential energy gains using the bimetallic catalyst made on *D.desulfuricans* would be 0.95 kWh/kg from starch-derived 5-HMF. The > 2-fold better performance of the catalyst made on the CAS as compared to *D. desulfuricans* prompted comparison of metal deposition by the two sulfidogenic cultures. As noted above, the *D. desulfuricans* loaded 60% of the Ru(III) and hence the approximate proportions of metals (Ru:Pd) were 0.6:1 and 1:1 respectively for the *D. desulfuricans* and CAS materials; other possible differences between them were sought.

3.3 Formation of bimetallic material by washed cells of the sulfidogenic cultures

3.3.1 Bio-Pd/Ru supported on *D.desulfuricans*

Palladium(II) was completely removed from the challenge solution by both sets of cells (estimated as in Omajali et al., 2015) and uptake into/into the cells to 5wt% Pd was concluded. Formation of Pd(0) on *D. desulfuricans* was described previously (Omajali et al., 2015). Here, at a loading of 20 wt% Pd both cell surface-localized and intracellular Pd-nanoparticles were observed (Supplementary information Figure S2). The occurrence of metal intracellularly implies an uptake mechanism but its relatively low occurrence in the cytoplasm could imply an effective efflux mechanism as a detoxification response which is a well known metal resistance mechanism and a way to ensure that cells retain essential metals while rejecting toxic ones (Waldron and Robinson, 2009).At a loading of 5 wt% Pd (i.e. for the Pd pre-loading as used in this study) little intracellular Pd(0) was observed (Supplementary information Fig. S3 and inset). This is in contrast to (non-

sulfidogenic) *E. coli* where Pd-NPs were visible throughout the cells (Figure. S3 and inset). While Pd deposition in *E. coli* did not co-map with either phosphorus or sulfur the elemental maps (Supplementary information Figure S3) indicated a co-deposition of Pd with S, at least in part, in the cell surface layers of washed cells of *D. desulfuricans*. This is in accordance with earlier data from X-ray photoelectron spectroscopy that indicated formation of Pd-S bonds (and hence some palladium sulfide species) in the cell surface (outermost ~ 10-30 nm) layers of *D. desulfuricans* (Omajali, 2015). It is not known if the putative palladium sulfide was formed from incoming or effluxing Pd(II).

Previous studies (Omajali et al., 2015; Williams, 2015) identified three populations of palladium nanoparticles (NPs) in *D. desulfuricans*: NPs in the cell surface layers, in the cytoplasm and localized within nuclear bodies (NBs: the intracellular inclusion nuclear body is shown in Supplementary information Figure S2). NBs are a condensed form of DNA that commonly occurs in cultures in stationary phase or when grown at a slow growth rate (Zaritsky et al., 2017). Pd is well known to bind to DNA (Pillai and Nandi, 1977) and/or histone-like, DNA-associated proteins. Actively growing cells produce H_2S, and a growing culture comprises a mixture of 'young' (freshly divided) and 'old' cells as well as dead cells. Hence, the *D. desulfuricans* culture would comprise a population of cells each at different stages of their cell cycle, with actively metabolizing and also senescent cells, from which H_2S would possibly not be produced from residual metabolism. The possibility that incoming Ru(III) faces a potential 'choice' between Pd(0), PdS (or other localization foci other than Pd-'seeds') has not been considered previously as sulfidogenic cultures have not been examined in detail (Omajali, 2015; Supplementary information Figure S3).

It was assumed that 5 wt% Pd(0) NPs serve as the putative ''seeds''. for Ru deposition, on the basis of earlier work on the formation of Pd/Au bimetallic catalysts (Deplanche et al., 2012). However, unlike with Au(III) reported previously using *E. coli* (Deplanche et al., 2012), the Ru(III) was incompletely removed by *D.desulfuricans* (see above) and the metal loading onto the cells was 5wt% Pd/3wt% Ru. Figure 2A shows the formation of metallic NPs in the nuclear bodies of *D. desulfuricans* (arrowed, white) and also localized at the cell surface. The deposition of Ru in the cells was greater than the background, but there was no clear association with Pd or any cellular feature in cells showing nuclear

bodies (Figure 2B, D) whereas a co-localization of Pd and Ru was evident in cell surface layers (Figure 2B; Supplementary information Figure S4). Putative bimetallic structures occurred at the cell surface, in addition to localizations where an association between Pd and Ru, (with apparent Ru outgrowths) was suggested (Figure S4). In contrast, in another example cell, discrete Pd-NPs in the surface layers showed no clear association of Pd and Ru and deposition of the latter appeared to be uniform throughout the cell surface (Figure 2e-h). The distribution of Ru appeared to be independent of the Pd-NPs (Supplementary information Figure S4) and it is not known whether the apparent Ru 'overgrowths' were coincidental or in association with Pd nucleation. Examination of examples of cell surface regions showed the large NPs to comprise agglomerations of smaller ones of sizes ~ 5-7 nm (Figure 3b, inset) with lattice fringes of 0.23 nm. This could correspond to the (110) plane of RuO_2 (Soin et al., 2012) but the (111) plane of Pd(0) was noted by Divakar and Raghunathan (2003) as 0.24 ± 0.01 nm and so the bio-NPs could equally be reporting the (111) facets of Pd(0). Pd(0)-NPs on *D. desulfuricans* were reported with Pd (111) lattice spacings of 0.250, 0.258 and 0.243 nm (Omajali et al., 2015). However, recent work in a purely chemical system has noted lattice spacings of palladium sulfide as 0.250 nm and 0.256 nm, attributed to the expansion of the Pd(0) lattice by sulfur (Albani et al., 2018). Hence, the identity of the bio-nano crystals we report here cannot be attributed with certainty (see later discussion).

3.3.2 Waste culture of consortium of acidophilic sulfidogens (CAS)

D. desulfuricans is a Gram negative anaerobic sulfate-reducing bacterium (SRB) that respires at the expense of sulfate in lieu of oxygen. The final product is H_2S. Early work to remediate acid mine drainage waters (AMD) developed the use of acidophilic (acid-tolerant) sulfate-reducing bacteria(see Introduction) to precipitate heavy metals as their sulfides. Later work developed a mixed sulfate-reducing bacterial consortium into a continuous process whereby the H_2S off-gas precipitated metal sulfides, leaving the bacterial cells as the waste for use in this study. Samples were taken from the culture (in two periods separated by several weeks) that had been operating in a continuous mode for > 5 years.

Examination of the CAS culture using scanning electron microscopy showed a variety of cell types (Supplementary information, Figure S5A), mostly comprising rod-shaped cells, some round structures and some small round bodies (presumably spores) both free and budding from some of the cells. Examination of the cell surfaces (bulk population) by XPS (see later) showed no calcium; calcium dipicolinate (CDP) is a major component of the bacterial spore and hence it may be concluded that the occurrence of bacterial spores in the mixture was below the limit of detection. However, the CDP resides below the outermost spore coat, being released upon germination (de Vries, 2004) and, since the penetration depth of XPS is in the order of 10-30 nm, this is not a definitive conclusion but may tend to confirm the low occurrence of spore-type small round structures visible by SEM (Figure S5A).

Analysis of the CAS cell population using molecular biology identification methods revealed its composition as 66% *Desulfosporosinus acididurans* (sp. *nova*: Sánchez-Andrea et al., 2015) 7% unidentified strain CEB, 10% *Acidocella aromatica* strain PFBC, 10% *Actinobacterium* AR3 and 7% *Acidithiobacillus ferrooxodans* (A.L.A.Santos and D.B. Johnson, unpublished) (Table 2) Hence, although the *D. desulfuricans* and 17% of the mixed culture would be united by their Gram-negative stain and non-sporeforming characteristic, 76% of the CAS would comprise Gram positive sporeformers.

The Gram-negative bacterial cell surface comprises a phospholipid outer membrane (OM) containing lipopolysaccharide that often bridges into extracellular hydrated polymeric materials which collapse upon drying. Beneath the OM the periplasmic space comprises a hydrated gel-compartment of width ~ 30 nm and beneath that the inner membrane (IM), which is the cellular permeability barrier bounding the cytoplasm. The periplasmic space contains structural peptidoglycan, the N-acetyl glucosamine components of which would provide amine groups for potential coordination of incoming metals. The classical Gram-positive cell lacks the OM and periplasmic space and its single membrane is bounded externally by a thick layer of peptidoglycan (as in the Gram-negative periplasmic space), which also contains phosphate in the form of teichoic acids embedded within it. In addition, there is often a coat of regular protein structures, the 'S-layer' (which can also be found on Gram-negative cells) which is present in many Gram positive bacteria including *Bacillus sphaericus* strains isolated from heavy metal-

contaminated sites (Merroun et al., 2005). This outermost surface layer plays a major role in the coordination of heavy metals and radionuclides through their carboxyl and phosphate groups (Merroun et al., 2005). In addition, archaea and Gram-positive bacterial S-layer has been used as a template for the fabrication of metallic NPs of Au (Merroun et al., 2007; Bartolome et al., 2012). Bacterial cell surfaces have been extensively reviewed *per se* and in the context of metal binding behaviour (e.g. Beveridge, 1989). It is assumed that binding of Ru(III) to Gram positive cells accesses more, or different, nucleation sites than onto Gram negative cells (e.g. via the higher content of surface-accessible petidoglycan in the former) but this was not tested.

3.3.3 Formation of metallic nanoparticles on CAS

The CAS was metallized with 5wt%Pd/5wt%Ru and examined in the light of the above discussions (Figure 4). Electron micrographs of the metallized CAS are also shown in supplementary information (Figure S5B and C, and S6). The cell heterogeneity is apparent in Figure S5 and expansion of cell surface areas (Figure 4 and Supplementary information Figure S6) shows four types on the basis of their pattern of metal deposition (c.f. Table 3) but each type could not be attributed to a taxonomic group on the basis of morphology alone. Type I cells (Figure 4A, B) showed heavy metallic deposits at the outer edge of the cell surface in addition to intracellular nanoparticles. Type II (Figure 4 C, D) showed no outermost metal deposits, but instead dense metallic deposits co-localized beneath the wall layers and some intracellular NPs. Type III (Figure 4E, F) showed metallic NPs within the wall layers and also intracellularly. Figure 4 E also shows a putative spore (type IV) but as the small round structures were numerically sparse (supplementary information Figure S5A) these were not considered to play a major role, although metallic deposits were apparent on the surface and within the putative spores (Supplementary information Figure S6G). Some cells showed outer membrane vesicles (Figure 4A; see Supplementary information Figure S6H), too few in number to contribute to the overall metal deposition.

Further examination of the metallic NPs is shown in Supplementary information, Figure S6. Note that in type I cells (Figure S6A, B) the NPs are generally separated, located on the outer face of the cell wall and of dimensions ~2nm whereas in type II cells (Figure

S6C, D) the NPs are larger (e.g. > 50 nm) and appear as agglomerations. Type III cells (Figure S6E, F) appear to have a layered cell surface structure (Figure S6F) typical of a Gram negative cell but this was not confirmed. As with *D.desulfuricans* (above) the lattice fringes were 0.23 nm (Figure 5) i.e. the nanocrystals could have been either Pd(0) or RuO_2or, indeed, a form of palladium sulfide (see above). Much of the NP material appeared to be amorphous or non-crystalline as evidenced by a lack of lattice fringes.

Elemental mapping by energy dispersive X-ray microanalysis (Figure 6) showed that, in type I cells, while Pd was dispersed throughout the cell surface and cytoplasmic layers, the Ru deposits were almost exclusively confined to the cell surface with occasional intracellular occurrences scarcely higher than the background between the cells (Figure 6C, D). Examination of cell areas (Supplementary information Figure S7) suggested that, where both elements occurred together, they tended to be co-localized, but areas of solely Pd-NPs were visible. The large Ru-NPs tended to occur as overgrowths onto Pd-NPs. While it is possible to assign a numerical correlation to the co-occurrence of specific elements in NPs (Omajali 2015) this was not possible in the present study due to the small size and poor definition of the NPs, preventing estimation of NP boundaries (e.g. Figure S7F).

Type II cells in the CAS showed metallic deposits mainly at the cell surface in a similar way to that described for *D. desulfuricans* (see earlier). On the basis of the lattice fringes (see earlier) metal sulfides could not be discounted; even though the cells were washed a faint odour of H_2S was detected in the CAS on standing after a few days. As no exogenous sulfate was provided this H_2S may have arisen due to protein turnover; the presence of cellular storage materials to provide metabolic energy for turnover in the resting cells was not sought. However, given that the CAS was a mixed culture consortium evolved over 5 years, the possibility of cross-feeding may provide an evolutionary advantage under nutritionally sparse conditions, e.g. the presence of sulfide-oxidizing bacteria *Acidithiobacillus ferrooxidans*, which accounted for 7% of the culture (Table 2) would likely generate oxidized sulfur species for re-reduction into metal-accessible sulfides. These could arise from thiols arising from protein degradation, from cellular molecules such as glutathione or from histone proteins released from DNA during senescence. Alternatively (or in addition), given that

polysulfides are now reported as cellular stores of sulfur in sulfide oxidizing bacteria and almost all of the sulfide in the reported case was oxidized to sulfate under low sulfide-flux conditions (Berg et al., 2014) there is a strong possibility that endogenous H_2S may be generated from within the culture (via nascent SO_4^{2-}) under 'resting' conditions via inter-species turnover. In addition, Newman et al. (1997) reported that *Desulfotomaculum* (a sulfate-reducer) precipitated arsenic trisulfide. The ability of bacteria to store sulfur is well recognised (e.g.Pickering et al., 2001; Pickering and George, 2002). In this case the storage material comprised globules of sulfur and not polysulfide (Pickering and George, 2002). Elemental mapping (Figure 7) showed co-localization of palladium and sulfur with a greater density of sulfur in the CAS sample as compared to *D. desulfuricans*, which had no access to additional oxidized forms of sulfur to reduce to thiols/H_2S during NP formation. Although the EDX mapping method is qualitative only the result was confirmed in hydrated samples by complementary X-ray mapping (below). As far as the authors are aware, this is the first report of potential bacterial sulfur cycling being harnessed to the generation of novel catalytic biomaterials.

3.4 Co-localization of Pd, Ru and S using X-ray mapping of hydrated specimens of CAS

Synchrotron radiation based scanning X-ray microscopy was used to determine the distribution of chemical elements (e.g. Pd, S) within the metallic NPs produced by hydrated specimens of CAS. X-ray fluorescence (XRF) elemental mapping analysis was carried out at K and L edge of S and Pd, respectively. The results obtained (Supplementary information Figure S7b) showed a close association of S and Pd at microscale (size of the analyzed region was 20 μm/70 μm). This microscale analysis is complemented by that of the EDX mapping method of the STEM/HAADF system. The major limitation of the EDX mapping method is that, while it is specific for the elements of interest (as long as their X-ray emission peaks are well separated) and can measure accurately most elements (but not the light elements like N, C) only a few cells can be examined within a field of view, albeit with mapping of specimen micro areas within a single cell. In contrast the sensitivity of mapping X-ray emissions under illumination by synchrotron radiation is greater than from EDX and can co-map the light elements but this method has a limit of resolution of about 20 microns and hence it can best image cell

clusters in a given field of view and provide a numerical analysis of 'population' co-occurrence; this then takes into account the presence of different cell types. The first images confirm co-localization of Pd and S by this method, where the areas of high Pd and S correspond to single cells (Supplementary information Figure S7B); numerical analysis of the data to gain whole-population correlations of co-localization of Pd, Ru as well as S, P and N is in progress.

3.5 Analysis of cell surfaces by X-ray photoelectron spectroscopy (XPS)

XPS analysis was carried out on the metallized *D.desulfuricans* (Pd5%/Ru3%) and the metallized CAS samples (Pd0%/Ru5% and Pd5%/Ru5%). Wide energy survey spectra recorded for the three types of samples (Figure 8A) identified the presence of C 1s +Ru 3d along with N 1s, O 1s and S 2p. In addition, a small signature of Pd 3d and Ru 3p was also noted for the *D.desulfuricans* material. In the CAS samples, apart from the above, S 2s and S 2p were identified. Bimetallic CAS consisted of a higher sulfur content (3.55 at%) than CAS (Ru5%), which revealed 1.18 at% sulfur content (see Table 3) from the elemental composition obtained from XPS, despite the similar wash procedures applied in each case. The production of H_2S by washed, resting cells was not quantified but may have arisen from protein turnover/degradation as sulfate was not supplied to the resting cell suspensions (see above discussion). Bimetallic CAS also confirmed the presence of Pd, identified as Pd 3d as well as a higher Ru (Ru 3p) content. Further detailed analysis of the elements and their chemical interactions was carried out using high-resolution spectra collected for all these elements. A comparison of the high resolution Pd 3d spectra for the two bimetallic systems revealed (Figure 8B) broader doublet peaks for D. *desulfuricans* centred at 336 eV and 341 eV. The CAS sample, on the other hand, revealed a sharper doublet peak shifted to higher binding energy (337 eV, 342 eV). Deconvolution of the two spectra into respective components can be seen in Figure 8C and 8D, respectively. *D.desulfuricans* samples consisted of Pd in its metallic (Pd (0)) as well as oxidized forms (Pd(II) and Pd(IV)), while the bimetallic CAS with its spectra shifted to higher binding energies suggested a complete absence of metallic Pd and consisted of Pd only in its oxidized forms. The presence of palladium sulfides (Pd_xS_y) which may have been formed due to exposure of H_2S during the growth of NPs cannot be ruled out in this case. This would further justify the shift in the Pd spectra and explain the complete

absence of Pd in its metallic form (unlike previous reports on bio-Pd), whereby any unoxidised Pd NPs were 'claimed' by the sulfur. The signature binding energies for (Pd_xS_y) in the high resolution Pd spectra are similar to those of oxidized Pd (Xu et al., 2013) and therefore, could not be identified as separate components here.

The high resolution C 1s + Ru 3d spectra for the three samples are compared in Figure 9a (comparison of Ru 3p spectra can be seen in Figure S8). Here again, bimetallic CAS shows a significantly larger 'bump' with a peak centred near 281 eV, attributable to the higher amount of Ru content as compared to other two samples. It must be noted that the Ru $3d_{5/2}$ region extends to 279 eV in case of bimetallic CAS unlike *D.desulfuricans* and Ru-only CAS where the signal was observed only up to 280 eV. Component peaks for the 3 samples can be seen in the deconvoluted spectra in Figures 8B-8D. Components identified in the three spectra were similar to those reported in similar bacterial systems reported earlier (Priestley et al., 2015; Omajali et al., 2019; Gomez-Bolivar et al., 2019). In the case of bimetallic CAS, the extended Ru $3d_{5/2}$ region (in which the Ru components are more easily identifiable compared to Ru $3d_{3/2}$ which is overshadowed by C 1s components), suggested the presence of an additional Ru component near 279.7 eV. This component is close to the binding energy (BE) of metallic Ru and RuS_2. The component is more likely RuS_2 in this case given: i), the presence of H_2S produced by the bacteria during the NP synthesis; ii), metallic Ru is highly unlikely to be present in the oxidizing environment near the surface layers of the bacteria given its oxophilic nature, as reported previously (Omajali et al., 2019; Gomez-Bolivar et al., 2019; this volume) and iii), this is agreement with the presence of sulfide in the Pd (and S2p) spectra, emphasizing the sulfidation of the available metal NPs taking place in this system.

Further clarity in the sulfidation/oxidation of the metal NP in these bacterial systems was attained with the help of high-resolution O 1s spectra for the three systems (Figure 10A-D). A simple comparison of the high resolution O 1s spectra (Figure 10A) revealed a clear shoulder below 530 eV in the bimetallic *D.desulfuricans,* suggesting a higher metal oxide content. The deconvolution of the three spectra revealed typical peaks attributed to metal oxide (Me-Ox), O=C/sulfate, O-C/O-N, phenolic O-C/SiO_2 and adsorbed H_2O.As seen in Figure 10d, the Me-Ox component for bimetallic *D.desulfuricans* in O 1s spectra has a much higher contribution as compared to that in the other two samples. Looking back at

the elemental compositions, the atomic % of oxygen and ruthenium was similar in the material of *D.desulfuricans* and Ru-CAS (Table 3) yet *D.desulfuricans* has higher Me-Ox component. Bimetallic CAS consisted of a slightly higher Ru content than the other two samples along with a higher S content. Hence, it can be concluded that the CAS samples must consist of Me-Ox as well as metal sulfides (for Pd and Ru) and that metallic Ru is unlikely to be present in the surface layers of the bacterial systems observed in the XPS.

High-resolution S 2p spectra are seen in Figure 11a-c (See Figure S9 for comparison of 2p spectra). Bimetallic CAS sample revealed a peak centred near 163 eV while the Ru-CAS sample showed a peak centred near 164 eV. Deconvolution of the two revealed four sets of components (2p doublets, $2p_{3/2}$ and $2p_{1/2}$), identified as S1, S2, S3 and S4. These component peaks were identified with 2 or more attributions, as listed in Table 4. The primary reason for these multiple attributions is the complex nature of these metallized CAS and *D.desulfuricans* samples as well as the similar omnipresent sulfur present in the form of H_2S, which was produced by the bacteria themselves. Various S-C bonds, SOx-Me bonds and S-C-Me (Me = Ca, Fe, Na, Cl, F; i.e trace metals naturally present in bacteria) complexes are possibly formed due to the interactions between polymeric/aliphatic/aromatic carbon structures within the bacterial structures and the available sulfur. The binding energies (BEs) for such bonds and complexes are very close to each other and hence single attributions to thee sulfur components cannot be identified in these systems. Similarly, the BEs for RuS_2 and Pd_xS_y are also close to reach other and components cannot be identified individually. Interestingly, bimetallic CAS with higher S at%, appears to have a higher metal sulfide component S1 which is in agreement with the Ru 3d and Pd 3d spectra.

4 Conclusions and future scope

This study shows clear potential for the harnessing of biomass waste side-streams into additional energy materials (via bio-NP catalysts) to help offset the ‘parasitic’ energy demand of biomass comminution and hydrothermal processing. A common solvent allowed a single stage processing, extraction and catalytic upgrading of 5- HMF to make DMF, a ‘drop in’ fuel. Commercial catalyst, although effective in upgrading of

commercial 5-HMF, had low activity against 5-HMF derived from thermochemical processing of starch and cellulose. Pd/Ru bimetallic nanoparticles made and supported on bacterial cells were effective in this reaction. Waste sulfidogenic bacteria from another, unrelated, biotechnology process outperformed the 'classical' sulfidogen *D.desulfuricans*. This may be attributed to the higher Ru content of the bimetallic of the former but could equally well be assigned to the higher proportion of metal sulfides formed in resting cells of the bacterial consortium without exogenous oxidized sulfur species. The role of palladium sulfide ensembles as enhanced hydrogenation catalysts is just emerging in the literature; as yet a role is not assigned for ruthenium sulfides in hydrogenation such as we suggest. The contributory roles of Pd(0) and oxidized Pd species, palladium sulfides and the various species of Ru (III) (IV) (VI) and RuS_2, await further elucidation via advanced characterization methods. However, the use of mixed metal NPs opens new opportunities for using metals recovered for wastes, as waste streams rarely contain single metals; neo-catalyst bio-genesis from waste is now well established in other published work.

Acknowledgements, author contributions and declaration.

The project was funded by NERC grant NE/L014076/1 to LEM (Program: '*Resource Recovery from Wastes*'). The Science City Photoemission Facility used in this research was funded through the Science Cities Advanced Materials Project 1: '*Creating and Characterizing Next Generation of Advanced Materials*' with support from AWM and ERDF funds. The microscopy work was conducted at 'Centro de Instrumentación Cientifica' at the University of Granada, Spain. The authors acknowledge with thanks, use of GC-FID/GC-MS supplied by Dr Daniel Lester within the Polymer Characterization Research Technology Platform, University of Warwick and the help of Drs B. Kaulich, T. Araki and M. Kazemian at beamline IO8, Diamond Light Source, UK, who funded the synchrotron study (Award No SP16407: *Scanning X-ray Microscopy Study of Biogenic Nanoparticles; Improved Bionanocatalysts by Design)* on I08 Scanning X-ray Microscopy beamline (SXM). Biomaterials were made and characterized by JGB and IPM; RLO developed the method for 5-HMF extraction from hyrolyzates and common reaction solvent system and made the energy balance calculations; RLO and JGB did catalytic testing, with analysis of products by RAH; SEM and high resolution

TEM/elemental mapping were by JGB and MM; XPS data acquisition was by MW with XPS interpretations by MW and SS; synchrotron measurements were done by MM, IPM and LEM with interpretation by MM; DBJ and BG maintained the SCW culture and provided the samples of CAS for use in this study. The paper was authored by LEM with contributions from all authors. The authors declare no competing conflicts of interest.

References

Al-Amin, A.Q., Rasiah, R. and Chenayah, S. (2015). Prioritizing climate change mitigation: An assessment using Malaysia to reduce carbon emissions in future. *Environ. Sci. Policy* 50, 24-33. DOI: https://doi.org/10.1016/j.envsci.2015.02.002

Albani D., Shahrokhi, M., Chen, Z., Mitchell S., Hauert R., López, N., Pérez-Ramiírez J (2018). Selective ensembles in supported palladium sulfide nanoparticles for alkyne semi-hydrogenation. *Nature Comm*9, Article No 2634, July 2018 DOI: 10.1038/s41467-018-05052-4

Aycock, D.F. (2007). Solvent applications of 2-methyltetrahydrofuran in organometallic and biphasic reactions. *Org. Proc. Res. Dev*., 11, 156−159. DOI: 10.1021/op060155c

Bartolome, J., Bartolome, F., García, L.M., Figueroa, A.I., Repolles, A., Martínez, M.J., et al. (2012). Strong magnetism of Au nanoparticles deposited on *Sulfolobus acidocaldarius* S-layer. *Phys. Rev. Lett*., 109, 247203- 247203. DOI:https://doi.org/10.1103/PhysRevLett.109.247203

Berg, J.S., Schwedt, A., Kreutzmann, A-C., Kuypers, MMM, and Miluckaa J (2014). Polysulfides as intermediates in the oxidation of sulfide to sulfate by *Beggiatoa*spp. *Appl Environ. Microbiol*. 80, 629-636. DOI: 10.1128/AEM.02852-13

Beveridge, T.J. (1989). Role of cellular design in bacterial metal accumnulaiton and mineralization. *Ann Rev Microbiol* 43, 147-171. DOI: doi.org/10.1146/annurev.mi.43.100.189.001051

Blumenthal, L.C., Jens, C.M., Ulbrich, J., Schwering, F., Langrehr, V., Turek, T., Kunz, U., Leonhard K, Palkovits R. (2016). Systematic identification of solvents optimal for the extraction of 5‑hydroxymethylfurfural from aqueous reactive solutions. *ACS Sust. Chem. Eng*. 4, 228−235. DOI: 10.1021/acssuschemeng.5b01036

Cadez, S.and Czerny, A., (2016). Climate change mitigation strategies in carbon-intensive firms. *J. Cleaner Prodn.* 112, 4132-4143. DOI:https://doi.org/10.1016/j.jclepro.2015.07.099

Charlot, G. (1978). Dosages Absorptiométriques des ElémentsMineraux, 2nd Edn. Paris, France, Masson.

Chu, S. and Majumdar, A. (2012). Opportunities and challenges for a sustainable energy future. *Nature* 488, 294–303. DOI: https://doi.org/10.1038/nature11475

Dang, Q., Hu, W., Rover, M., Brown, R.C., and Wright, M.M. (2016). Economics of biofuels and bioproducts from an integrated pyrolysis biorefinery. *Biofuel, Bioprod and Bioref.* 10, 790-803. DOI: https://doi.org/10.1002/bbb.1681.

De Los Reyes, J.A., Gidbolos, S., Vrinat, M. and Breysse, M. (1990). Preparation and characterization of highly active ruthenium sulphide supported catalysts, *Catal. Lett.* 5, 17-24. DOI: https://doi.org/10.1007/BF00772089

Da Silva J.R. and Aznar, M. (2014). Thermophysical properties of 2,5-dimethylfuran and liquid–liquid equilibria of ternary systems water + 2,5-dimethylfuran + alcohols (1-butanol or 2-butanol or 1-hexanol). *Fuel* 136, 316-325. DOI: https://doi.org/10.1016/j.fuel.2014.07.039

Deplanche K., Caldelari, I., Mikheenko, I.P., Sargent, F. and Macaskie, L.E. (2010). Involvement of hydrogenases in the formation of highly catalytic Pd(0) nanoparticles by bioreduction of Pd(II) using *Escherichia coli* mutant strains. *Microbiology* 156, 2630-2640.DOI: 10.1099/mic.0.036681-0

Deplanche, K., Merroun, M.L., Casadesus, M., Tran, D.T., Mikheenko, I.P., Bennett, J.A., et al. (2012). Microbial synthesis of core/shell gold/palladium nanoparticles for applications in green chemistry. *J. Roy. Soc. Interface* 9, 1705-1712. DOI: 10.1098/rsif.2012.0003

Deplanche, K.,. Bennett J. A, Mikheenko I. P., Omajali J., Wells A. S., Meadows R. E., Wood J. and Macaskie L. E. (2014). Catalytic activity of biomass-supported Pd nanoparticles: influence of the biological component in catalytic efficacy and potential application in 'green' synthesis of fine chemicals and pharmaceuticals. *Appl. Catal. B: Environ.*, 147, 651–65.DOI:10.1016/j.apcatb.2013.09.045.

De Vries Y.P. (2004). The role of calcium in bacterial; spore germination. *Microbes Environ*. 19, 199-202. DOI:https://doi.org/10.1264/jsme2.19.199

Dogaris, I., Karapati, S., Mamma, D., Kalogeris, E. and Kekos, D. (2009). Hydrothermal processing and enzymatic hydrolysis of sorghum bagasse for fermentable carbohydrates production. *Biores. Technol.*100, 6543-6549. DOI: https://doi.org/10.1016/j.biortech.2009.07.046

Divakar, R. Raghunathan, V.S. (2003). Characterisation of interfaces in nanocrystalline palladium.*Sadhana*, 28, 47–62. DOI:https://doi.org/10.1007/BF02717125

Dunleavy, J.K. (2006). Sulfur as a catalyst poison. *Plat. Met. Rev*. 50, 110-110. DOI: 10.1595/147106706X111456

Ezeji, T., Qureshi, N. andBlaschek, H.P. (2007). Butanol production from agricultural residues: Impact of degradation products on *Clostridium beijerinckii* growth and butanol fermentation. *Biotechnol.Bioeng.* 97, 1460-1469. DOI: https://doi.org/10.1002/bit.21373

Gawade, A.B., Tiwari, M.S. and Yadav G.D. (2016). Biobased green process: selective hydrogenation of 5-hydroxymethylfurfural to 2,5-dimethyl furan under mild conditions Using Pd-$Cs_{2.5}H_{0.5}PW_{12}O_{40}$/K-10 Clay*ACS Sustainable Chem. Eng.*, *4*, 4113–4123. DOI: 10.1021/acssuschemeng.6b00426

Gollakota, A.R.K., Kishore, N. andGu, S. (2018). A review on hydrothermal liquefaction of biomass. *Renew. Sust. En. Rev.* 81, 1378-1392. DOI: https://doi.org/10.1016/j.rser.2017.05.178

Gomez-Bolivar, J., Mikheenko, I.P., Orozco, R.L. Sharma, S., Banerjee, D., Walker, M. et al. (2019). Synthesis of Pd/Ru bimetallic nanoparticles by *Escherichia coli* and potential as a catalyst for upgrading 5-hydroxymethyl furfural into liquid fuel precursors.*Front. Microbiol*., in submission

Gotterbarm, K.M., Luckas, N., Hoefert O., Lorenz, M.P.A., Streber. R., Papp. C., et al. (2012). Kinetics of the sulfur oxidation on palladium; a combined in situ x-ray photoelectron spectroscopy and density-functional study. *J Chem. Phys*. 136. DOI: https://doi.org/10.1063/1.3687676

Govindan, K. and Hasanagic, M., (2018). A systematic review on drivers, barriers, and practices towards circular economy: a supply chain perspective, *Int. J. Prodn. Res*., 56, 278-311. DOI: https://doi.org/10.1080/00207543.2017.1402141.

Haldar, D., Sen, D and Gayen, K. (2016). A review on the production of fermentable sugars from lignocellulosic biomass through conventional and enzymatic route—a comparison, *Int. J. Green En*., 13, 1232-1253. DOI: https://doi.org/10.1080/15435075.2016.1181075

Hansen, T.S., Barta, K. andAnastas P.T. (2012). One-pot reduction of 5-hydroxymethylfurfural via hydrogen transfer from supercritical methanol. *Green Chem.*,14, 2457-2461. DOI: 10.1039/C2GC35667H

Hodge, D.B., Anderson, C., Berglund, K.A. andRova, U. (2009). Detoxification requirements for bioconversion of softwood dilute acid hydrolyzates to succinic acid. *Enz. Microb. Technol*., 44,309-316. DOI: https://doi.org/10.1016/j.enzmictec.2008.11.007

Hu, L., Tang, X., Xu, J., Wu, Z., Lin, L. and Liu, S. (2014). Selective transformation of 5-hydroxymethylfurfural into the liquid fuel 2,5dimethylfuran over carbon-supported ruthenium.*Ind.Eng. Chem. Res.*. 53, 3056-3064. DOI: 10.1021/ie404441a

Jin H., Li, Y., Liu, X., Ban, Y., Peng, Y., Jiao, W. and Yang, W. (2015). Recovery of HMF from aqueous solution by zeoliticimidazolate frameworks.*Chem. Eng. Sci*. 124, 170-178. DOI: https://doi.org/10.1016/j.ces.2014.07.017

Kamio, E., Takahashi, S., Noda, H., Fukuhara, C. and Okamura, T. (2006). Liquefaction of cellulose in hot compressed water under variable temperatures. *Ind. Eng. Chem. Res*., 45, 4944-4953. DOI: 10.1021/ie060136r

Kunwar B., Deilami S.D., Macaskie L.E., Wood J., Biller P. and Sharma, B. K. (2017). Nanoparticles of palladium supported on bacterial biomass for hydroprocessing bio oil from continuous hydrothermal liquefaction (NTL) ofalgae.*Fuel* 209, 449-456. DOI: https://doi.org/10.1016/j.fuel.2017.08.007

Lei H., Tang X., Xu J., Wu Z., Lu, L. and Liu, S. (2014). Selective transformation of 5-hydroxymethylfurfural into the liquid fuel 2,5-dimethylfuran over carbon-supported ruthenium. *End. Eng. Chem. Res*. 53, 3056-3064. DOI: 10.1021/ie404441a

Lindberg, B.J., Hamrin, I.K., Johansson, G., Gelius, U., Fahlman, A., Nordling, A.C. and Siegbahn, K., (1970). Molecular spectroscopy by means of ESCA II.sulfur compounds. Correlation of electron binding energy with structure. *Phys. Scripta* 1, 286-298.

Liu, Y., Mellmer, M.A., Alonso, D.M. and Dumesic, J.A. (2015). Effects of water on the copper-catalyzed conversion of hydroxymethyl furfural in tetrahydrofuran. *Chem. Sus. Chem.*, 8, 3983-3986. DOI: https://doi.org/10.1002/cssc.201501122

Love, J.C., Wolfe, D.B., Haasch, R., Chabinyc, Kateri, M.L., Paul E., Whitesides, G.M.and Nuzzo, R.G. (2003). Formation and structure of self-assembled monolayers of alkanethiolates on palladium *J. Am. Chem. Soc*., 125, 2597-2609. DOI**:** 10.1021/ja028692

Lu, Y.J., Guo, L.J. and Zhang, X.M. (2006). Thermodynamic modeling and analysis of hydrogen production process by biomass gasification in supercritical water. *Abstr. Pap. Am. Chem. Soc*., 2006. 231: p. 9-PETR.

Lu Y,J., Guo L,J., Zhang X.M Yan, Q. (2007). Thermodynamic modeling and analysis of hydrogen production process by biomass gasification in supercritical water.*The Chem. Eng. J.* 131, 233-244. DOI: https://doi.org/10.1016/j.cej.2006.11.016

Lu, Y., Mellmer, M.A., Alfonso, D.M. and Dumesic, J.A. (2015). Effects of water on the copper-catalysed conversion of hydroxymethyl furfural in tetrahydrofuran. *Chem. Sus. Chem.* 8, 3983-3986. DOI: 10.1002/cssc.201501122.

Luo, W., Sanker, M.., Beale, A.M., He, Q., Kiely, C.J., Bruijnincx, P.C.A. and Weckhuysen, B.M. (2015). High performing and stable supported nano-alloys for the catalytic hydrogenation of levulinic acid to gamma- valerolactone. *Nature Comm.* 6, 6540. DOI: https://doi.org/10.1038/ncomms7540

Ma, H., Ji, X., Tian, Z., Fang, G. and Yang, G. (2017). Adsorption removal of inhibiting compounds by modified activated carbon. *J. Energ. Nat. Res*., 6, 24-30. DOI: 10.11648/j.jenr.20170602.12

Merroun, M.L., Raff, J., Rossberg, A., Hennig, C., Reich, T and Selenska-Pobell S. (2005). Complexation of uranium by cells and S-layer sheets of *Bacillus sphaericus* JG-A12. *Appl Environ Microbiol.* 71, 5542-5553. DOI: 10.1128/AEM.71.9.5532-5543.2005

Merroun, M.L., Rossberg, A., Hennig, C., Scheinost, A.C. and Selenska-Pobell, S. (2007). Spectroscopic characterization of gold nanoparticles formed by cells and S-layer protein of *Bacilus sphaericus* JG-A12. *Mat Sci Eng C -Biomimetic Supramol. Systems* 27, 188-192.

Miao, Z., Grift, T.E., Hansen.A.C. and Ting, K.C. (2011). Energy requirement for comminution of biomass in relation to article physical properties. *Ind. Crops Prod.,*33, 508-513. DOI: https://doi.org/10.1016/j.indcrop.2010.12.016

Minowa, Z.F., Tomoko O.G.I. and Varheghyi, G. (1998). Decomposition of cellulose and glucose in hot-compressed water under catalyst-free condtitions. *J. Chem. Eng. Jap.*, 31, 131-134. DOI: https://doi.org/10.1252/jcej.31.131

Mitra, J., Zhou, X and Rauchfuss, T. (2015). Pd/C-catalyzed reactions of HMF: decarbonylation, hydrogenation, and hydrogenolysis*Green Chem.*17, 307-313. DOI: 10.1039/C4GC01520G

Miyazawa, T.-F., (2005). Polysaccharide hydrolysis accelerated by adding carbon dioxide under hydrothermal conditions. *Biotechnol. Progr.*, 21 1782-1785.DOI: https://doi.org/10.1021/bp050214q

Modenbach, A.A. and Nokes, S.E. (2013). Enzymatic hydrolysis of biomass at high-solids Loadings: A review. *Biomass Bioen*. 56, 526-544. DOI: https://doi.org/10.1016/j.biombioe.2013.05.031

Murray, A.J., Zhu, J., Wood, J. and Macaskie, L.E. (2017). A novel biorefinery: Biorecovery of precious metals from spent automotivecatalyst leachates into new catalysts effective in metal reduction and in thehydrogenation of 2-pentyne. *Mins. Eng*. 113, 102-108. DOI: doi.org/10/1016/j.mineng.2017.08.011

Murray, A.J., Mikheenko, I.P., Deplanche, K, J.B., Gomez-Bolivar, J, Merroun, M.L. and Macaskie, L.E. (2019). Biorefining of metallic wastes into new nanomaterials for green chemistry, environment and energy. 'Resource Recovery from Wastes: Towards a Global Circular Economy Eds Macaskie, L.E., Sapsford, D.J. and Mayes, W.M Ch 9. Royal Society of Chemistry, in press

Nagpure A.S., Venugopal A.K., Lucas N., Manikandan M., Thirumalaiswamy, R. and Chilukuri, S. (2015). Renewable fuels from biomass-derived compounds: Ru-containing hydrotalcites as catalysts for conversion of HMF to 2,5-dimethylfuran.*Catal. Sci. Technol.*5, 1463-1472. DOI: 10.1039/C4CY01376J

Ňancucheo, I. and Johnson, D.B. (2012). Selective removal of transition metals from acidic mine waters by novel consortia of acidophilic sulfidogenic bacteria. *Microb. Biotechnol.* 5,34-44. DOI: https://doi.org/10.1111/j.1751-7915.2011.00285.x

Newman, D.K., Beveridge, T.J., and Morel, F.M.M. (1997). Precipiation of arsenic trisulfide by *Desulfotomaculum auripigmentum. Appl. Environ. Microbiol*. 63, 2022-2028.

Nishimura S., Ikeda N. and Ebitani K. (2014). Selective hydrogenation of biomass-derived 5-hydroxymethylfurfural (HMF) to 2, 5-dimethylfuran (DMF) under atmospheric hydrogen pressure over carbon supported PdAu bimetallic catalyst. *Catal. Today*. 232, 89-98. DOI: https://doi.org/10.1016/j.cattod.2013.10.012

Omajali, J.B. (2015). Novel bionanocatalysts for green chemistry applications PhD Thesis, University of Birminham, UK

Omajali, J.B., Mikheenko I.P., Merroun M.L., Wood J. and Macaskie L.E. (2015). Characterization of intracellular palladium nanoparticles synthesized by *Desulfovibrio desulfuricans* and *Bacillus benzeovorans*. *J. Nanopart. Res.* 17, 264-281. DOI:10.1007/s11051-015-3067-5.

Orozco, R. L., Redwood M. D., Yong P., Caldelari I., Sargent F. and Macaskie L. E. (2010). Towards an integrated system for bio-energy: hydrogen production by *Escherichia coli* and Use of palladium-coated waste cells for electricity generation in a fuel cell. *Biotechnol. Lett.*, 32, 1837–1845. DOI:10.1007/s10529-010-0383-9.

Orozco, R.L., Redwood, M.D., Leeke, G.A., Bahari, A., Santos, R.C.D. and Macaskie, LE. (2012). Hydrothermal hydrolysis of starch with CO2 and detoxification of the hydrolysates with activated carbon for bio-hydrogen fermentation. *Int. J. Hyd. Energ*. 37, 6545-6553. DOI: https://doi.org/10.1016/j.ijhydene.2012.01.047

Orozco R.L (2012). Hydrogen production from biomass by integrating thermochemical and biological processes' PhD Thesis, University of Birmingham, UK

Priestley, R.E., Mansfield, A. Bye, J., Deplanche, K., Jorge, A.B., Brett, D., Macaskie, L.E. and Sharma, S (2015). Pd nanoparticles supported on reduced graphene–*E. coli* hybrid with enhanced crystallinity in bacterial biomass. *RSC Adv.* 5, 84093-84103. DOI: https://doi.org/10.1039/c5ra12552a

Palmqvist, E. and Hahn-Hägerdal., B. (2000). Fermentation of lignocellulosic hydrolysates. II: inhibitors and mechanisms of inhibition. *Biores. Technol*., 7425-7433. DOI:https://doi.org/10.1016/S0960-8524(99)00161-3

Pickering, I.J., George, G.N., Yu, E.Y., Brune, D.C., Tuschak, C., Overmann, J. et al (2001). Analysis of sulfur biochemistry of sulfur bacteria using X-ray absorption spectropscopy. *Biochemistry*. 40, 8138-8145.

Pickering, I.J. and George, G.N. (2002). Bacterial sulfur storage globules SSRL Science highlights:https://www-ssrl.slac.stanford.edu/content/science/highlight/2002-01-31/bacterial-sulfur-storage-globules. Accessed 13/12/2018

Pillai, C.K. and Nandi, U.S. (1977). Interactions of palladium (II) with DNA. *Biochim. Biophys. Acta* 474, 11-16. DOI: https://doi.org/10.1016/0005-2787(77)90209-X

Redwood, M.D., Orozco, R.L., Majewski, A.J. and Macaskie, L.E. (2012). An integrated biohydrogen refinery: Synergy of photofermentation, extractive fermentation and hydrothermal hydrolysis of food wastes. *Biores. Technol*. 119, 384-392. DOI: https://doi.org/10.1016/j.biortech.2012.05.040

Roman-Leshkov, Y., Barrett, C., Liu, Z.Y. and Dumesic, J.A. (2007). Production of dimethylfuran for liquid fuels from biomass-derived carbohydrates. *Nature*, 447, 982-985. DOI : https://doi.org/10.1038/nature05923

Saha, B. and Abu-Omar, M. M. (2014). Advances in 5-hydroxymethylfurfural production from biomass in biphasic solvents. *Green Chem.* 16, 24-38. DOI: 10.1039/C3GC41324A

Sánchez-Andrea I., Stams, A.J., Hedrich, S., Ňancucheo, I and Johnson, D.B. (2015). *Desulfosporosinus acididurans* sp. nov.: an acidophilic sulfate-reducing bacterium

isolated from acidic sediments. *Extremophiles*. 19, 39-47. DOI: 10.1007/s00792-014-0701-6.

Santos, A.L. and Johnson, D.B. (2017). The effects of temperature and pH on the kinetics of an acidophilic sulfidogenic bioreactor and indigenous microbial communities.*Hydrometall.* 168, 116-120.DOI:org/10.1016/j.hydromet.2016.07.018

Santos, A.L. and Johnson, D.B. (2018). Design and Application of a low pH upflow biofilm sulfidogenic bioreactor for recovering transition metals from synthetic waste water at a Brazilian copper mine. *Front. Microbiol.* 9, 2015 DOI: 10.3389/fmicb.2018.02051

Shi, W., Gao, Y., Yang, G. andAhao, Y. (2013). Conversion of corn stalk to bio-oil in hot compressed water: effects of ultrasonic pretreatment on the yield and chemical composition of bio-oil, carbon balance, and energy recovery. *J Agric. Food Chem.* 61, 7574-7582. DOI: 10.1021/jf401975p

Soin, N., Roy, S. S., Mitra, S. K., Thubdat, T. and McLaughlin, J. A. (2012). Nanocrystalline ruthenium oxide dispersed Few Layered Graphene (FLG) nanoflakes as supercapacitor electrodes. *J. Mat. Chem.*22, 14944-14950. DOI: 10.1039/C2JM31226C

Thananatthanachon, T. and Rauchfuss, T.B. (2010). Efficient production of the liquid fuel 2,5-dimethylfuran from fructose using formic acid as a reagent. *Angew. Chem.* 122, 6616-6618.DOI: https://doi.org.10.1002/ange.201002267

Vardon, D.R., Sharma, B.K., Blazina, G.V., Rajagopalan, K and Strathmann, T.J. (2012) Thermochemical conversion of raw and defatted algal biomass via hydrothermal liquefaction and slow pyrolysis. *Biores. Technol.* 109, 178-187. DOI: https://doi.org/10.1016/j.biortech.2012.01.008

Waldron, K.J. and Robinson, N. (2009). How do bacterial cells ensure that metalloprotiens get the correct metal? *Nat Rev Microbiol* 7, 25-35. DOI: https://doi.org/10.1038/nrmicro2057

Williams, A. R. (2015). Biogenic precious metal-based magnetic nanocatalyst for enhanced oxygen reduction. PhD Thesis, University of Birmingham , UK

Xu, W., Ni, J., Zhang, Q., Feng, F., Xiang, Y. and Li, X. (2013) Tailoring supported palladium sulfide catalysts through H+-assisted sulfidation with H_2S. *J. Mater. Chem. A,* 1, 12811–12817. DOI: 10.1039/C3TA12277H

Yang, Y., Liu, Q., Li, D., Tan, J., Zhang, Q.I., Wang. C. and Ma, L. (2017). Selective

hydrodeoxygenation of 5-hydroxymethylfurfural to 2,5-dimethylfuran on Ru–MoO_x/C catalysts. *RSC Adv.* **7**, 16311-16318. DOI: 10.1039/C7RA00605E

Yong, P., Paterson-Beedle M., Mikheenko I. P. and Macaskie L. E. (2007). From bio-mineralisation to fuel cells: biomanufacture of Pt and Pd nanocrystals for fuel cell electrode catalyst. *Biotechnol. Lett.* 29, 539–544. DOI:10.1007/s10529-006-9283-4.

Yong, P., Mikheenko I. P., Deplanche K., Redwood M.D. and Macaskie L. E. (2010). Biorefining of precious metals from wastes:an answer to manufacturing of cheap nanocatalysts for fuel cells and power generation via an integrated biorefinery? *Biotechnol. Lett.* 32, 1821–1828. DOI:10.1007/s10529-010-0378-6.

Yong, P., Liu, W., Zhang Z., Beauregard, D., Johns, M.L. and Macaskie, L.E. (2015). One step bioconversion of waste preciousmetals into *Serratia* biofilm-immobilized catalyst for Cr(VI) reduction, *Biotechnol. Letts.* 37, 2181-2191.DOI: 10.1007/s10529-015-1894-1

Yu, M.A. and Antal, Jr., M.J. (1993). Hydrogen Production by Steam Reforming Glucose in Supercritical Water. *En.Fuels*, 7, 574-577.

Zaritsky, A., Rabinovitch, A., Liu, C. and Woldringh, C.L. (2017) Does the ecslipse limit bacterial nucleoid complexity and cell width? *Synth Syst Biotech.* 2, 267-275. DOI:https://doi.org/10.1016/j.synbio.2017.11.004.

Zhang, F., Liu, Y., Niu, X., Zhu, Y. (2017). Efficient production of the liquid fuel 2,5-dimethylfuran from 5-hydroxymethylfurfural in the absence of acid additive over bimetallic PdAu supported on graphitized carbon.*En. Fuels* 31, 6364-6373. DOI**:** 10.1021/acs.energyfuels.7b00428

Zhu J., Wood J., Deplanche K., Mikheenko I.P. and Macaskie L.E. (2016). Selective hydrogenation using palladium bioinorganic catalyst. *Appl. Catal. B: Environ.* 199, 108–122. DOI: https://doi.org/10.1016/J.APCATB.2016.05.060.

Zu, Y.H., Yang, P.P., Wang, J.J., Liu, X.H., Ren, J.W., Lu, G.Z. and Wang, Y.Q. (2014). Efficient production of the liquid fuel 2, 5-dimethylfuran from 5-hydroxymethylfurfural over Ru/Co_3O_4 catalyst. *Appl. Catal*. B, 146, 244-248. DOI: https://doi.org/10.1016/j.apcatb.2013.04.026

Table 1. Conversion of starch and cellulose to 5-HMF and extraction efficiency of MTFH

	Starch	Cellulose
Conversion to 5-HMF (mg 5-HMF/g SM*)	130	40
MTHF extraction efficiency of 5-HMF (%)	59.6	62.8
[5-HMF] in MTHF (Supernatant; mM)	70	21

*SM = Starting Material (Starch or Cellulose)

Table 2. The sulfidogenic waste culture used in the study compared to *D.desulfuricans*

Bacterium	% representation	Gram stain	Spore former
D.desulfuricans	100%	Gram negative	-
CAS: Desulfosporosinus			
*acididurans**	66%	Gram positive	+
CAS: Unidentified strain CEB	7%	NK	NK
CAS: *Acidocella aromatica*	10%	Gram negative	-
CAS:*Actinobacterium*	10%	Gram positive	+
CAS:*Acidithiobacillus* *ferroroxidans*	7%	Gram negative	-

NK: not known. Only 17% of the CAS population were the same cell type as *D. desulfuricans* (Gram negative, non-sporeformer). The majority were Gram positive spore formers (76%).

Table 3. Atomic percentages of outermost ~ 10 nm of metallized bacterial cells determined by XPS

Sample	Ru	Pd	C	O	N	S	Cl	P	Ca
E.coli 5%Pd/4.7%Ru* *D.desulfuricans*	2.42	0.14	71.48	19.81	4.30	0	0	0.80	0
5%Pd/3%Ru	1.03	0.12	68.88	21.44	5.18	0.38	0.17	0.38	0.21
CAS 5% Ru	1.40	0	64.37	21.95	7.08	1.18	0	0.41	0
CAS 5%Pd/5%Ru	5.30	0.41	64.36	18.78	6.01	3.55	0.11	1.39	0

**E. coli* was included as a comparator Gram negative bacterium that is non-sulfidogenic. (Gomez-Bolivar et al., 2019). The low content of the Pd at the cell surface is attributable to internalization into the lower cellular layers beyond the detection of XPS.

Table 4: Binding energies for the components identified in sulfur spectra along with peak attributions.

Component	Binding Energy, eV		Attributions	Ref.
	CAS Ru 5%	CAS Pd5%/Ru5%		
S1	162.5, 163.7	162.5, 163.8	RuS_2, Pd_xS_y	De Los Reyes et al., 1990; Love et al., 2003
S2	163.9, 165.1	163.9, 165.1	-S-S- , S=C=S, -S-CH_3	Lindberg et al., 1970; Love et al., 2003;
S3	166.3, 167.5	166.4, 167.6	SO_2-Na, aromatic -C-S-O-,	Lindberg et al., 1970
S4	168.2, 169.4	168.2, 169.4	Sulfided Pd/C, $SOCl_2$	Lindberg et al., 1970; Xu et al., 2013

Legends to Figures.

Figure 1. Conversion of 5-HMF from commercial source (A) and from starch (B) and cellulose (C) hydrolyzates by commercial 5%Ru on carbon catalyst, 5wt% bio-Ru on *D. desulfuricans*, 5wt% bio-Ru on sulfidogenic waste culture (CAS), 5wt%Pd/3wt%Ru on *D. desulfuricans* and 5wt%Pd/5wt%Ru on CAS as shown. Experiments were done at least twice on separate occasions and data are shown in Supplementary Information Table S1B.X axis: *: Conversion of 5-HMF (%). #: Yield of 2,5-DMF (%). ^: Selectivity to 2,5-DMF (%).

Figure 2. Deposition of 5wt% Pd/3wt% Ru by *Desulfovibrio desulfuricans* and co-localization of the metals on the cells. Arrows: dense nuclear bodies typical of slowly-growing cells. A: HAADF image where metallic NPs appear bright. B: elemental map of Pd (green) and Ru (magenta); individual elemental maps are shown in C and D. E: HAADF image of discrete NPs in the cell surface region mapped for Pd (F, green) and Ru (G, magenta) and co-localization of Pd and Ru (H).

Figure 3. Region of cell surface shown in Figure 2E-H. Enlarged image (Fig. 3b, inset) shows that the large NPs are agglomerations of smaller ones. Crystal lattice spacings are shown for a NP outside (C,D) and within (E.F) an agglomeration.

Figure 4. Examination of the CAS bacteria loaded with 5wt%Ru/5wt%Pd. Three main patterns of metal deposition are attributed to type I (AB), type II (C,D) and type III (E,F) cells.

Figure 5. High resolution-TEM analysis of cell sections showing cluster (A, B) taken from Figure 4B (panel B) and (C, D) taken from figure 4B (panel D) shows lattice spacing of 0.23 nm.

Figure 6. Elemental mapping of distribution of Ru and Pd in two type I cells (as in figure 4) showing superimposition of Pd (green B) and Ru (magenta, D) occurrences. Individual maps (C, D) show very little Ru inside the cells although Pd is distributed uniformly between the cell surface and intracellular regions.

Figure 7. HAADF/STEM images of *D.desulfuricans* (A) loaded with 5wt% Pd/3wt% Ru and CAS cells type II loaded with 5%Pd/5%Ru (B). Magnifications show similar clusters on sulfidogenic bacteria (D) and *D. desulfuricans* (C) located in the periplasm. Qualitative analysis using EDX elemental mapping shows superimposition in CAS bacteria for Pd (F) and sulfur (H) and also in *D. desulfuricans* (E and G).

Figure 8. XPPS analysis showing A) Wide energy survey spectra for the metallised bacterial samples, B) High-resolution Pd 3d comparison for the two bimetallic samples, C) Pd 3d fitted components for the *D. desulfuricans* Pd5/Ru3 sample and D) Pd 3d fitted components for the CAS Pd5/Ru5 sample.

Figure 9. High Resolution C 1s + Ru 3d spectra showing A) comparison of the three metallized bacterial samples, B) fitted components for the *D. desulfuricans* Pd5/Ru3 sample, C) fitted components for the CAS Pd0/Ru5 sample, and D) fitted components for the CAS Pd5/Ru5 sample

Figure 10. High Resolution O 1s spectra showing A) comparison of the three metallized bacterial samples, B) fitted components for the CAS Pd0/Ru5 sample, C) fitted components for the CAS Pd5/Ru5 sample fitted and D) components for the *D. desulfuricans* Pd5/Ru3 sample.

Figure 11. High Resolution S 2p spectra showing A) comparison of the three metallized bacterial samples, B) fitted components for the CAS Pd0/Ru5 sample, and C) fitted components for the CAS Pd5/Ru5 sample.

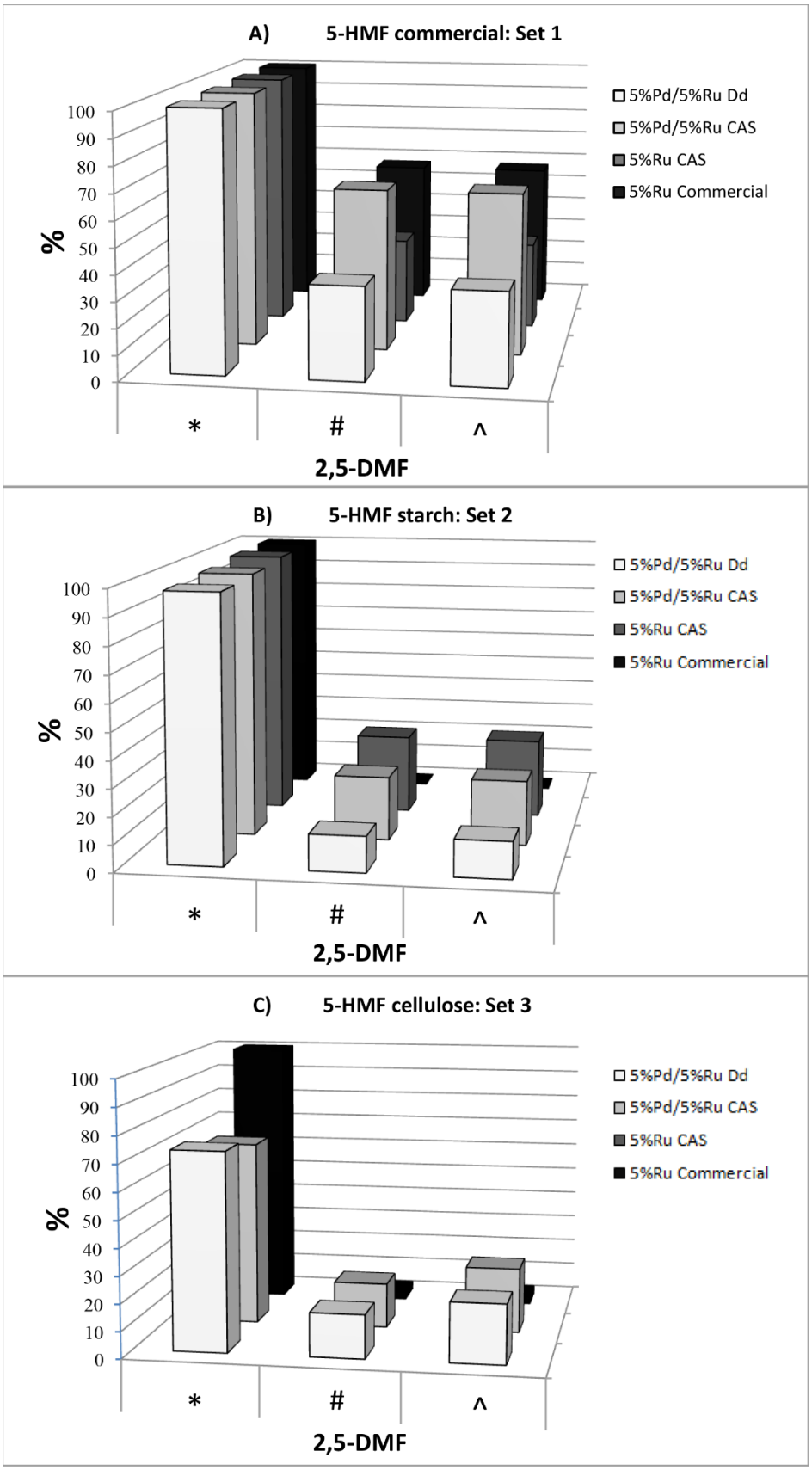
A)
5-HMF commercial: Set 1
%
100
90
80
70
60
50
40
30
20
10
0
*
#
^
2,5-DMF
5%Pd/5%Ru Dd
5%Pd/5%Ru CAS
5%Ru CAS
5%Ru Commercial
B)
5-HMF starch: Set 2
%
100
90
80
70
60
50
40
30
20
10
0
*
#
^
2,5-DMF
5%Pd/5%Ru Dd
5%Pd/5%Ru CAS
5%Ru CAS
5%Ru Commercial
C)
5-HMF cellulose: Set 3
%
100
90
80
70
60
50
40
30
20
10
0
*
#
^
2,5-DMF
5%Pd/5%Ru Dd
5%Pd/5%Ru CAS
5%Ru CAS
5%Ru Commercial

Figure 1.

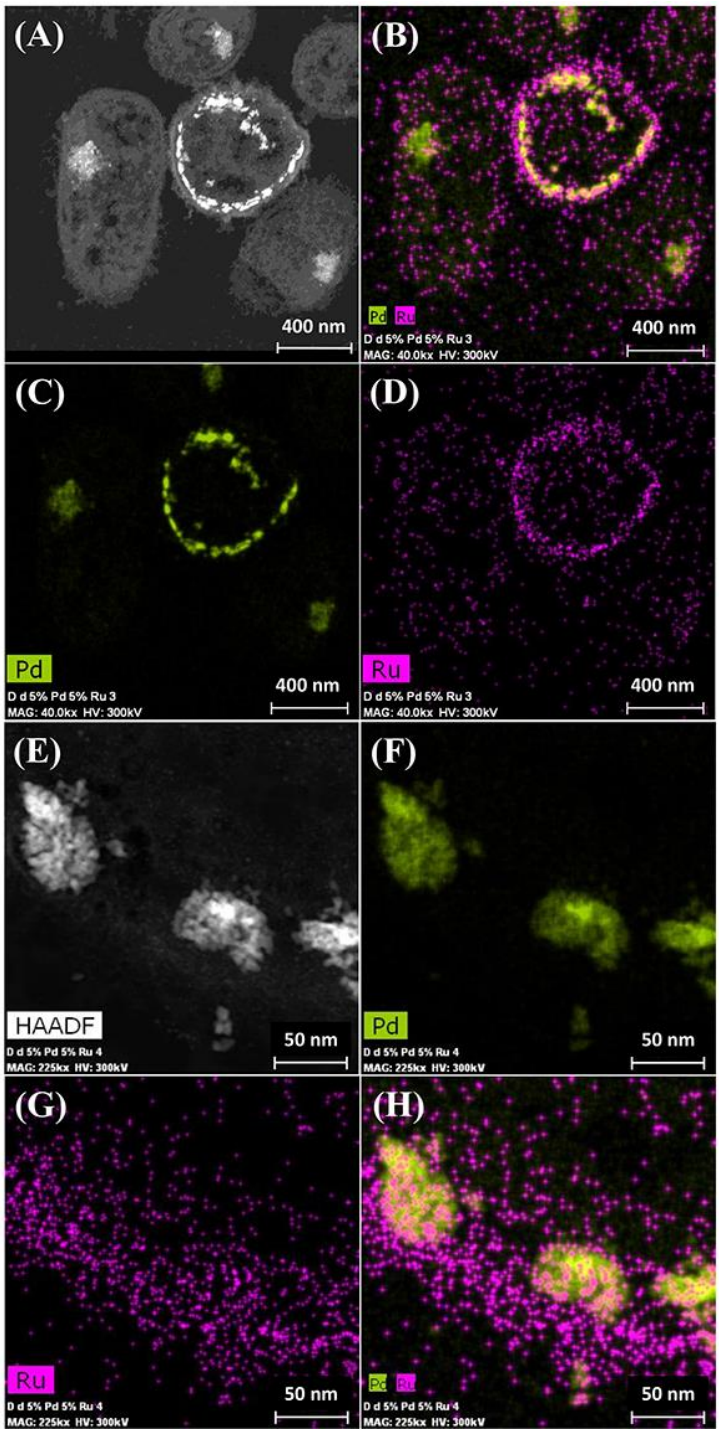
(A)
400 nm
(B)
Pd Ru
D d 5% Pd 5% Ru 3
MAG: 40.0kx HV: 300kV
400 nm
(C)
Pd
D d 5% Pd 5% Ru 3
MAG: 40.0kx HV: 300kV
400 nm
(D)
Ru
D d 5% Pd 5% Ru 3
MAG: 40.0kx HV: 300kV
400 nm
(E)
HAADF
D d 5% Pd 5% Ru 4
MAG: 225kx HV: 300kV
50 nm
(F)
Pd
D d 5% Pd 5% Ru 4
MAG: 225kx HV: 300kV
50 nm
(G)
Ru
D d 5% Pd 5% Ru 4
MAG: 225kx HV: 300kV
50 nm
(H)
Pd Ru
D d 5% Pd 5% Ru 4
MAG: 225kx HV: 300kV
50 nm

Figure 2.

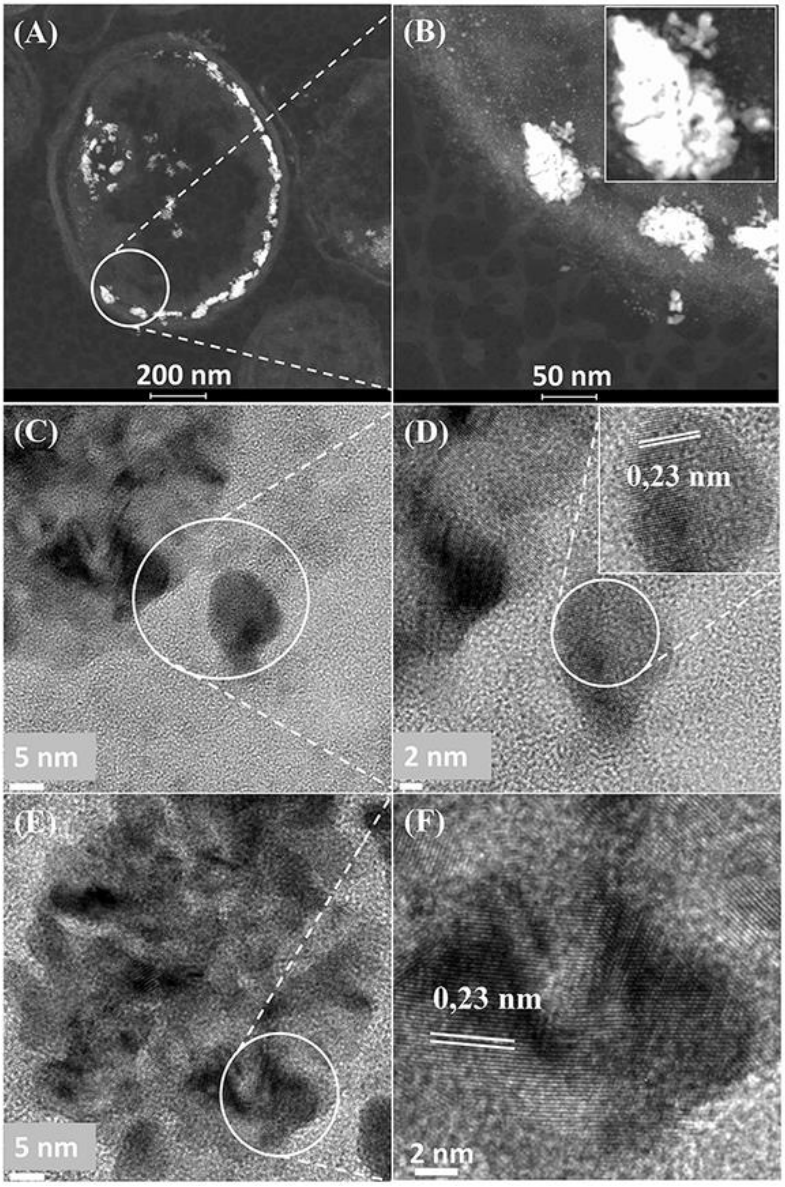

Figure 3.

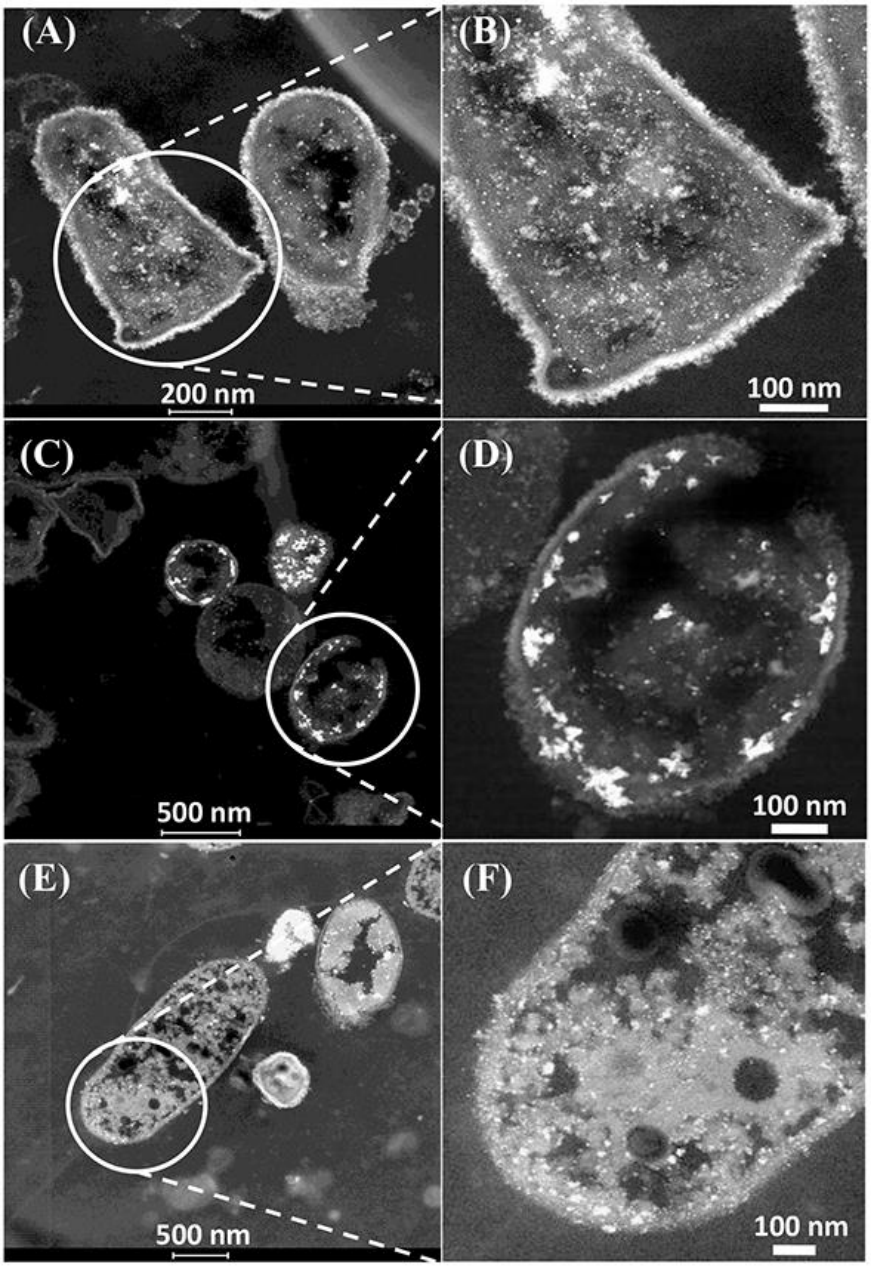

Figure 4.

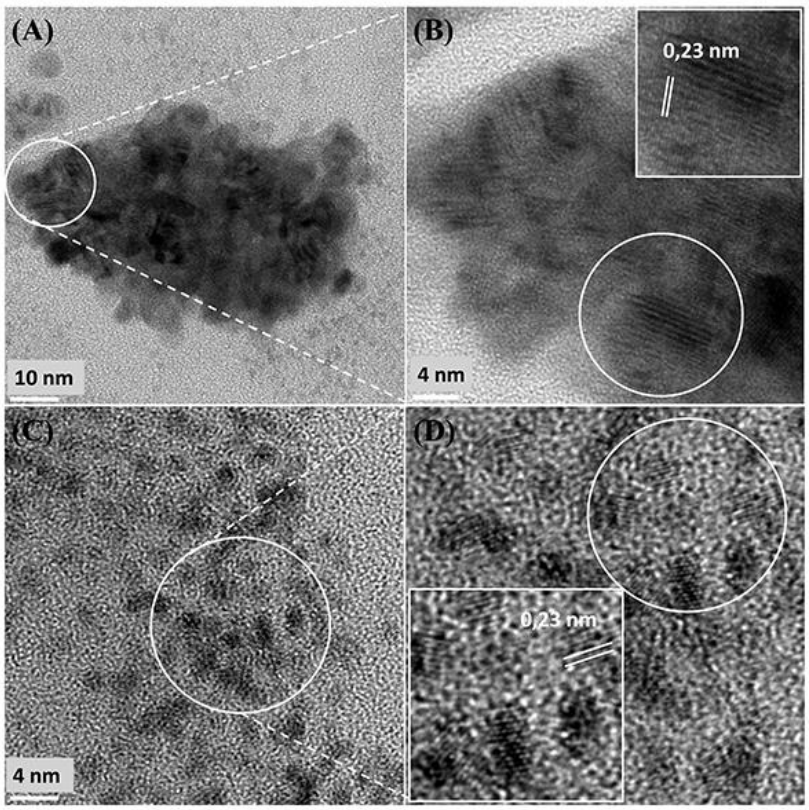
(A)
10 nm
(B)
0,23 nm
4 nm
(C)
4 nm
(D)
0,23 nm

Figure 5.

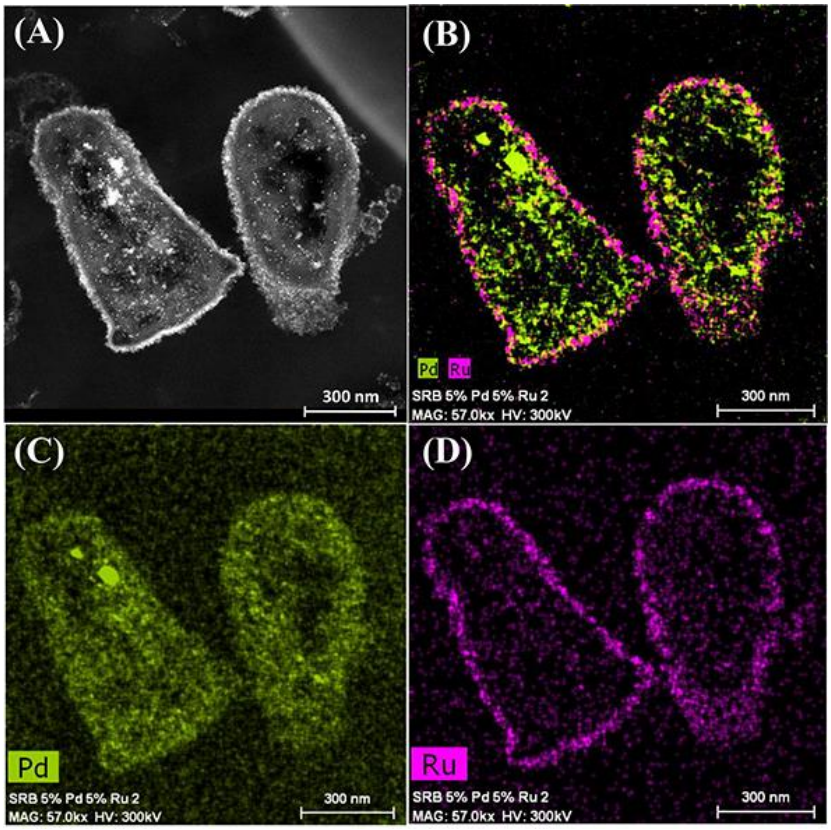
(A)
300 nm
(B)
Pd Ru
SRB 5% Pd 5% Ru 2
MAG: 57.0kx HV: 300kV
300 nm
(C)
Pd
SRB 5% Pd 5% Ru 2
MAG: 57.0kx HV: 300kV
300 nm
(D)
Ru
SRB 5% Pd 5% Ru 2
MAG: 57.0kx HV: 300kV
300 nm

Figure 6.

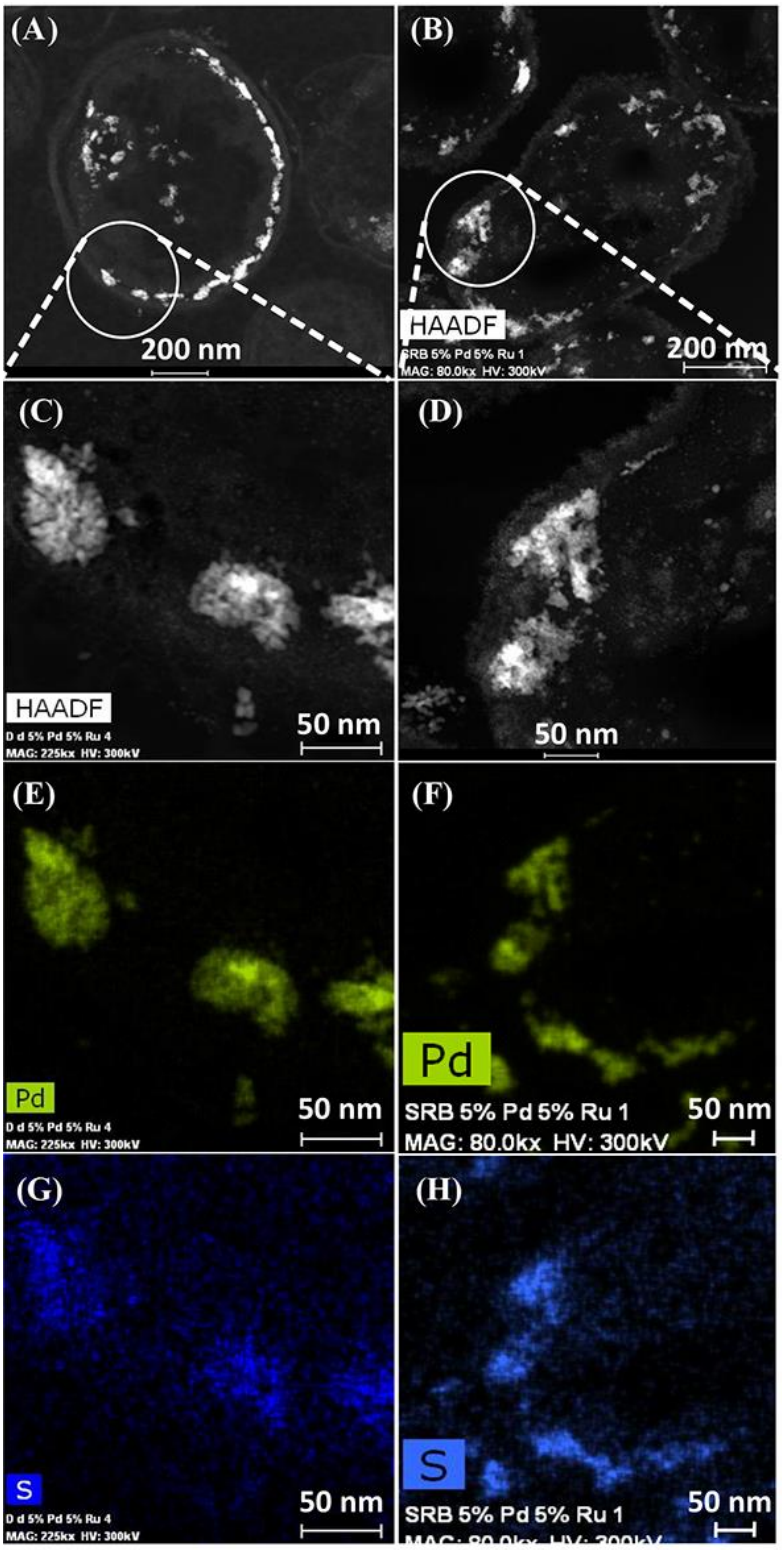

Figure 7.

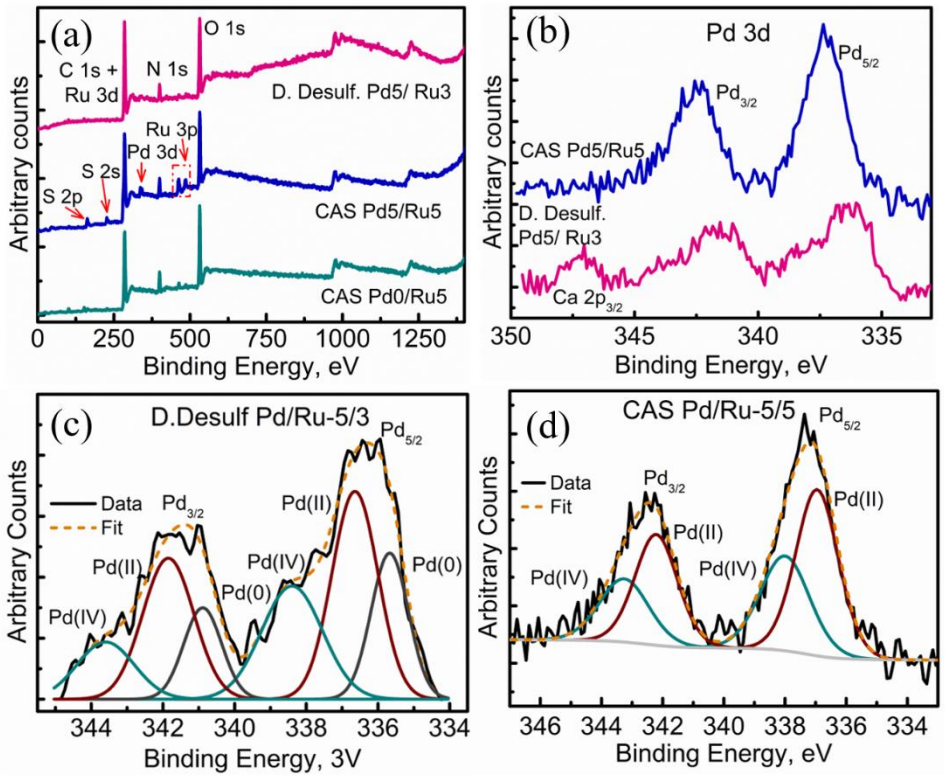
(a)
O 1s
C 1s +
Ru 3d
N 1s
D. Desulf. Pd5/ Ru3
Ru 3p
Pd 3d
S 2s
S 2p
CAS Pd5/Ru5
CAS Pd0/Ru5
Arbitrary counts
0 250 500 750 1000 1250
Binding Energy, eV
(b)
Pd 3d
Pd5/2
Pd3/2
CAS Pd5/Ru5
D. Desulf.
Pd5/ Ru3
Ca 2p3/2
Arbitrary counts
350 345 340 335
Binding Energy, eV
(c)
D.Desulf Pd/Ru-5/3
Pd5/2
Data
Fit
Pd3/2
Pd(II)
Pd(IV)
Pd(II)
Pd(0)
Pd(IV)
Pd(0)
Arbitrary Counts
344 342 340 338 336 334
Binding Energy, 3V
(d)
CAS Pd/Ru-5/5
Pd5/2
Data
Fit
Pd3/2
Pd(II)
Pd(IV)
Pd(II)
Pd(IV)
Arbitrary Counts
346 344 342 340 338 336 334
Binding Energy, eV

Figure 8.

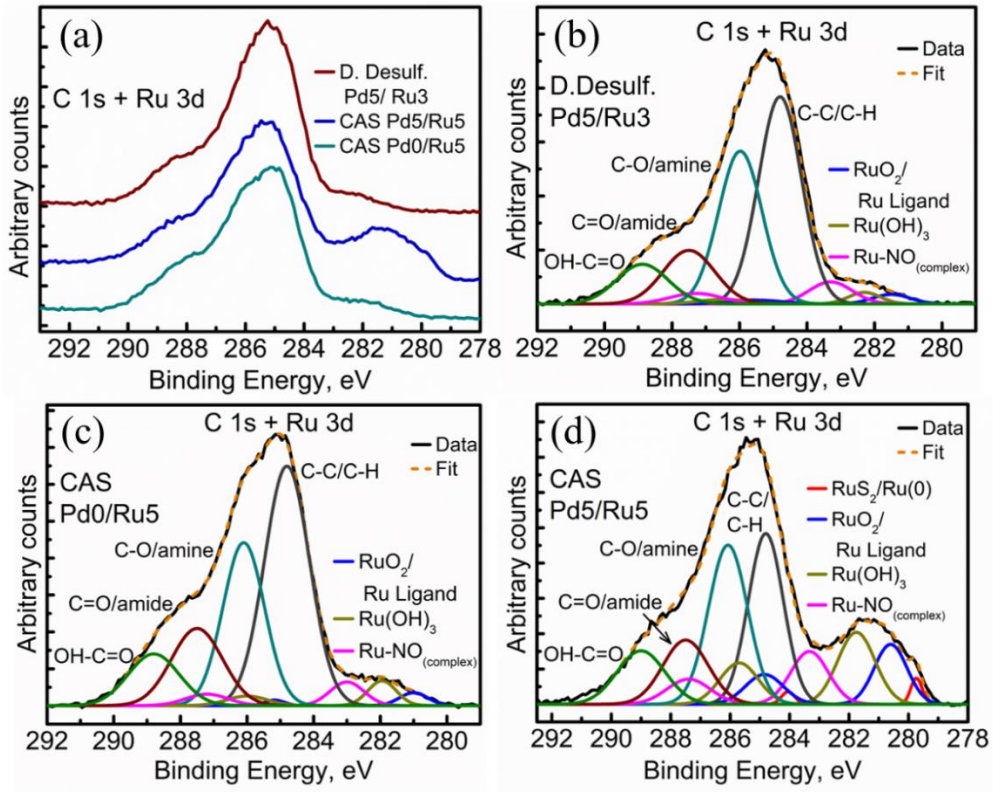

Figure 9.

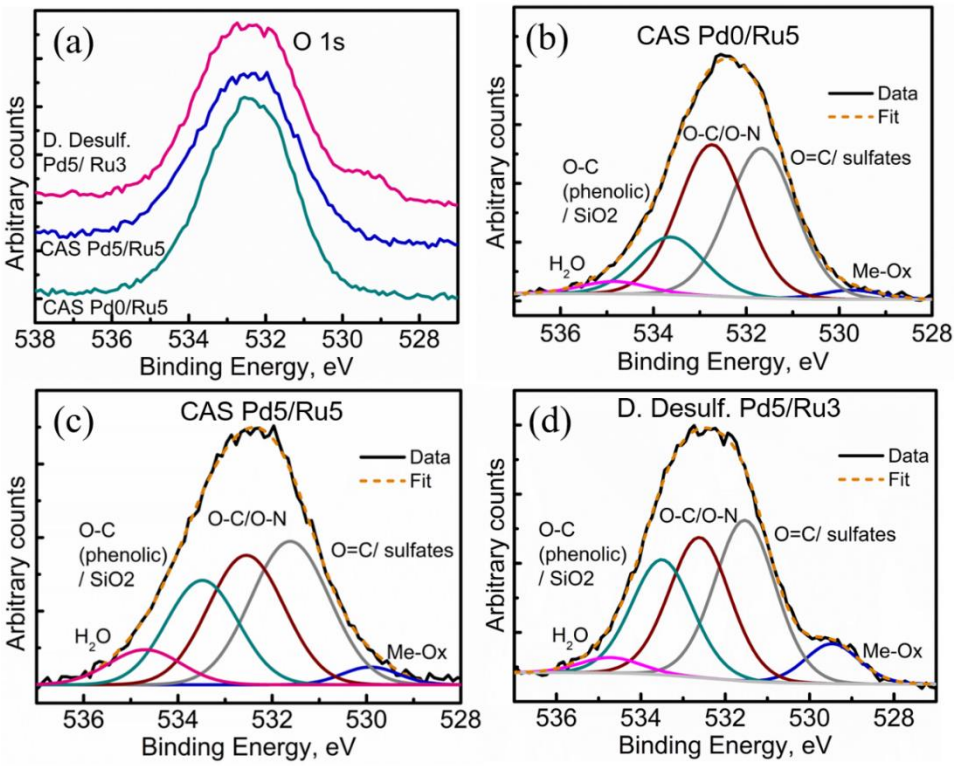

Figure 10.

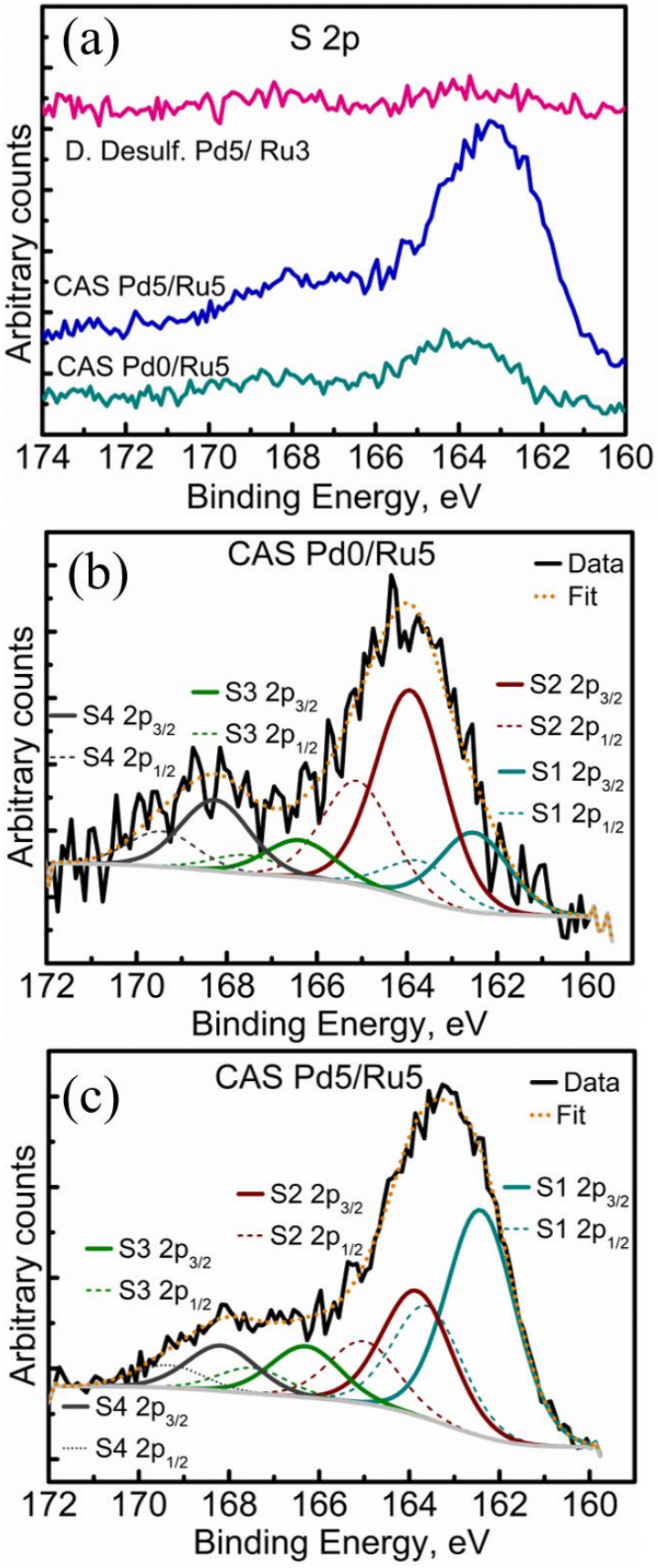
(a)
S 2p
D. Desulf. Pd5/ Ru3
CAS Pd5/Ru5
CAS Pd0/Ru5
Arbitrary counts
174 172 170 168 166 164 162 160
Binding Energy, eV
(b)
CAS Pd0/Ru5
Data
Fit
S4 2p3/2
S4 2p1/2
S3 2p3/2
S3 2p1/2
S2 2p3/2
S2 2p1/2
S1 2p3/2
S1 2p1/2
Arbitrary counts
172 170 168 166 164 162 160
Binding Energy, eV
(c)
CAS Pd5/Ru5
Data
Fit
S2 2p3/2
S2 2p1/2
S1 2p3/2
S1 2p1/2
S3 2p3/2
S3 2p1/2
S4 2p3/2
S4 2p1/2
Arbitrary counts
172 170 168 166 164 162 160
Binding Energy, eV

Figure 11.

Supplementary information

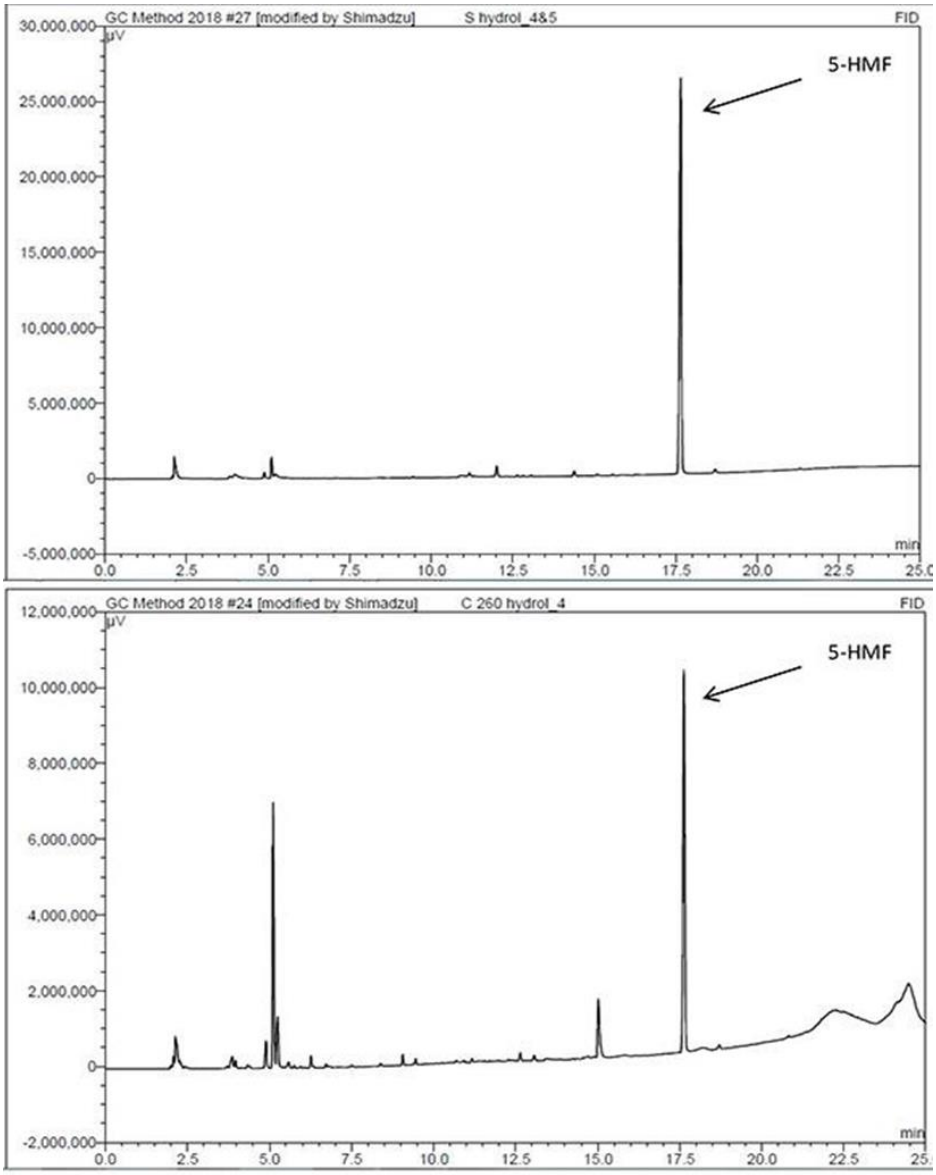

Figure S1A. Example GC chromatograms of products from hydrothermal hydrolysis of starch @ 220 ^{o}C (top) and cellulose @ 260 ^{o}C (bottom)

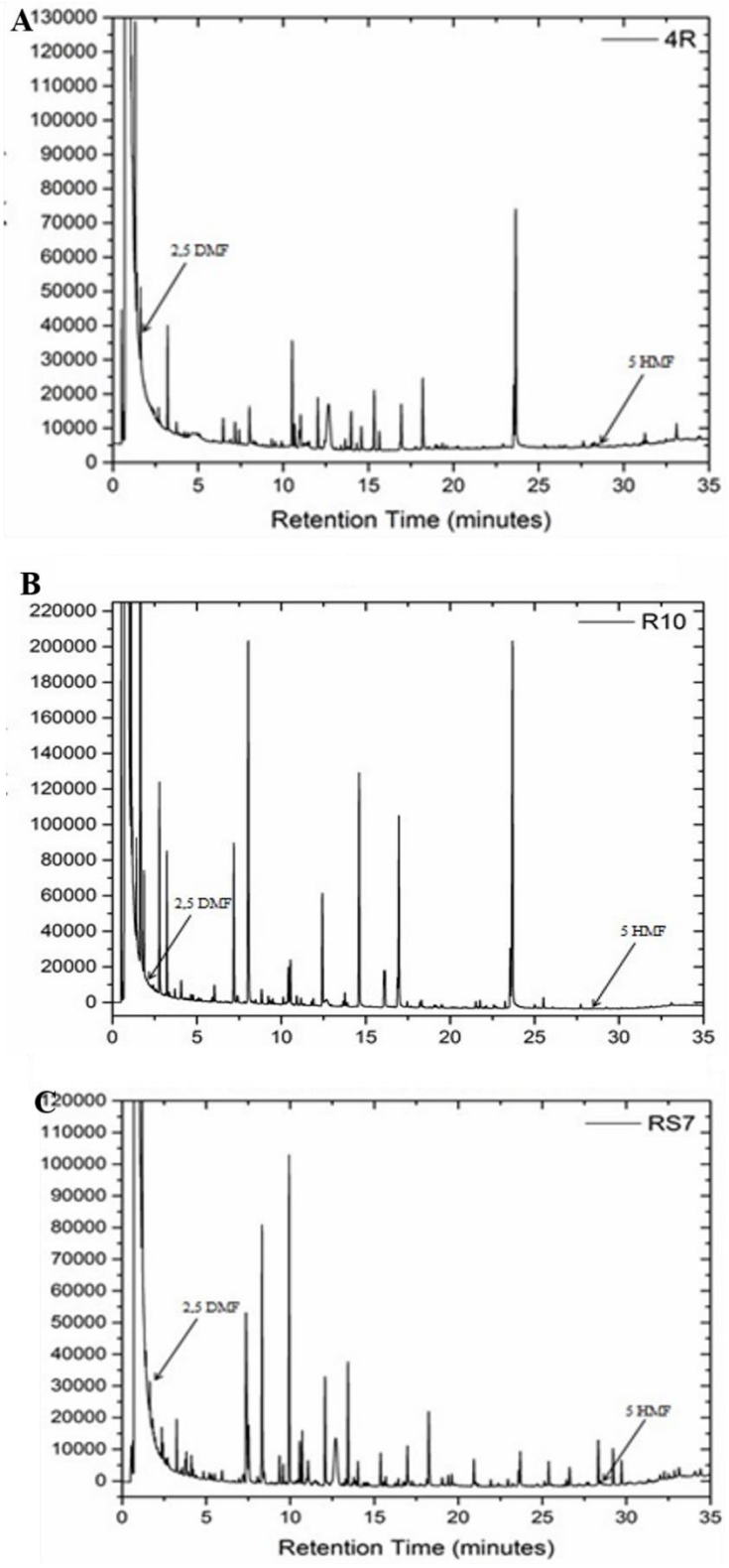

Figure 1SB: Example chromatograms of products from catalytic upgrading of 5-HMF. Products from 5-HMF upgrading using 5wt% Ru-C commercial catalyst and commercially obtained 5-HMF (46 mM DMF, no 5-HMF) (A). Products from 5-HMF upgrading using 5wt% Ru-C catalyst and 5- HMF obtained via starch hydrolysis (No

DMF, no 5-HMF) (B). Products from 5-HMF upgrading using Pd/Ru catalyst on CAS and 5- HMF obtained via starch hydrolysis (20 mM DMF, 0.2 mM 5-HMF) (C).

Table S1A. Comparative hydrogenation reactions converting commercial 5-HMF to DMF under two catalyst loadings and different reaction conditions in MTHF and THF as solvents. The reaction volume was 25 mL in al reactions and the reaction time was 2h. In all cases the conversions to DMF are higher with MTHF compared to THF suggesting that MTHF is a better reaction solvent under these conditions.

	MTHF			**THF**		
Catalyst	DMF (mM)	5-HMF (mM)	Reaction conditions	DMF (mM)	5-HMF (mM)	Reaction conditions
5% Ru-C	45.7	0	100 mg cat; 260 ºC; 50 bar	16.7	0	50 mg cat; 260 ºC; 50 bar
5% Ru-C				12.4	2.9	100 mg cat; 200 ºC; 20 bar
Bio-5%Pd/5%Ru	9.0	6.4	100 mg cat; 200 ºC; 20 bar	0.25	52	100 mg cat; 200 ºC; 20 bar
Bio-5%Pd/5%Ru	15.1	1.5	50 mg cat; 260 ºC; 50 bar	5.1	14	50 mg cat; 260 ºC; 50 bar
No catalyst	0.6	74.2	200 ºC; 20 bar	0	74	200 ºC; 20 bar

Table S1B. Yields of main product 2,5 DMF for the different catalytic reactions and 5-HMF sources (set 1, 2 and 3 as described). Values are average of 2 experiments ± S.E.

* DD: *Desulfovibrio desulfuricans*;

** CAS: consortium of acidophilic sulfidogens Pd/Ru on bacteria was 5wt%Pd/5wt%Ru. 5%RuComm: commercial 5wt%Ru on carbon catalyst.

5%PdComm: commercial 5%wtPd on carbon catalyst Convers: conversion (%); Select: Selectivity to 2,5 DMF (%)

Note lack of activity of commercial catalysts to obtain 2,5-DMF from 5-HMF in starch/cellulose hydrolysates, whereas bio-derived catalyst achieved selective conversion to 2,5-DMF.

Catalyst	**5-HMF commercial (set1)**			**5-HMF starch (set2)**			**5-HMF cellulose (set3)**		
	5-HMF Convers	2,5 DMF Yield %	2,5 DMF Select	5-HMF Convers	2,5 DMF Yield %	2,5 DMF Select	5-HMF Convers	2,5 DMF Yield %	2,5 DMF Select
Pd/Ru DD*	100	35.88 ± 2.3	35.88 ± 2.3	97.8	13.23 ± 1.1	13.53 ± 1.1	73.38 ± 6.8	16.19 ± 1.4	22.06 ± 1.9
Pd/Ru CAS**	99.88	63.13 ± 4.1	63.2 ± 4.1	**98.54**	**23.64 ± 0.8**	**23.99 ± 0.9**	**68.71 ± 6.5**	**16.67 ± 1.7**	**24.26 ± 2.5**
5%Ru CAS	100	33.75 ± 0.9	33.75 ± 0.9	99.84	29.3 ± 2.5	29.33 ± 2.5		Not done	
5%Ru $_{Comm.}$	100	**57.06 ± 3.8**	**57.06 ± 3.8**	100	0 ± 0	0 ± 0	100	3 ± 0.29	3 ± 0.3
5%Pd $_{Comm.}$	100	6.44 ±0.75	6.44 ± 0.75	100	2.16 ±0.42	2.16 ± 0.4		Not done	

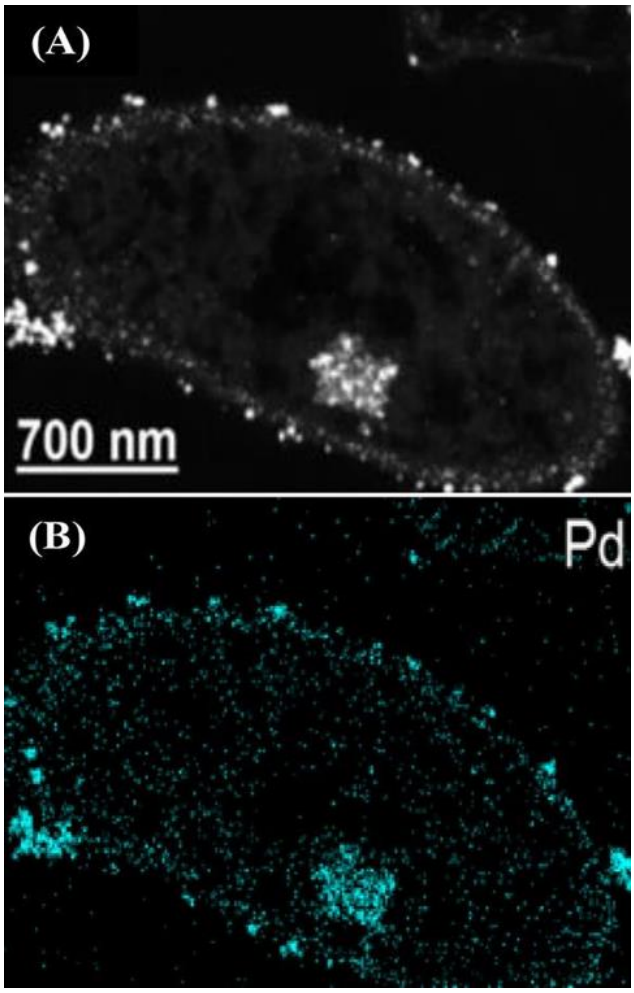

Figure S2. Pd deposition by D. desulfuricans at 20 wt% loading onto cells.

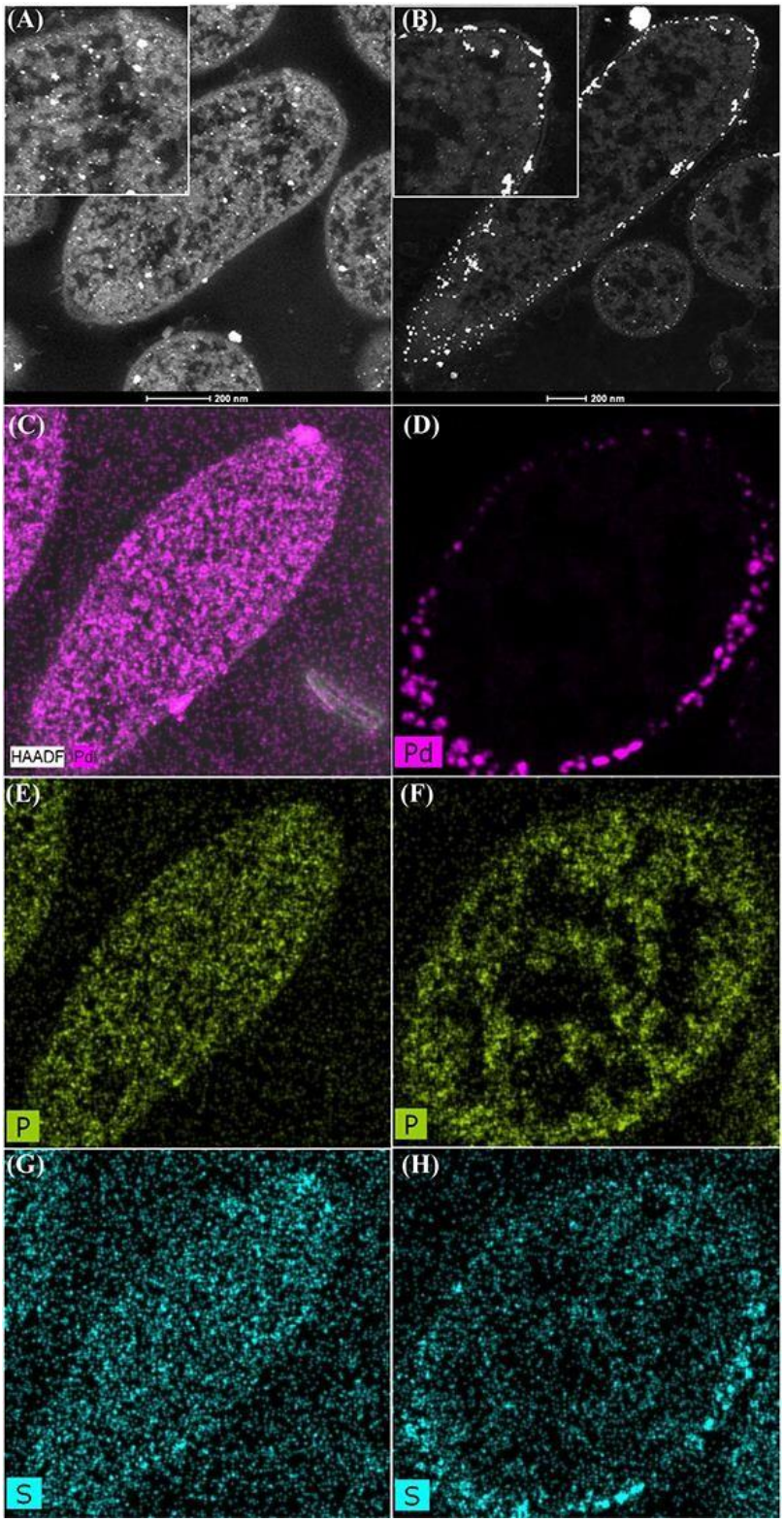

Figure S3. HAADF-STEM micrographs of Pd(0) on cells of E. coli (A) and D. desulfuricans (B) at 5wt% loading onto biomass, with elemental mapping for Pd, P and S

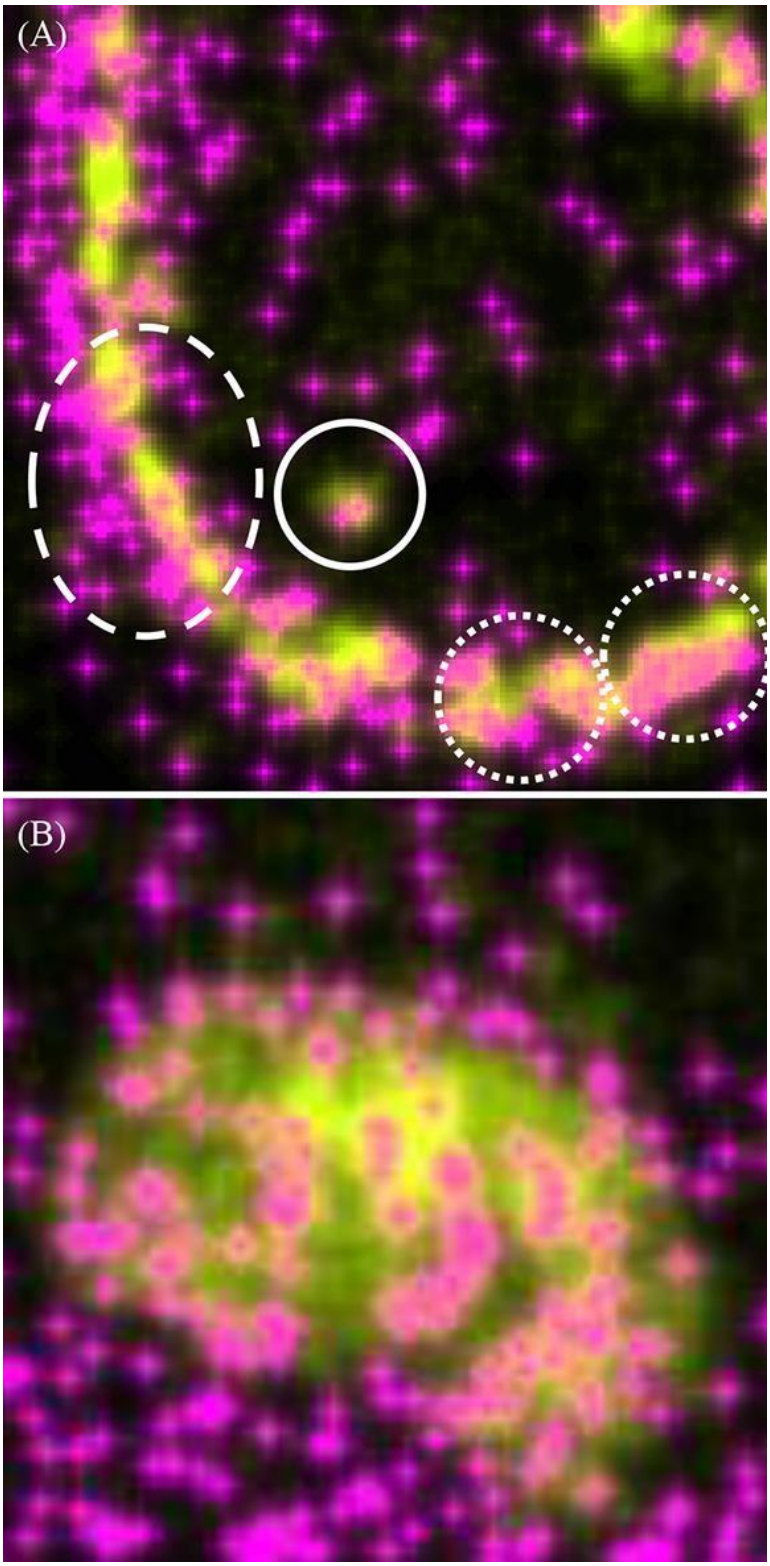

Figure S4. STEM/HAADF images of D. desulfuricans loaded with 5%wtPd/3wt%Ru

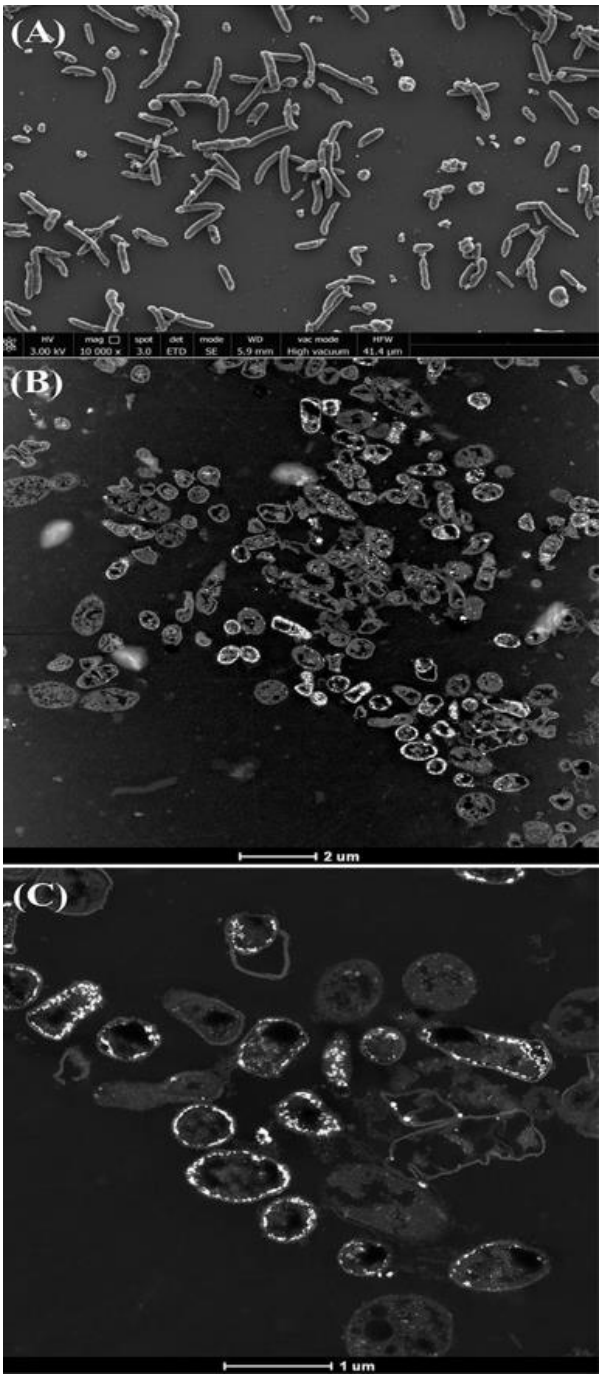

Figure S5. Consortium of acidophilic sulfidogenic bacteria (CAS) viewed by SEM (A) and images of cells loaded to 5wt%Pd/5wt%Ru (B, C).

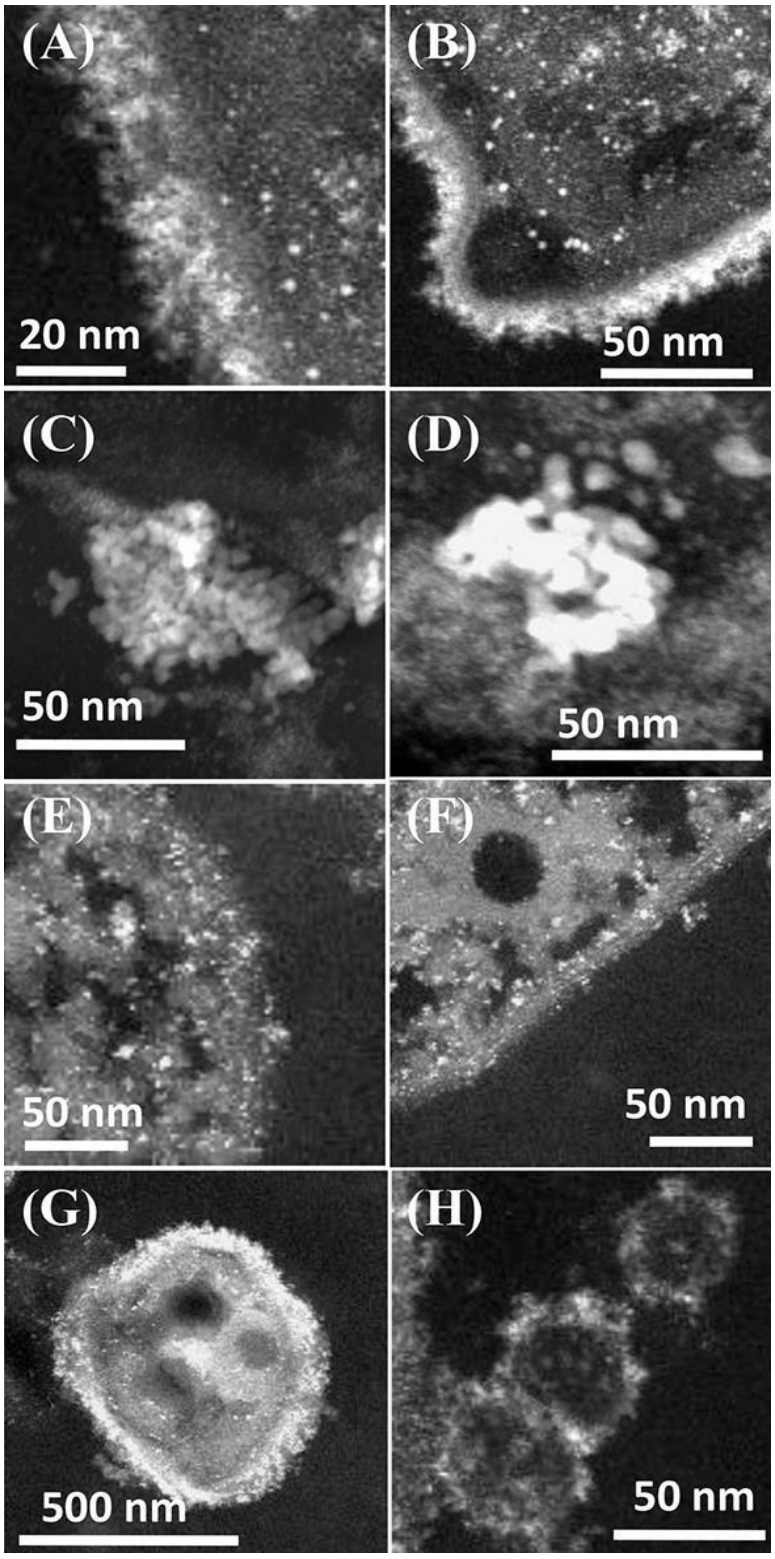

Figure S6. Four types of metal-accumulating bacteria within the CAS, loaded to 5wt%Pd/5wt%Ru. A, B: surface layers of CAS Type I cells. C,D: surface layers of CAS Type II cells. E,F: surface layers of CAS Type III cells. G: CAS Type IV cells (probable spore) H: Extruded outer membrane vesicles from a type I cell

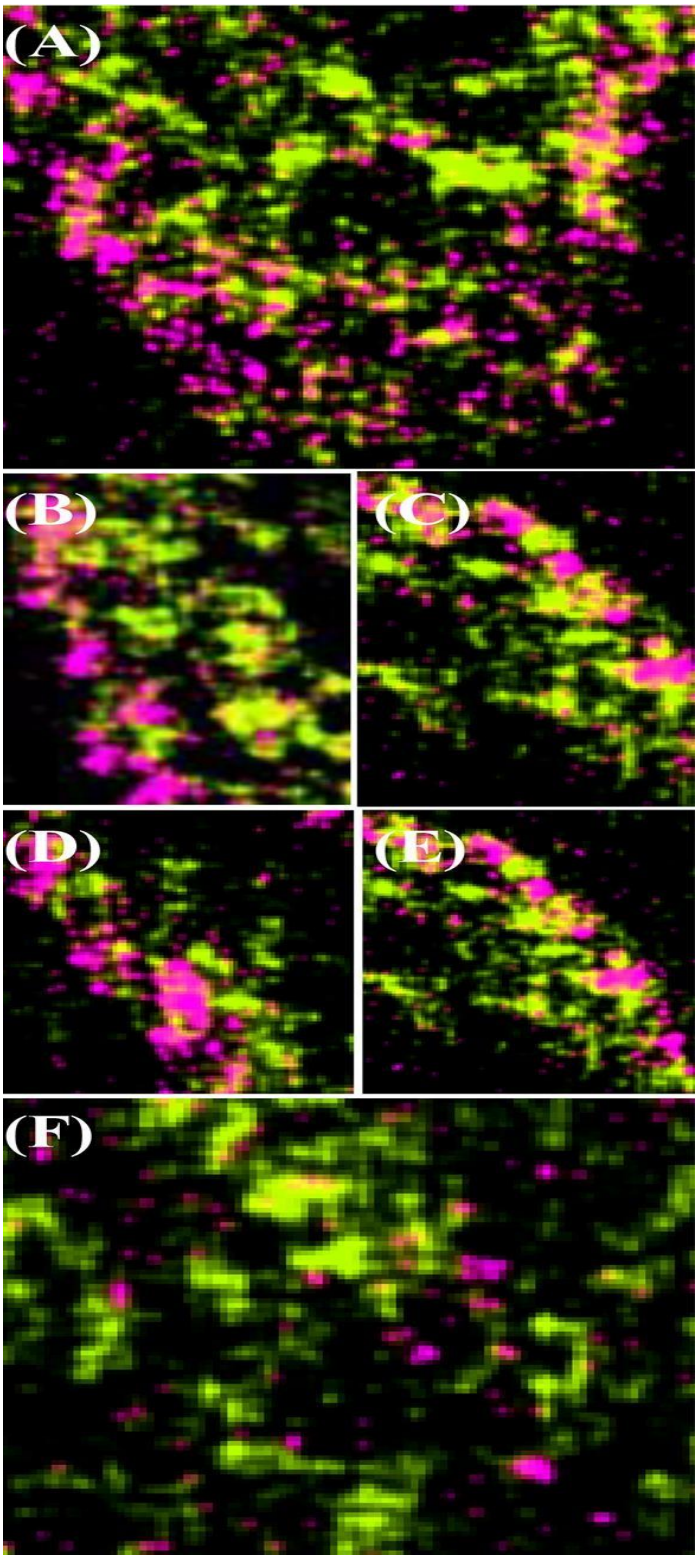

Figure S7A. Expanded regions of cell surfaces of CAS bacteria loaded with 5wt%Pd/5wt%Ru

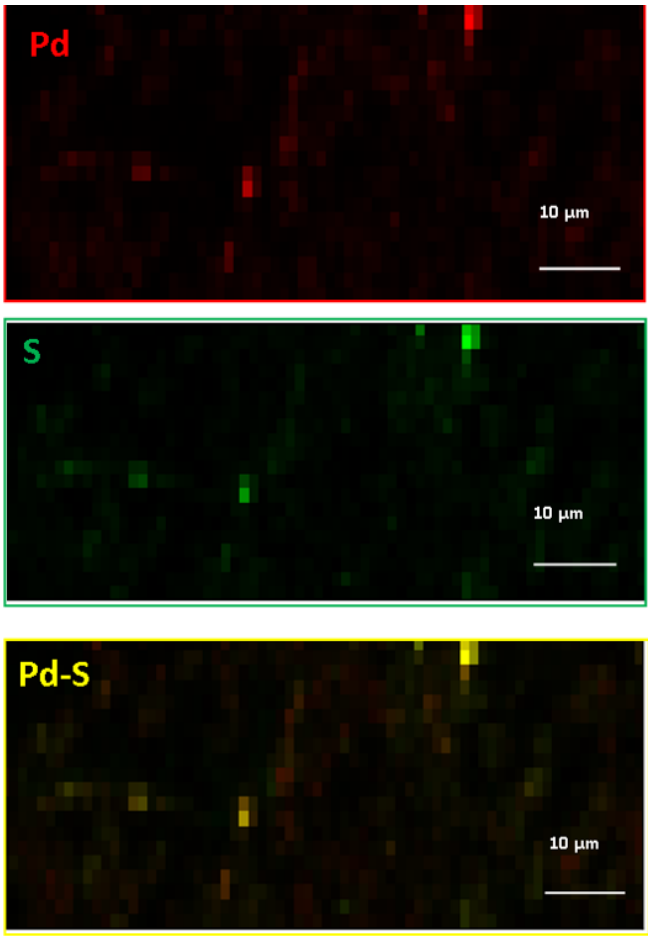

Figure S7B. Preliminary data showing use of X-ray microscopy via synchtrotronradiation to promote element- specific X-ray emission

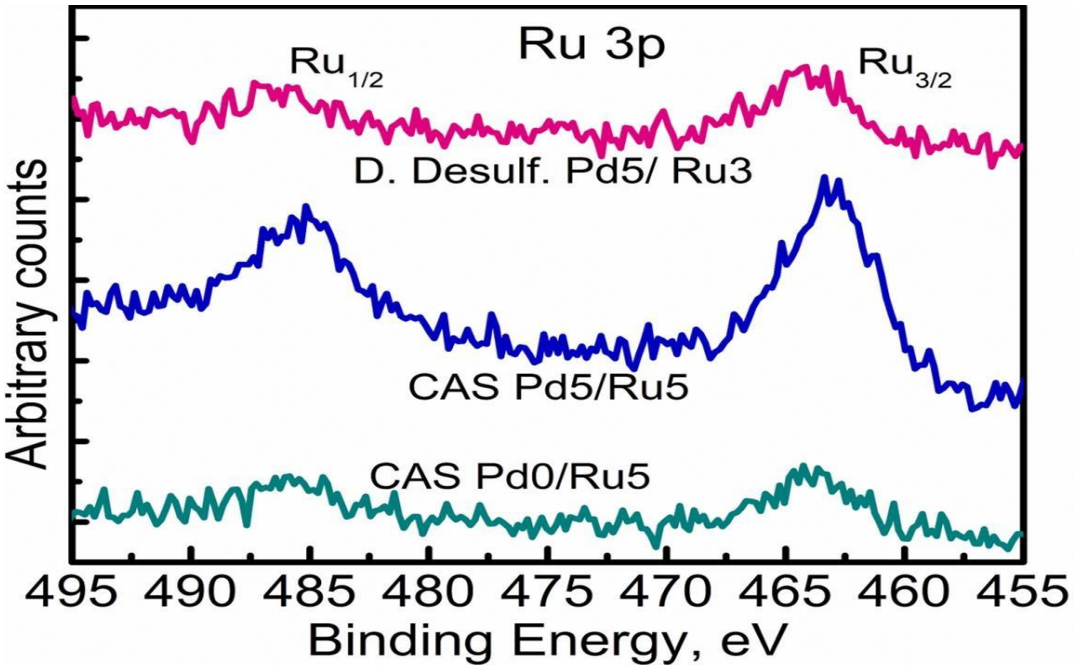

Figure S8. Ru3p XPS spectra for 3 biometallic samples

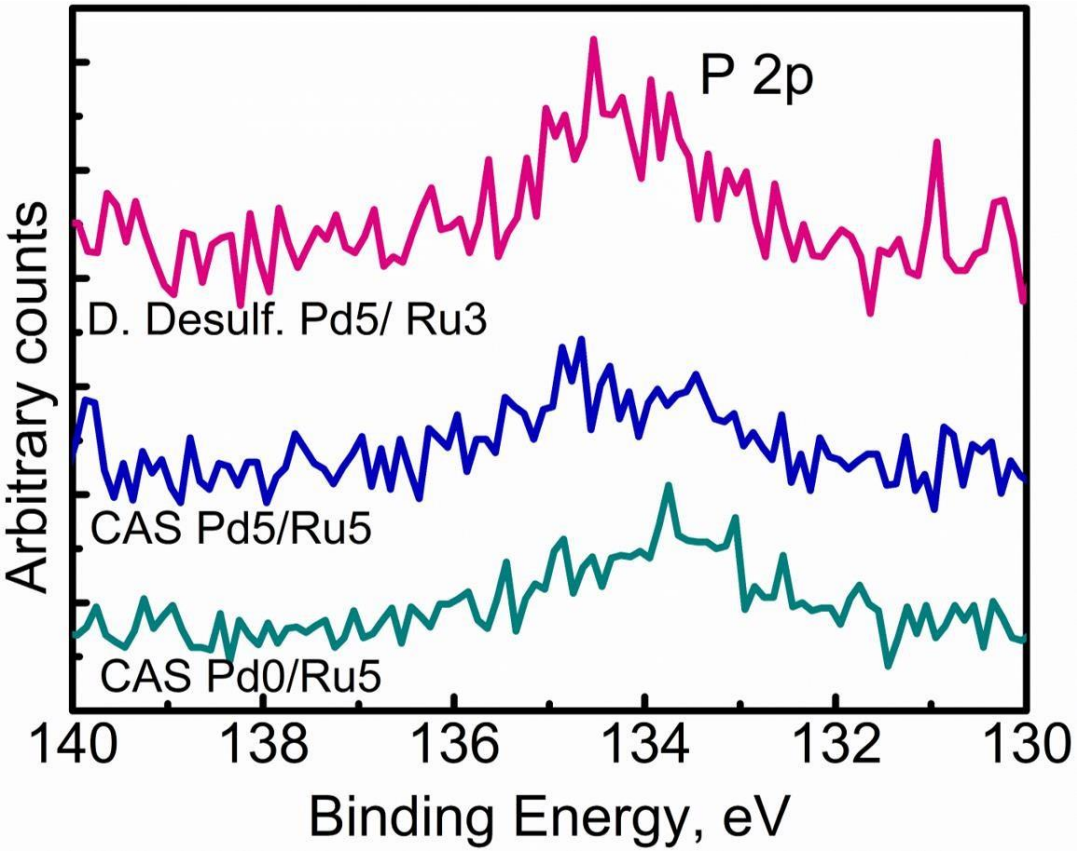

Figure S9. P2p XPS spectra for 3 biometallic samples

CHAPTER III

Characterization of Palladium Nanoparticles Produced by Healthy and Microwave-Injured Cells of *Desulfovibrio desulfuricans* and *Escherichia coli*

Jaime Gomez-Bolivar[1,*], Iryna P. Mikheenko[2], Lynne E. Macaskie[2] and Mohamed L. Merroun[1]

[1] Department of Microbiology, Faculty of Sciences, University of Granada, Campus Fuentenueva, 18071 Granada, Spain; merroun@ugr.es (M.L.M.)

[2] School of Biosciences, University of Birmingham, Edgbaston, Birmingham B15 2TT, UK; I.Mikheenko@bham.ac.uk (I.P.M.); L.E.Macaskie@bham.ac.uk (L.E.M.);

* Correspondence: jagobo@ugr.es; Tel.: +34-958-24-98-34

nanomaterials

MDPI

Article

Characterization of Palladium Nanoparticles Produced by Healthy and Microwave-Injured Cells of *Desulfovibrio desulfuricans* and *Escherichia coli*

Jaime Gomez-Bolivar [1,*], Iryna P. Mikheenko [2], Lynne E. Macaskie [2] and Mohamed L. Merroun [1]

Abstract

Numerous studies have focused on the bacterial synthesis of palladium nanoparticles (bio-Pd NPs), via uptake of Pd (II) ions and their enzymatically-mediated reduction to Pd (0). Cells of *Desulfovibrio desulfuricans* (obligate anaerobe) and *Escherichia coli* (facultative anaerobe, grown anaerobically) were exposed to low-dose radiofrequency (RF) radiation (microwave (MW) energy) and the biosynthesized Pd NPs were compared. Resting cells were exposed to microwave energy before Pd (II)-challenge. MW-injured Pd (II)-treated cells (and non MW-treated controls) were contacted with H_2 to promote Pd(II) reduction. By using scanning transmission electron microscopy (STEM) associated with a high-angle annular dark field (HAADF) detector and energy dispersive X-ray (EDX) spectrometry, the respective Pd NPs were compared with respect to their mean sizes, size distribution, location, composition, and structure. Differences were observed following MWinjury prior to Pd(II) exposure versus uninjured controls. With *D. desulfuricans* the bio-Pd NPs formed post-injury showed two NP populations with different sizes and morphologies. The first, mainly periplasmically-located, showed polycrystalline Pd nano-branches with different crystal orientations and sizes ranging between 20 and 30 nm. The second NP population, mainly located intracellularly, comprised single crystals with sizes between 1 and 5 nm. Bio-Pd NPs were produced mainly intracellularly by injured cells of *E. coli* and comprised single crystals with a size distribution between 1 and 3 nm. The polydispersity index was reduced in the bio-Pd made by injured cells of *E. coli* and *D. desulfuricans* to 32% and 39%, respectively, of the values of uninjured controls, indicating an increase in NP homogeneity of 30%–40% as a result of the prior MW injury. The observations are discussed with respect to the different locations of Pd(II)-reducing hydrogenases in the two organisms and with respect to potential implications for the catalytic activity of the produced NPs following injury-associated altered NP patterning.

Keywords: palladium nanoparticles; microwave injured cells; microwave energy; *Escherichia coli*; *Desulfovibrio desulfuricans.*

1. Introduction

Platinum group metals (PGMs) (e.g., Pd, Pt, Ru, Rh, Os, Ir) are widely used as catalysts in many different reactions to obtain valuable products with industrial applications [1]. They are of particular importance due to their unique properties (i.e., high catalytic activity, oxidation resistant properties, mechanical strength, and outstanding resistance to corrosion) [2]. PGM catalysts are used to control the emission of gaseous pollutants from automobiles. Due to this high global demand the price of PGMs has increased substantially since the mid-2000s [3], while high demand for PGMs [4,5] has also increased the focus on recovery processes. Chemical methods offer an alternative for PGM recovery from wastes; these methods include ion exchange, solvent extraction or electrochemical recovery, but they have the challenge of using strong chemicals which are often toxic and environmentally damaging [6].

Bacterially-mediated recovery of PGMs is considered as an emerging green and cheap alternative to traditional physical and chemical approaches. Bio-derived methods can exhibit numerous advantages since bacterial species used as templates are easy to grow in large amounts and are capable of rapid metal reduction to form metallic nanoparticles that are comparably active to commercial catalysts in chemical synthesis [7].

Bacteria can interact with soluble metal species in many different ways (e.g., via enzymatic reduction, biosorption, biomineralization, etc.) [8–10]. Bacterially-mediated reduction of metals into a neo-catalyst has attracted much interest with other potential applications in, for example, fuel cells [11], decontamination of groundwater [12], and catalytic upgrading of heavy fossil and pyrolysis oils [13,14]. Some microorganisms are able to recover Pd (II) from acidic solutions similar to the conditions that are present in industrial wastes (and from actual waste leachates) and convert waste PGMs into a green neo-catalyst [15,16]. A life cycle analysis of the latter, as applied to catalytic upgrading of heavy fossil oil, showed the economic potential of this approach even before factoring in the energy (carbon) savings in refinery and mitigation of the high carbon impact and environmental damage involved in mining and metal extraction from primary ores [17].

The use of bacteria for synthesis of metallic nanoparticles (NPs) offers the advantage of NP size control via bio-patterning and the use of enzymes for the Pd reduction avoids the

use of toxic chemicals as capping agents that would add to the process cost [18]. Additionally, living systems operate at ambient temperatures, making the process of synthesis of NPs economically attractive. For example, *Desulfovibrio desulfuricans*, a Gram-negative strain, has been shown to use periplasmic hydrogenases supplied with hydrogen to form Pd NPs in the periplasm [9]. NP-synthetic capability has been shown also in other Gram-negative bacteria like *Shewanella oneidensis*, *Escherichia coli*, and *Pseudomonas putida* [7,19–21] as well as Gram-positive bacteria such as *Bacillus sphaericus* and *Arthrobacter oxydans* [22,23]. With the use of modern microscopes, recent studies reported the accumulation of small intracellular Pd NPs in both bacterial types [24], as well as in cell surface layers. Although the former brings possible limitations of substrate access, the use of acetone-washed cells permeabilizes them, whereas NPs stripped of their biochemical scaffold agglomerated and lost activity [25], while partial cleaning altered the catalytic activity as the metal surface was progressively unmasked [26]. However, such processing would add to the production cost and hence this study reports the use of a supported Pd catalyst made on whole cells.

In addition to cellular location, particle size, and shape, dispersity can play an important role in catalyst reactivity in some reactions [27]. In the case of microbial synthesis of Pd NPs, some studies have shown an influential role of the biological component in the control of shape, size, and distribution of NPs and, as a consequence, their catalytic activity [7]. A possible association of the initial Pd "seeds" with intracellular phosphate structures has been postulated in cells of *Bacillus benzoevorans*, preventing the Pd NPs from agglomeration [24]. Electron donors such as formate or hydrogen used in NP fabrication can influence the sizes of the biochemically-formed PdNPs and, with this, their electrocatalytic activity [28]. Taking into account these different factors a method of manipulating the formation of NPs to influence their size and distribution could result in a tailored catalyst for increased reaction rates and selectivity in a given reaction.

The main challenges that face the synthesis of nanoparticles are: control of the size and shape of the NPs and monodispersity. It is known that thermal factors can affect the size and uniformity of nanoparticles [29]. Localized heating can be achieved by the use of microwave radiation. Any material (but particularly water) can absorb microwave energy and this is expressed by its dielectric loss factor combined with the dielectric constant.

When the microwave heats the desired material through the dielectric loss, it converts the radiation energy into thermal energy [30]. In organic synthesis this has been shown to accelerate processes involved in homogeneous catalysis [31]. The efficiency of microwave energy for the synthesis of a variety of nanomaterials including metals, metal oxides, and bimetallic alloys has been shown [32]. The effect of microwave (MW) radiation on microorganisms has also been studied [33,34]. Some authors noted that application of radiofrequency (RF) microwave radiation (2.45 GHz) altered the activities of some enzymes expressed in *Staphylococcus aureus* resulting from some changes in the cell that could not be explained by the thermal effect [35]. More recently, Shamis et al. [34] confirmed that MW radiation on cells could result in toxic effects when the heating effect was discounted. By modulating the frequency of the MW radiation [36] different biological effects in terms of protein structures were observed, together with alterations in the routes of some biochemical reactions.

In this study MW energy was applied to cells of *E. coli* and *D. desulfuricans* before their exposure to palladium solution. Following the MW treatment, synthesis of Pd NPs was performed using molecular hydrogen as the electron donor. Characterization of size, shape, cellular localization, and atomic structure of the fabricated NPs was conducted by means of scanning transmission electron microscopy (STEM) associated with a high-angle annular dark field (HAADF) detector and energy dispersive X-ray micro analysis (EDX). The use of X-ray diffraction analysis of bulk material was largely precluded by the small nanoparticle sizes and hence poorly resolved powder patterns of the largely amorphous biomaterial [37]. The possible application of the MW treatment to moderate the synthesis of more dispersed and homogeneous Pd NPs is discussed with reference to data obtained from high-resolution electron microscopy in conjunction with image analysis.

2. Materials and Methods

2.1. Bacterial Strains and Culture Conditions

Two Gram-negative bacterial strains were used in this study, a facultatively anaerobic strain *Desulfovibrio desulfuricans* NCIMB 8307 and the facultatively anaerobic *Escherichia coli* MC4100 as described previously [19, 24]. *D. desulfuricans* was grown anaerobically under oxygen-free nitrogen (OFN) in Postgate's medium C (Sigma-

Aldrich) (pH 7.5 ± 0.2) at 30 °C (inoculated from a 24 h pre-culture, 10%*v/v*) in sealed anaerobic bottles [24], while *E. coli* was grown anaerobically (37 °C) on nutrient broth N° 2 (Sigma-Aldrich) supplemented with 0.5%(*v/v*) glycerol (Sigma-Aldrich) and 0.4% (*w/v*) fumarate (Sigma-Aldrich) as described previously [19]. Cells were grown to mid-exponential phase and harvested (Beckman Coulter Avati J-25 Centrifuge, U.S.A) by centrifugation (12,000 g, 15 min), washed 3 times in 20 mM MOPS-NaOH buffer (pH 7), concentrated in a small volume of buffer to between 20 and 30 mg dry weight per ml and stored under OFN at 4 °C until next day [38]. Cell dry weight was calculated from optical density (OD_{600}) by a previously-determined dry weight conversion factor (mg dry cells= $CF \times OD_{600} \times n$, (where n is the dilution factor)).

2.2. Microwave Irradiation of E. coli and D. desulfuricans cells

2.2.1. Microwave Irradiation Conditions

This study was carried out using a portable commercial apparatus (CEM corporation, North Caroline, United States) (CEM Discover SP microwave digestion system; single-mode energy source; 300 W magnetron; ~3GHz, 300W). Vials containing cells in 6mL volume re-suspended in 20 mM buffer with concentration between 20 and 30 mg dry weight/ml were exposed in short bursts (10 s) interspersed with periods of 30 s of cooling in ice cold acetone after exposure. This process was repeated three times (total irradiation period of 30 s). During the microwave irradiation sample vials were cooled in hexane.

2.2.2. Microwave Irradiation of Resting Cells Suspended in MOPS Buffer

A 5 mL volume of concentrated cell suspension between 20 and 30 mg/mL in 20 mM MOPS-NaOH buffer (Sigma-Aldrich) pH 7 was added into a 6 mL sealed tube under OFN and treated as above. After microwave exposure, a known amount of treated cells was taken and added immediately to a new sealed tube containing Pd (II) solution (below), representing a final 5 wt% of Pd on the cells. As a control, a 6mL sealed tube under OFN of Pd(II) solution in buffer was added and exposed to microwave radiation under the same conditions as above.

2.3. Preparation of Palladium-Challenged Cells

2.3.1. Palladium Solution

For "palladization" of cells a Pd(II) solution was used: 2 mMNa_2PdCl_4 (Sigma-Aldrich, St. Louis, Missouri, United States) pH 2 in 0.01M HNO_3 placed in sealed tubes (final volume of 6 mL) and degassed with oxygen-free nitrogen (OFN) under vacuum prior to addition of bacteria.

2.3.2. Formation of Pd Nanoparticles by Control and MW-Treated Cells

Following microwave treatment, tubes with cells (and untreated controls) were allowed to stand in a water bath (30 min, 30 °C) for uptake of the Pd (II) ions in order to form nucleation sites on the biomass. Hydrogen was added as an electron donor by bubbling H_2 gas through the suspensions in the sealed bottles (15 min) which were left under H_2 (24 h) for complete reduction of palladium on the cells (confirmed by assay of residual soluble Pd (II)). Palladized cells were harvested by centrifugation (12,000g, 15 min) and washed with distilled water twice prior to fixation (2.5% glutaraldehyde in 0.1 M cacodylate buffer (pH 7)) for examination by electron microscopy. Controls of palladium-challenged cells without MW treatment were prepared in the same way.

2.3.3. Residual Pd(II) Quantification Using the Tin(II) Chloride Method

In order to confirm complete depletion of Pd (II) ions from the solution, the spectrophotometric tin (II) chloride-based method was used as described previously [39].

2.4. High-Resolution Scanning Transmission Electron Microscopy (STEM) with HAADF (High-Angle Annular Dark Field) Detector and EDX Analysis

For STEM analysis, thin sections of palladized MW-treated and non-treated *E. coli* and *D. desulfuricans* cells were prepared according to the method described by Merroun et al. [40]. To determine the location of palladium NPs in the cells, palladized cells were examined under a high-angle annular dark field scanning transmission electron microscope (HAADF–STEM) FEI TITAN G2 80–300 at 300 KeV. For elemental analysis, EDX (energy dispersive X-ray microanalysis of specimen microareas) was used with a spot size of 4 Å and a live counting time of 50s coupled with a high-resolution STEM and HAADF detector. Element co-localizations (Pd, P, S) were enumerated by use

of the Manders overlap coefficient (MOC) [41] implemented in ImageJ via the JACoP [38] and co-localization was assumed if the Manders coefficient was greater than 0.9.

2.5. Image Processing, Lattice Spacing Determination and Particle Size Analysis

The HAADF–STEM images were used to determine the average size of Pd NPs produced in different experiments as well as their distribution by means of the image processing software ImageJ (National Institutes of Health, Maryland, United States) [42]. In order to distinguish the Pd nanoparticles on/in cells from background signals and artifacts the same methodology as described by Omajali et al. [24] was used and mean particle size was calculated (mean ± SEM from at least 3 different areas of samples; total NPs analyzed was>100). Significant differences were assigned using the two sample test of the variance at P= 0.95. The polydispersity index or coefficient of variation was calculated from the particle size distribution dividing the standard deviation of the means by the means [43]. At least 100 particles were counted in each case using ImageJ software. The particle size distribution was estimated using Origin Pro 8. The lattice spacing was determined using ImageJ through profiling of HR-TEM images and compared against lattice spacing of bulk palladium from the database generated using Powder cell 2.400 software (2.4, Informer Technologies, Inc).

3. Results

3.1. Microwave-Injury of Bacteria

Examination of the cells by electron microscopy post-injury showed cellular damage as compared to uninjured controls (Supplementary information Figure S1), similar to the response observed by Shamis et al. [34], i.e., shrinkage of the cytoplasmic compartment away from the wall layers with an enlarged periplasmic space. Shamis et al. [34] attributed this to the electromagnetic radiation and not the heating effect. Even though cooling was applied, it was not possible to make this distinction unequivocally using the commercial equipment in this study. Instead, a prior study [44] was carried out using purpose-built equipment that decoupled the electromagnetic and thermal effects at a comparable applied dose (Supplementary information Figure S1). This showed an identical cellular response visually to that using the commercial equipment (with cooling) in the present study and hence, as noted by Shamis et al. [34] the reported cellular response can be attributed to the effect of the MW irradiation.

3.2. Examination of the Pd Nanoparticles Produced by Native and MW-Injured Cells of E. Coli MC4100 and D. Desulfuricans NCIMB 8307

Controls of Pd(II) solution in buffer alone exposed to microwave radiation showed no removal of Pd (II) from the solution after microwave exposure using the tin (II) chloride method, nor the appearance of any black Pd(0), indicating that microwave irradiation had no active role in the reduction of Pd (II) under the condition tested in this work.

In order to examine and identify the Pd NPs made by native and injured cells, high-resolution HAADF–STEM with EDX was used. For both strains the Pd loading was 5wt% (1:19 mass of Pd:dry weight of cells). Electron opaque NPs, identified as Pd by EDX (Supplementary information Figure S2) were found in the cell surface layers and within the intracellular matrices (Figure 1B, E and Figure 2B,E). In the case of untreated cells of *E. coli* (Figure 1A–C) large clusters were observed within the intracellular matrices (Figure 1C inset bottom left) and membrane (Figure 1C, main panel, arrowed) at high magnification while MW-treated cells showed apparently more dispersed intracellular NPs with few clusters (Figure 1F).

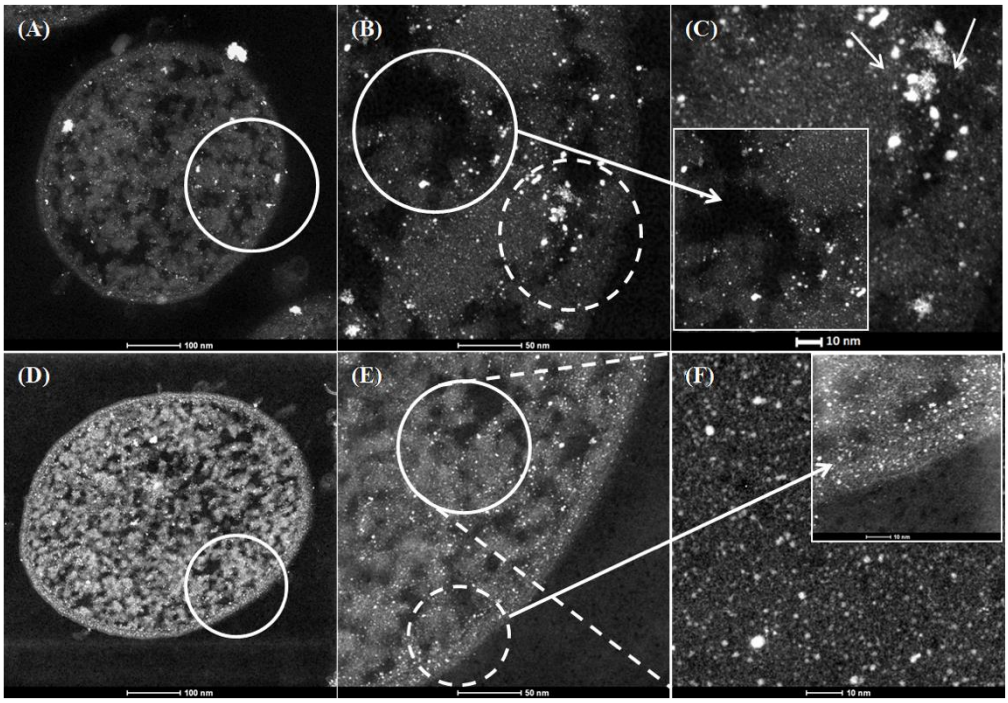

Figure 1. High-angle annular dark field scanning transmission electron microscope (HAADF–STEM) micrographs of Pd nanoparticles synthesized using 5wt% Pd loading (1:20) on *E. coli* MC4100 from 2 mM Na_2PdCl_4 solution,

in0.01 M HNO_3 using hydrogen as an electron donor without prior microwave (MW) treatment (**A**,**B**,**C**) and with 30 s prior MW treatment (**D**,**E**,**F**).

In contrast, untreated cells of *D. desulfuricans* showed a deposition of surface bound NPs in clusters (Figure 2B,C) in agreement with Omajali et al. [24]. Pd NPs located at the level of the periplasm showed inclusions in the form of nano-branches with sizes ranging from 20 to 30 nm (Figure 2C arrowed), while intracellular NPs were visible which were smaller with sizes between 1 and 5 nm (Figure 2C inset top left). Following MW treatment, and in contrast to *E. coli* (above), the cytoplasmic compartment of MW-treated *D. desulfuricans* remained contracted to reveal NPs in the outer and inner membranes (Figure 2D) with NP-deposition also in the periplasmic space (Figure 2D circled area). The main differences were in morphology of the NPs observed at the level of the surface (Figure 2F) in comparison with untreated cells (Figure 2C), where larger clusters were observed at high magnification. No major differences in number and morphology of Pd NPs were apparent visually by HR-TEM alone within the intracellular matrices in treated (Figure 2C top left) and untreated cells of *D. desulfuricans* (2F bottom right).

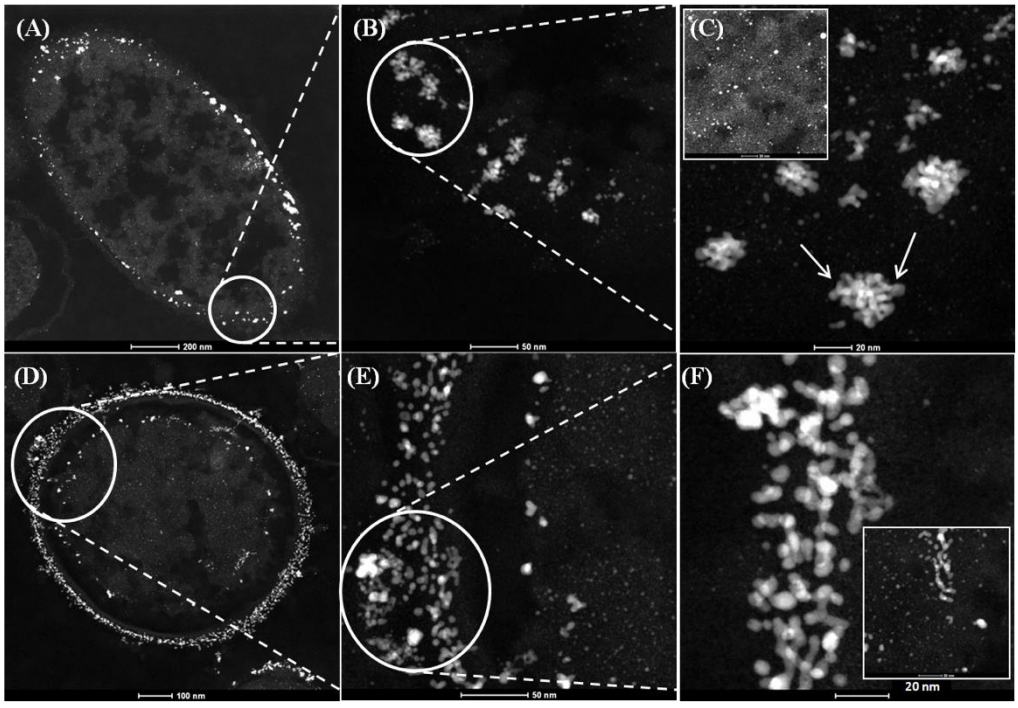

Figure 2.HAADF–STEM micrographs of Pd nanoparticles synthesized using 5wt% Pd loading (1:20) on *D. desulfuricans* from 2 mM Na_2PdCl_4 solution, in0.01 M HNO_3 using hydrogen as electron donor without MW treatment (**A**,**B**,**C**) and with 30 second MW treatment (**D**,**E**,**F**).

The distribution of Pd NPs within the intracellular matrices, cell surface layers, and membrane was established by using elemental mapping (Figure 3 and 4). The main elements associated with Pd were phosphorus (P) and sulfur (S). Statistical analysis using ImageJ software [41] was done in order to determine the Manders overlap coefficient to reveal any correlation in localization between Pd and S, and Pd and P in each strain and the effect of the MW treatment on any co-localizations. The Manders overlap coefficient was above 0.9 for both strains and treatments (Figure 3 and 4). According to the statistics analysis done using ImageJ, no differences in the degree of co-location for the selected elements for control and MW-treated cells were observed for either strain (Figure 3 and Figure 4).

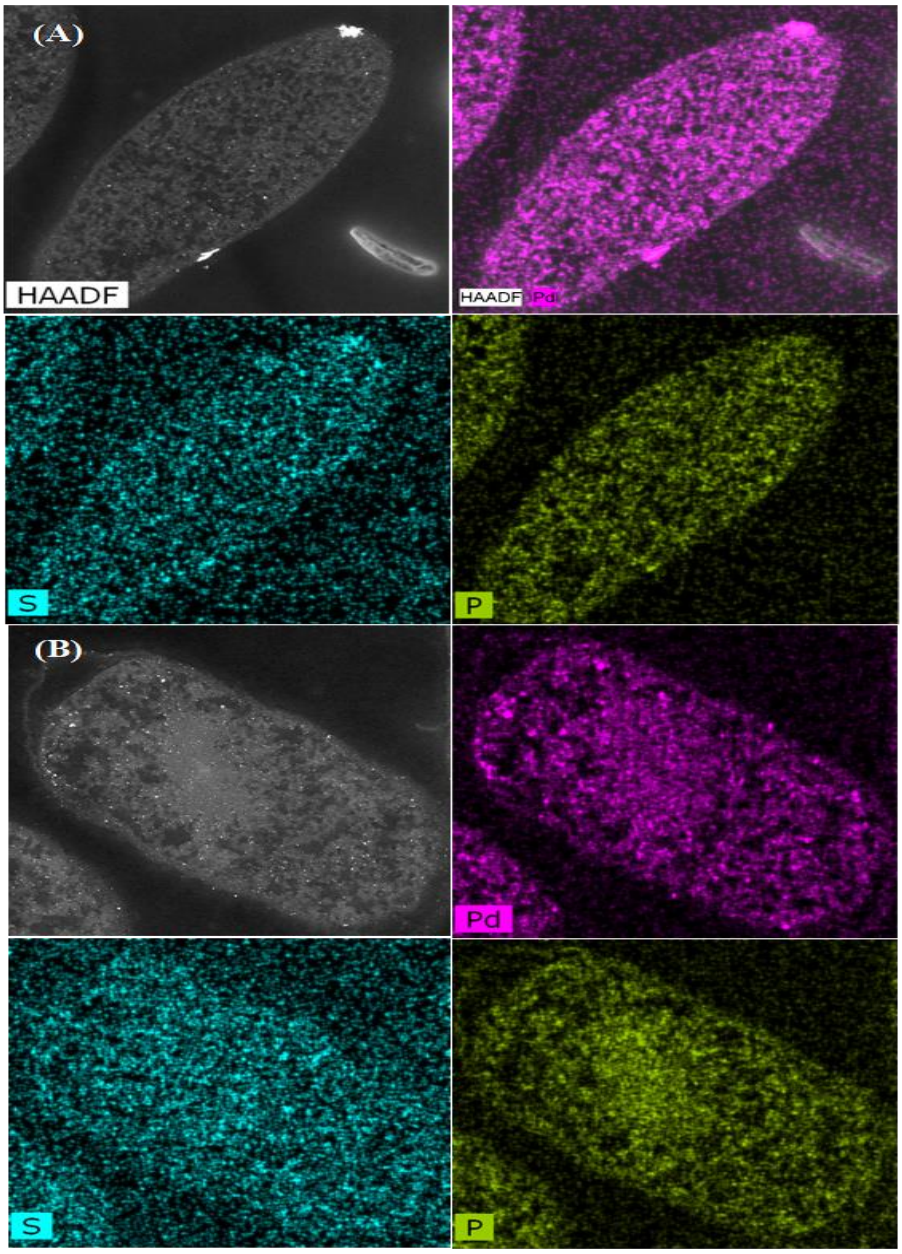

Figure 3. Elemental mapping showing distribution of Pd, P, and S in untreated cells of *E. coli* MC4100 (**A**) and cells treated with MW for 30 sec (**B**). The Manders overlap coefficients were higher than 0.9 for Pd/P and Pd/S in control and MW-treated cells.

The co-location of Pd with S in *D.desulfuricans* is assumed to be PdS resulting from biogenic H_2S from residual metabolism [24] and the formation of PdS was confirmed in cell surface layers of sulfidogenic bacteria using X-ray photoelectron spectroscopy [45]. In addition, sulfur is present in the amino acids, cysteine and methionine (components of

proteins), while phosphorus is ubiquitous within deoxyribonucleic acids, ribonucleic acids, phospholipids, etc., as well as phosphorylated proteins and ATP. The role of these biological components in the patterning of palladium deposition is under current consideration.

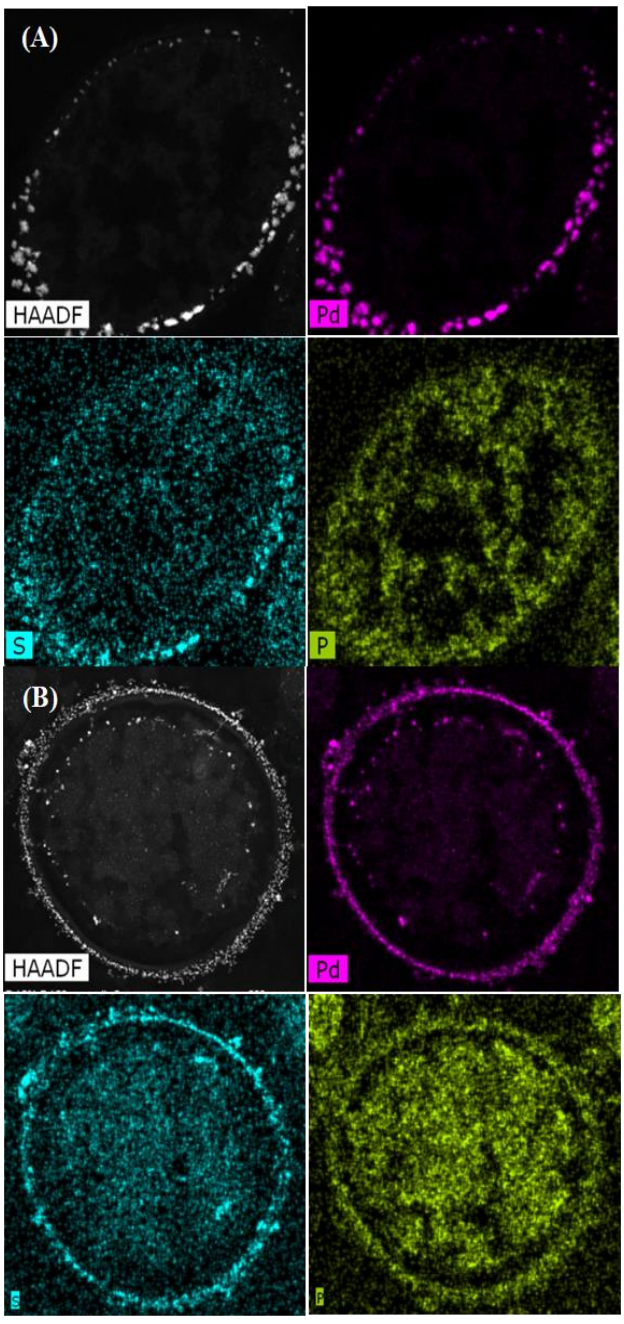

Figure 4. Elemental mapping showing distribution of Pd, P, and S in untreated cells of *D. desulfuricans* (**A**) and cells treated with MW for 30 sec (**B**). The Manders overlap coefficients were higher than 0.9 for Pd/P and Pd/S in control and MW-treated cells.

3.3. Dispersity and Size Distribution of Pd Nanoparticles

Analysis of the nanoparticles size distribution was performed using high-resolution images and ImageJ software [46]. Cells previously MW-treated and then exposed to Pd (II) followed by reduction to Pd (0) were analysed. The mean particle size of the intracellular Pd nanoparticles was 1.28 nm and 1.17 nm for the control and treated cells of *E. coli* MC4100, respectively (Figure 5A,B).

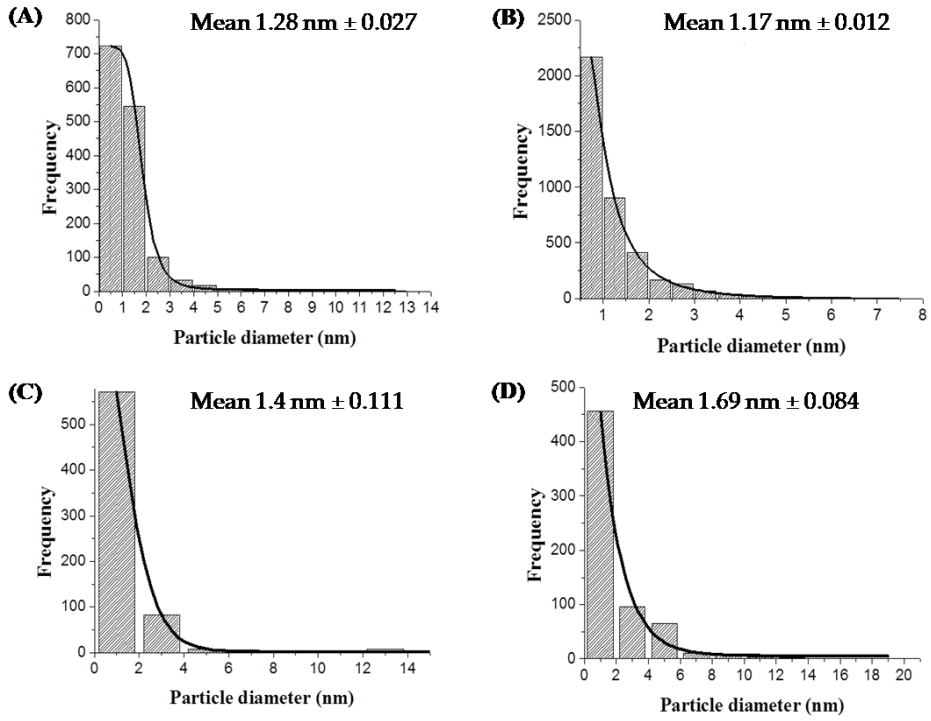

Figure 5. Size distribution and mean nanoparticle (NP) sizes of Pd nanoparticles made by *E. coli* MC4100 untreated (**A**) and MW-treated cells (**B**) and *D. desulfuricans* untreated (**C**) and MW-treated cells (**D**).The mean NP sizes (nm, mean ± SEM) were (A): 1.28 ± 0.027; (B): 1.17 ± 0.012; (C): 1.40 ± 0.11; (D): 1.69 ± 0.084.

For *D. desulfuricans* the major differences in terms of shape and size of the NPs were observed on the surface so the analyses were mainly focused on these areas. The corresponding mean particle sizes of membrane Pd NPs produced by treated cells was 1.69 nm and 1.4 nm for control cells (Figure 5D and 5C, respectively). These differences were significant at P = 0.95 (two sample test of the variance) and hence *E. coli* makes smaller intracellular NPs in response to MW irradiation whereas the NP size increases in

the case of *D. desulfuricans* surface-located NPs. However since the differences were small (~10%–20%), a mechanistic biological significance cannot be attributed to them at this stage and further work is required to reveal the underlying reasons which may be attributed to the mechanisms of NP deposition in the two strains (see Discussion).

Despite the small differences in mean sizes of the Pd nanoparticles, notable differences were found in their degree of dispersity. The polydispersity value of Pd nanoparticles produced by treated cells of *E. coli* was 0.55 as compared to 0.80 for untreated cells. In the case of *D. desulfuricans* the polydispersity value was 1.26 and 2.07 for MW-treated and untreated cells, respectively. The lower value of polydispersity indexes (32% and 39% lower than controls for *E. coli* and *D. desulfuricans*, respectively) for the two strains resulting from the MW injury suggests a higher degree of homogeneity of the size of nanoparticles. This is accordance with the visual appearance of the cells as noted above.

3.4. Crystallinity and Lattice Spacing of Pd Nanoparticles

No differences were observed in terms of crystallinity of the particles under these conditions (Figure6 and Figure7). The most representative lattice spacing for *E. coli* was 0.204 nm and 0.213 nm consistent with the (200) facets, and 0.241 nm and 0.23 nm consistent with the (111) facets of Pd, showing a mixed-facet arrangement for both membrane and intracellular Pd nanoparticles (Figure6A and B).

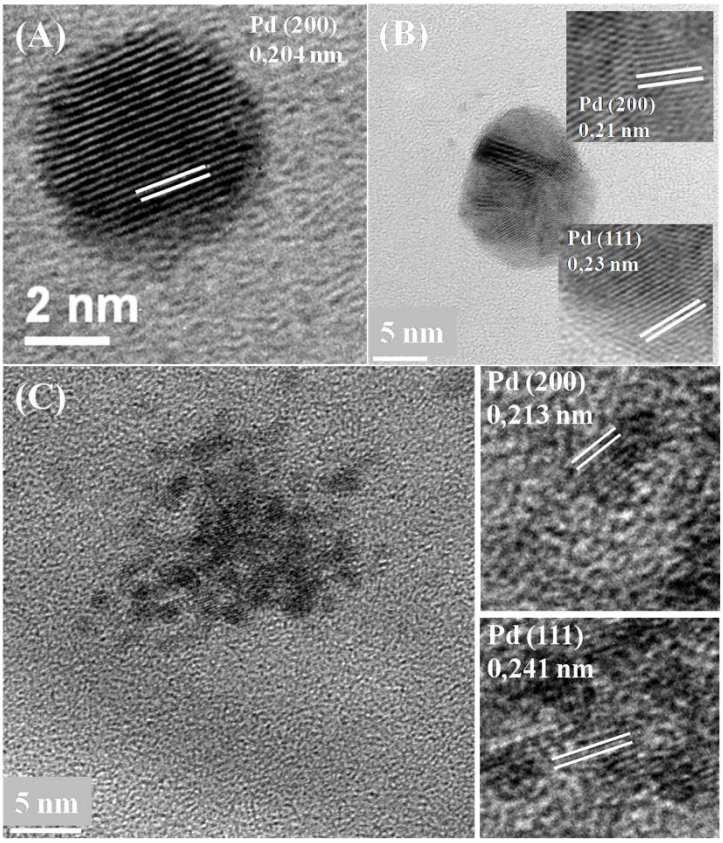

Figure 6.TEM images of intracellular Pd crystals made by *E. coli* MC41005% bio-Pd 30 seconds MW treatment before being exposed to Pd(II) (**A**,**B**) and untreated cells (**C**) revealing lattice spacing in crystals.

MW-treated cells of *D. desulfuricans* showed lattice spacing of 0.223 nm and 0.199 nm, again consistent with the (111) and (200) facets (Figure 7A) and, similarly, 0.231 and 0.202 nm for untreated cells. A similar NP structure was observed in previous studies by Omajali et al. [24] of Pd nanoparticles in *D. desulfuricans* with a mix-facet arrangement of (111) and (200) with different crystal orientations in the case of the larger clusters (Figure 7A) when made under H_2 as in the present study.

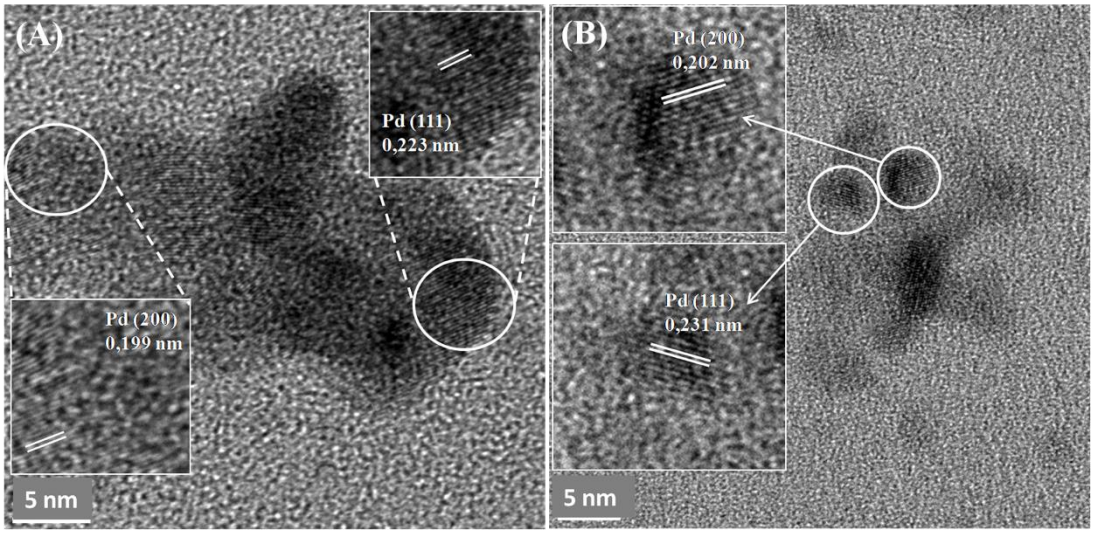

Figure 7.TEM images of membrane-bound Pd crystals made by *D. desulfuricans* 5% bio-Pd 30 seconds MW treatment before being exposed to Pd(II) (**A**) and untreated cells (**B**) revealing lattice spacing in crystals.

4. Discussion

This study focuses on the synthesis and characterization of palladium nanoparticles produced by two different bacterial strains that were previously injured via application of microwave energy compared to cells that had no MW exposure. The capacity of these two related genera for the synthesis of Pd NPs is well known via the activity of hydrogenases [9,19] as well as via other (unidentified) mechanisms in cells under conditions in which hydrogenases are not expressed [47]. The chemical reduction of Pd (II) under hydrogen or with formate as an electron donor using killed cells was almost negligible [9,19]. Few studies have been published using cells previously treated with MW energy and none involve the synthesis of Pd NPs. Previous studies proposed that the application of radiofrequency (RF) energy in *E. coli* under similar conditions to those used in this work might cause electrokinetic modification of the cell surface with a destabilization of the cell membrane [34]. Another observation made by this group was that the application of MW energy resulted in disruption of the cellular membrane and, as a consequence, cytosolic fluids within the *E. coli* cells could pass out through the membrane. However, this was a temporary effect as the shape of the cells was restored within a 10 min recovery period. In the present study the Pd (II) was applied immediately after the removal of the cells from the MW apparatus within 1 min at the early stage of

the 10 min “recovery window”. However, follow-up work showed that incorporating the Pd (II) at the outset, during MW exposure, gave similar results as with MW exposure during the pre-Pd (II) period [44] using the experimental setup described here as well as that of the earlier study (Supplementary information Figure S1).

In normal processes of formation of Pd NPs on *E. coli*, a possible mechanism to explain the transport of Pd inside the cells was highlighted by Deplanche et al. [7], while a previous report [47] showed that Pd (II) is transported across the membrane through an unknown translocation mechanism. It is known that Ni (II) is a key component in many metalloenzymes [48,49] that are located in the cytoplasm (e.g., ureases and hydrogenases); the latter are also located in the cell membrane and, in the case of *D. desulfuricans*, in the periplasmic space. Deplanche et al. [7] suggested that, due to the similar chemistry of Ni (II)and Pd (II), the latter could be transported inside the cells through the Ni (II) “trafficking system” and deposited as NPs in the cytoplasm as a possible mechanism to forestall cytotoxicity if the Pd (II) is taken up in lieu of Ni (II), but cannot substitute for Ni (II) functionally.

Considering cells exposed to MW energy followed by exposure to Pd (II) solution, apart from the mechanisms mentioned above, additional responses could be activated in the cells that could influence the deposition of Pd inside the cells. According to Shamis et al. [34] cytosolic fluids would be extruded from the cells as a response to the MW radiation and the Pd (II) ions may have more sites becoming available for initial formation of NPs on re-absorption of extruded material along with Pd (II) ions. As a consequence, a higher number of initial binding sites would be occupied by Pd (II) due to the higher accessibility to the binding ligands originating from the cytoplasm caused by the MW. Deplanche et al. [7] confirmed a correlation between the initial uptake of Pd (II) onto cellular components and the initial formation of nuclei at many coordination sites, resulting in smaller Pd NPs per given biomass per constant amount of Pd. Once the effect of MW radiation is finished and cells are recovered in shape and membrane permeability (with re-absorption of the cytosolic fluids [34]) the resulting cells would have a greater proportion of Pd (II) ions contained intracellularly (as compared to surface-localized) than untreated cells. Once the intracellular reduction of Pd (II) into Pd (0) occurs, the association of the resulting Pd NPs with phosphate or sulfide structures would reduce NP

mobility, reducing NP agglomeration. The combination of the translocation mechanisms combined with mechanisms activated in the cells as a response to the MW energy may lead to the formation of Pd NPs with higher dispersity than native cells.

A recent study using *S. oneidensis* for the synthesis of Pd/Au nanoparticles showed how a post-treatment consisting of a doping process, carbonization of bacteria, and reduction of graphene oxide avoided NP agglomeration and, as a consequence, increased the dispersity of the nanoparticles, resulting in higher electrochemical activity than a commercial electrocatalyst [50]. Earlier work had shown co-formation of bio-Pd and reduced graphene oxide on cells of *E. coli* [51] but the catalytic activity of the *E. coli* material was not tested. In contrast, for use as a chemical catalyst the cells are not carbonized but are washed in acetone which destabilizes the membrane and lipid structures, making the intracellular Pd NPs more accessible for the reaction. Recent work showed biogenic palladium catalyst of *D. desulfuricans* cells that had been exposed to MW energy had a higher hydrogenation activity and product selectivity in the hydrogenation of 2-pentyne [44], which will be reported as a companion to the present study. Further, follow-up work showed cells of *E. coli* MW injured under the conditions described here had a similarly increased activity as a selective oxidation catalyst when developed as Pd/Au core-shell NP structures.

By the altered deposition of the NPs observed in the biogenic Pd NPs synthesized by MW-treated cells of *D. desulfuricans* in the present work, a causal relationship may be suggested although conclusive proof is awaited. Since the deposition of the derived Pd NPs of untreated cells differs between *E. coli* and *D. desulfuricans* (Figure 1A and Figure 2A) it may be suggested that both types of cell may have different mechanisms relevant to the synthesis of NPs in terms of shape and location via cellular responses during exposure to MW energy and during the recovery period. The process of the synthesis of Pd NPs in *Desulfovibrio* strains has been studied previously [9,24]. With respect to the derived Pd NPs synthesized by *D. desulfuricans*, with cells exposed to MW energy, the main differences were observed in the periplasm where the hydrogenases are predominantly located [52,53]. A higher porosity of the membrane may facilitate the deposition of the Pd (II) in many different nucleation sites for the initial seeds that without the increased porosity of the membrane caused by the MW energy would not be possible.

This hypothesis could explain why the polydispersity index decreases when the cells were previously exposed to MW energy, indicating a higher number of NPs with homogeneous size, given the same dose of Pd (II). This effect was seen regardless of the bacterial strain used.

The relationship between the catalytic activity and the size of the NPs in these two strains has previously been shown [10]. A related study [44]to evaluate the effect of the MW treatment of resting cells (by the method shown in Supplementary information Figure S1) showed the initial rate of conversion of 2-pentyne to be increased by 50% (from 1.1 μmol per litre per second) by Pd NPs made following MW injury of the cells, with selectivity to the desired product cis-2-pentyne, being approximately doubled. One of the major goals in the optimization of the catalytic reactions using NPs as a catalyst is the NPs size control that will help to further understand the relationship between the size and location of the Pd NPs and the product selectivity for a specific reaction. A good example of size control and good dispersion of Au and Pd NPs is the S-layer protein of the Gram-positive strain *Lysinibacillus sphaericus* JG-A12 [54, 55]. The monomer of the S-layer offers a good biotemplate for the formation of NPs with a regular structure, pores with identical size (1–5 nm), and good binding sites for Pd(II) such as glutamic and aspartic groups. The crystal structure of the Pd NPs synthesized by the MW-treated cells in the present study did not differ from the untreated cells, showing similar results for *D. desulfuricans* as those obtained by Omajali et al. [24] where twinned NPs were also seen (Figure 7 and Figure 2b). Future studies will focus on comparative studies of the catalytic activity of the Pd NPs synthesized by MW-treated cells versus untreated cells that will inform the controlled synthesis of bio-Pd NPs with higher catalytic activity.

5. Conclusions

This study shows the application of microwave radiation on Gram-negative cells of *D. desulfuricans* and *E. coli* prior to the exposure of Pd (II) solution for the synthesis of Pd NPs with a higher degree of dispersity compared to cells that had no MW exposure. The response to the MW on the synthesis of the Pd NPs is strain specific. The main differences of the NPs made by treated cells of *E. coli* were at the level of the cytoplasm with an increase of 32% approximately in the level of homogeneity compared to untreated cells. However, the main differences in treated cells of *D. desulfuricans* were observed at the

level of the surface with an increase of 39% in the level of homogeneity of the size of the nanoparticles compared to the control.

Author Contributions: Biomaterials were made and characterized by J.G.B. and I.P.M.; high-resolution SEM/TEM/elemental mapping were done by J.G.B. and M.L.M.; the paper was lead-authored by J.G.B. and work was supervised by L.E.M. and M.L.M.

Funding: The study was supported by NERC (grant NE/L014076/1) to LEM.

Acknowledgments: We acknowledge the assistance of María del Mar Abad Ortega and Concepción Hernández-Castillo (Microscopy Service, Centro de Instrumentación Científica, and University of Granada, Spain).

Conflicts of Interest: the authors declare no conflicts of interest.

References

1. Rao, C.R.M.; Reddi, G.S. Platinum group metals (PGM); occurrence, use and recent trends in their determination. *TrAC-Trends Anal. Chem.* **2000**, *19*, 565–586. doi:10.1016/S0165-9936(00)00031-5.
2. Rao, C.R.K.; Trivedi, D.C. Chemical and electrochemical depositions of platinum group metals and their applications. *Coord. Chem. Rev.* **2005**, *249*, 613–631. doi:10.1016/j.ccr.2004.08.015.
3. Cowley, A.; Woodward, B. A healthy future: Platinum in medical applications platinum group metals enhance the quality of life of the global population. *Platinum Metals Rev.* **2011**, *55*, 98–107. doi:10.1595/147106711×566816.
4. Gavin, H. Platinum group metals research from a global perspective. *Platin. Met. Rev.* **2010**, *54*, 166–171. doi:10.1595/147106710×500125.
5. Kononova, O.N.; Melnikov, A.M.; Borisova, T.V.; Krylov, A.S. Simultaneous ion exchange recovery of platinum and rhodium from chloride solutions. *Hydrometallurgy* **2011**, *105*, 341–349. doi:10.1016/j.hydromet.2010.11.009.
6. De Corte, S.; Bechstein, S.; Lokanathan, A.R.; Kjems, J.; Boon, N.; Meyer, R.L. Comparison of bacterial cells and amine-functionalized abiotic surfaces as support for Pd nanoparticle synthesis. *Colloids Surf. B* **2013**, *102*, 898–904. doi:10.1016/j.colsurfb.2012.08.045.
7. Deplanche, K.; Bennett, J.A.; Mikheenko, I.P.; Omajali, J.; Wells, A.S.; Meadows, R.E.; Wood, J.; Macaskie, L.E. Catalytic activity of biomass-supported Pd nanoparticles: Influence of the biological component in catalytic efficacy and potential application in "green" synthesis of fine chemicals and pharmaceuticals. *Appl. Catal. B Environ.* **2014**, *147*, 651–665. doi:10.1016/j.apcatb.2013.09.045.
8. Merroun, M.L.; Nedelkova, M.; Ojeda, J.J.; Reitz, T.; Fernández, M.L.; Arias, J.M.; Romero-González, M.; Selenska-Pobell, S. Bio-precipitation of uranium by two bacterial isolates recovered from extreme environments as estimated by potentiometric titration, TEM and X-ray absorption spectroscopic analyses. *J. Hazard. Mater.* **2011**, *197*, 1–10. doi:10.1016/j.jhazmat.2011.09.049.
9. Mikheenko, I.P.; Rousset, M.; Dementin, S.; Macaskie, L.E. Bioaccumulation of palladium by *Desulfovibrio fructosivorans* wild-type and hydrogenase-deficient strains. *Appl. Environ. Microbiol.* **2008**, *74*, 6144–6146. doi:10.1128/AEM.02538-07.

10. Macaskie, L.E.; Humphries, A.C.; Mikheenko, I.P.; Baxter-Plant, V.S.; Deplanche, K.; Redwood, M.D.; Bennett, J. a.; Wood, J. Use of *Desulfovibrio* and *Escherichia coli* Pd-nanocatalysts in reduction of Cr(VI) and hydrogenolytic dehalogenation of polychlorinated biphenyls and used transformer oil. *J. Chem. Technol. Biotechnol.* **2012**, *87*, 1430–1435. doi:10.1002/jctb.3763.
11. Macaskie, L.E.; Mikheenko, I.P.; Omajai, J.B.; Stephen, A.J.; Wood, J. Metallic bionanocatalysts: Potential applications as green catalysts and energy materials. *Microb. Biotechnol.* **2017**, *10*, 1171–1180. doi:10.1111/1751-7915.12801.
12. Deplanche, K.; Snape, T.J.; Hazrati, S.; Harrad, S.; Macaskie, L.E. Versatility of a new bioinorganic catalyst: Palladized cells of *Desulfovibrio desulfuricans* and application to dehalogenation of flame retardant materials. *Environ. Technol.* **2009**, *30*, 681–692. doi:10.1080/09593330902860712.
13. Omajali, J.B.; Hart, A.; Walker, M.; Wood, J.; Macaskie, L.E. In-situ catalytic upgrading of heavy oil using dispersed bionanoparticles supported on gram-positive and gram-negative bacteria. *Appl. Catal. B Environ.* **2017**, *203*, 807–819. doi:10.1016/j.apcatb.2016.10.074.
14. Kunwar, B.; Deilami, S.D.; Macaskie, L.E.; Wood, J.; Biller, P.; Sharma, B.K. Nanoparticles of Pd supported on bacterial biomass for hydroprocessing crude bio-oil. *Fuel* **2017**, *209*, 449–456. doi:10.1016/j.fuel.2017.08.007.
15. Macaskie, L.E.; Mikheenko, I.P.; Yong, P.; Deplanche, K.; Murray, A.J.; Paterson-Beedle, M.; Coker, V.S.; Pearce, C.I.; Cutting, R.; Pattrick, R.A.D.; et al. Today's Wastes, Tomorrow's Materials for Environmental Protection.*Hydrometallurgy***2010**, *104*, 483–487.
16. Murray, A.J.; Zhu, J.; Wood, J.; Macaskie, L.E. A novel biorefinery: Biorecovery of precious metals from spent automotive catalyst leachates into new catalysts effective in metal reduction and in the hydrogenation of 2-pentyne. *Miner. Eng.***2017**, 113, 102–108. doi:10.1016/j.mineng.2017.08.011.
17. Archer, S.A.; Murray, A.J.; Omajali, J.B.; Paterson-Beedle, M.; Sharma, B.K.; Wood, J.; Macaskie, L.E. In: *Resource Recovery from Wastes: Towards a Circular Economy*. Eds L.E. Macaskie, D.J. Sapsford and W.M. Mayes. Green Chemistry Series No 62. The Royal Society of Chemistry, in press (publication date Oct 2019).

18. Narayanan, K.B.; Sakthivel, N. Biological synthesis of metal nanoparticles by microbes. *Adv. Colloid Interface Sci.* **2010**, *156*, 1–13. doi:10.1016/j.cis.2010.02.001.
19. Deplanche, K.; Caldelari, I.; Mikheenko, I.P.; Sargent, F.; Macaskie, L.E. Involvement of hydrogenases in the formation of highly catalytic Pd(0) nanoparticles by bioreduction of Pd(II) using *Escherichia coli* mutant strains. *Microbiology* **2010**, *156*, 2630–2640. doi:10.1099/mic.0.036681-0.
20. Mabbett, A.N.; Sanyahumbi, D.; Yong, P.; Macaskie, L.E. Biorecovered precious metals from industrial wastes: Single-step conversion of a mixed metal liquid waste to a bioinorganic catalyst with environmental application. *Environ. Sci. Technol.* **2006**, *40*, 1015–1021. doi:10.1021/es0509836.
21. Søbjerg, L.S.; Gauthier, D.; Lindhardt, A.T.; Bunge, M.; Finster, K.; Meyer, R.L.; Skrydstrup, T. Bio-supported palladium nanoparticles as a catalyst for Suzuki-Miyaura and Mizoroki-Heck reactions. *Green Chem.* **2009**, *11*, 2041–2046. doi:10.1039/b918351p.
22. Creamer, N.J.; Mikheenko, I.P.; Yong, P.; Deplanche, K.; Sanyahumbi, D.; Wood, J.; Pollmann, K.; Merroun, M.; Selenska-Pobell, S.; Macaskie, L.E. Novel supported Pd hydrogenation bionanocatalyst for hybrid homogeneous/heterogeneous catalysis. *Catal. Today* **2007**, *128*, 80–87. doi:10.1016/j.cattod.2007.04.014.
23. Wood, J.; Bodenes, L.; Bennett, J.; Deplanche, K.; Macaskie, L.E. Hydrogenation of 2-butyne-1, 4-diol using novel bio-palladium catalysts. *Ind. Eng. Chem. Res.***2010**, *49*, 980–988. doi:10.1021/ie900663k.
24. Omajali, J.B.; Mikheenko, I.P.; Merroun, M.L.; Wood, J.; Macaskie, L.E. Characterization of intracellular palladium nanoparticles synthesized by *Desulfovibrio desulfuricans* and *Bacillus benzeovorans*. *J. Nanoparticle Res.***2015**, *17*, 264. doi:10.1007/s11051-015-3067-5.
25. Williams, A.R. Biogenic precious metal-based magnetic nanocatalyst for enhanced oxygen reduction. PhD Thesis, University of Birmingham, Birmingham, UK. (25th September, 2015).
26. Attard, G.A.; Casadesus, M.; Macaskie, L.E.; Deplanche, K. Biosynthesis of platinum nanoparticles by *E.scherichia coli* MC4100: Can such nanoparticles exhibit intrinsic surface enantioselectivity? *Langmuir* **2012**, *28*, 5267–5274. doi:10.1021/la204495z.

27. Michael, B.C.; Donazzi, A.; Schmidt, L.D. Effects of H_2O and CO_2 addition in catalytic partial oxidation of methane on Rh. *J. Catal.* **2009**, *265*, 117–129. doi:10.1016/j.jcat.2009.04.015.
28. Courtney, J.; Deplanche, K.; Rees, N.V.; Macaskie, L.E. Biomanufacture of nano-Pd(0) by *Escherichia coli* and electrochemical activity of bio-Pd(0) made at the expense of H_2 and formate as electron donors. *Biotechnol. Lett.* **2016**, *38*, 1903–1910. doi:10.1007/s10529-016-2183-3.
29. Zhou, Y.; Itoh, H.; Uemura, T.; Naka, K.; Chujo, Y. Synthesis of novel stable nanometer-sized metal (M = Pd, Au, Pt) colloids protected by a π-conjugated polymer. *Langmuir* **2002**, *18*, 277–283. doi:10.1021/la011323r.
30. Saifuddin, N.; Wong, C.W.; Yasumira, A.A.N. Rapid biosynthesis of silver nanoparticles using culture supernatant of bacteria with microwave irradiation. *E-Journal Chem.* **2009**, *6*, 61–70. doi:10.1155/2009/734264.
31. Larhed, M.; Moberg, C.; Hallberg, A. Microwave-accelerated homogeneous catalysis in organic chemistry. *Acc. Chem. Res.* **2002**, *35*, 717–727. doi:10.1021/ar010074v.
32. Panda, A.B.; Glaspell, G.; Samy El-Shall, M. Microwave synthesis and optical properties of uniform nanorods and nanoplates of rare earth oxides. *J. Phys. Chem. C* **2007**, *111*, 1861–1864. DOI: 10.1021/jp0670283.
33. Banik, S.; Bandyopadhyay, S.; Ganguly, S. Bioeffects of microwave - a brief review. *Bioresour. Technol.***2003**, *87*, 155–159. doi:10.1016/S0960-8524(02)00169-4.
34. Shamis, Y.; Taube, A.; Mitik-Dineva, N.; Croft, R.; Crawford, R.J.; Ivanova, E.P. specific electromagnetic effects of microwave radiation on *Escherichia coli*. *Appl. Environ. Microbiol.* **2011**, *77*, 3017–3022. doi:10.1128/aem.01899-10.
35. Dreyfuss, M.S.; Chipley, J.R. Comparison of effects of sublethal microwave radiation and conventional heating on the metabolic activity of *Staphylococcus aureus*. *Appl. Environ. Microbiol.* **1980**, *39*, 13–16.
36. Rai, S.; Singh, S.P.; Samarketu; Tiwari, S.P.; Mishra, A.K.; Pandey, K.D.; Rai, A.K. Effect of modulated microwave frequencies on the physiology of a cyanobacterium, Anabaena doliolum. *Electro- Magnetobiol.* **1999**, *18*, 221–232. doi:10.3109/15368379909022578.
37. Chang, C.K.; Chen, J.Y.; Yeh, C.T. Characterization of alumina-supported gold with temperature-programmed reduction. *Appl. Catal. A* **1998**, *174*, 13–23.

38. Mikheenko, I.P.; Gomez-Bolivar, J.; Merroun, M.; Sharma, S.; Macaskie, L.E. High resolution electron microscopy study of biologically derived ruthenium and palladium/ruthenium nanoparticles. In Proceedings of the 6th International Conference Nanomaterials: Applications and Properties, NAP 2016. Lviv, Ukraine (14^{th}-19^{th} September 2016). doi: 10.1109/NAP.2016.7757229.
39. Charlot G., in Dosages Absorptionmétriques des Éléments Mineraux, 2^{nd} ed.; Masson Ed.; Paris, France, 1978.
40. Merroun, M.L.; Raff, J.; Rossberg, A.; Hennig, C.; Reich, T.; Selenska-Pobell, S. Complexation of uranium by cells and S-layer sheets of *Bacillus sphaericus* JG-A12. *Appl. Environ. Microbiol.* **2005**, *71*, 5532–5543. doi:10.1128/AEM.71.9.5532-5543.2005.
41. Manders, E.M.M.; Verbeek, F.J.; Aten, J.A. Measurement of co-localization of objects in dual-colour confocal images. *J. Microsc.* **1993**, *169*, 375–382. doi:10.1111/j.1365-2818.1993.tb03313.x.
42. Bolte, S.; Cordelières, F.P. A guided tour into subcellular colocalization analysis in light microscopy. *J. Microsc.* **2006**, *224*, 213–232. doi:10.1111/j.1365-2818.2006.01706.x.
43. Baalousha, M.; Lead, J.R. Nanoparticle dispersity in toxicology. *Nat. Nanotechnol.* **2013**, *8*, 308–309. doi:10.1038/nnano.2013.78.
44. Mikheenko, I.P.; Macaskie, L.E. Enhanced hydrogenation rate and selectivity of biogenic palladium catalyst synthesized by *Desulfovibrio desulfuricans* exposed to a radio frequency magnetic field. *Biotechnol. Bioeng.* Under review.
45. Mikheenko, I.P.; Gomez-Bolivar, J.; Merroun, M.L.; Macaskie, L.E.; Sharma, S.; Walker, M.; Hand, R.A.; Grail, B.; Johnson, D.B.; Orozco, R.L. Upconversion of cellulosic waste into a potential 'drop in fuel' via novel catalyst generated using *Desulfovibrio desulfuricans* and consortium of acidophilic sulfidogens. *Front. Microbiol.* **2019**. doi:10.3389/fmicb.2019.00970.
46. Schneider, C.A.; Rasband, W.S.; Eliceiri, K.W. NIH Image to ImageJ: 25 years of image analysis. *Nat. Methods* **2012**, *9*, 671–675. doi:10.1038/nmeth.2089.
47. Foulkes, J.M.; Malone, K.J.; Coker, V.S.; Turner, N.J.; Lloyd, J.R. Engineering a biometallic whole cell catalyst for enantioselective deracemization reactions. *ACS Catal.* **2011**, *1*, 1589–1594. doi:10.1021/cs200400t.

48. Mulrooney, S.B.; Hausinger, R.P. Nickel uptake and utilization by microorganisms. *FEMS Microbiol. Rev.* **2003**, *27*, 239–261. doi:10.1016/S0168-6445(03)00042-1.
49. Liermann, L.J.; Hausrath, E.M.; Anbar, A.D.; Brantley, S.L. Assimilatory and dissimilatory processes of microorganisms affecting metals in the environment. *J. Anal. At. Spectrom.* **2007**, *22*, 867–877. doi:10.1039/b705383e.
50. Liu, J.; Zheng, Y.; Hong, Z.; Cai, K.; Zhao, F.; Han, H. Microbial synthesis of highly dispersed PdAu alloy for enhanced electrocatalysis. *Sci. Adv.* **2016**, *2*, e1600858. doi:10.1126/sciadv.1600858.
51. Priestley, R.E.; Mansfield, A.; Bye, J.; Deplanche, K.; Jorge, A.B.; Brett, D.; Macaskie, L.E.; Sharma, S. Pd nanoparticles supported on reduced graphene-*E. coli* hybrid with enhanced crystallinity in bacterial biomass. *RSC Adv.* **2015**, *5*, 84093–84103. DOI: 10.1039/c5ra12552a
52. Hatchikian, C.E.; Traore, A.S.; Fernandez, V.M.; Cammack, R. Characterization of the nickel-iron periplasmic hydrogenase from *Desulfovibrio fructosovorans*. *Eur. J. Biochem.* **1990**, *187*, 635–643. doi:10.1111/j.1432-1033.1990.tb15347.x.
53. Casalot, L.; Hatchikian, C.E.; Forget, N.; De Philip, P.; Dermoun, Z.; Bélaïch, J.P.; Rousset, M. Molecular study and partial characterization of iron-only hydrogenase in *Desulfovibrio fructosovorans*. *Anaerobe* **1998**, *4*, 45–55. doi:10.1006/anae.1997.0137.
54. Fahmy, K.; Merroun, M.; Pollmann, K.; Raff, J.; Savchuk, O.; Hennig, C.; Selenska-Pobell, S. Secondary structure and Pd(II) coordination in S-layer proteins from *Bacillus sphaericus* studied by infrared and X-ray absorption spectroscopy. *Biophys. J.* **2006**, *91*, 996–1007. doi:10.1529/biophysj.105.079137.
55. Merroun, M.; Rossberg, A.; Hennig, C.; Scheinost, A.C.; Selenska-Pobell, S. Spectroscopic characterization of gold nanoparticles formed by cells and S-layer protein of *Bacillus sphaericus* JG-A12. *Mater. Sci. Eng. C* **2007**, *27*, 188–192. doi:10.1016/j.msec.2006.05.001.

Supplementary information

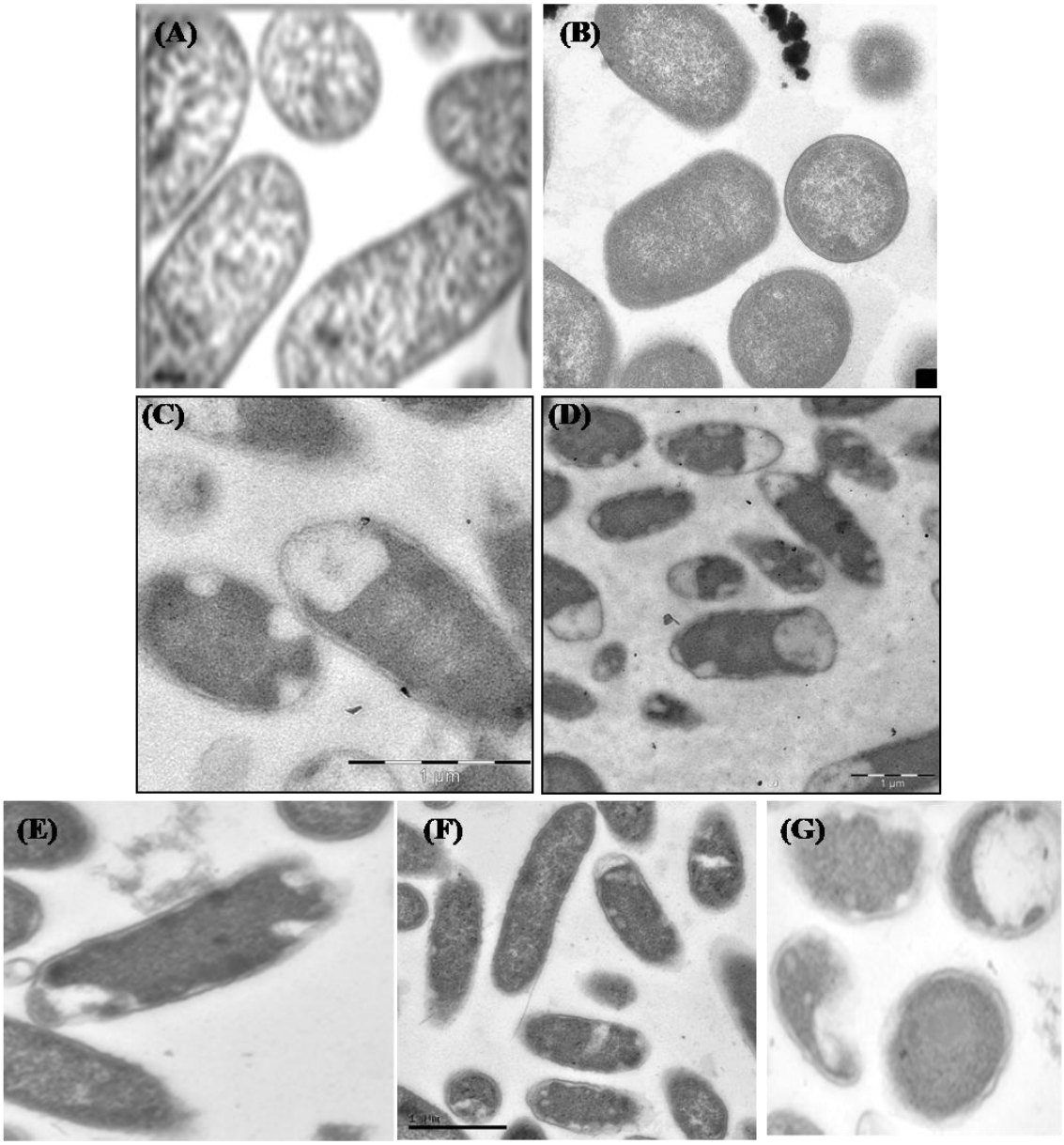

Figure S1. Effect of RF irradiation (microwaves) on cells of *E. coli* and *D. desulfuricans* in the absence of microwave treatment (A,B, respectively) and following exposure to MW in short bursts with cooling (C, D, respectively) (this study: see text). A companion study was done (E,F,G) which applied RF radiation at 2W (E),4W (F) or 8W (G) (20 min) using purpose-built equipment to decouple the thermal and electromagnetic components. The equipment was developed in house at C-Tech Innovation Ltd. via adaptation of commercial equipment. The *E* (electric) component of electromagnetic radiation produces heating in dielectric (non-conducting) materials so it is important to exclude heating from the sample by isolating the *H* (magnetic) component. This was achieved

using a series LC circuit tuned with an external matching box. This generated a magnetic field inside the induction coil and an electric field in the air gap between the two conducting plates. The sample vial, placed in the centre of the induction coil, was exposed to a magnetic field for the desired time. After exposure, the final temperature of the bottle was checked and absence of heating confirmed. The samples were treated by exposure inside a solenoid coil as the electromagnetic field within the coil will be almost entirely magnetic; consequently, as the magnetic susceptibilities of the components of the sample being treated (glass, water, bacteria) are very low at this frequency there would be minimal heating of the sample, allowing long treatment times. The total dose in the two studies was similar: The commercial equipment (this study) delivered 300W which was applied for 30 sec (9,000 'units of stress'). In the purpose-built equipment the cells were treated with 2-8 W over 20 min (up to 9,600 'units of stress'); the power level can be considered as a rate (power = energy per second; 8W; 20 x 60 sec) and a dose as rate x time of the integral of rate over time.

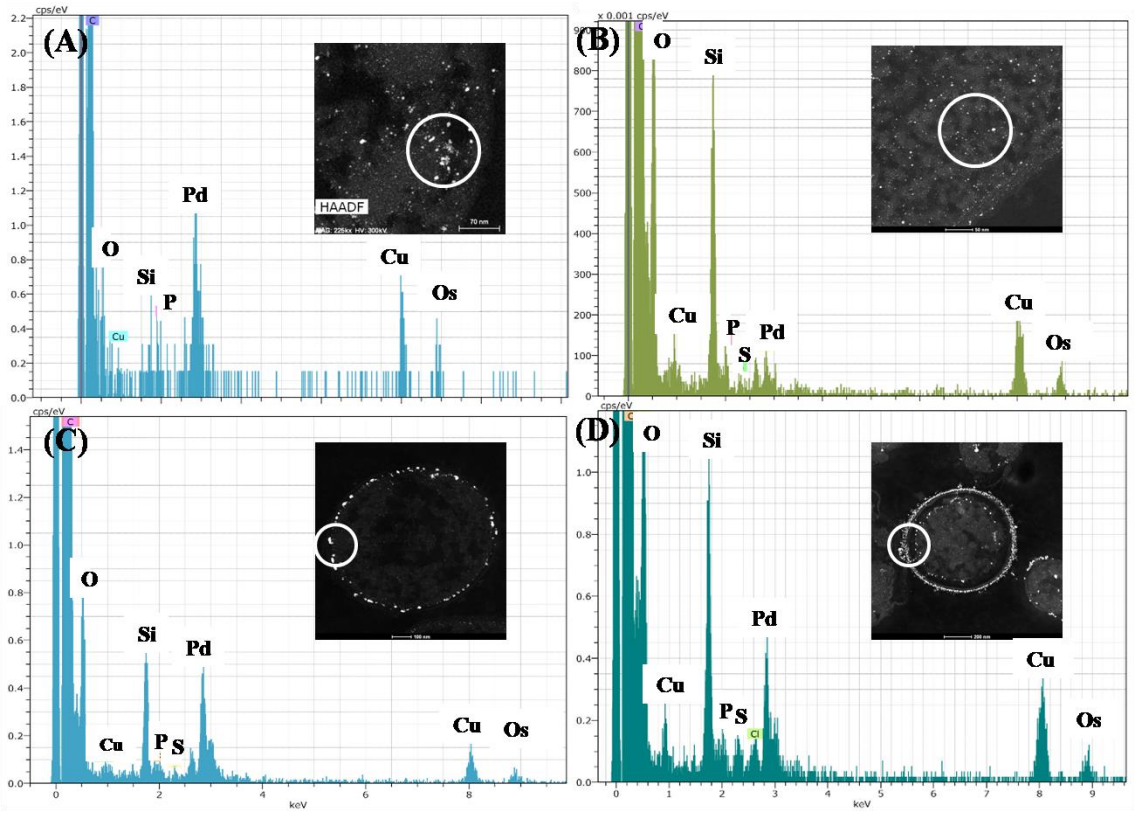

Figure S2. HAADF–STEM–EDX analysis of Pd nanoparticles (circled areas shown) with phosphorus (P) and sulfur (S) of untreated cells of *E. coli* MC4100 (A) and *D.*

desulfuricans (C), 30 second MW treated cells of *E. coli* MC4100 (B) and *D. desulfuricans* (D). Silicon is from the oil diffusion pump of the column of the TEM system, copper is from the TEM grid and osmium from the staining

CHAPTER IV

Enhanced Hydrogenation Catalyst Synthesized by *Desulfovibrio desulfuricans* Exposed to a Radio Frequency Magnetic Field (Paper in submission)

Lynne E. Macaskie[1], John Collins[2], Iryna P. Mikheenko[1], Jaime Gomez-Bolivar[3], Mohamed L. Merroun[3], James A. Bennett[1]

1 School of Biosciences, University of Birmingham, Edgbaston, Birmingham B15 2TT, UK

2 C-Tech Innovation Ltd. Capenhurst Technology Park, Capenhurst, CH1 6EH, UK

3 Department of Microbiology, Faculty of Sciences, University of Granada, Campus Fuentenueva, 18071, Granada, Spain

*Corresponding author: L.E. Macaskie@bham.ac.uk

Abstract

Desulfovibrio desulfuricans reduces Pd(II) to Pd(0)-nanoparticles (Pd-NPs) which are catalytically active in 2-pentyne hydrogenation. To make Pd-NPs resting cells are challenged with Pd(II) ions (uptake step), followed by addition of electron donor to promote bioreduction of cellular Pd(II) to Pd(0) (bio-Pd). Application of radiofrequency (RF) radiation to prepared 5 wt% bio-Pd catalyst (60 W power, 60 min) increased the hydrogenation rate by 70% with no adverse impact on selectivity to cis-2-pentene. Such treatment of a 5 wt% Pd/carbon commercial catalyst did not affect the conversion rate but reduced the selectivity. Lower-dose RF radiation (2-8 W power, 20 min) was applied to the bacteria at various stages during synthesis of the bio-scaffolded Pd-NPs. The reaction rate (μ mol 2-pentyne converted/sec) was increased threefold by treatment during bacterial catalyst synthesis but the selectivity for cis-2-pentene was reduced by ~ 25%. Application of RF radiation (2 or 4W power) to resting cells prior to Pd(II)-exposure affected the catalyst made subsequently, increasing the reaction rate by 50% as compared to untreated cells, while nearly doubling selectivity for cis- 2-pentene. The results are discussed with respect to a greater homogeneity of the Pd-NPs made during or following exposure of the cells to the RF field.

Keywords: *Desulfovibrio desulfuricans*; bio-palladium catalyst; microwave injury, 2-pentyne hydrogenation

1. Introduction

Bacteria can reduce precious metals, forming metallic nanoparticles (NPs) in cell surface layers (Mikheenko *et al*., 2008; Deplanche et al., 2010; 2014) and intracellularly (Omajali et al., 2015; Gomez-Bolivar et al., 2019). Some bio-NPs are promising catalysts for remediation and 'green chemistry' (Deplanche et al., 2011; De Corte et al., 2012; Hennebel et al., 2012; Singh, 2015). NP size, shape, structure, and distribution affects activity and selectivity (Lee et al., 2009, Schmidt et al., 2009). Hence, a method of manipulating bio-NP formation could steer the properties of the resulting catalyst.

A population of Pd-NPs are located in or near bacterial cell membranes, and also within the periplasmic space of Gram-negative bacteria (Mikheenko et al., 2008; Deplanche et al., 2010). Conditions which are known to change the structure or function of the cell membrane(s) and/or associated enzymes may impact upon the size, distribution, shape or hydrophobicity of the associated metallic NPs. The role of bacterial hydrogenases in Pd-NP synthesis was shown using mutants deficient in one or more hydrogenase enzymes; such alterations, affecting the patterning of Pd-NPs (Mikheenko et al., 2008; Deplanche et al., 2010), also enhanced the catalytic activity as shown in Cr(VI) reduction (Skibar et al., 2005) and in the hydrogenation of itaconic acid (I. Mikheenko unpublished; supplementary information Fig. S1).

Other mechanisms of Pd-NP synthesis occur: aerobically-grown cells (i.e. not expressing hydrogenases) of *E. coli* (Foulkes et al. 2011) and a Serratia sp. (Deplanche et al., 2014) made catalytically-active biogenic-Pd(0) nanoparticles (bio-Pd). Killed cells made negligible Pd-NPs (Mikheenko et al., 2008; Deplanche et al., 2010). A contribution of bacterial membrane material was suggested in the ability of bio-Pd to dechlorinate hydrophobic polychlorinated biphenyls (Redwood et al., 2008), while more recent work showed the ability of bio-Pd to hydrogenate hydrophobic soybean oil (Zhu et al., 2016) as well as 2-pentyne (Bennett et al., 2010; 2013), the latter reaction forming the focus of this study.

Radio frequency (RF) electric fields cover frequencies of 3 kHz to 300 GHz and in some cases they are known to affect cell membranes; such irradiation may be used for non-thermal bacterial inactivation (Geveke and Brunkhorst, 2008). The voltage formed across the membrane in the presence of an electric field is thought to cause membrane-thinning,

electroporation and, eventually, cell rupture (Zimmerman et al., 1974, 1986; Hulshleger et al., 1981) but in practice it is difficult to attribute cellular damage to decoupled electromagnetic and local heating effects.

Shamis et al. (2011) confirmed that microwave (MW) radiation (a subset of the RF range occupying the higher frequencies at 300MHz to tens of GHz) produced a transient toxic effect on bacteria when the effects of heating were discounted. They confirmed an increased porosity in the membrane of *E. coli* when exposed to MW radiation at a frequency of 18 GHz and an electric field, with the temperature maintained below 40 ºC. Efflux of cytosolic contents was observed, and also solute penetration of cells, with increased influx, attributed to transient pores created during RF-injury.

Although the application of radiofrequency (RF) electromagnetic radiation has been suggested to be able to change the structure and properties of matter it is not usually considered for samples with a high water content due to dielectric loss. However, inorganic, dried or deep frozen materials can be examined at higher RF strengths and powers (dielectric processing) which are known to promote alterations in crystal and surface structures. Hence, the first aim of this study was to compare the effect of application of RF radiation on commercial 5 wt% Pd on carbon catalyst with dried 5 wt% bio-Pd catalyst, with respect to their catalytic activity and selectivity in the hydrogenation of 2-pentyne.

The second aim was to evaluate the scope for intervention by applying a lower RF dose during catalyst synthesis, and also before exposure to Pd(II), to evaluate the response of the cells to RF-injury with respect to their ability to make an altered Pd-catalyst subsequently (‘memory’). The hypothesis is that such an intervention in cellular processes could predispose the cells to making altered Pd(0)-NPs showing increased reaction rates and/or selectivities via altered NP dispersions; the latter was reported previously (Gomez-Bolivar et al., 2019).

While hydrogenase mutants produced NPs with higher catalytic efficacy (above) a bio-catalyst must be markedly better than what is commercially available and/or more economic to produce in order to impact upon well established markets (Catalytic Technology Management Ltd; commissioned consultancy report 2009). The goal of this study is to establish the scope for using electromagnetic intervention as a tool to produce

bio-NPs with enhanced catalytic properties, as a first step towards 'steering' NPs engineered towards specific reaction outcomes.

Biogenesis of Pd-NPs typically (but not exclusively) uses bacteria expressing hydrogenase(s) (above), which oxidize H_2 to $2H^+ + 2e^-$, with the electrons reducing Pd(II) to Pd(0) which becomes localized as Pd-NPs nearby (Mikheenko et al., 2008; Deplanche et al., 2010). To make 'bio-Pd' catalyst resting cells are suspended in a solution of Pd(II) ions which coordinate to ligands in/on the bacterial surface. The Pd is trafficked to the site of its reduction by an unknown mechanism which may also relate to Ni(II) recognition and transport (discussion in Omajali et al., 2015; Torgeman, 2017). With an added electron donor (H_2 or formate) the Pd(II) is reduced to metallic nanoclusters which remain patterned onto the supporting biomatrix to grow into larger NPs, of size as determined by the amount of Pd(II) supplied.

It is convenient to use acetone-washed (i.e. permeabilized), dried, catalyst preparations. These showed good activity and selectivity in the hydrogenation of 2-pentyne (Bennett et al., 2010; 2013) soybean oil (Zhu et al., 2016) and itaconic acid (supplementary information Fig. S1). Towards evaluating the scope for physiological intervention this study used radiofrequency (RF) magnetic fields that were isolated from the heating effects produced by electric fields, applied to bacterial cells at various stages in the preparation of bio-Pd catalyst as well as onto resting cells before exposure to Pd(II) (Table 1). The study used bespoke equipment which allows the application of RF fields to cell suspensions while allowing isolation of the thermal component to minimise thermal effects on the cells. Pd(II) exposure is optimally done at pH ~2-2.3 in order to protonate the cell surface and facilitate access of $PdCl_3^-$ that predominates in solution. This imposes an additional dual stress (metal plus pH-stress) on the cells and cellular responses to both stresses have been the focus of widespread study by many authors. Delineating the combined effects of multiple stresses is beyond this scoping study which aims to show cause and effect and hence establish the scope for RF-injury as a simple interventional tool. The 'palladized' cells (bio-Pd) were evaluated as catalysts in the hydrogenation of 2-pentyne, seeking impacts on catalytic activity and selectivity for the production of the desired product, cis-2-pentene. Commercial hydrogenations comprise a very large industrial sector and the cis-alkene product is favoured over the trans-isomer for a number of reasons and hence catalyst selectivity is of paramount importance (see Zhu et al., 2016).

2. Materials and Methods

2.1. RF delivery system

The system (Figure 1) comprised a 27.5 MHz RF generator (10P Plasma Products Inc.), matching network to tune the circuit, and an applicator circuit of a capacitor plate and a solenoid induction coil situated in a Faraday cage. The coil was of a slightly larger internal diameter than the glass sample vial, which was fully immersed in the coil and stood on a ceramic holder (Figure 1). The test vials (glass, Wheaton) were 51 mm x 22 mm diameter (working volume 12 mL) containing 10 mL of cell suspension.

2.2. High dose radiofrequency magnetic field treatment of pre-formed palladium catalyst

Bio-Pd catalyst (5 wt% Pd) was prepared on cells of *D. desulfuricans* as described previously (Bennett et al., 2010; 2013) with 0.1 M sodium formate solution substituted for H_2 gas for metal reduction (2.5 mmol sodium formate to 1 mmol Pd(II), left overnight). Following complete removal of Pd (determined by assay) the sample was washed in water then acetone, dried and ground. The comparator was commercial 5 wt% Pd/C catalyst (Creamer et al., 2007). A sample of dry, preweighed catalyst was added to the sample tube and placed in the centre of the coil in the RF treatment system (Figure 1). A radiofrequency magnetic field (27.5 MHz) of 60 W power was applied (60 min). The temperature of the sample was monitored throughout and the sample was reweighed after RF exposure to check for any change of mass.

2.3. Low-dose RF magnetic field treatment of live cells followed by bio-Pd synthesis

A suspension of resting cells in 20 mM MOPS–NaOH buffer (pH 7) of known dry weight/mL was added to a sealed sample tube under a N_2 atmosphere and placed in the centre of the coil in the RF generator. A radiofrequency magnetic field (27.5 MHz; 2 – 60 W) was applied (5 - 30 minutes). The sample was removed from the field and the temperature was checked. Parallel controls were left in buffer without application of RF and allowed to make Pd(0) alongside the RF-treated samples. Na_2PdCl_4 solution (2 mM in 10 mM HNO_3), previously degassed and stored under N_2, was added by syringe; the volume was that required to give 5 wt% Pd (mass of cells was calculated from the OD_{600} of the suspension). The solution was left (20 min) for the bacteria to take up the Pd(II) before adding 0.1M sodium formate solution (electron donor: 2.5 mmol sodium formate

to 1 mmol Pd(II)) and left overnight. The cells were centrifuged, washed and dried as described previously, including an acetone wash (Bennett et al., 2010; 2013).

2.4. Examination of RF-injured cells

Before or immediately following RF-injury the cells were fixed in glutaraldehyde and dehydrated (ethanol series), sectioned and routinely examined by electron microscopy as described previously (Deplanche et al., 2010). Examination of 'palladized' cells was as described by Gomez-Bolivar et al. (2019).

2.5. RF magnetic field treatment of live cells during bio-Pd synthesis

To evaluate the effect of RF radiation on the process of initial uptake of Pd(II) and initial Pd-deposition the resting cells (and untreated controls) were placed in the RF magnetic field with Pd(II) during the period of Pd(II) uptake (20 min or as stated) and removed from it before formate addition (2.5 mmol sodium formate to 1 mmol Pd(II)). Alternatively, cells were untreated during Pd(II)-uptake and then transferred to the RF field during the reduction of Pd(II) to Pd(0) (20 min) and then left overnight (no field). The treatments are summarized in Table 1.

2.6. Catalytic testing in the hydrogenation of 2-pentyne

5% wt Pd catalyst (30 mg) (i.e. 1.5 mg Pd(0) and 150 mL 2-propanol) were added to a 500 mL Baskerville autoclave reactor, sealed, purged with N_2 and stirred (500 rpm, 40 ºC) with hydrogen bubbled through (0.1 L/min; 10 min) to 'prime' the catalyst. The reactor was purged with N_2 and 2-pentyne (4 mL) was added. The reactor was flushed with H_2, sealed and pressurized (2 bar). The stirred (1000 rpm) mixture was sampled periodically; analysis used GC (Varian CP-3380 GC with a flame ionization detector and a 25M ChrompackPlot CP7576 capillary column with an Al_2O_3/KCl coating). The oven temperature ramp was: initial temperature of 95 ºC (30 min) ramp to 220 ºC (50 ºC/min) and hold (20 min).

3. Results

3.1. Developed experimental system for RF radiation delivery and decoupling of electric and magnetic fields

The equipment used for RF treatment of cells and catalyst was developed in house at C-Tech Innovation Ltd. via adaptation of commercial equipment (Figure 1). Some sample heating (to above 30 ºC) was observed using a power of 8W or higher, and with exposure times in excess of 20 minutes. The most likely mechanisms for this are radiation or conduction of heat across the air gap from the coil (which is subject to some resistive heating) and also possibly imperfections in the coil, leading to small electric field components within the coil. An empty glass vial showed similar heating to a full sample vial. For already-prepared, dried bio-Pd catalyst (and the commercial comparator) a higher power (60 W) was used; the cells were already permeabilized and killed (using acetone: Canovas et al., 2005; Jamur and Oliver, 2010), dried and ground. Such dried bio-Pd was used previously in hydrogenation and also in the Heck synthesis at temperatures in excess of 100 ºC (Bennett et al., 2013; Zhu et al., 2016). Where living cells were to be treated before or during Pd(0) synthesis a lower exposure was used; at a power of 8W, a temperature increase of between 2 and 6 ºC was observed after 20 min. Therefore, these experiments were restricted to 8W or less (usually 2-4 W; see below) for a maximum of 20 min in order to avoid thermal damage or stress to the bacteria (details in individual experiments).

3.2. Comparison of commercial catalyst and bio-Pd catalyst without and following RF treatment

An earlier study compared commercial 5 wt% Pd/TiO_2 catalyst with dried bio-Pd (Zhu et al., 2016). The use of TiO_2 was avoided in this study (to avoid solid metallic components other than Pd) and the comparator was 5 wt% Pd on carbon catalyst, as with the hydrogenation of itaconic acid (Creamer et al., 2007; Skibar et al., 2005; supplementary information Figure S1). The commercial 5 wt% Pd/C catalyst outperformed bio-Pd in the hydrogenation of 2-pentyne (Figure 2A). Early work using mutants deficient in Pd(II)-reducing periplasmic hydrogenases showed the extent of itaconic acid conversion by dried bio-Pd to become more comparable to the commercial comparator but this was, to some extent, dependent on the Pd-loading on the cells, with 5 wt% Pd being optimal

(supplementary information Figure S1). Mutants were not tested in this study; the previous study used mutants of *D. fructosovorans* (Mikheenko et al., 2008) while other work has shown that the efficacy of bio-Pd also depends on the *Desulfovibrio* strain used, even within the species *D. desulfuricans* (Omajali, 2015). *D. desulfuricans* NCIMB 8307 was used in this work to facilitate comparison with the earlier hydrogenation studies.

Dried catalyst samples were exposed to RF of 60 W for 30 min (Figure 2A). The reaction rate with commercial Pd/C catalyst was ~ 8 fold higher than with the bio-Pd (Figure 2A). The rate was little-affected by RF treatment of the commercial catalyst whereas that of the bio-Pd was increased by ~ 70%. At higher temperatures (without RF treatment) a thermogravimetric analysis showed that ~ 5% of the weight was lost, corresponding to bound water (Omajali et al., 2017). The samples in this study, weighed before and after treatment, showed no change in mass, i.e. biological material was not lost. The RF-induced changes cannot be metabolic since the palladized cells were dried and acetone-treated prior to RF-exposure and hence the effect of RF would reflect changes in the structure of the composite biomaterial. Microwave electromagnetic radiation is used to sinter materials (Louzguine-Luzgin et al., 2009; Prette et al., 2011; Singh et al., 2015) but the sintering temperatures were much greater than those generated in this work. The sample temperatures reached a maximum of only 36 ºC after 30 min RF at 60W and hence heat-mediated structural changes could be ruled out.

RF treatment had minimal effect on the selectivity of the 5 wt% Pd/C commercial catalyst up to 40% conversion but beyond this the treatment promoted a marked decrease in selectivity towards cis-2-pentene (Figure 2B) and in pentene to pentane (Figure 2C). The selectivity of bio-Pd towards 2-pentene was generally lower than for the 5 wt %Pd/C comparator (Figure 2B,C) but the RF treatment increased its selectivity by a small, constant amount which was maintained at high conversion efficiencies (above 80%) where the activity of the commercial comparator became negligible (Figure 2B,C). Hence, although the bio-Pd catalyst was, overall, less effective in the conversion of 2-pentyne, at a high conversion the RF-treated bio-Pd shows potential advantages in maintaining selectivity.

3.3. Comparison of commercial catalyst with bio-Pd catalyst made in the presence of RF radiation

Using untreated cells the 5 wt% bio-Pd gave an initial rate of 2-pentyne consumption of 1 μmol/L/sec. A bio-Pd catalyst prepared identically but at 40 ºC without RF treatment gave the same reaction rate, establishing that below this temperature observed changes were not attributable to thermal effects. Use of 20 min exposure gave a temperature of between 36º – 40 ºC in the samples.

A power of 8W was selected to determine the effects of RF applied during bio-Pd biomanufacture with respect to its subsequent catalytic activity. The RF was applied during Pd(II) uptake or during the subsequent reduction step whereby Pd(0) is formed (Table 1). Applying the RF immediately after addition of Pd(II) solution allows the RF to take effect during uptake of the metal onto cellular nucleation sites. Application of RF after uptake of Pd(II) along with sodium formate addition allows the RF to take effect during reduction of the metal to Pd(0) at its nucleation sites. Figure 3 shows that RF applied to cells taking up Pd(II) (and also to those exposed to RF before Pd(II) exposure-see later) was the most effective in terms of increased reaction rate via the resulting bio-Pd, which was increased by > 2-fold as compared to untreated controls (Figure 3A). The advantage in selectivity towards cis-2-pentene was negated by treatment of resting cells at this dose (Figure 3B) but was unaffected with respect to pentene selectivity over pentane (Figure 3C). For catalysts prepared with bacteria exposed to RF during the Pd(II) uptake stage, the selectivity of the bio-Pd was higher and was similar to where RF was applied during Pd(II) reduction only (Figure 3B,C). The data are summarized in Table 2. This shows that the advantages in reaction rate and cis-selectivity were the same regardless of where the RF was applied in the process of Pd(0) biomanufacture; both treatments enriched the final mixture with respect to cis-pentene (Figure 3C; Table 2), while selectivity to pentene over the fully hydrogenated pentane was nearly doubled as compared to the bio-Pd made by untreated cells. This choice of method was based on the maximum reaction rate coupled with the maximum selectivity, i.e. 8W RF applied during Pd(II) uptake (Figure 3A, 3B). Since injury prior to Pd-exposure promoted enhanced catalytic activity of the catalyst made subsequently this was examined further.

3.4. Effect of lower dose RF treatment of resting cells before exposure to Pd(II)

To indicate a potentially altered biochemical basis for making altered Pd(0) ('memory') the effect of 8W of RF (20 min) and lower RF doses ('injury') was investigated using resting cells prior to Pd(II) addition. The activities of these catalysts are shown in Figure 4 and summarized in Table 3. A RF dose before exposure to Pd(II) improved the reaction rate of the resulting bio-Pd(0) in a dose-dependent manner (Figure 4A); the rate obtained from 4W-pretreated samples was half of that of 8W-pretreated samples (Table 3). Although the overall rate using bio-Pd(0) samples made using cells pre-treated under milder RF conditions was lower (Figure 4A) advantages emerged in the product selectivities, inversely related to the dose at low conversions while at 80% conversion little difference was seen between the treatments, with the selectivity to cis-2-pentene approaching that of the commercial catalyst (Figure 4B; c.f. Figure 1B).

Fixed samples were examined by electron microscopy. The cells sustained damage with increasing field power, showing vacuoles, enlargement of the periplasmic space and shrinkage of cell contents (Figure 5). The use of markers was not used to follow leakage of cell contents, but the limit of tolerance of the cells (with respect to visible injury but no fragmentation) appeared to be 8W for 20 min (c.f. Table 3). At a dose of 15W and above (20 min) the cells were unable to reduce Pd(II), while a 30W dose (20 min) revealed extensive cell destruction (Figure 5).

A companion study (Gomez-Bolivar et al., 2019) examined the Pd-NPs made by untreated and RF-treated cells. The NPs comprised Pd, as shown using energy dispersive X-ray microanalysis (supplementary information, Figure S2). The shrinkage of the cellular compartment was confirmed, with the Pd-NPs visualizing the retracted cytoplasmic membrane (supplementary information, Figure S2C,D) and enlarged periplasmic space which contained few NPs (Figure S2B). Gomez-Bolivar et al. (2019) also reported the lattice spacings (Å) of Pd-NPs of RF untreated and treated cells to be 0.223 and 0.199, and 0.231 and 0.202 nm respectively, corresponding to the (111) and (200) facets of Pd(0) and indicating no differences in the crystal structure between them.

Addition of RF along with Pd(II) (as above) would allow more facile production. Little difference was seen in NPs made by *D. desulfuricans* during Pd(II) addition or during Pd(II) reduction as compared to cells injured before exposure to Pd(II) (J. Gomez-Bolivar and I. Mikheenko, unpublished work; supplementary information Figure S3).

4. Discussion

This study reveals different responses of dried bio-Pd catalyst and of cells in response to RF-treatment, the former in finished catalyst on dried cells and the latter of catalyst being made by live cells (with or without Pd(II)) at a lower RF dose.

Our first conclusion is that higher dose RF-processing is beneficial for bio-Pd catalyst but not for the commercial counterpart. This may suggest alterations in the supporting matrix offered by the dried cells; direct interactions between cellular materials and Pd(0) were reported previously by analysis (Priestley et al., 2015) and by electron microscopy, which showed a 'pancaking' of the Pd-NPs out onto the supporting biomatrix at the bio-metallic interface (Bennett et al., 2013). Differences between the bio-Pd and metallic Pd were also shown by 105Pd NMR (Hooper et al., 2018), while an electron paramagnetic resonance study of commercial Pd and bio-Pd, mixed with activated carbon and sintered, showed enhanced electronic interactions (free radical quenching) between the bio-supported catalyst and activated carbon, to an extent related to the electrocatalytic activity (Carvalho et al., 2009).

The conversion rate using the RF-treated biomaterial was less than the commercial comparator, although marked advantages in selectivity occurred at high conversions (i.e. long reaction times). The potentially increased yield of product per unit of starting material (2-pentyne) would reduce the carbon impact via reduced requirement for petrochemically-derived substrate per unit of product yielded as well as a reduction in waste. The bio-Pd was recovered and functioned in sequential reactions (Bennett et al., 2013) while the continuous use of biofilm-immobilized bio-Pd catalyst was also established (Beauregard et al., 2010; Yong et al., 2015). Potential advantages should be evaluated on a case by case basis, e.g. the potential scope may differ between well-established large scale hydrogenation operations as compared to other, possibly niche, applications and/or where the cost of the starting material (and disposal of waste co-products) are major considerations.

The Pd-bionanoparticles, like chemically-made Pd-NPs, contain Pd-(111) facets, are icosahedral (Bennett et al., 2013; Omajali et al., 2015) and they are supported on the (hydrated) biomatrix. Although the biomaterial was dried in air, bound water in (e.g.) hydrated polymers would remain (deduced from thermogravimetric analysis: Omajali et

al., 2017); local perturbations in bound water molecules could result in morphological rearrangement of the biochemical/metal interface which was not investigated here. However, normally water absorption is an electric field effect; the field in this case was almost exclusively magnetic.

Two studies using muon spin rotation spectroscopy of bio-Pd-NPs have shown that they are ferromagnetic (Creamer et al., 2011; Williams, 2016) a property that is shared with chemically-made Pd-NPs within particular size boundaries (see Williams, 2016 for discussion). Pd-NPs tend to agglomerate into larger NPs unless stabilized by capping agents. This stabilizing function would be provided at the biomatrix/Pd-NP interface, where Pd atoms were 'pancaked' at the edge of the NP, increasing the planar surfaces (Bennett et al., 2013). Chemical interactions between the cell-bound Pd-NPs and the biomatrix were noted in previous studies (see above) but the extent to which the biomatrix may moderate the catalytic activity by stabilizing the bio-Pd NPs and/or preventing their agglomeration and/or, indeed, contribute by increasing the amount of 'planar' Pd-surface is currently unknown and would be difficult to measure. Other workers have reported that semihydrogenation of 2-methyl-3-butyn-2-ol to 2-methyl-3-butene-2-ol takes place preferentially at plane sites of the crystal whereas hydrogenation of alkene to alkane occurs mainly at edge sites (Crespo-Quesada et al., 2011). Hence the presence of stabilizing biomaterial may also have conferred some protection of the NPs to fragmentation (which would otherwise make more edge sites, promoting undesirable alkane production, above) which occurs during energetic treatment of crystals (Collins & Bettens, 2015).

Teschner et al. (2006) showed that selectivity in pentyne hydrogenation is also related to the exclusion of bulk hydrogen via the buildup of a Pd-C layer, explaining that this buildup process is not effective on the surface of bulk (111). It follows that bio-NPs with predominantly (111) surface planes might be less selective in hydrogenation because hydrogen (made in situ from formate) can saturate the bulk of the particle, which becomes too reactive (i.e. a faster reaction; note that the rate with bio-Pd was slower: above) at the expense of selectivity. They also suggest that structural defects may be required to start a C- dissociation reaction in order to facilitate initiation of the Pd-C surface phase that then retards participation of energetic bulk-dissolved hydrogen in the reaction, hence favouring selectivity at the expense of rate. In this mechanistic context, a more detailed

examination of the bacterial Pd-NPs would be warranted, with and without RF treatment, also using mutants (Figure S1) to 'steer' the NP localization onto sites giving 'preferred' crystal arrangements.

Our second conclusion is that pre-injury of bacteria using 2 W or 4 W RF power gave a faster (by ~ 50%) rate of hydrogenation via the resulting bio-Pd catalyst than that shown by untreated bacteria. The rate enhancement was ~ half that shown by bio-Pd of 8 W-treated cells (Figure 4A; Table 3) but the latter suffered substantial injury (Figure 5). Hence, for the maximum reaction rate, the optimal dose for cell treatment was 8 W but for enhanced selectivity 2-4 W was preferable (Table 3). It is important to note that commercial catalysts have been extensively developed and optimized prior to market whereas this is the first study of its kind using bio-Pd and with no attempt made at bio-catalyst optimization nor application in different reactions. In another study Zhu et al. (2016) showed that bio-Pd(0) (on E. coli) outperformed a commercial catalyst (Pd/TiO_2) in the selective hydrogenation of soybean oil, while Deplanche et al. (2014) showed comparable application of 'native' bio-Pd in the Heck synthesis, in an industrial laboratory validation against commercial comparators used routinely for that reaction. Since different catalysts may have different optimal Pd loadings (e.g. see Figure S1 showing variation in three catalysts within mutants of a single organism) a stringent comparison is only realistic under the optimal loading and reaction conditions for each reaction, compared against the best commercial catalyst for each, which were not attempted. Indeed, it was shown previously that two independent commercial catalysts gave different results when compared to bio-Pd (Creamer et al., 2007; Skibar et al., 2005; Zhu et al., 2016) and hence a 'like for like' comparison is not trivial. In this study 5 wt% Pd on carbon was chosen as the comparator; the use of metallic supports or components (other than Pd) was avoided to preclude possible deflection of the RF field and the formation of localized 'hot spots', i.e. to be confident that the field distribution in the sample chamber was the same in each treatment.

The beneficial effect of a low RF dose on living cells before Pd(II) exposure indicates that formation of the improved catalyst is rooted in a biological response to RF-injury that predisposes the cells to making a better catalyst subsequently. Attempts to gain dynamic insight into the nature of the cellular injury using flow cytometry were not possible due to the separate locations of the RF apparatus and flow cytometry equipment,

while the time required for microwave-injured cells to recover was shown to be in the order of ~ 10 min (Shamis et al., 2011); hence it is difficult to transfer injured bacteria sufficiently quickly for meaningful data. Examination of the *D. desulfuricans* cells by electron microscopy (Figure 5) shows a similar response to that described by Shamis et al. (2011) in terms of retraction of the cytoplasmic membrane, shrinkage of the cellular compartment and enlargement of the periplasmic space. This is reflected in Figure S2 where the injury has resulted in Pd-internalization to the inner membrane, not seen in untreated cells at 5 wt% Pd loading. In other studies where native cells were heavily loaded (to 20 wt% Pd), the Pd-NPs were located in the outer membrane and wall layers, the cytoplasmic membrane, to some extent in the periplasm and also in association with nuclear bodies in the cytoplasm, showing that the cells are able to take up Pd(II) (Omajali et al., 2015). Williams (2015) showed by magnetic analysis (bulk population), with direct examination (individual cells) using high resolution electron microscopy, the presence of three subpopulations of bio-Pd-NPs of different sizes. Pd-particle size, and also topography, are known to affect the reactivity in olefin hydrogenation/isomerization (Lee et al., 2009; Schmidt et al., 2009) and these features may not be offered identically by NPs in each subpopulation, while a possible shift in the proportions of each subpopulation in MW-injured cells was not examined. A high-resolution EM study using *E. coli* (Gomez-Bolivar at al., 2019) used elemental mapping to show that more Pd was internalized within the cells following RF treatment, suggesting enhancement of cellular permeability under RF-stress as proposed by Shamis et al., (2011). However, in contrast, little or no evidence was seen for discrete Pd-NPs in the cytoplasm of *D. desulfuricans* at 5 wt% Pd (supplementary information Figures S2, S3).

The means by which Pd(II) ions are assimilated by cells is currently unknown but, since cells have well defined metal trafficking pathways (uptake and also efflux) for essential metals which require homeostasis to avoid toxicity, an association with the metal-transport and assimilation/effflux pathway(s) may be anticipated. It may be conjectured, for example, that Pd(II) is 'recognized' in lieu of, for example, Ni(II) (see Omajali et al., 2015 for discussion). Not only hydrogenases, but other enzymes, contain Ni which gives a large number of potential 'destination' sites for an outcome that may involve cellular 'recognition' of Pd(II) but an inability to then produce a functional enzyme that is dependent on the precise incorporation of the specific metal required for enzymatic activity. An ability to take up Pd(II) but not produce functional enzymes may, in turn,

upregulate pathways for (e.g.) Ni(II) transport; the cells would 'perceive' Ni-starvation under conditions of Pd(II) saturation (e.g. 20 wt% loading of Pd as compared to 5 wt%: see above) and this may lead to over-internalization of Pd(II) into the cells with potentially, reduction to Pd(0) as a detoxification mechanism; once reduced to Pd(0) the metal toxicity was reduced as compared to Pd(II) when compared using flow cytometry (Omajali et al., 2018). The lack of observable intracellular Pd NPs in *D. desulfuricans* at 5 wt% Pd may relate to a more effective efflux mechanism for Pd(II) and metal reduction occurring during exit from the cells and not during uptake of Pd(II). Evidence for or against this hypothesis has been limited by a lack of rapid screening assay of mutants deficient in genes known to be involved in metal metabolism. A rapid method to visualize altered Pd accumulation was developed by Torgeman (2017) to screen 21 d-block metal transporter gene mutants of *E. coli*, showing, to date, influential effects of several genes: *cusA* (encodes copper efflux, resistance to silver (Randall et al., 2015) and biofabrication of silver nanoparticles (Lin et al., 2014)); *modF* (part of the molybdate ATPase transporter system (Grunden et al, 1996; Ma et al., 2009)); *apaG* (involved in efflux of Co(II) (Ecogene); *fur* (global regulator for Fe repression (Iwig et al., 2006; Seo et al., 2014; Bagg & Neilands, 1987) and *fieF* (involved in efflux of Fe(II) (Grass et al., 2005). Hence, several mechanisms are probably involved in cellular processing of Pd(II), any one or more of which may have an altered regulation in response to RF injury. An unrelated study examining the effect of RF exposure on gene expression in *E. coli* showed a 3-4 fold upregulation of a suite of genes including functionalities relating to Ni(II) metabolism (Supplementary Information S4).

It is interesting to note that, in contrast to *D. desulfuricans*, *E. coli* localized more Pd(0)-NPs intracellularly (Gomez-Bolivar et al., 2019) but no biochemical insight can be assigned to this without further understanding of the pathways involved in Pd(II) processing. However it can be concluded that the effect of RF radiation on living cells prior to exposure to Pd(II) is to predispose them to making a more homogeneous distribution of Pd-NPs in *E. coli* (Gomez-Bolivar et al., 2019) and *D. desulfuricans* (supplementary information, Figure S2, Figure S3), which suggests a cellular injury response that affects NP nucleation and patterning but it is not known if this is solely a rapid and transient response (Shamis et al., 2011) or to a more enduring upregulation of injury stress-related genes (above), or both.

Prior to the work we report here it was known that exposure of cells to an electric field influences various cellular processes (Knowles et al., 2007) and, also relevant, an electric field was shown in E. coli to enhance hydrogenase-mediated hydrogen production (Redwood, 2007); the membrane-bound hydrogenase-3 (part of the FHL complex) is known to be involved in the manufacture of bio-Pd(0), acting in Pd(II) reduction via H_2-splitting (Deplanche et al., 2010). However, these two unrelated studies did not attempt to isolate electric from magnetic field components. RF-injured cells, while showing outer membrane rearrangement and increased permeability (Shamis et al., 2011) apparently recovered within 10-15 min. Altered gene expression and protein synthesis (Supplementary Information S4) may be initiated in response to the immediate membrane perturbations and loss of permeability barrier and hence invoking a secondary response, persisting beyond the immediate RF recovery period. Hence two responses may be suggested, an initial rapid membrane disruption and also a genetic response, the trigger for which may be the electromagnetic field per se (via an unknown mechanism) and/or the altered membrane permeability in response to the stimulus. Both periplasmic and inner membrane-bound hydrogenases are involved in Pd(0) deposition in *D. desulfuricans* (Mikheenko et al., 2008); it is likely that the RF magnetic field induced changes to the membrane-environment and hence perturbs the transmembrane processes of hydrogen cycling which are key to the metabolism of *D. desulfuricans*.

The overall benefit at 8 W dose was similar irrespective of whether the RF was applied before or during Pd(II) uptake and reduction (Table 2); adding the RF with Pd in both stages increased the selectivity by 50% (Table 2). However, as these cells were placed under three simultaneous stresses (RF, pH and metal) proper interpretation is difficult without applying each stress in isolation, which was beyond the present scope. Examination of Pd-NPs produced prior to and during/after cell injury, showed that the response was, overall, similar with respect to the NPs produced (Gomez-Bolivar and I. Mikheenko, unpublished; supplementary information Figure S3), along with the similar catalytic activities (Table 2).

With cells injured in the absence of Pd a simple increase in subsequent NP homogeneity (Gomez-Bolivar et al., 2019) via a post-stress injury response and altered Pd-patterning might account for the decreased (halved) rate and doubled selectivity at lower doses (Table 3). It could be argued that the short transfer time between Pd(II)-addition and the

introduction of the RF field may have been sufficient to promote the rapid response during Pd(II) uptake but this cannot account for the changes seen in cells pre-challenged with Pd(II) and only exposed to RF during the reduction stage. Hence, a further response may be suggested which relates to the interaction of the Pd(II) with the cellular matrix (e.g. akin to the effect on pre-formed bio-Pd: see earlier). Once the NPs were initiated, the catalytic activity was identical with respect to application of RF during Pd(II) uptake or, later, to reduction to Pd(0) (Table 2). As the latter cells showed only small additional changes in NP size and dispersion (Figure S3) this would argue against a contributory effect of pH or metal stress since both sets of Pd-challenged cells were treated identically with the difference being the time of RF addition. However, the catalytic outcome was the same in each case (Table 2) but was less favourable than that of cells injured prior to Pd(II) exposure (Table 3).

With regards to catalysis, the mechanism of selective hydrogenation relates to several factors (see above), with the actual catalytic site comprising a layer of Pd/carbon on the NP surface and not the metallic surface per se (Teschner et al., 2006). In this case it is possible that some material is 'donated' by the biomass components to interact with the Pd-NPs. A direct interaction between the Pd-NPs in the cell surface layers and the biomaterial-carbon was shown using X-ray photoelectron spectroscopy (Priestley et al., 2015), while single electron transfer between bio-Pd and activated carbon was reported (see above).

Teschner et al. (2006) also pointed out that pentane does not form from trans-2-pentene over Pd (111) (the predominant plane in bio-Pd-NPs), potentially resulting in less pentane occurring from trans-2-pentene and thereby reducing the ratio of cis to trans-2-pentene. The crystal faces of the cell surface and intracellular Pd-NPs have not been examined in detail over a sufficiently large population of NPs but this would repay a detailed comparison in native and RF-injured cells to enumerate the proportions of Pd (111) and (200) faces produced. This consideration is prompted by work of Bennett et al. (2013) and Omajali et al. (2015) which noted (111) and also (200) planes. Since Teschner et al. (2006) showed that selectivity in pentyne hydrogenation is also related to the exclusion of bulk hydrogen via the buildup of a Pd-C layer (explaining that this build up process is not effective on the surface of bulk (111)), it follows that bio-NPs with solely (111) surface planes should be less selective in hydrogenation because hydrogen can saturate

the bulk of the particle, which becomes too reactive at the expense of selectivity, and hence a greater predominance of (200) planes may be beneficial. This discussion assumes that biomatrix components interact with Pd-NPs biomimetically. Techner et al. (2006) also suggest, however, that in addition structural defects may be required to start the C-C dissociation reaction in the hydrogenation mixture in order to facilitate the start of the Pd-C surface phase that then acts to prevent participation of energetic bulk-dissolved hydrogen in the reaction, i.e. favouring selectivity at the expense of rate. Clearly in this mechanistic context, a more detailed examination of a larger population of bacterial Pd-NPs would be warranted, with and without RF treatment, especially looking at the imperfections observed on (111) planes (Bennett et al., 2013) and (111) distortion (~ 5%) noted by Omajali et al. (2015).

Enhanced selectivity was observed by bio-Pd(0) made in the presence of Pd(II) (Table 2) although the NP homogeneity was greater (supplementary information Figure S3) . This may indicate a possible change in the surface atomic arrangement (including defects) of the bio-supported palladium particles (above) as well as their precise interactions with influential biochemical scaffolding matrices. Relevant to this conjecture, temperature-programmed desorption studies of cis- and trans-2-butene over various platinum surfaces (Lee et al., 2009) showed that the cis- isomer was more thermodynamically stable upon close-packed Pt(111), (100) planes than the trans-isomer. Conversely, the latter was more stable on a more open Pt(110); clearly the facets and atomic arrangements of the Pd atoms on bio-Pd warrant a more exhaustive study.

A previous study (Gomez-Bolivar et al., 2019) noted that, whereas RF dosing resulted in larger NPs being produced by *D. desulfuricans* smaller NPs were made by *E. coli* (however, the differences, although statistically significant, were small, within 10-20%). This may relate to different activities and patterning of (e.g.) formate hydrogen lyase (FHL) in the two organisms. FHL is key to the fermentative growth of *E. coli* as it breaks down formate when this is produced as a toxic fermentation end product. On the other hand, *Desulfovibrio* spp. normally grow via dissimilatory sulfate reduction and FHL, while reported in early work, was not normally considered to be a major enzyme of this organism. However, while the importance of a cytoplasmic FHL as a component in formate cycling and key to the energy conservation of *Desulfovibrio* has been advanced

(Price et al., 2014) this would seem to be an unlikely factor in *D. desulfuricans*, given that little intracellular Pd was observed (above).

Intuitively, larger NPs (such as those produced by *D. desulfuricans* under RF stress: above (Gomez-Bolivar et al., 2019)) should result in a slower reaction rate for the same mass of metal (due to the relatively lower overall surface area to volume) but, on the other hand, Doyle et al. (2004; 2005) showed that pentenes react faster on larger particles; the smaller particles observed in other work following RF treatment of E. coli (Gomez-Bolivar et al., 2019) are in accordance with this (i.e. reduced formation of pentane) but the unpublished observations we report (whereby the NPs become larger with cell injury; Figure S3) would anticipate more pentane (at the expense of pentene) but this was not observed (Table 2, Table 3). However, the larger NPs may represent agglomerations of smaller ones, e.g. as observed previously (Courtney et al., 2016) with individual small NPs retained and stabilized by biomatrix components within a larger entity.

The cellular responses leading to the formation of altered NPs and catalytic activities are complex (above); over-interpretation at this stage is premature but, altered Pd-NPs can be regarded a providing a 'fossil record' of the history of such changes which cannot easily be followed dynamically. From this concept, a dynamically self-reporting metal such as Au(0) may prove useful; the size and shape (and complexation) of Au(0) nanoparticles self-report as emitted color (red/pink/orange though to various shades of blue/purple) via the surface plasmon vibrations of the gold atoms. For example, a color change was used to report conformational changes of Au(0) bound to cytochrome C as this undergoes a pH-dependent conformational change (Chah et al., 2005). Changes to the membrane organization, and transient collapse of the transmembrane proton gradient upon poration in an RF field may report dynamically via the emitted color of metallic NPs but interpretation may be complicated if the color represents a combined effect of several mechanisms of Au deposition. Moreover, Pd does not self-report in this way. The situation is further complicated by the recent observation that the Pd-species on sulfidogenic cells is not solely Pd(0) but also comprises an oxidized form (PdO; the catalyst was stored in air) as well as a sulfided form of Pd (e.g. PdS, Pd_3S, Pd_4S or Pd_xS_y) (Mikheenko et al., 2019). Although the cells were washed before use the possibility of residual H_2S production was not precluded. Although sulfide is a classical catalyst poison Pd4S was reported as one of the most selective hydrogenation catalysts in the

hydrogenation of alkynes to alkenes, with PdS also showing high –ene selectivity (McCue et al., 2016). More recent work (Albani et al., 2018) has reported the high activity of a nanostructured Pd_3S phase as well as noting that ethane desorption from Pd3S and Pd4S surfaces (0.08 and 0.22 eV respectively) is energetically preferred over further hydrogenation of the -ene (0.79 and 0.55 eV respectively). This is the opposite situation to Pd(111) where the over hydrogenation is favoured (barrier is 0.45 eV), this being much lower than that of the alkene desorption (0.85 eV).

In the light of these two recent developments (Albani et al., 2018; Orozco et al., 2019) a full crystallographic and ultrastructural examination (by EXAFS) of the Pd-products of sulfidogenic cells is underway. This is made difficult by the fact that the lattice spacings are very similar (see Orozco et al. (2019) for discussion). If a pivotal role for Pd-sulfide is confirmed than a potential advantage offered by sulfidogenic bacteria would be that the dissimilatory sulfate metabolism of the cells under RF-stress may provide another interventional target for fine tuning. As the RF field has profound effects on membrane integrity and potentially on hydrogen cycling (earlier) the proton gradient would be affected so that ATP cannot be formed by ATP synthase. In this respect the RF may be acting like a classical uncoupling agent and thus promote increased flux into sulfate reduction, H_2S formation and more predominance of palladium sulfide components of the NPs.

Acknowledgements

This work was supported by EPSRC (grants No EP/I007806/1 and EP/D05768X/1), BBSRC (grant No BB/C516128/1), NERC (grant NE/L014076/1) and by a Royal Society/BBSRC Industrial Fellowship to LEM for secondment into C-Tech Innovation Ltd., who provided the custom-made apparatus used in this work. We acknowledge with thanks the contributions of the late Dr Ruth Wroe of C-Tech Innovation Ltd. into useful discussions and the kind permission of Drs Steve Megit, Colin Berry and Andy Morby (University of Cardiff, UK) to describe their unpublished work in Supplementary Information.

This work was partially supported by the Spanish Government Sistema Nacional de Garantía Juvenil grant PEJ-2014-P-00391 (Promoción de Empleo Joven e Implantación

de la Garantia Juvenil 2014, MINECO) with a scholarship to JGB. We also thank the EM Centre at U. Granada for access to high resolution electron microscopy in supplementary information (Figures S2 and S3).

References

Albani, D., Shahrokhi, M., Chen, Z., Mitchell, S., Hauert, R., López, N. & Pérez-Ramírez, J. (2018) Selective ensembles in supported palladium sulfide nanoparticles for alkyne semi-hydrogenation. Nature Comm. 9, 2634-2645. Doi: 10.1038/s41467-018-05052-4.

Bagg, A. & Neilands, J.B. (1987) Ferric uptake regulation protein acts as a repressor, employing iron(II) as a cofactor to bind the operator of an iron transport operon in Escherichia coli. Biochemistry, 26, 5471-5477. https://doi.org/10.1021/bi00391a039

Beauregard, D.A., Yong, P., Macaskie, L.E & Johns, M.L. (2010) Using non-invasive magnetic resonance imaging (MRI) to assess the reduction of Cr(VI) using a biofilm–palladium catalyst. Biotechnol. Bioeng. 107, 11–20. https://doi.org/10.1002/bit.22791

Bennett, J.A., Creamer, N.J., Deplanche, K., Macaskie, L.E., Shannon, I.J. & Wood J. (2010) Palladium supported on bacterial biomass as a novel heterogeneous catalyst: A comparison of Pd/Al2O3 and bio-Pd in the hydrogenation of 2-pentyne, Chem. Eng. Sci., 65, 282-290. https://doi.org/10.1016/j.ces.2009.06.069

Bennett, J.A., Mikheenko, I.P., Deplanche, K., Shannon, I.P., Wood, J. & Macaskie, L.E. (2013) Nanoparticles of palladium supported on bacterial biomass; new, recyclable heterogeneous catalyst with comparable activity to homogeneous colloidal Pd in the Heck reaction. Appl. Catal. B Environ. 140-141, 700-707. https://doi.org/10.1016/j.apcatb.2013.04.022

Canovas, M., Torroglosa, T. & Iborra, J.L. (2005) Permeabilization of Escherichia coli cells in the biotransformation of trimethylammonium compounds into l-carnitine. Enz. Microb. Technol. 37, 300-308. https://doi.org/10.1016/j.enzmictec.2004.07.023

Carvalho, R.P., Yong, P., Mikheenko, I.P., Peterson-Beedle, M. & Macaskie, L.E. (2009) Electron paramagnetic resonance analysis of active bio-Pd based electrode for fuel cells. Adv. Mats. Res. 70-73, 737-720. https://doi.org/10.4028/www.scientific.net/AMR.71-73.737

Chah S., Hammond, M.R. & Zare, R.N. (2005) Gold nanoparticles as a colorimetric sensor for protein conformational changes. Chem. Biol. 12, 323-328. https://doi.org/10.1016/j.chembiol.2005.01.013

Collins, M.A. & Bettens, R.P.A. (2015) Energy-based molecular fragmentation methods. Chem. Rev. 115, 5607-5642. https://doi.org/10.1021/cr500455b

Courtney, J., Deplanche, K., Rees, N.V. &E. Macaskie, L.E. (2016) Biomanufacture of nano-Pd(0) by Escherichia coli and electrochemical activity of bio-Pd(0) made at the expense of H2 and formate as electron donors. Biotechnol Lett. 38, 1903-1910. https://doi.org/10.1007/s10529-016-2183-3

Creamer N.J., Mikheenko, I.P.; Yong, P., Deplanche, K., Sanyahumbi, D., Wood, J., Pollmann, K.., Merroun, M., Selenska-Pobell, S. & Macaskie, L.E. (2007) Novel supported Pd hydrogenation bionanocatalyst for hybrid homogeneous/heterogeneous catalysis. Catal. Today 128, 80-87. https://doi.org/10.1016/j.cattod.2007.04.014

Creamer N.J., Mikheenko, I.P., Johnson, C, Cottrell, S.P. & Macaskie L E. (2011) Local magnetism in palladium bionanomaterials probed by muon spectroscopy. Biotechnol Lett. 33, 969-976. doi: 10.1007/s10529-011-0532-9.

Crespo-Quesada, M., Yarulin, A., Jin, M., Xia, Y. & Kiwi-Minsker, L. (2011) Structure sensitivity of alkynol hydrogenation on shape and size controlled palladium nanocrystals-which sites are most active and selective? J. Am. Chem. Soc. 133, 12787-12794. https://doi.org/10.1021/ja204557m

De Corte S., Hennebel T., de Gusseme B., Verstraete W. & Boon, N. (2012) Bio-palladium: from metal recovery to catalyic applications. Microb. Biotechnol. 5, 5-17. https://doi.org/10.1111/j.1751-7915.2011.00265.x

Deplanche, K., Caldelari, I., Mikheenko, I. P., Sargent, F. & Macaskie, L. E. (2010) Involvement of hydrogenases in the formation of highly catalytic Pd(0) nanoparticles by bioreduction of Pd(II) using Escherichia coli mutant strains. Microbiology, 156, 2630-2640. https://doi.org/10.1099/mic.0.036681-0

Deplanche, K., Murray, A.J., Mennan, C., Taylor, S. and Macaskie, L.E. (2011) Biorecycling of precious metals and rare earth elements. In Nanomaterials (first edition). Rahman, M. (Ed). Intech, Croatia, ISBN: 978-953-307-913-4 pp. 279-314.

Deplanche, K., Bennett, J.A., Mikheenko, I.P., Omajali, J.B., Wells, A.S., Meadows, R.E., Wood, J. & Macaskie, L.E. (2014) Catalytic activity of biomass-supported Pd nanoparticles: Influence of the biological component in catalytic efficacy and potential

application in ‘green’ synthesis of fine chemicals and pharmaceuticals. Appl. Catal. B Environ. 147, 651-665. https://doi.org/10.1016/j.apcatb.2013.09.045

Doyle, A.M., Shaikhutdinov, S. & Freund, H-J. (2004) Alkene chemistry on the palladium surface: nanoparticles versus single crystals. J. Catal. 223, 444-453. https://doi.org/10.1016/j.jcat.2004.02.020

Doyle, A.M., Shaikhutdinov, S. & Freund, H-J. (2005) Surface-bound precursor determines particle size effects for alkene hydrogenation on palladium Ang. Chem. 44, 629 -631. https://doi.org/10.1002/anie.200461614

Foulkes, J.M., Malone, K.J., Coker, V.S, Turner, N.J. & Lloyd, J.R. (2011) Engineering a biometallic whole cell catalyst for enantioselective deracemization reactions. ACS Catal. 1, 1589-1594. https://doi.org/10.1021/cs200400t

Geveke, D.J. & Brunkhorst, C. (2008) Radio frequency electric fields inactivation of Escherichia coli in apple cider. J. Food Eng. 85, 215-221. https://doi.org/10.1016/j.jfoodeng.2007.06.029

Gomez-Bolivar, J., Mikheenko, I.P., Macaskie, L.E. & Mohamed L. Merroun, M.L. (2019) Characterization of palladium nanoparticles produced by healthy and microwave-Injured cells of Desulfovibrio desulfuricans and Escherichia coli. Nanomaterials 9, 857-873. doi:10.3390/nano9060857

Grass, G., Otto, M., Fricke, B., Haney, CJ,, Rensing, C,, Nies, D.H. & Munkelt, D. (2005) FieF (YiiP) from Escherichia coli mediates decreased cellular accumulation of iron and relieves iron stress. Arch. Microbiol. 183, 9- 18. https://doi.org/10.1007/s00203-004-0739-4

Grunden, A.M, Ray, R.M., Rosentel, J.K., Healy, F.G, & Shanmugam, K.T. (1996) Repression of the Escherichia coli modABCD (molybdate transport) operon by ModE. J Bacteriol. 178, 735-44. doi: 10.1128/jb.178.3.735-744.1996

Hennebel, T., de Corte S., Verstraete, W. & Boon, N. (2012) Microbial production and environmnetal application of palladium nanoparticles for treatement of halogenated compounds Curr. Opin. Biotechol. 23, 555-561. https://doi.org/10.1016/j.copbio.2012.01.007

Hooper, T.J.N., Partridge, T.A., Rees, G.J., Keeble, D.S., Powell, N.A., Smith, M.E., Mikheenko, I.P., Macaskie, L.E., Bishop, P.T. & Hanna, J.V. (2018). Direct solid state NMR observation of the 105Pd nucleus in inorganic compounds and palladium metal systems. Phys. Chem. Chem. Phys. 20, 26734-26743. doi:10.1039/c8cp02594k 2018

Hulshleger, H., Potel, J. & Niemann, E.G. (1981) Killing of bacteria with electric pulses of high field strength. Rad. Environ. Biophys. 20, 53-65. https://doi.org/10.1007/BF01323926

Iwig, J.S., Rowe, J.L. & Chivers, P.T. (2006) Nickel homeostasis in Escherichia coli - the rcnR-rcnA efflux pathway and its linkage to NikR function. Mol. Microbiol., 62, 252-62. https://doi.org/10.1111/j.1365-2958.2006.05369.x

Jamur, M.C. & Oliver, C. (2010) Permeabilization of cell membranes. Meth. Mol. Biol. 588, 63-66.

Knowles, C.J., Jackman, S., Li, H., Mustacchi, R. & Sunderland, J. (2007) Control of biocatalysis reactions International patent IPC8 Class AC25B300FI:USA Classi 205701

Lee, I., Delbecq, F., Morales, R., Albiter, M. A. & Zaera, F. (2009) Tuning selectivity in catalysis by controlling particle shape. Nat. Mats. 8, 132-138. https://doi.org/10.1038/nmat2371

Lin, I.W.-S., Lok, C-N & Che, C-M. (2014) Biosynthesis of silver nanoparticles from silver(i) reduction by the periplasmic nitrate reductase c-type cytochrome subunit NapC in a silver-resistant E. coli. Chem. Sci., 5, 3144- 3150. Doi: 10.1039/C4SC00138A

Louzguine-Luzgin, D.V., Xie, G.Q., Li, S., Inoue, A., Yoshikawa, N., Mashiko, K., Taniguchi, S. & Sato, M. (2009) Microwave-induced heating and sintering of metallic glasses. J. Alloys Compounds 483, 78-81. https://doi.org/10.1016/j.jallcom.2008.07.158

Ma, Z., Jacobsen, F.E. & Giedroc, D.P. (2009) Metal transporters and metal sensors: how coordination chemistry controls bacterial metal homeostasis. Chem. Rev., 109, 4644-4681. doi: 10.1021/cr900077w

McCue, A.J., Guerrero-Ruiz, A., Rodríguez-Ramos, I. & Anderson, J.A. (2016) Palladium sulphide- a highly selective catalyst for the gas phase hydrogenation of alkynes to alkenes J. Catal. 340, 10-16. doi: 10.1016/j.cat.2016.05.002

Mikheenko, I.P., Rousset, M., Dementin, S. & Macaskie, L.E. (2008) Bioaccumulation of palladium by Desulfovibrio fructosovorans and hydrogenase deficient mutants. Appl. Environ. Microbiol. 74, 6144–6146. DOI: 10.1128/AEM.02538-07

Mikheenko, I.P., Gomez-Bolivar, J., Merroun, M.L., Macaskie, L.E., Sharma, S., Walker, M., Hand, R.A., Grail, B.M., Johnson, D.B., & Orozco, R.L. (2019) Upconversion of cellulosic waste Into a potential "drop in fuel" via novel catalyst generated using Desulfovibrio desulfuricans and a consortium of acidophilic sulfidogens. Front. Microbiol., 10 May 2019 | https://doi.org/10.3389/fmicb.2019.00970

Omajali, J.B. (2015) Novel Bionanocatalysts for Green Chemistry Applications. PhD Thesis University of Birmingham UK.

Omajali, J., Mikheenko, I.P., Merroun, M.L., Wood, J. & Macaskie, L.E. (2015) Characterization of intracellular palladium nanoparticles synthesized by Desulfovibrio desulfuricans and Bacillus benzeovorans. J Nanopart. Res. 17, 264-281. Doi: 10.1007/s11051-015-3067-5

Omajali, J.B., Hart, A., Walker, M., Wood, J. & Macaskie. L.E. (2017) In situ catalytic upgrading of heavy oil using dispersed bio-nanoparticles supported on Gram-positive and Gram-negative bacteria. Appl. Catal. B Environ. 203, 807-819. https://doi.org/10.1016/j.apcatb.2016.10.074

Omajali, J.B., Mikheenko, I.P., Overton, T.W., Mohamed L Merroun, M.L. & Macaskie, L.E. (2019) Probing the viability of palladium-challenged bacterial cells using flow cytometry. J. Chem. Technol. Biotechnol. 94, 295-301. https://doi.org/10.1002/jctb.5775

Prette, A.L.G., Cologna, M., Sglavo, V. & Raj, R. (2011) Flash-sintering of Co2MnO4 spinel for solid oxide fuel cell applications. J. Power Sources 196, 2061-2065. https://doi.org/10.1016/j.jpowsour.2010.10.036

Price, M.N., Ray, J., Wetmore, K.M., Kuehl, J.V., Bauer, S. & Deutschbauer, A.M. (2014) The genetic basis of energy conservation in the sulfate reducing bacterium Desulfovibrio alaskensis G20. Front. Microbiol. 5, 577-585. https://doi.org/10.3389/fmicb.2014.00577

Priestley, R.E., Mansfield, A., Bye, J., Deplanche, K., Jorge, A.B., Brett, D., Macaskie, L.E. & Sharma, S. (2015) Pd nanoparticles supported on reduced graphene– E. coli hybrid

with enhanced crystallinity in bacterial biomass. RSC Adv. 5, 84093-84103. Doi: 10.1039/C5RA12552A

Randall, C.P., Gupta, A., Jackson, N., Nusse, D & O, Neill, A.J. (2015) Silver resistance in Gram-negative bacteria: a dissection of endogenous and exogenous mechanisms. J. Antimic. Chemother., 70, 1037-46. doi: 10.1093/jac/dku523.

Redwood, M.D. (2007) Biohydrogen and Biomass–supported Palladium Catalyst for Energy Production and Waste Minimisation. PhD Thesis University of Birmingham, UK.

Redwood, M.D., Deplanche, K., Baxter-Plant, V.S. & Maakie, L.E. (2008) Biomass-supported palladium catalysts on Desulfovibrio desulfuricans and Rhodobacter sphaeroides. Biotechnol. Bioeng. 99, 1045-54. https://doi.org/10.1002/bit.21689

Seo, S.W., Kim, D., Latif, H., Brien, E.J., Szubin, R. & Palsson, B.O. (2014) Deciphering Fur transcriptional regulatory network highlights its complex role beyond iron metabolism in Escherichia coli. Nature Comm. 5, 4910-4910. https://doi.org/10.1038/ncomms5910

Shamis, Y., Taube, A., Mitik-Dineva, N., Croft, R., Crawford, R.J. & Ivanova, E.P. (2011) Specific electromagnetic effects of microwave radiation on Escherichia coli. Appl. Environ. Microbiol. 77, 3017-3023. Doi: 10.1128/AEM.01899-10

Schmidt, E., Vargas, A., Mallat, T. & Baiker, A. (2009) Shape-selective enantioselective hydrogenation on Pt nanoparticles. J. Am. Chem. Soc. 131, 12358-12367. https://doi.org/10.1021/ja9043328

Singh O.V. Ed., Bionanoparticles: Biosynthesis and Sustainable Biotechnological Implications Wiley, New York (2015a).

Singh, S., Gupta, D., Jain, V. & Sharma, A.K. (2015) Microwave processing of materials and applications in manufacturing industries: a review. Mats. Manuf. Proc. 30, 1-29. https://doi.org/10.1080/10426914.2014.952028

Skibar, W.S, Pompe, W., Fratzl, P., Selenska-Pobell, S., Rousset, M. & Macaskie, L.E. (2005) Novel precious metal-based bionanocatalysts from scrap. Final report Contract No G5RD-CT-2002-00750. The European Commission, Brussels.

Teschner, D., Vassm E., Hävecker, M., Zafeiratos, S., Schnörch, P., Sauer, H., Knop-Gericke, A., Schlogl, R., Chamam, M., Wootsch, A., Canning, A.S., Gamman, J.J., Jackson, S.D., McGregor, J. & Gladden, L.F. (2006) Alkyne hydrogenation over Pd catalysts: a new paradigm. J. Catal. 242, 26-37. https://doi.org/10.1016/j.jcat.2006.05.030

Torgeman, E. (2017) Biosynthesis of gold and palladium nanoparticles via bacteria. Master Thesis, University of Oslo

Williams, A.R. (2016) Biogenic precious metal-based nanocatalysts for enhanced oxygen reduction. PhD Thesis, University of Birmingham, UK.

Yong. P., Liu, W., Zhang, Z., Beauregard, D., Johns, M.L. & Macaskie, L.E. (2015) One step bioconversion of waste precious metals into Serratia biofilm-immobilized catalyst for Cr(VI) reduction. Biotechnol Lett 37, 2181–2191 DOI 10.1007/s10529-015-1894-1

Zhu, J., Deplanche, K., Wood, J. & Macaskie, L.E. (2016) Selective hydrogenation using palladium bioinorganic catalyst Appl. Catal. B Environ. 199, 108-122. https://doi.org/10.1016/j.apcatb.2016.05.060

Zimmerman, U., Pilwat, G. & Riemann, F. (1974) Dielectric breakdown of cell membranes. Biophys. J. 14, 881-899. https://doi.org/10.1016/S0006-3495(74)85956-4

Zimmerman, U. (1986) Electrical breakdown, electropermeabilization and electrofusion. Rev Physiol Biochem Pharmacol 105, 176-256. https://doi.org/10.1007/BFb0034499

Table 1. Treatments used in this study

Treatment	Resting cells	Initial Pd(II) sorption*	Pd(II) reduction*	Finished catalyst**
Pre-formed	-	-	-	+
Catalyst				
During Pd(0) reduction	-	-	+	N/A
During Pd(II) uptake	-	+	-	N/A
Resting cells (before Pd)	+	-	-	N/A
Control (no RF)	-	-	-	N/A

The control was left untreated and used to make bio-Pd(0) as described in Materials and Methods. An electromagnetic field (see text) was applied to the cells (shown as +) at different stages of catalyst preparation: (a) to resting cells before addition of palladium salt or reductant; (b) during uptake of Pd(II) onto/into the cells or (c) during reduction of palladium by the cells after addition of formate. Short and long exposure times (5 and 20 minutes) were tested using living cells at a range of powers (2-60 W). The effect of RF radiation on dried 5% bio-Pd powder used high power (60W, 60 min). Samples using live cells were each treated with 2W, 4 or 8W RF (20 mins unless stated otherwise). A control using Pd(II) solution with no cells showed no reduction of Pd(II).

Table 2. Effect of RF treatment on cells and bio-Pd catalyst when dosed at 8W RF for 20 min

Catalyst Treatment	Initial rate* (μmol/L/sec)	Ave cis/trans 2-pentene	Ave pentene/ pentane
No RF	1.1	12.8	6.7
RF during Pd(II) uptake	2.2	15.2	11.8
RF during Pd(II) reduction	1.9	15.3	11.5

*Initial rate up to 20% conversion. Errors as shown in Figure 3.

Table 3. Effect of RF treatment on resting cells prior to addition of Pd(II)

Catalyst Treatment	Initial rate* (μmol/L/sec)	Ave cis/trans 2-pentene	Ave pentene/ pentane
No RF resting cells	1.1	12.8	6.7
5 min 2 W resting cells	1.2	18.3	10.4
20 min 2 W resting cells	1.5	22.1	11.8
20 min 4 W resting cells	1.6	21.0	12.9
20 min 8 W resting cells	3.3	9.4	7.6

*Initial rate up to 20% conversion. Errors as shown in Figure 4.

Legends to Figures

Figure 1. RF equipment used in this study. A Faraday cage was used to separate the magnetic field from the electrical heating components. The E (electric) component of electromagnetic radiation produces heating in dielectric (non-conducting) materials hence it is important to exclude heating from the sample by isolating the H (magnetic) component. This used a series LC circuit tuned with an external matching box to generate a magnetic field inside the induction coil (denoted L) and an electric field in the air gap between the two conducting plates (C). The sample vial, placed in the centre of the induction coil, was exposed to the magnetic field. The samples were treated by exposure inside a solenoid coil as the electromagnetic field within the coil will be almost entirely magnetic; consequently, as the magnetic susceptibilities of the components of the sample being treated (glass, water, bacteria and a very low concentration of Pd) are very low at this frequency there would be minimal heating of the sample. After exposure, the final external temperature of the bottle was checked. The temperature of the sample was monitored using a fibre optic temperature probe. Samples were treated at a power output levels of 2-60 Watts for up to 60 min as stated in individual experiments. These power levels are regarded as levels of magnetic field intensity and are proportional to the magnetic field strength but cannot be regarded as fully quantitative power densities. Samples received a dose of radio frequency magnetic field determined by the power level and the treatment time but again this cannot be fully quantified and data should be regarded as a semi quantitative for comparison.

Figure 2. Conversion of 2-pentyne and product selectivities using 5 wt% bio-Pd and commercial Pd/C catalysts (open symbols) and their RF-treated analogues (60 W; 60 min; filled symbols). A: Pentyne conversion (%). B: Cis/trans selectivity of pentene. C: Pentene/pentane selectivity. □,□: 5% Pd/C. □□: 5% bio-Pd. Data are means □ SEM. Where no error bars are shown these were within the dimensions of the symbols.

Figure 3. Conversions and product selectivities for cells manufacturing bio-Pd (5 wt%) without RF treatment (control, □) or treated with RF (8W) as follows: □, resting cells before addition of Pd(II); □, during sorption of Pd(II); □, during reduction of Pd(II) following sorption. A: Pentyne conversion (%). B: Cis/trans selectivity of pentene. C: Pentene/pentane selectivity. Data are means □ SEM. Where no error bars are shown these were within the dimensions of the symbols

Figure 4. Conversions and product selectivities for bio-Pd (5 wt% Pd) made by resting cells without exposure to RF (control, □) and with Pd loading following RF treatment of the resting cells as follows: □, 2W, 5 min; □, 2W, 20 min; □, 4W, 20 min; □, 8W, 20 min. A: Pentyne conversion (%). B: Cis/trans selectivity of pentene. C: Pentene/pentane selectivity. Data are means □ SEM. Where no error bars are shown these were within the dimensions of the symbols.

Figure 5. Morphological effects of RF treatment on cells of *D. desulfuricans*. A: Control cells without RF treatment. Cells are shown following RF treatment at B: 2W (5 min); C: 2W (20 min); D: 4W (20 min); E: 8W (20 min); F: 30W (20 min). Bars are 2 μm. Images correspond to the data shown in Fig. 4.

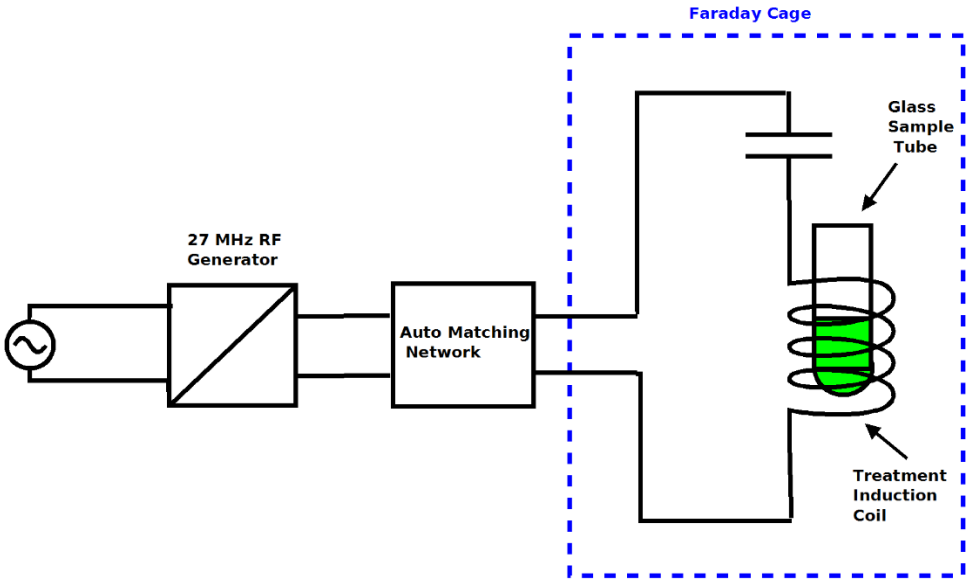

Figure 1.

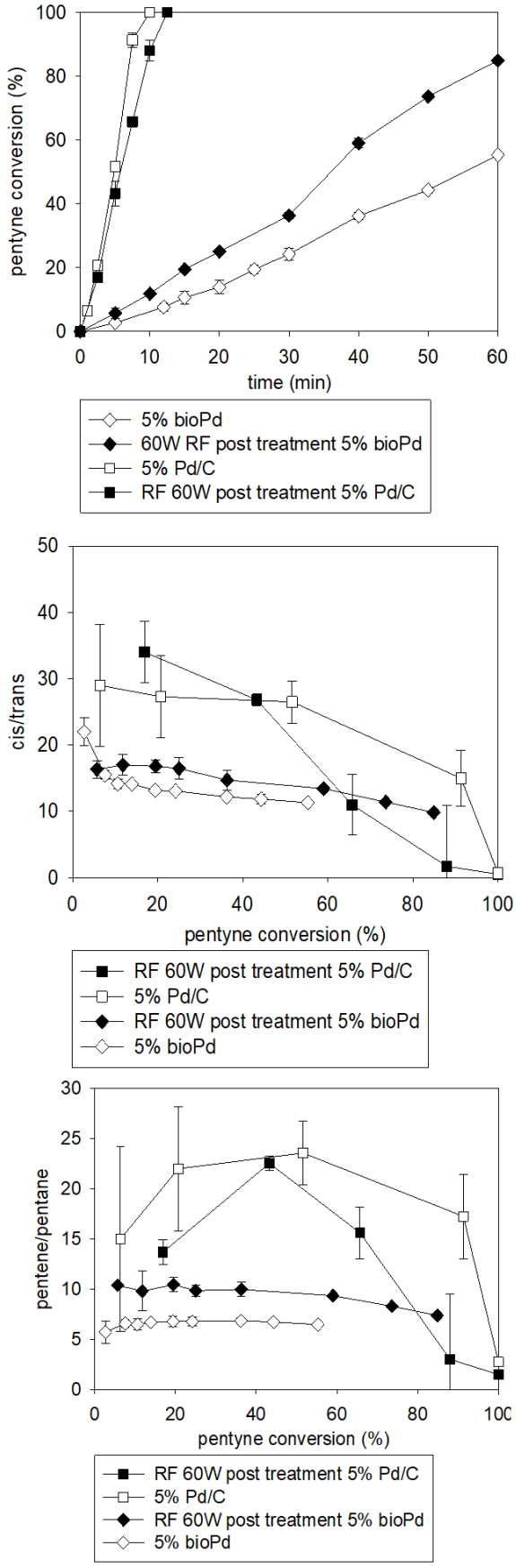
pentyne conversion (%)
time (min)
5% bioPd
60W RF post treatment 5% bioPd
5% Pd/C
RF 60W post treatment 5% Pd/C
cis/trans
pentyne conversion (%)
RF 60W post treatment 5% Pd/C
5% Pd/C
RF 60W post treatment 5% bioPd
5% bioPd
pentene/pentane
pentyne conversion (%)
RF 60W post treatment 5% Pd/C
5% Pd/C
RF 60W post treatment 5% bioPd
5% bioPd

Figure 2.

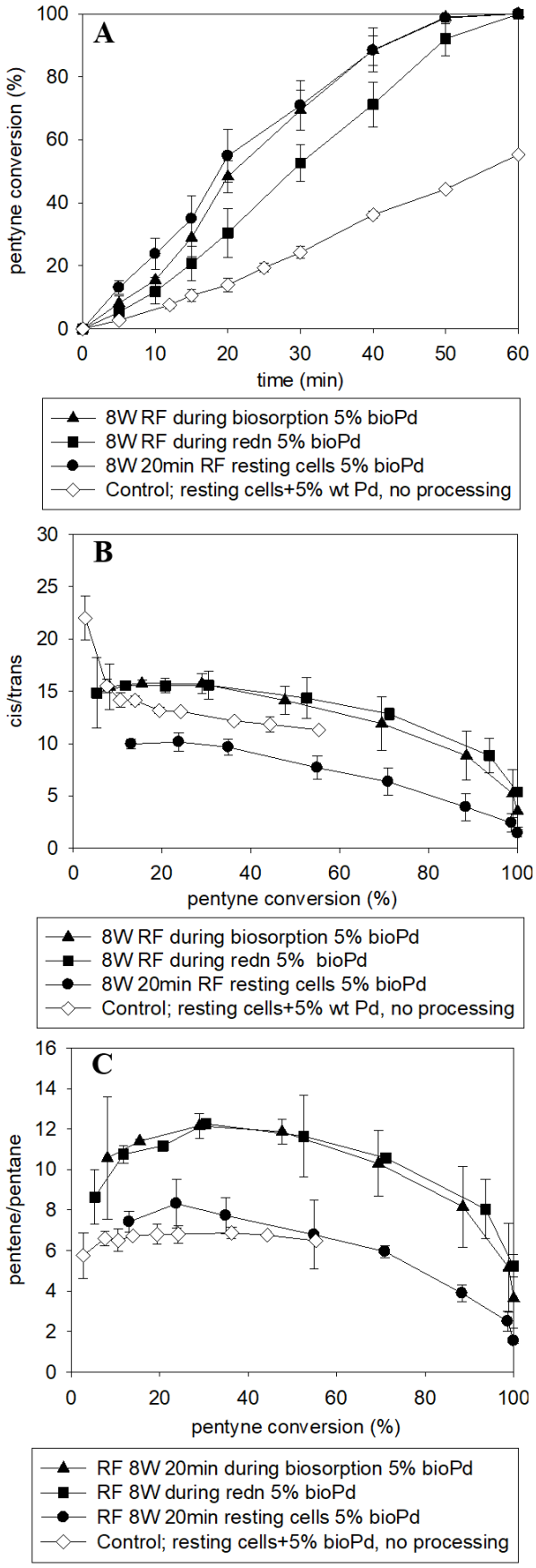
A
pentyne conversion (%)
time (min)
8W RF during biosorption 5% bioPd
8W RF during redn 5% bioPd
8W 20min RF resting cells 5% bioPd
Control; resting cells+5% wt Pd, no processing
B
cis/trans
pentyne conversion (%)
8W RF during biosorption 5% bioPd
8W RF during redn 5% bioPd
8W 20min RF resting cells 5% bioPd
Control; resting cells+5% wt Pd, no processing
C
pentene/pentane
pentyne conversion (%)
RF 8W 20min during biosorption 5% bioPd
RF 8W during redn 5% bioPd
RF 8W 20min resting cells 5% bioPd
Control; resting cells+5% bioPd, no processing

Figure 3.

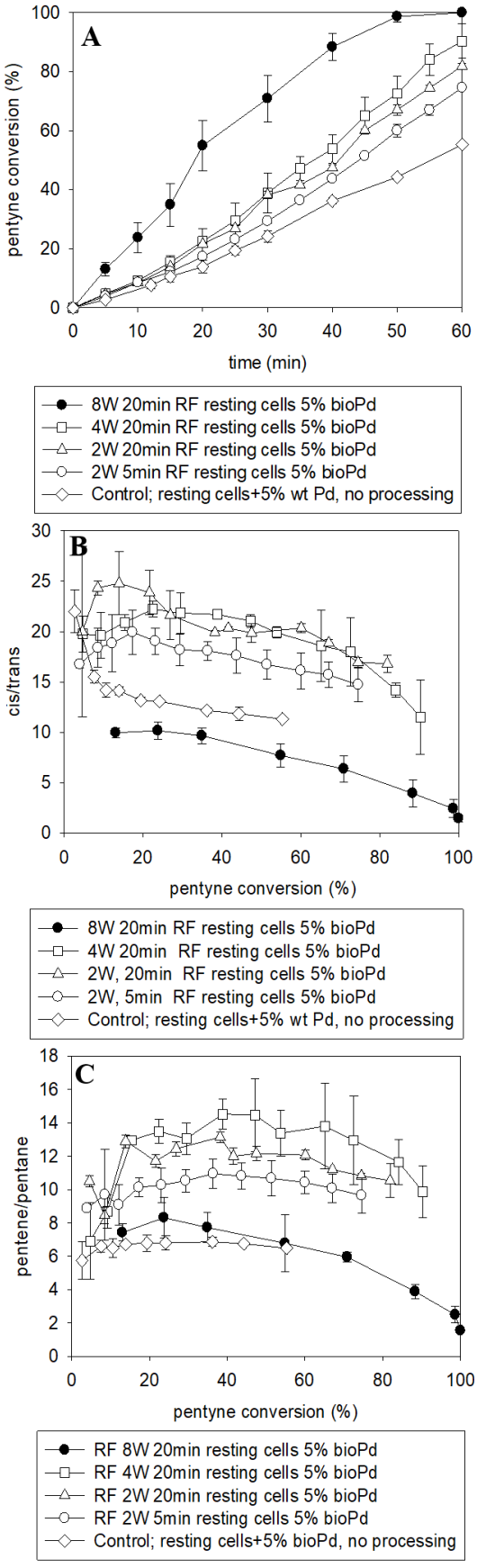
A
pentyne conversion (%)
time (min)
8W 20min RF resting cells 5% bioPd
4W 20min RF resting cells 5% bioPd
2W 20min RF resting cells 5% bioPd
2W 5min RF resting cells 5% bioPd
Control; resting cells+5% wt Pd, no processing
B
cis/trans
pentyne conversion (%)
8W 20min RF resting cells 5% bioPd
4W 20min RF resting cells 5% bioPd
2W, 20min RF resting cells 5% bioPd
2W, 5min RF resting cells 5% bioPd
Control; resting cells+5% wt Pd, no processing
C
pentene/pentane
pentyne conversion (%)
RF 8W 20min resting cells 5% bioPd
RF 4W 20min resting cells 5% bioPd
RF 2W 20min resting cells 5% bioPd
RF 2W 5min resting cells 5% bioPd
Control; resting cells+5% bioPd, no processing

Figure 4.

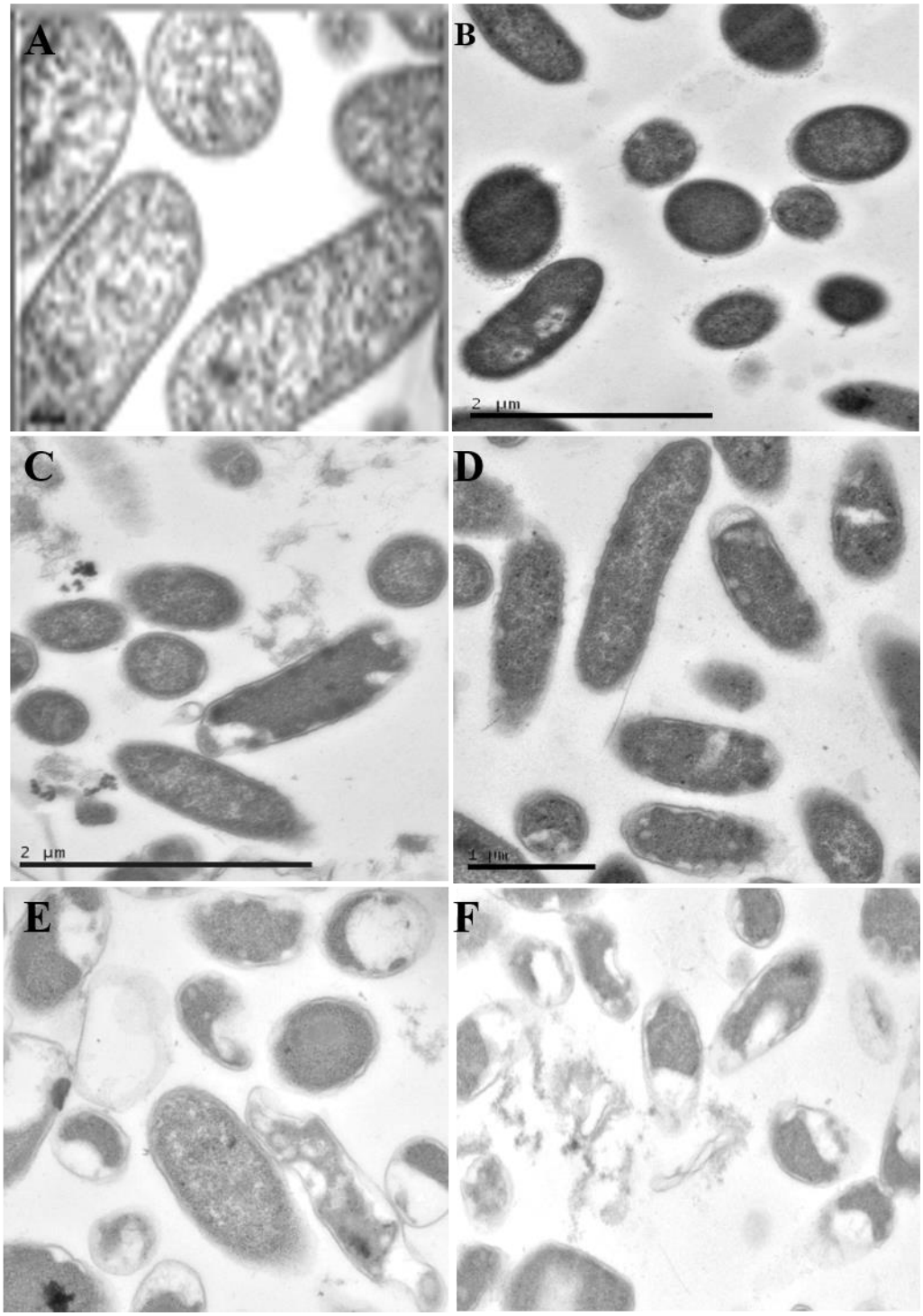

Figure 5.

Supplementary information

Figure S1. Hydrogenation of itaconic acid by bio-Pd of *Desulfovibrio fructosovorans*. Bio-Pd (5 wt% Pd or as shown) was made on *Desulfovibrio fructosovorans* using parental cells (wild type, WT) and a mutant deleted with respect to its two periplasmic hydrogenases (double negative mutant: Mikheenko et al., 2008). The commercial comparator was 5wt% Pd on carbon catalyst (Creamer et al., 2007). This work was described by Skibar et al., (2005).

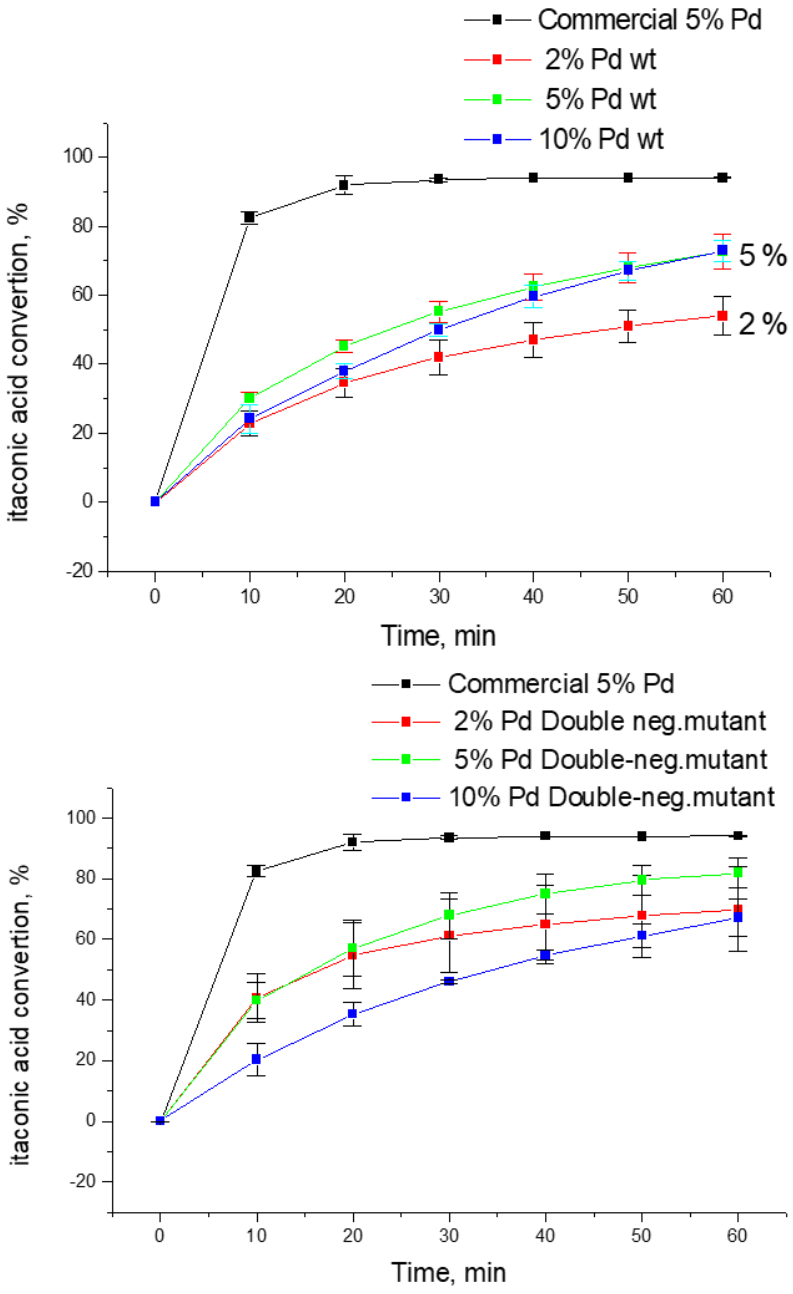

Figure S2. *Desulfovibrio desulfuricans* cells without (left panels) and following exposure to RF radiation (right panels) and corresponding X-ray microanalysis of specimen microareas. Details as in Gomez-Bolivar *et al*., 2019. Note the presence of P and S along with Pd, that are co-localized according to Mander's coefficient (see Gomez- Bolivar et al., 2019). Note also the retraction of the cytoplasmic membrane in response to RF-stress applied before addition of Pd(II) and relative paucity of Pd-nanoparticles in the periplasm except in some locations where they appear to bridge between the cytoplasmic and outer membranes

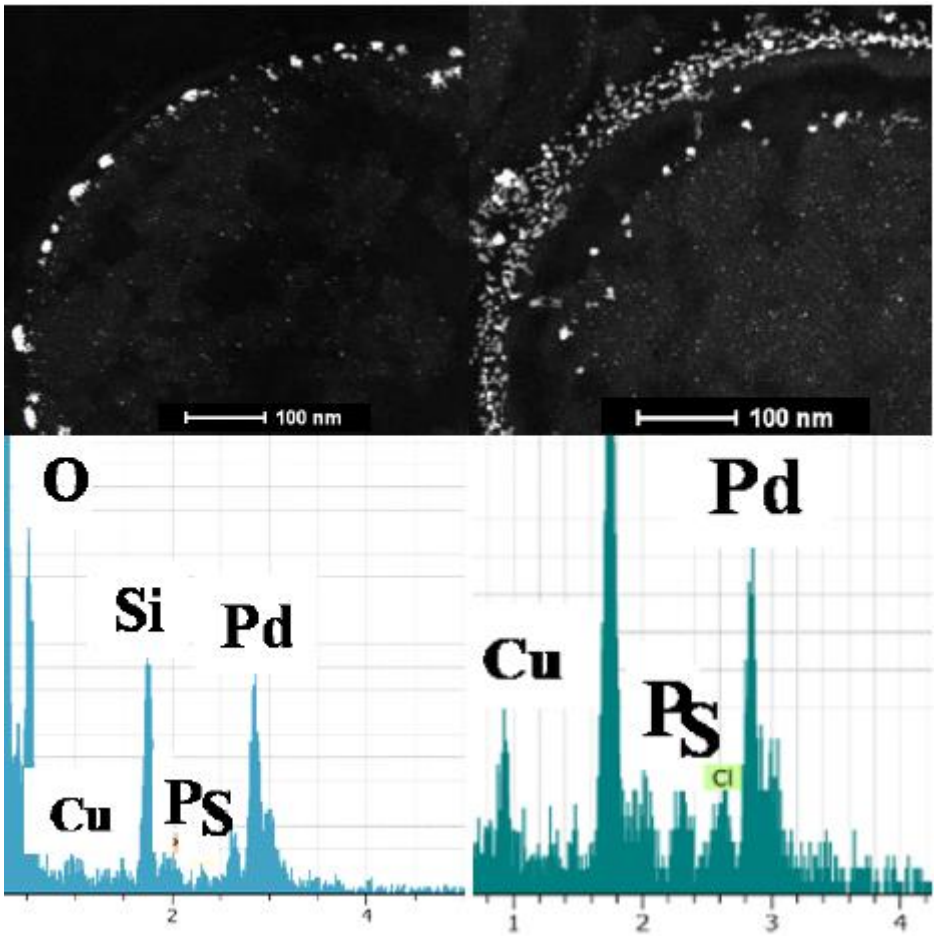

Figure S3. Pd-NPs produced by RF-injured *D. desulfuricans* (Gomez-Bolivar et al., 2019). A: no RF application (control) and RF applied to resting cells before Pd(II) addition (B) or during Pd(II) uptake (C). Dispersivity indexes were A: 2.07; B: 1.26; C: 0.98 (calculated according to Gomez-Bolivar et al.,2019).

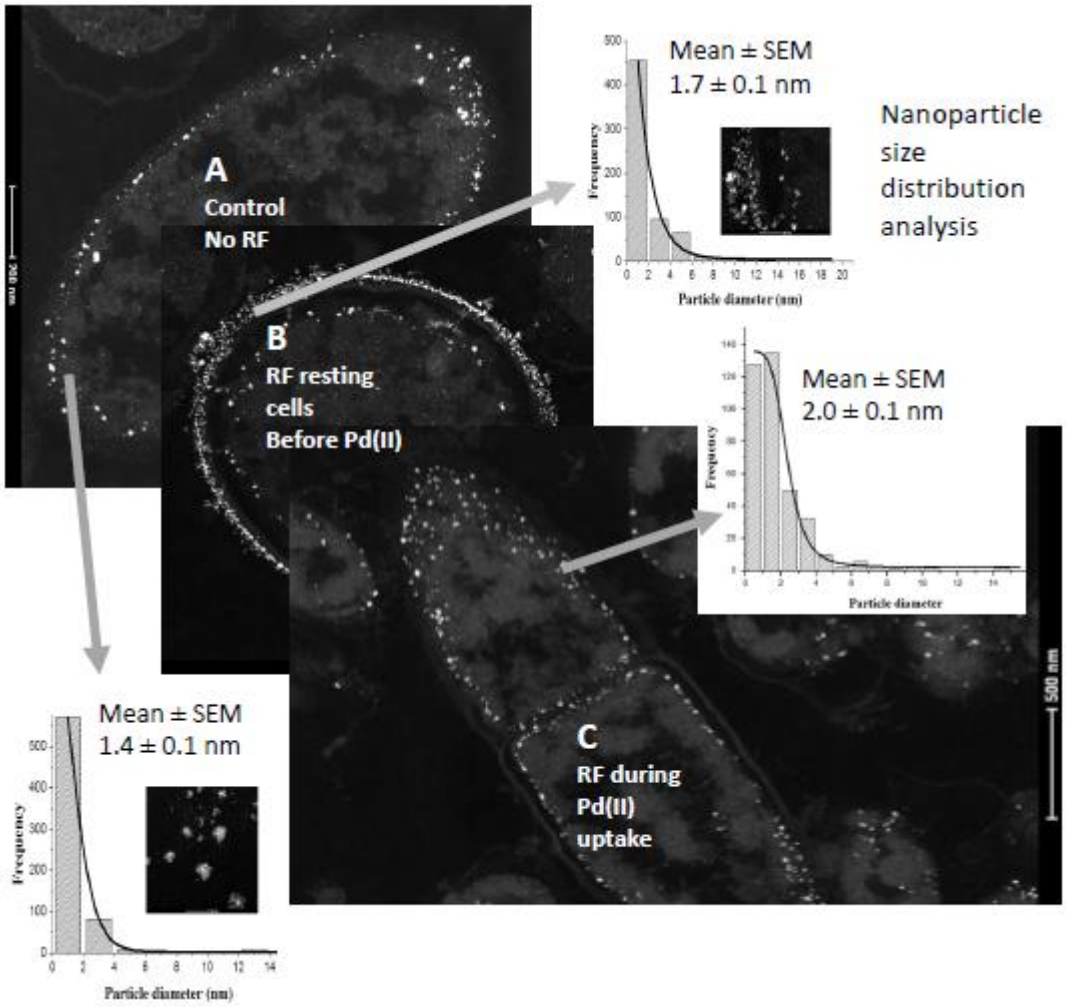

Figure S4. Mobile phone 'communication' with *E. coli* perturbs the expression of genes involved in fundamental cellular processes

Steven J. Megit, Colin Berry and Andrew P. Morby (unpublished work, shown with permission)
Cardiff School of Biosciences, Cardiff University Museum Avenue, Cardiff CF10 3US, UK

Fold Change in Transcript Abundance	Gene Designation	Gene Product Function
-4.6	*yacG*	Unknown
+4.0	*minE*	Cell division factor *Reverses MinC inhibition of ftsZ ring formation*
+3.9	*holA*	DNA-replication/repair, restriction/modification
+3.2	*insA_1*	Transposon-related functions
+4.6	*nohA*	Lambda terminase homologue
+2.4	*ydgR*	Putative transport protein
+2.2	*yohG*	Putative channel / filament protein
+2.4	*yifK*	Putative amino acid / amine transport protein
+3.0	*nrfE*	Energy metabolism *Formate-dependent nitrite reductase; possible assembly function*
+3.1	***hyaF***	**Energy metabolism** ***Nickel incorporation into hydrogenase-1 proteins***
+3.2	***hyfI***	**Energy metabolism *Hydrogenase 4Fe-S subunit***
+3.6	***nikD***	**Transport of small molecules** ***ATP-binding protein of nickel transport system***
+1.8	*betT*	High-affinity choline transport

Table 1 Genes with altered transcript abundance in response to mobile phone radiation
Only those genes are listed for which the alteration (increase (+) or decrease (-)) in transcript abundance was at least two standard deviations greater than the mean value calculated in each case from three independent experiments. The value presented is the

average fold-alteration in comparison with control cells. Data show that 13 genes undergo significant alterations in expression on exposure to radiation from a mobile phone. The changes in transcript abundance were detected for genes involved in cell division, DNA replication, phage mobilisation and transposition, so that mobile phone radiation appears to perturb fundamental cell processes, including three functions involved in nickel transport and metabolism (bold: see main text for relevance).

Methods: *E. coli* strain TG1 was grown in LB medium (100 ml) to an A_{600} of 0.040 ± 0.005. The culture was divided (30ml $flask^{-1}$) between two 500 ml conical flasks, to one of which, a 900MHz GSM digital mobile phone (MAXON 3204: 2W maximal output) was attached externally (inverted to increase the proximity of the aerial to the growing culture). The phone was activated to transmit and both cultures were grown in separate but identical incubators with shaking (200 rpm) for two hours at 37°C. Cultures were confirmed to be isothermal using a Hanna Instrument HI93510 thermometer and liquid probes. Cells were harvested (A_{600} 0.46 ± 0.01) and total RNA was extracted immediately. Transcript abundance was determined using duplicate Sigma-Genosys Panorama *E. coli* gene arrays and quantified with a BIO-RAD Molecular Imager FX phosphoimager/Quantity One software. The experiments were performed in triplicate and to control for possible variations between incubators and/or the individual filters in a duplicate pair, these were alternated between non-irradiated control and irradiated cultures in sequential experiments.

Details and wider relevance: Ubiquitous mobile phone usage world-wide has led to concerns about possible health effects from the use of a microwave emitter in proximity to live cells.

Microwave energy was shown to induce alterations in cellular function both in whole organisms and in isolated neural tissues[1,2], but such studies often employ defined microwave sources (transverse electromagnetic cells) and exaggerated power levels. We exposed cells of a model system (*E. coli* TG1) to radiation emitted by a commercially-available mobile phone. By employing array technology, the transcriptional levels of all identified open reading frames in the genomic sequence of this organism[3] were measured.

The transcript abundance of 13 from 4255 genes (Table 1) was significantly altered (>95% confidence limit) on exposure to mobile phone radiation in each of 3 separate experiments. One gene (*yacG*) which encodes a product of unknown function exhibited diminished expression, whereas increased transcript levels were detected for 12 genes, 8 of which encode known or predicted membrane associated proteins. These can be functionally classified into cell proliferation (MinE, HolA), DNA mobilisation (InsA, NohA), transport (NikD, BetT), putative transport (YdgR, YohG, YifK) and energy metabolism (NrfE, HyaF, HyfI).

The protein product of the cell cycle-associated gene *minE* stimulates cell-division at internal division sites whilst suppressing secondary division sites which form at the poles of an *E. coli* cell, thereby generating topological specificity. The *holA* gene encodes the delta sub-unit of DNA polymerase III and since this enzyme is the major replicative complex in *E. coli*, the increased transcript abundance for *minE* and *holA* may both reflect alterations in cell division. These findings are in keeping with those previously reported[4,5] which suggested an increase in the division rate of eukaryotic cells exposed to microwave energy.

Many copies of insertion elements (IS) are present within *E. coli* DNA and their movement is capable of driving rearrangement by recombination within the genome. Increased expression of *insA* was detected in response to mobile phone radiation and, again, this is consistent with elevated transcription of IS genes in *E. coli* cells in response to stress[6]. Another enzyme involved in DNA scission is NohA which cleaves replicating phage genomes into linear fragments with prior to association with phage coat proteins. Both InsA and NohA are capable of generating "free" DNA termini *in vivo*. Chromosomal damage has been shown to occur in eukaryotic cells exposed to microwaves but it was postulated that this damage did not occur by direct absorption of the microwave energy by DNA[7,8]. The induction of genes which represent functional analogues of *insA* and/or *nohA* in mammalian systems may explain the chromosomal damage observed due to microwave exposure.

Three genes encoding hydrogenase associated proteins (NrfE, HyaF, HyfI) were induced in this study together with *nikD* encoding a Ni(II)-export ATPase. These 4 genes are

functionally associated given the Ni(II) requirement of many membrane-associated hydrogenases[9]. Osmotic stress and a range of other conditions e.g. growth under anaerobiosis, has been shown to modulate the expression of hydrogenase genes in *E. coli*[10,11]. An increase in medium osmolarity has been shown previously to result in elevated transcription of the *betT* gene which encodes a choline import protein[12] (glycine-betaine, which acts as a neutral osmolyte in these cells, is synthesised from the precursor, choline). An increase in *betT* expression was seen in response to mobile phone radiation. Thus, induction of *nrfE*, *hyaF*, *hyfI*, *nikD* and *betT* by mobile phone radiation may be linked to alterations in membrane status leading to changes in the perception of osmotic potential or actual changes in cytoplasmic ion composition. Indeed, in mammalian cells, membrane integrity and/or membrane transport, including choline import in neural tissue[13], has been reported to be affected by exposure to microwave radiation[14,15].

These experiments provide incontrovertible proof of significant change in gene expression in response to mobile phone radiation. In addition, the changes observed have direct parallels with reported effects on eukaryotic cells elicited by similar exposure.

References

1. Preece, A.W., *et al*., *Int. J. Radiation Biology* 75, 447-456 (1999).

2. Tattersall, J.E.H., Wood, S.J. & Scott, I.R. *Proc IEE Seminar*, *Electromagnetic assessment and antenna design relating to health implications of mobile phones London* 5/1-5/4 (1999).

3. Blattner, F.R., *et al*., *Science* 277, 1453-1474. (1997).

4. Daniells C., *et al*.*Mutat. Res.* 399, 55-64. (1998).

5. Velizarov, S. Raskmark, P. & Kwee, S. *Bioelectrochem. Bioenerg.* 48, 177-180 (1999).

6. Naas, T., Blot, M., Fitch, W. M. & Arber, W. *Genetics* 136, 721-730 (1994).

7. Lai, H. & Singh, N.P. *Bioelectromagnetics* 18, 446-54 (1997).

8. Saffer, J.D. & Profenno, L.A. Bioelectromagnetics. 13, 75-78. (1992).

9. Wu, L.F. & Mandrand, M.A. *FEMS Microbiol. Rev.* 10, 243-69 (1993).

10. NiBhriain, N., Dorman, C.J. & Higgins, C.F. *Molec. Microbiol.* 3, 933-944 (1989).

11. Gousebet, G., *et al J. Bacteriol.* 175, 214-221 (1993).

12. Lamark T., *et al*. *Molec. Microbiol*. 5, 1049-1064 (1991).

13. Lai, H., *et al*. *Pharmacol. Biochem. Behav.* 33, 131-138 (1989).

14. Dwivedi, R.S. Dwivedi, U. & Chiang, B. *Exp. Cell Res.* 180, 253-265 (1989).

15. Geletyuk, V.I., *et al*. *FEBS Lett.* 359, 85-88 (1995).

GENERAL DISCUSSION

**Note: At the end of this section an appendix with all the mentioned figures is provided by order of appearance (see appendix below).*

This doctoral thesis achieved all the primary objectives, characterising via microscopic and spectroscopic techniques the monometallic and bimetallic Pd and Pd/Ru NPs synthesized by *Escherichia coli* MC4100 and *Desulfovibrio desulfuricans*. It was also confirmed that a waste consortium of acidophilic sulfidogenic bacteria (CAS) generated from an unrelated biotechnology process was also to make bio-Pd/Ru NPs. All the three groups of bacteria (as pure culture and consortium) synthesized active Pd/Ru NPs for the catalytic conversion of 5-HMF into 2,5-DMF.

In addition, the objectives of chapters III and IV were successfully achieved. It was confirmed that application of microwave (MW) energy to cells of *E. coli* and *D. desulfuricans* before the exposure to Pd(II) solution resulted in altered Pd NPs. The resulting Pd NPs synthesized by MW treated cells of *E. coli* and *D. desulfuricans* showed more homogeneous distribution than untreated cells, as was confirmed using STEM/HAADF analysis. Finally, the catalytic activity of the Pd NPs synthesized by MW treated cells of *D. desulfuricans* for the hydrogenation reaction of 2-pentyne was tested, resulting in higher catalytic activity than the Pd NPs of untreated cells. This section will discuss the main advantages and challenges of the use of bacteria for recovery of precious metals and its potential as a green alternative to the conventional methods of synthesis of catalyst, in the context of what is known about the mechanisms by which bacteria bio-manufacture metallic NPs against a 'background' of low pH and toxic metal stresses, that may complicate identification of precise metal-specific mechanisms. Identification of key genes that are upregulated by Pd(II) exposure is underway (Torgeman, 2017)

The ability of a wide range of microorganisms to reduce palladium is a well-established process since it was first reported by Lloyd *et al*., (1998). Prior to the beginning of this doctoral thesis, substantial information about the potential applications of microbial reduction of Pd(II) and formation of Pd NPs was available. Yong *et al*., (2003) reported a new process to recover Pd as well as other precious metals, consisting of the use of preloaded Pd-Ag biofilm capable to recover Pt, Pd and Rh from 50% (aq.) diluted *aqua regia* with a continuous flow of electrochemically derived hydrogen delivered from the

back-side of a thimble electrode that delivered hydrogen to the biofilm. About 80% of the metals contained in the diluted *aqua regia* were recovered in 10-15 min. Another approach was described using gas bubbled hydrogen recovering Pd and Au (Creamer *et al*., 2006). With the use of analytical technologies and equipment such as X-ray power diffraction (XRD), transmission and scanning electron microscopy the crystalline nature and the small size of the Pd deposit formed by *D. desulfuricans* was revealed (Yong *et al*., 2002). It was reported thereafter that these small crystalline deposits showed excellent catalytic properties for a wide range of reactions. Palladized bacteria were active for the reduction of Cr(VI) (Mabbett *et al*., 2004), the dehalogenation of chlorinated aromatic compounds (Baxter-Plant *et al*., 2003) and hydrogenation reactions (Mikheenko *et al*., 2008). Other microorganisms like *Rhodobacter sphaeroides* have shown the ability to form active bio-Pd for different reactions (Redwood *et al*., 2008). Other works showing the formation of bio-Pd by Gram-negative and Gram-positive bacteria (Creamer *et al*., 2007; Deplanche *et al*., 2014; De Windt *et al*., 2005; Bunge *et al*., 2010) reported a different distribution of the Pd NPs between the two types. A different distribution of the Pd NPs might be expected due to the different membrane and cell surface composition in Gram-negative and Gram-positive bacteria. Pd NPs penetrated the cell surface of the Gram-negative strains whereas in *Bacillus sphaericus* Pd NPs were mostly located between the peptidoglycan and the S-layer (Creamer *et al*., 2007). Later, with the improvement of high-resolution equipment NPs inside the cytoplasm of Gram-positive cells was confirmed (Omajali *et al*., 2015).

E. coli is a model microorganism largely studied for different purposes and has well-defined molecular tools to elucidate the mechanism involved in the process of synthesis of NPs. Work has been limited until recently due to the lack of a rapid screening method for cells that deposit Pd but such methodology has recently been described (Torgeman 2017). *E. coli* has been reported to produce highly active Pd NPs for the reduction of Cr(VI). The work reported by Deplanche *et al*., (2010) showed that the reduction of Cr(VI) to Cr(III) varied according to the *E. coli* mutant strain used for the initial bioreduction of Pd(II). The enzymes potentially involved in the bioreduction of palladium by *E. coli* under the latter conditions are the nickel dependent hydrogenase enzymes Hyd-1, Hyd-2, and Hyd-3, and the formate dehydrogenase molybdoenzymes FDH-N, and FDH-H. In addition, *E. coli* was also capable to recover Au(III) reducing it and forming active Au(0) NPs for oxidation reactions (Deplanche *et al*., 2007). It is also known that

addition of other metals solutions to bio-Pd biomass after an initial formation of Pd 'seeds' results in the formation of bimetallic NPs and in some cases with very specific structures like core/shell structures which is the case of bio-Pd/Au, with activity in the oxidation of benzyl-alcohol or bio-Pd/Pt with alloy structure (Stephen *et al*., 2019) and also in the case of bio-Pd/Ru where core shells and alloys are rarer in the bimetallic (Gomez-Bolivar *et al*., 2019).

With all the previous information about the potential ability of *E. coli* to form active monometallic and bimetallic NPs, one of the scopes of this doctoral thesis was to investigate the potential applications of this bacterium as a nano-catalyst. In this project, the formation of catalytically active bio-Pd/Ru NPs by cells of *E. coli* was successfully achieved and the NPs were characterized.

With the preliminary study reported by Omajali *et al*. (2019) using a Gram-positive bacterium *B. benzoevorans* for the formation of bio-Pd/Ru NPs, the idea of ~~the~~ chapter I was to report a more detailed study about the interactions of bacteria with ruthenium and palladium using a well-studied model organism, here *E. coli* MC400 strain. According to the literature bio-NP catalyst synthesized by Gram negative bacteria was more active than Gram-positive bacteria (Zhu et al., 2016; Deplanche *et al*., 2014). Deplanche *et al*. (2011) previously reported a biocatalyst of bio-Pd/Au using *E. coli* for the partial oxidation of benzyl alcohol.

In chapter I, the first objective was to study through a multidisciplinary approach the interactions of "naked" cells of *E. coli* with a 1 mM solution of $RuCl_3$ salt following the addition of bubbling hydrogen as electron donor and then the same procedure with pre-palladized cells of *E. coli*. Using "naked" cells of *E. coli* to uptake Ru(III), only about 50% of Ru(III) from solution was removed after 96h. The use of STEM/HAADF and EDX analysis confirmed the presence of opaque Ru-NPs located in the cell surface (chapter I, Figure 1A-E) and no Ru was observed inside the cells. However, when cells of *E. coli* were previously palladized about 90% of Ru(III) was removed from solution for cells with 5 wt% Pd/5% wt% Ru and 5 wt% Pd/20% wt% Ru. This, agreed with previous works of bio-Pd/Ru NPs using *B. benzoevorans* (Omajali *et al*., 2019) and for bio-Pd/Au NPs with *E. coli* (Deplanche *et al*., 2011), suggesting that bio-Pd promotes the deposition of other metals with faster and higher metal recovery. It was confirmed the presence of NPs at the level of the surface but also at the level of the cytoplasm (chapter

I, Figure 2A-B). Surprisingly, the presence of Ru was also confirmed in the cytoplasm using EDX (chapter I, Figure 2D and 2H). The intracellular accumulation of Ru raises some questions about the role of Pd in the internalization of Ru in the cytoplasm. The addition of Pd(II) could activate the Ni transport system of *E. coli* due to the similar chemistry of both elements establishing a possible route to unproductively deliver some Pd inside the cells as previously suggested by Deplanche *et al*., (2014) and discussed by Omajali *et al*., (2015) but the hypothesis was not tested. It is likely that Pd(II) may be recognised and transported but unable to substitute functionally for Ni(II) (e.g. in incorporation into enzymes) and hence the cells will 'perceive' Ni(II) starvation, and, indeed, be placed under Ni-starvation stress. (c.f. later). During the addition of the second metal this route might be opened (during the pre-loading of Pd) allowing some Ru to be deposited inside the cell, but future studies should be performed to elucidate this mechanism. However, in cells with higher Ru concentration (cells 5 wt% Pd/20% wt% Ru) no intracellular Ru was observed indicating a possible lethal effect to cells that inactivates the internalisation mechanism. Future work based in the use of flow cytometry technique could give insights onto the toxic effect of Ru on the cell viability and metabolic activity, in the same way as was shown by Omajali et al in the case of Pd-only, where reduction of the Pd(II) to Pd(0) reduced the metal toxicity (Omajali *et al*., 2019).

For the purpose of catalyst application, the surface bound material would be more relevant to examine. The amount of Ru appeared to increase when metal loading was increased as observed using STEM/EDX analysis (chapter I, Figure 2H and Figure 3G) and confirmed later using XPS (chapter I, Figure 7B-D). The presence of core/shell structures (Ru core/Pd shell) in bio-Pd/Ru NPs (chapter I, Figure 3H) confirmed the previous investigations by Deplanche *et al*., (2012). This mechanism implies an oxidation of the initial bio-Pd NPs acting as seeds for deposition of Au(III). The latter oxidize Pd(0) via galvanic reduction of Au(III) that makes Pd(II) migrate around the NP, which is re-reduced thanks to the presence of H_2 forming the shell of Pd around the core of Au(0). However, the presence of Ru(0) NPs was not proved in this study.

Note that XPS is a surface technique, examining only the outermost 10-20 nm of the cell, whereas EXAFS is a bulk method. The spectroscopic characterisation of the bimetallic using EXAFS analysis of bulk material suggested the presence of mainly Ru(III) and Ru(IV) species but also some Ru(0) was suggested ranging between 6-10% of the total

amount of Ru. This Ru would be invisible to XPS if the metallic Ru had been internalised. It would seem possible, as discussed in chapter I, that Ru(0) might be initially formed in bio-Pd/Ru cells and after air exposure this may lead to an oxidation of the small and very reactive Ru NPs forming RuO_2 at the cell surface. This hypothesis could agree with the analysis using HR-TEM showing lattice fringes of 0.201 nm (chapter I, Figure 3D) that could be associated with Ru(0) (101) or RuO_2 (210). The remaining 6-10% could belong to the Ru core of the bimetallic NPs observed being protected by the Pd shell from the oxygen, where PdO would be formed. Recent studies showed that a synergistic effect between Ru and RuO_2 species worked as a vital role to produce 2,5-Dimethylfuran (Jae *et al*., 2014).

Once the samples were fully characterised, the next objective in chapter I was the catalytic testing of the NPs. Due to the potential application of the Pd/Ru NPs in certain hydrogenation reactions and with the recent focus on sustainable energy and green chemistry the bio-NPs were tested for the conversion of 5-HMF into 2,5-DMF. Since one of the goals of this project is to recycle resources from wastes and convert them into new re-usable products, 5-HMF was recovered from thermochemical hydrolysis processes of starch and cellulose. In order to compare the reaction process, the bio-NPs were tested against commercial 5-HMF and 5-HMF against hydrolysate extracts in MTHF which is a common solvent for extraction and separation of 5-HMF from other compounds derived from the reaction of cellulose and starch hydrolysis. The bio-NPs were also compared with the commercial catalyst of Ru/C and Pd/C available. By using MTHF as a solvent for the reaction, Ru/C gave 100% conversion and 57.1% selectivity while Pd/C gave 100% conversion and 3.3% selectivity, so the latter was not considered further. The bio-derived catalysts tested were 5% Ru on *E. coli*, 5%Pd/5%Ru on *E. coli* and 5%Pd/20%Ru on *E. coli*. The reaction rates of the NPs synthesized by *E. coli* gave low yield on 5% bio-Ru and 5%/20% bio-Pd/Ru (about 10% and 21% selectivity respectively). In order to efficiently use the precious material, reduce cost and get the maximum performance of the catalyst, the 5%/20% bio-Pd/Ru was not considered further. It would be possible that the high Ru contain of the sample could result in additional by-products out of the scope of this project as was shown previously (Nagpure *et al*., 2015). However, the 5%/5% bio-Pd/Ru catalyst gave similar results as did the commercial Ru/C but the latter, under the conditions used here, gave little activity against the 5-HMF made from starch and cellulose. Hence, the bio-derived catalyst fulfils one of the major criteria for adoption of

a new catalyst: being able to achieve an outcome that a chemical catalyst cannot. The second criterion is to be able to produce a catalyst economically and potentially scalable.

With the initial test performed by *E. coli* cells on the synthesis of a novel biocatalyst of bio-Ru and bio-Pd/Ru and the potential of the bio-Pd/Ru catalyst (5 wt% of each metal) in the production of 2,5-DMF from 5-HMF made from starch and cellulose, the next step on the chapter II was to test the same reaction using waste bacteria for the synthesis of the catalyst. The decision to select a waste culture of sulfidogenic bacteria was made according to previous works published using sulfidogenic bacteria for the synthesis of NPs and its application for different hydrogenation reactions. It was discussed at the beginning of this section the importance of the supporting biomass for the synthesis of NPs and the catalytic activity. The different organic material of different types of bacteria can influence in the size, location and shape and therefore influence the catalytic activity (Deplanche *et al*., 2014; Zhu *et al*., 2016). Among all these bacteria used for applications as a nanocatalyst, as an example *D. desulfuricans* gave better results in some catalytic reactions when compared with *E. coli*, for example reduction of Cr(VI) and hydrogenolytic dehalogenation of polychlorinated biphenyls and used transformer oil (Macaskie *et al*., 2012). For this reason, a group of bacteria related sulfidogenically (but not taxonomically) to *D. desulfuricans* was selected for this chapter. This culture, evolved over several years to produce H_2S as a primary product to remediate acidic mine waters, was not composed entirely of sulfidogenic organisms (Santos and Johnson 2017) and hence data interpretation is made more difficult but the major advantage is that the bacteria are generated as a waste potentially at large scale, since tonnages would be needed to make enough H_2S to treat the very large volumes of waste mine water (e.g. 5 million litres per day from a Rio Tinto Zinc site with no on-site storage (L.E. Macaskie personal communication)).

D. desulfuricans is an anaerobic microorganism and working with anaerobic bacteria is sometimes more difficult than aerobic bacteria. Anaerobic bacteria can be difficult to grow, sometimes requiring special growth media causing additional cost and being time-consuming. Working with waste bacteria offers the advantage to remove the operational cost of growing the bacteria in the lab (chemicals equipment and time of growth) and the time required to scale up the process to get enough biomass for the catalyst. In addition, use of a mixed culture is a well established way to harness aerobic organisms to remove

O_2, enabling the anaerobic organisms to grow without special precautions. Another advantage of working with the CAS from waste, is the acidic conditions in the reactor. Contrary to the commercial-scale sulfidogenics reactors that use neutrophilics species, this reactor was operating as a continuous flow system for 462 days with pH values between 4 and 5 and temperature between 30-45ºC (Santos and Johnson 2017). Thus, these microorganisms could have a better response (i.e. less acid stress) to the acidic conditions of the metal solutions (Pd(II) and Ru(III)) that could be related with the higher catalytic activity of the Pd/Ru CAS culture than Pd/Ru *D. desulfuricans.* The yield of 2,5-DMF using starch 5-HMF using CAS was double than that using *D. desulfuricans* (chapter II, Figure 1B). Comparative molecular analysis could provide useful information regarding to the gene expression in SRB exposed to acidic conditions for a long term like CAS culture and SRB growth in the lab under neutral pH.

In the chapter II the formation of bio-NPs of Pd/Ru and Ru by *D. desulfuricans* and Consortium of Acidophilic Sulfidogen culture was successfully achieved. *E. coli* was also used in this work as a comparator of non-sulfidogenic Gram negative bacteria. The STEM/HAADF and EDX-Mapping images showed the presence of Pd and Ru (chapter II, Figure 2B) in the membrane that might confirm the previous hypothesis of Pd NPs acting as seeds for ruthenium deposition. However, images at higher resolution (chapter II, Figure 2E-H) showed more uniform deposition of Ru in the membrane and no clear association with Pd is observed. In addition Ru(III) was not completely removed and the final metal loading was 5wt%Pd/3wt% Ru.

The CAS culture showed a variety of cell types with different shapes using SEM (chapter II, Supplementary figure S5A) in agreement with the diversity revealed using molecular biology identification methods (see chapter II, table 2). The heterogeneous composition of the CAS culture can be correlated with the heterogeneous shapes and location of the Pd/Ru NPs observed using STEM/HAADF analysis (chapter II, Figure 4). In total, 3 types of NPs were observed with depositions in the surface (type I and II) and throughout the cell surface and cytoplasm (type III); any of the 3 types could not be attributed to a specific taxonomic group. However, some characteristic deposits in CAS culture could be compared with the ones formed by *D. desulfuricans* (chapter II, Figure 2E and Figure 4D) with the formation of big clusters forming branches. The thick membrane observed in figure 6A (chapter II) gives clues of Gram-positive strain with Ru mainly located in

the surface (chapter II, Figure 6D) with eventual deposit inside the cell, and Pd located throughout the cell surface and cytoplasm. This pattern of distribution for Pd and Ru NPs was observed in a previous work published by Omajali *et al*., (2019) using *Bacillus benzoevorans* as a support for Pd/Ru NPs formation.

The three samples (5%Pd/5%Ru *D. desulfuricans*, 5%Pd/5%Ru CAS and 5%Ru CAS) were tested for the 5-HMF (commercial 5-HMF, 5-HMF from starch and 5-HMF from cellulose) reaction and compared with 5%Ru commercial catalyst (chapter II, Figure 1 and Table S1B). The commercial 5%Ru showed 57% yield of DMF while for starch and cellulose 5-HMF it was almost negligible. Again, this highlights the opportunity for application of the bio-catalyst in reactions that chemical catalysts cannot perform. The 5%Pd/5%Ru on CAS showed 63.13%, 23.64% and 16.67% yield of 2,5-DMF from commercial, starch and cellulose 5-HMF respectively. The lower yield of 2,5-DMF would be attributed to the other derived by-products from cellulose hydrolysis that could be present and interfere in the reactions. In addition, it should be noticed that cellulose was not pre-treated in any way; it is known that mechanical treatment can lower the crystallinity of cellulose improving degradability (Shimizu *et al*., 2009; Geboers *et al*., 2010), but mechanical treatments consume power and impact adversely on the overall energy balance. It should be highlighted that the bio-catalysts used here, were not further-treated after formation of NPs. The commercial catalysts as used here are the result of several years of investment by the industries to optimize the efficiency of the catalyst. Future studies should be focused on the optimization of the catalyst's efficiency as well as detailed studies to understand why the CAS-derived catalyst shows the positive attributes reported here. However this task is not trivial since many bacterial components of mixed populations cannot grow in isolation, as an example, synergistic interactions among bacteria can occur promoting the production of β-1,4-glucosidase for lignocellulose degradation that would not be possible to occur with isolated bacteria (Deng *et al*., 2016). In the same way that mixed cultures can produce β-1,4-glucosidase for lignocellulose degradation (that is not possible in isolated strains) a synergistic effect during the synthesis of NPs in CAS culture might occur with the production of specific enzymes that give NPs with higher catalytic activity than NPs synthesized by isolated microorganisms might be possible here.

With the requirement to examine the mixed culture, the first report of the use of X-ray scanning microscopy to combine elemental co-localization over a mixed population (tens to hundreds of cells) at high sensitivity, was made (chapter II figure S7B). This method, using synchrotron radiation, can acquire substantial numerical data that single cell elemental mapping cannot, being able to examine a population. Hence subtle changes in the microbial population composition could be related to changes in the elemental proportions; the resolution of this method is insufficient at current state of the art to examine single cells individually and it is not known the extent to which a sample divided for X-SM could be used on another beamline specialized in microscopically resolved synchrotron radiation based techniques like micro(μ) EXAFS/XANES. These microfocused techniques would allow to determine speciation and spatial heterogeneity of chemical elements associated with the NPs at single cell scale within complex biological/environmental samples (Kuzmin *et al*., 2014).

The comparison of the CAS bimetallic culture with *D. desulfuricans* bimetallic resulted in 2-fold better performance of CAS as compared with *D. desulfuricans*, a possible reason could be the lower content in Ru of *D. desulfuricans* (5%Pd/3%Ru). Interestingly, the highest yield of 2,5-DMF using 5-HMF from starch was obtained using 5%Ru on CAS (29.3%) being higher than Pd/Ru CAS (23.64%). The possible reasons for the higher activity in the latter were not further investigated but in order to use wisely and efficiently the recovered metals, future studies of the catalyst performance at different metal loadings and composition should be interesting to investigate to optimize the amount of metal used. During the NPs synthesis bacteria are exposed to multiples stress such as low pH, Pd and Ru toxicity etc. An additional stress for the CAS culture (apart from low pH and high Pd and Ru concentration) is the long-time exposition to a rich metal medium (0.27 mM Ni(II), 0.15 Mn(II), 0.04 mM Co(II), 0.02 mM Zn(II)) in the reactor prior to be collected. This long-term exposure to a rich metal medium could lead to additional bacterial mechanism for NPs synthesis as a response to the stress, or, indeed ‘prepare’ the cells for exposure to Pd(II).

The critical role of the biological support matrix in the synthesis of Pd NPs has been demonstrated previously by Deplanche *et al*. (2014). This study showed that among all the bacteria tested, *E. coli* and *D. desulfuricans* showed the higher dispersion of the Pd NPs and a correlation was observed (Deplanche *et al*., 2014) with the initial rate of Pd(II)

bioreduction and the amount of Pd(II) removed during the uptake phase. The higher catalytic activity of the bio-Pd nanparticles was previously attributed to the small particle size (Yong *et al*.,2002). Increasing the dispersion of the NPs (as achieved using MW-processing (see below)) would make Pd NPs more accessible for the reaction by improving the mixture with the substrate for the catalyst reaction. The evidence to support this hypothesis was proved by Deplanche *et al*., (2014) using bio-Pd on *Rhodobacter* for the hypophosphite test, increasing the activity when metal loading was decreased. An increased proportion of support could lead to more accessible Pd NPs (meaning more dispersed NPs and less aggregates). It was shown that catalytic activity increased when metal loading was reduced to 100% to 25% to 5% (w/w). However, with other strains like *D. desulfuricans* the behaviour was different in terms of metal loading (i.e. higher metal loading higher catalytic activity (Deplanche *et al*., 2014)) so other factors are also important.

With the critical existing correlation between the NPs size and dispersion and catalytic activity, two main hypotheses in the last two chapter were stated. For the chapter III the main hypothesis was: the application of an external source of MW energy applied on cells of *E. coli* and *D. desulfuricans* before their exposure to palladium solution resulted in a higher degree of dispersion of the NPs. Both types of cells had specific response to MW energy with main differences observed at the level of the periplasm in *D. desulfuricans* (chapter III, Figure 2) while the differences in terms of size and dispersity of NPs in *E. coli* manifested in the cytoplasm (chapter III, Figure 1). Presumably, in a catalytic reaction especially after acetone washing of the palladized cells the surface located NPs would be more accessible to the reaction. If main differences in the synthesis of NPs in MW *E. coli* were observed in the cytoplasm, a future study comparing catalytic activity of treated and not treated cells of *E. coli* could provide valuable information about the role of cytoplasmic Pd NPs in the reaction. It was also relevant in this study that the effect of the MW in the synthesis of Pd NPs was more in terms of homogeneity than in terms of mean size of the NPs when it was compared to the controls. Thus, the polydispersity index was reduced by 32% in *E. coli* and 39% in *D. desulfuricans*.

One of the difficulties of working with living microorganisms for the synthesis of NPs is that cell population are not synchronised, and bacteria can be found at different growth phase (exponential, stationary, etc.) which could affect the metallic NPs synthesis. For

instance, Pd is known to bind DNA (Pillai and Nandi, 1977), bacteria can form nuclear bodies which is a condensed form of DNA that occurs in cultures in stationary phase (Zaritsky *et al*., 2017) so the stage of the cell in the moment of formation of Pd NPs is relevant. This is just one example of the high number of variables influencing the synthesis of NPs and the size of the formed NPs which in turn affect their catalytic activity. To achieve a constant population continuous culture is a useful tool to maintain the bacteria at a constant proportion of the specific growth rate (steady-state). Continuous culture was the condition for the CAS cells and hence this population, although mixed, was stable (D.B. Johnson, personal communcation). The findings in this chapter, increasing the homogeneity of the Pd NPs by applying an external source of MW energy on cells can reduce the number of variants to elucidate the influence of the bio-Pd NPs in catalytic reactions.

The last chapter (chapter IV) of the present doctoral thesis successfully confirmed that Pd NPs synthesized by MW treated cells of *D. desulfuricans* show higher catalytic activity for the hydrogenation reaction of 2-pentyne to 2-pentene than Pd NPs of control cells. In order to fully understand the role of MW energy in the synthesis and catalytic activity of Pd NPs by cells of *D. desulfuricans* different dose of MW-radiation was applied in different stages of NP formation (i.e. prior to MW exposure and during NP synthesis). The conversion rate for the hydrogenation reaction was lower than for the commercial comparator used, but at long reaction times the yield of desired product was higher. The beneficial effects of low dose of energy (2 W or 4 W) were achieved giving faster rate of hydrogenation by catalyst of treated cells than untreated cells (50% faster). At higher dose (8 W) the conversion rate was higher than at 2-4 W, but cells resulted substantially injured (chapter IV, Figure 5) affecting adversely the selectivity of their catalyst (chapter IV, table 3).

A main conclusion from the microwave-processing is that the cells are pre-injured before exposure to Pd(II) and they retain this ‘memory’ during formation of the Pd-NPs.

The first response to MW-injury is the disruption of the cellular membrane with the cytosolic fluids passing outwards through the membrane and then being re-absorbed (Shamis *et al*., 2011) allowing Pd(II) (carried in’ in the inflow) to access more nucleation sites without the necessity to go through the intact membrane. This membrane disruption will be perceived as stress by the cells even without Pd(II).

Other work has shown that RF exposure (injury was not verified) of *E. coli* from a mobile phone resulted in upregulation of various genes, some involved in metal processing (chapter IV supplementary 4). The gene upregulation was caused by the RF here as there was no Pd. So, in our case we must ask what is happening when the cells have the double stress of MW and then Pd (with also the low pH of the Pd solution).

Looking at the effects of specific stresses would be possible by making specific gene mutations, but cause and effect has been hampered by the lack of rapid diagnostic for Pd deposition. That barrier is overcome by method development (Torgeman, 2017 U. Oslo Thesis) and the path is now opened to establish what are the key steps in formation of NPs with the highest catalytic activity. On the one hand we have the highly developed model system (*E. coli*, bottom up approach) and on the other hand the unknown of the mixed culture in CAS (top down approach). A good first step would be to try and establish which components of the CAS make the best Pd and try and steer the CAS culture towards these without losing the functionality in the primary metal remediation process.

APPENDIX

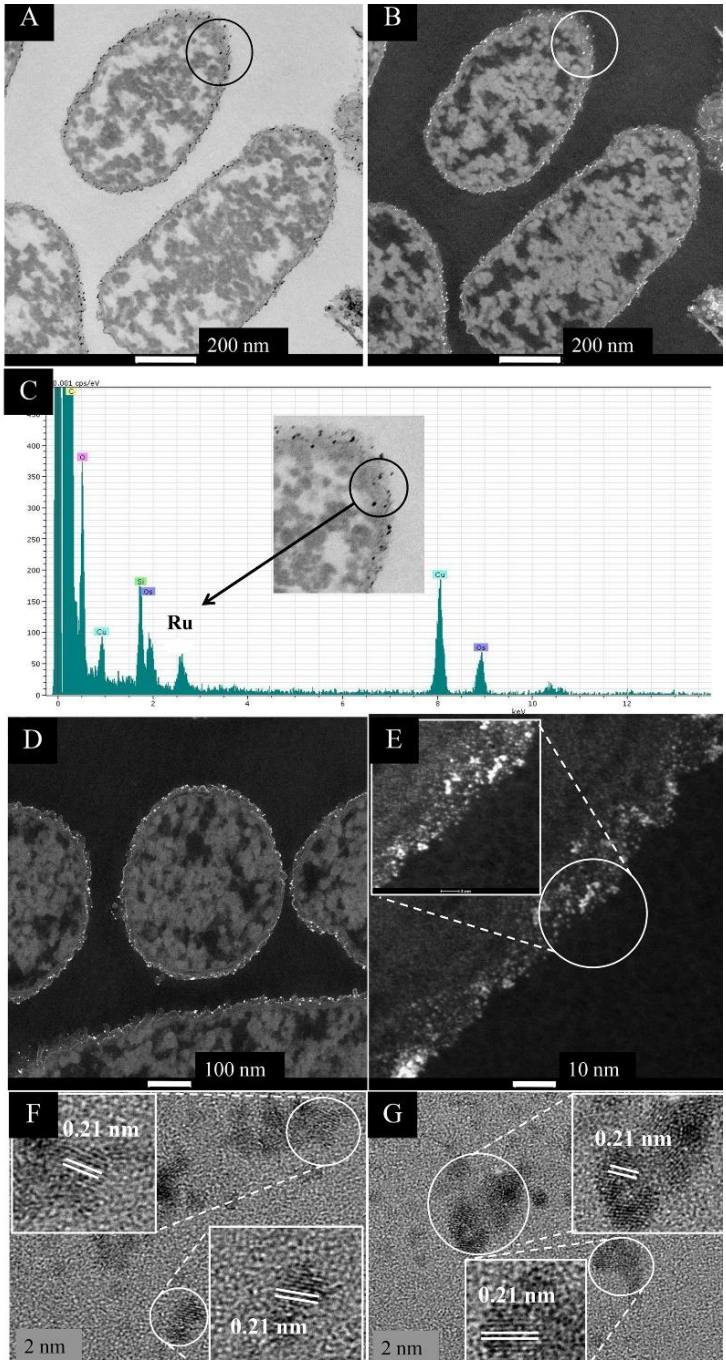

Figure 1. EM study of *E. coli* MC4100 cells loaded to 2.6wt% of Ru. A,B: STEM/HAADF images of cell sections. For comparison cells with no added metal are shown in Supplementary Information Fig S2. Magnification of the circled section (inset) shows the presence of nanoparticles located in the membrane (C, inset.) EDX analysis confirmed the presence of Ru in the cell surface NPs (C). Cu is from the EM grid and Os from the stain. Bars are 500 nm (A and B). HAADF image is shown

enlarged (D,E) revealing heterogeneity of Ru- NP sizes (E) and NP localization only in the periplasm (width of periplasm ~ 35 nm). HR-TEM analysis of the circled area in E revealed consistent lattice spacing of 0.21 nm (F,G) which can be attributed to either Ru metal or RuO2 (see text).

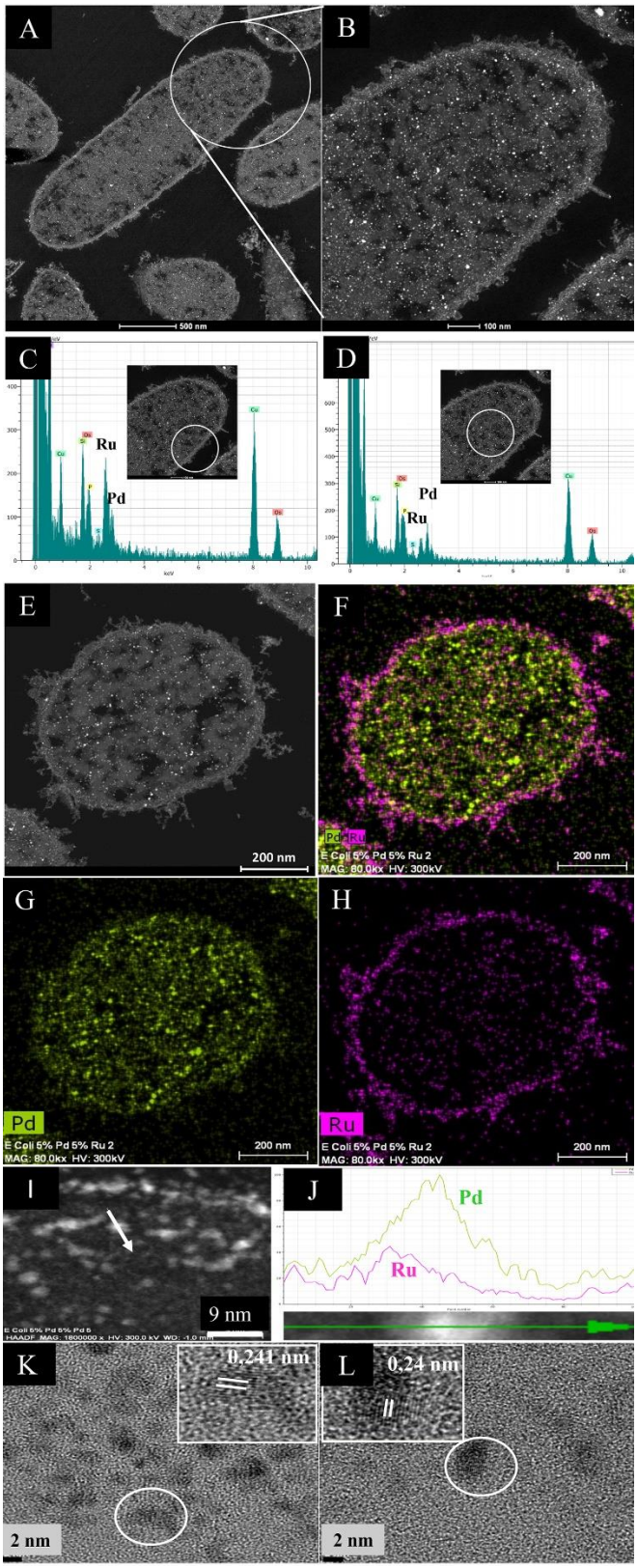

Figure 2. HAADF/STEM micrographs of cell sections (A) and magnified view (B) of 5wt%Pd/5wt%Ru NPs. Bars are 500 nm. EDX is shown of the cell surface (C) and intracellular (D) regions. A single cell (E) is shown mapped for areas of Pd (G) and Ru

(H) localization and co-mapped to show distribution of the two elements (F). Bars are 200 nm. An enlarged image of (F) is shown in supplementary information Figure S4 to show overall lack of co-mapping of the two elements on visual inspection but also that intracellular Ru is very evident. An example NP in the cell surface region (I, arrowed; scale bar is 9 nm) was analyzed by transect (J) to show association between Pd (green) and Ru (magenta), especially evident one side of the NP as a skewed distribution. The green arrow (bottom) shows distance across the transect (as a percentage 0-100%) and the Y axis is counts (arbitrary). K and L: HRTEM Images of single NPs from membrane-bound (K) and cytoplasmic (L) NPs showing lattice fringes. Scale bar is 7 nm.

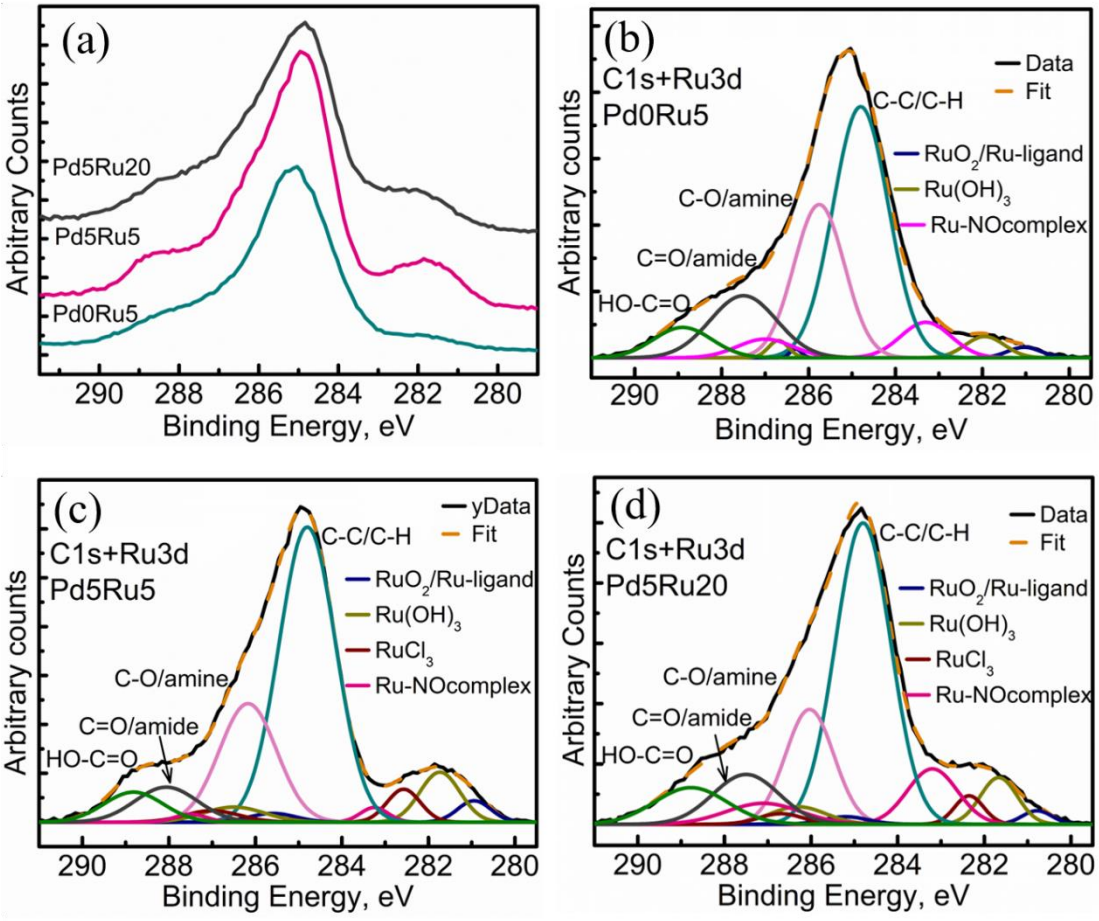

Figure 7. Carbon and Ruthenium XPS spectra showing (a) comparison of high resolution C 1s + Ru 3d region for all three samples, (b) C 1s + Ru 3d peak fitting for low Ru only sample, (c) C 1s + Ru 3d peak fitting for low Pd and low Ru loading sample, (d) C 1s + Ru 3d peak fitting for low Pd and high Ru loading sample

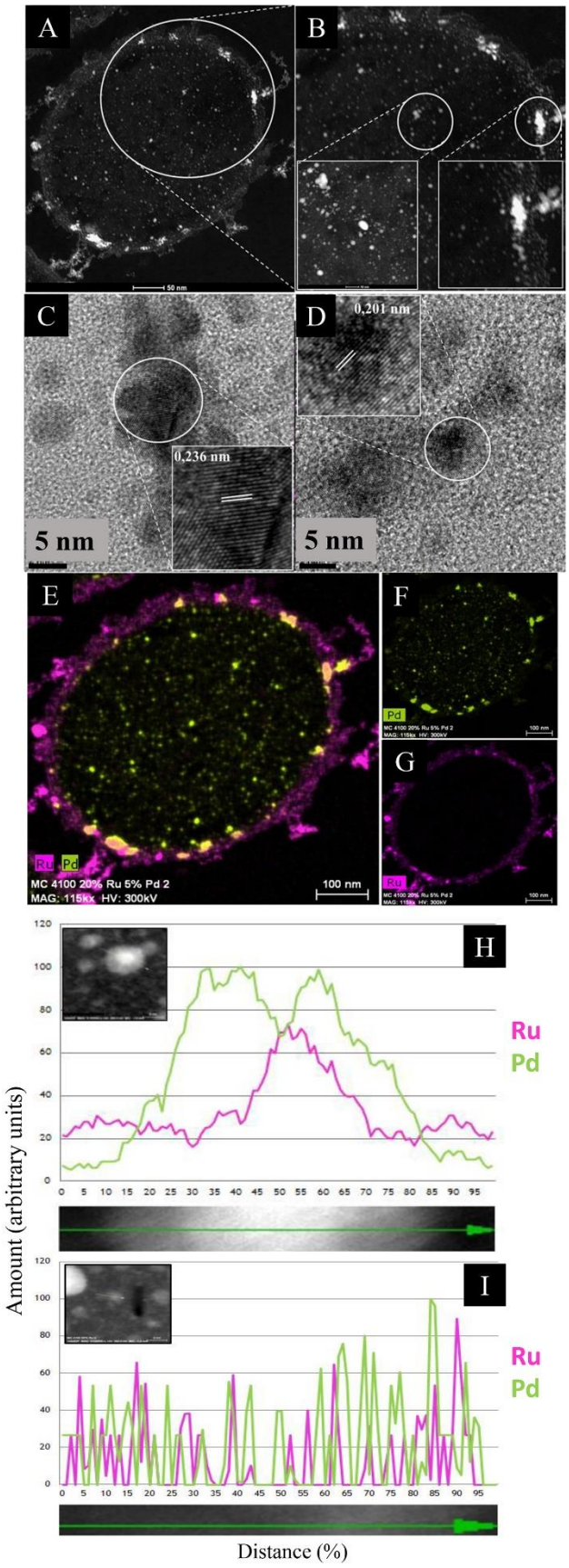
A
B
C
D
0,201 nm
0,236 nm
5 nm
5 nm
E
F
G
Ru
Pd
MC 4100 20% Ru 5% Pd 2
MAG: 115kx HV: 300kV
100 nm
H
I
Ru
Pd
Amount (arbitrary units)
Distance (%)

Figure 3. HAADF/STEM micrographs of cell sections showing Pd/Ru NPs (5wt%Pd/20wt%Ru). (A). A higher magnification (B) shows NPs located in the cell surface layers (B inset right) and in the bulk region (B inset left). Lattice spacing of example NPs in cell wall layers and intracellularly are shown in respectively (C) and (D). Elemental maps (by EDX) of cells show co-localization of Pd and Ru (E) and individually Pd (F) and Ru (G). Figure3 HAADF/STEM micrographs of cell sections showing Pd/Ru NPs (5 wt%Pd/20wt%Ru). (A). A higher magnification (B) shows NPs located in the cell surface layers (B inset right) and in the bulk region (B inset left). Lattice spacing of example NPs in cell wall layers and intracellularly are shown in respectively (C) and (D). Elemental maps (by EDX) of cells show localization of Pd and Ru (E) and individually Pd (F) and Ru (G).

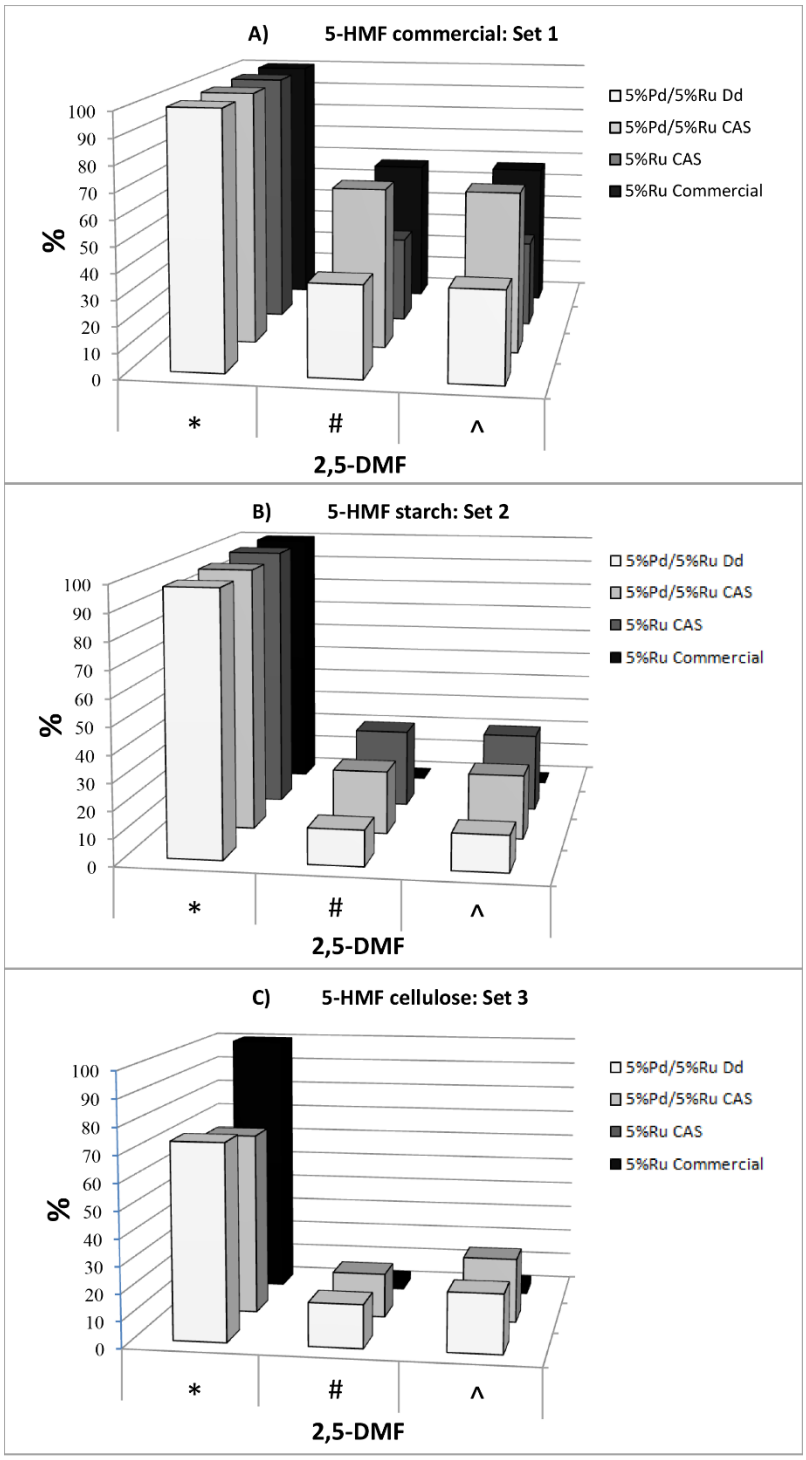

Figure 1. Conversion of 5-HMF from commercial source (A) and from starch (B) and cellulose (C) hydrolyzates by commercial 5%Ru on carbon catalyst, 5wt% bio-Ru on *D. desulfuricans*, 5wt% bio-Ru on sulfidogenic waste culture (CAS), 5wt%Pd/3wt%Ru on *D. desulfuricans* and 5wt%Pd/5wt%Ru on CAS as shown.

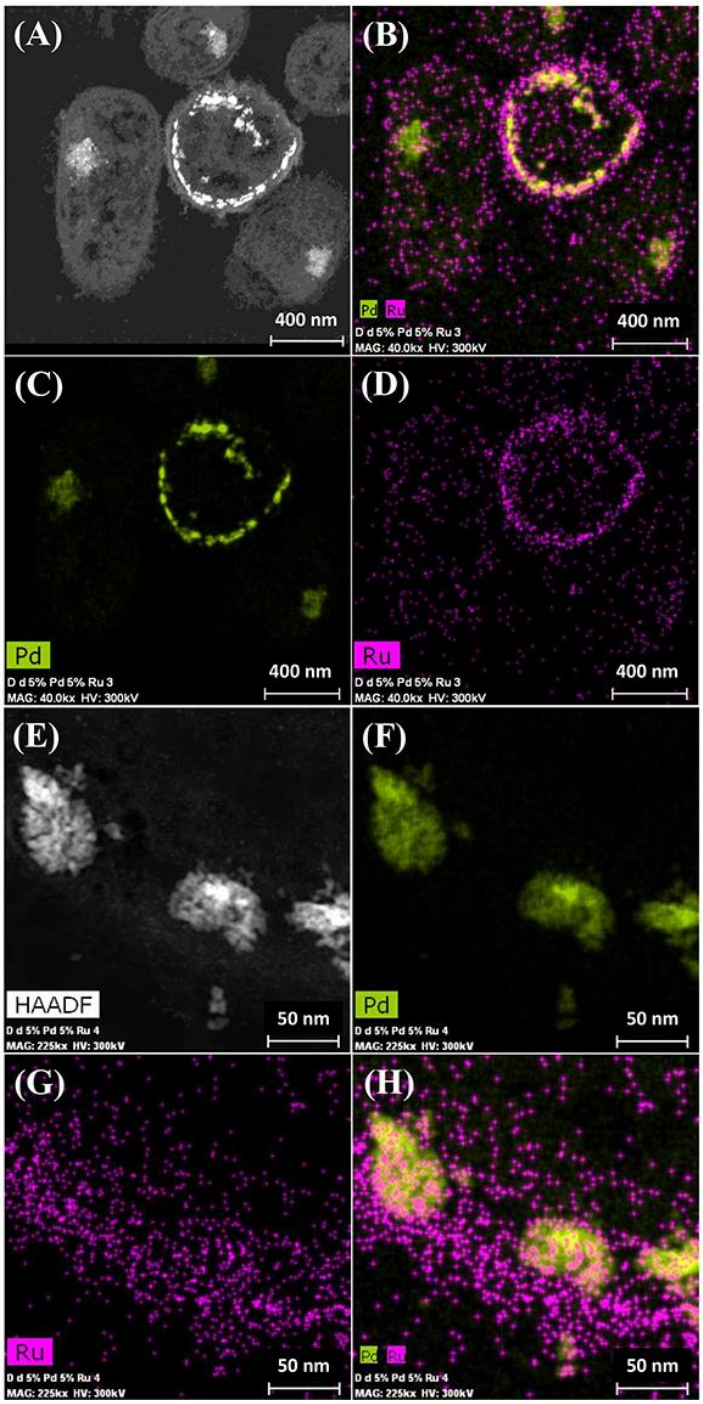

Figure 2. Deposition of 5wt% Pd/3wt% Ru by *Desulfovibrio desulfuricans* and co-localization of the metals on the cells.Arrows: dense nuclear bodies typical of slowly-growing cells. A: HAADF image where metallic NPs appear bright. B: elemental map of Pd (green) and Ru (magenta); individual elemental maps are shown in C and D. E: HAADF image of discrete NPs in the cell surface region mapped for Pd (F, green) and Ru (G, magenta) and co-localization of Pd and Ru (H).

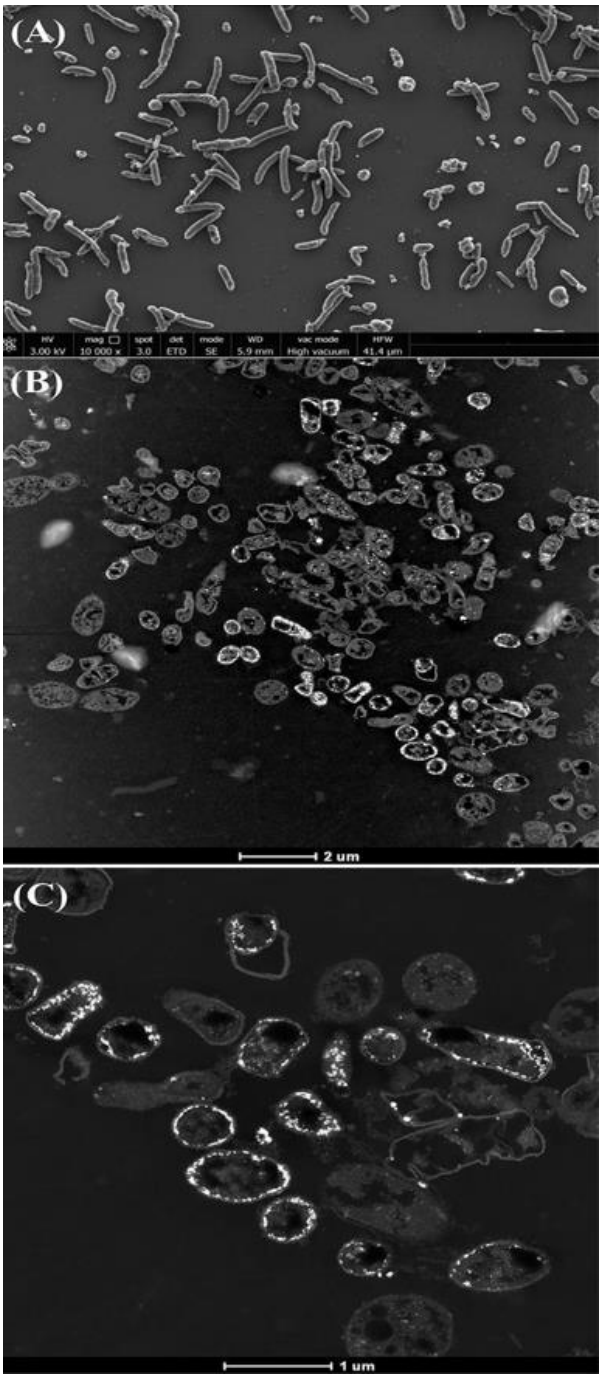

Figure S5. Consortium of acidophilic sulfidogenic bacteria (CAS) viewed by SEM (A) and images of cells loaded to 5wt%Pd/5wt%Ru (B,C).

Table 2. The sulfidogenic waste culture used in the study compared to *D.desulfuricans*

Bacterium	% representation	Gram stain	Sporeformer
D.desulfuricans	100%	Gram negative	-
*CAS: Desulfosporosinus acididurans**	66%	Gram positive	+
CAS: Unidentified strain CEB	7%	NK	NK
CAS: *Acidocella aromatica*	10%	Gram negative	-
CAS:*Actinobacterium*	10%	Gram positive	+
CAS:*Acidithiobacillus ferroroxidans*	7%	Gram negative	-

NK: not known. Only 17% of the CAS population were the same cell type as *D. desulfuricans* (Gram negative, non-sporeformer). The majority wereGram positive sporeformers (76%).

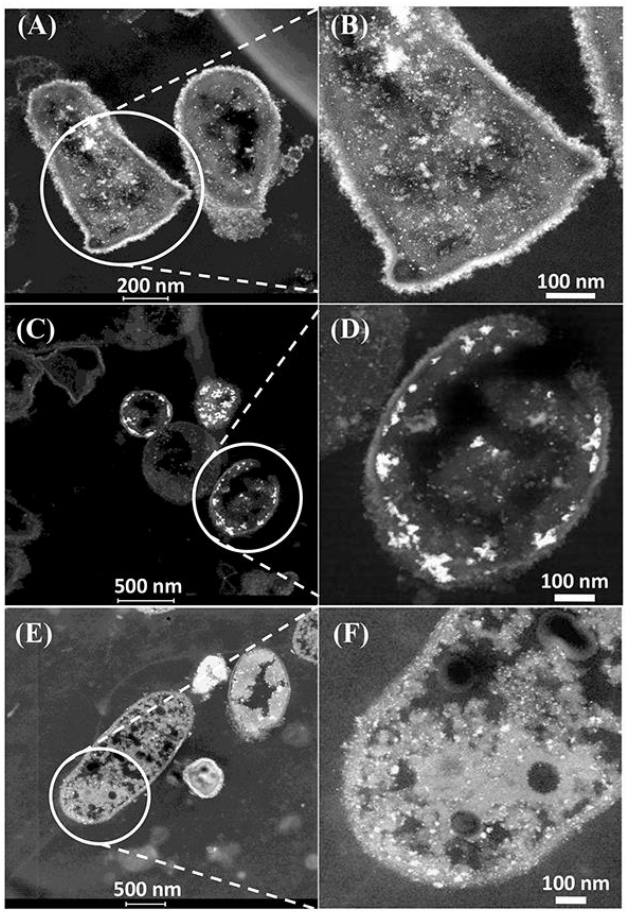

Figure 4. Examination of the CAS bacteria loaded with 5wt%Ru/5wt%Pd. Three main patterns of metal deposition are attributed to type I (A, B), type II (C, D) and type III (E, F) cells.

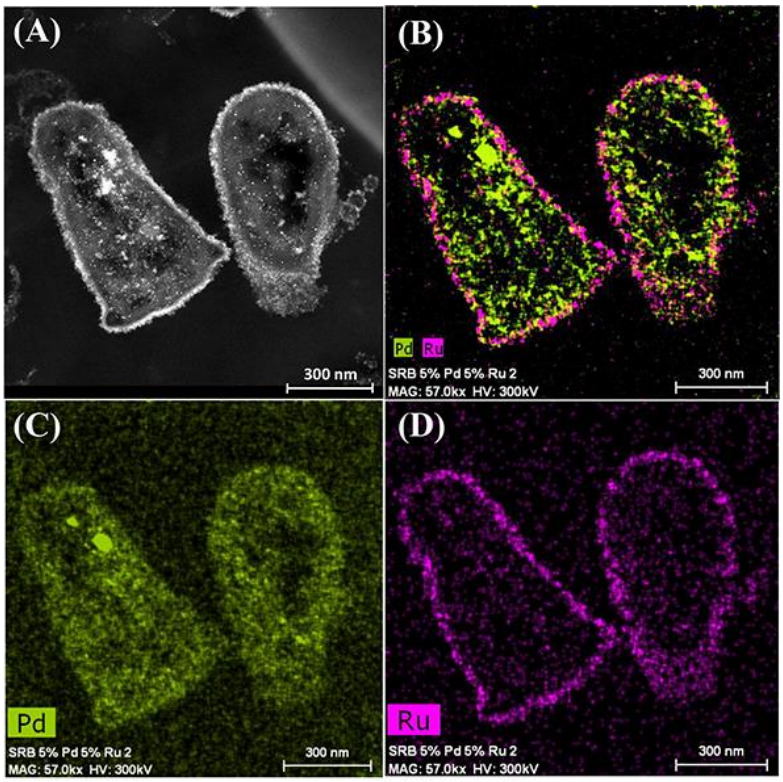

Figure 6. Elemental mapping of distribution of Ru and Pd in two type I cells (as in figure 4) showing superimposition of Pd (green B) and Ru (magenta, D) occurrences. Individual maps (C, D) show very little Ru inside the cells although Pd is distributed uniformly between the cell surface and intracellular regions.

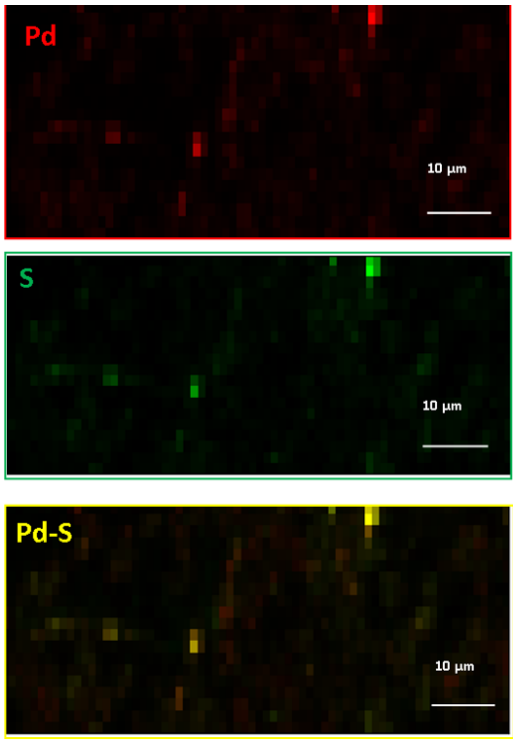

Figure S7B. Preliminary data showing use of X-ray microscopy via synchtrotronradiation to promote element- specific X-ray emission

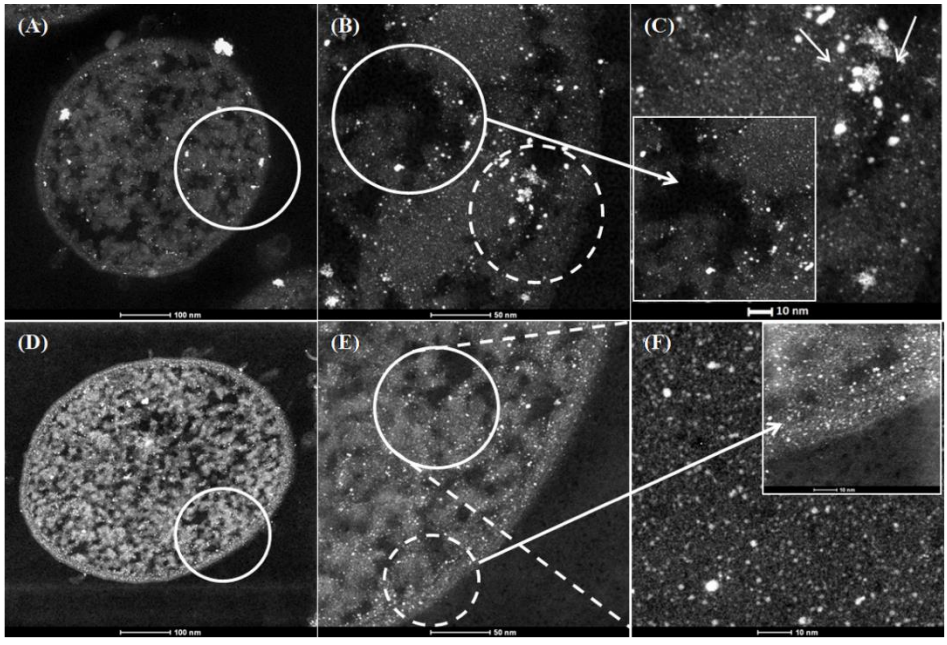

Figure 1. High-angle annular dark field scanning transmission electron microscope (HAADF–STEM) micrographs of Pd nanoparticles synthesized using 5wt% Pd loading (1:20) on *E. coli* MC4100 from 2 mM Na_2PdCl_4 solution, in0.01 M HNO_3 using hydrogen as an electron donor without prior microwave (MW) treatment (**A**,**B**,**C**) and with 30 s prior MW treatment (**D**,**E**,**F**).

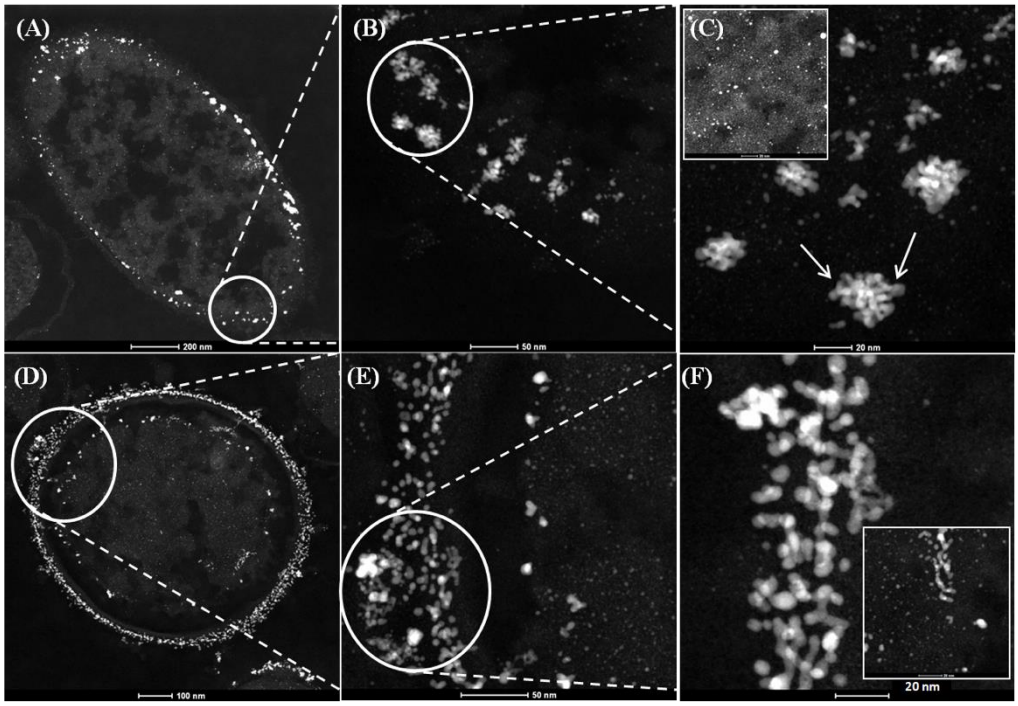

Figure 2.HAADF–STEM micrographs of Pd nanoparticles synthesized using 5wt% Pd loading (1:20) on *D. desulfuricans* from 2 mM Na_2PdCl_4 solution, in 0.01 M HNO_3 using hydrogen as electron donor without MW treatment (**A**,**B**,**C**) and with 30 second MW treatment (**D**,**E**,**F**).

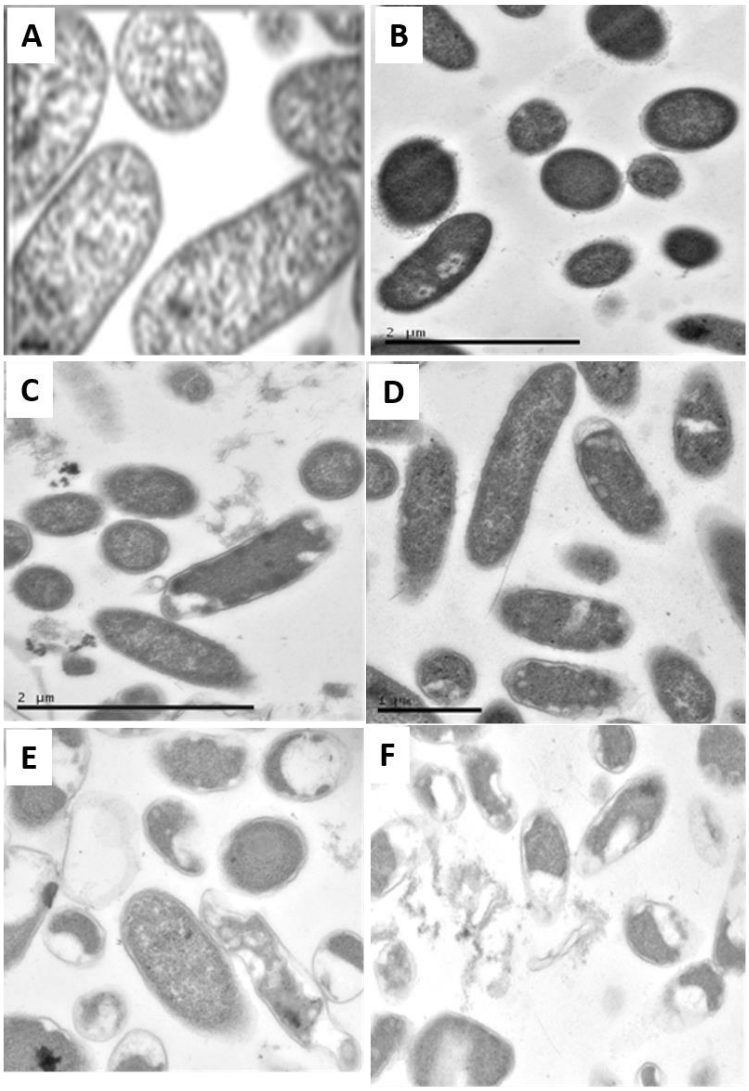

Fig. 5. Morphological effects of RF treatment on cells of *D. desulfuricans.* A: Control cells without RF treatment. Cells are shown following RF treatment at B: 2W (5 min); C: 2W (20 min); D: 4W (20 min); E: 8W (20 min); F: 30W (20 min). Bars are 2 μm.

References

Baxter-Plant, V. S., Mikheenko, I. P., & Macaskie, L. E. (2003). Sulphate-reducing bacteria, palladium and the reductive dehalogenation of chlorinated aromatic compounds. *Biodegradation*, *14*(2), 83–90. Retrieved from http://www.ncbi.nlm.nih.gov/pubmed/12877464

Bunge, M., Søbjerg, L. S., Rotaru, A. E., Gauthier, D., Lindhardt, A. T., Hause, G., … Meyer, R. L. (2010). Formation of palladium(0) nanoparticles at microbial surfaces. *Biotechnology and Bioengineering*, *107*(2), 206–215. https://doi.org/10.1002/bit.22801

Creamer, N. J., Baxter-Plant, V. S., Henderson, J., Potter, M., & Macaskie, L. E. (2006). Palladium and gold removal and recovery from precious metal solutions and electronic scrap leachates by *Desulfovibrio desulfuricans*. *Biotechnology Letters*, *28*(18), 1475–1484. https://doi.org/10.1007/s10529-006-9120-9

Creamer, N. J., Mikheenko, I. P., Yong, P., Deplanche, K., Sanyahumbi, D., Wood, J., … Macaskie, L. E. (2007). Novel supported Pd hydrogenation bionanocatalyst for hybrid homogeneous/heterogeneous catalysis. *Catalysis Today*, *128*(1-2 SPEC. ISS.), 80–87. https://doi.org/10.1016/j.cattod.2007.04.014

Torgeman, E. *Biosynthesis of gold and palladium nanoparticles via bacteria*. Master Thesis 2017.

Lloyd, J. R., Yong, P., & Macaskie, L. E. (1998). Enzymatic recovery of elemental palladium by using sulfate-reducing bacteria. *Applied and Environmental Microbiology*, *64*(11), 4607–4609.

Yong, P., Macaskie, L. E., Rowson, N. A., Farr, J. P. G., & Harris, L. R. (2003). A novel electrobiotechnology for the recovery of precious metals from spent automotive catalysts. *Environmental Technology (United Kingdom)*, *24*(3), 289–297. https://doi.org/10.1080/09593330309385561

Yong, P., Rowson, N. A., Farr, J. P. G., Harris, I. R., & Macaskie, L. E. (2002). Bioreduction and biocrystallization of palladium by *Desulfovibrio desulfuricans*

NCIMB 8307. *Biotechnology and Bioengineering*, *80*(4), 369–379. https://doi.org/10.1002/bit.10369

Mabbett, A. N., Yong, P., Farr, J. P. G., & Macaskie, L. E. (2004). Reduction of Cr(VI) by "palladized" biomass of Desulfovibrio desulfuricans ATCC 29577. *Biotechnology and Bioengineering*, *87*(1), 104–109. https://doi.org/10.1002/bit.20105

Mabbett, A. N., Sanyahumbi, D., Yong, P., & Macaskie, L. E. (2006). Biorecovered precious metals from industrial wastes: Single-step conversion of a mixed metal liquid waste to a bioinorganic catalyst with environmental application. *Environmental Science and Technology*, *40*(3), 1015–1021. https://doi.org/10.1021/es0509836

Mikheenko, I. P., Rousset, M., Dementin, S., & Macaskie, L. E. (2008). Bioaccumulation of palladium by Desulfovibrio fructosivorans wild-type and hydrogenase-deficient strains. *Applied and Environmental Microbiology*, *74*(19), 6144–6146. https://doi.org/10.1128/AEM.02538-07

Redwood, M. D., Mikheenko, I. P., Sargent, F., & Macaskie, L. E. (2008). Dissecting the roles of Escherichia coli hydrogenases in biohydrogen production. *FEMS Microbiology Letters*, *278*(1), 48–55. https://doi.org/10.1111/j.1574-6968.2007.00966.x

Deng, Y. J., & Wang, S. Y. (2016). Synergistic growth in bacteria depends on substrate complexity. *Journal of Microbiology*, *54*(1), 23–30. https://doi.org/10.1007/s12275-016-5461-9

Deplanche, K., Attard, G. A., & Macaskie, L. E. (2007). Biorecovery of gold from jewellery wastes by Escherichia coli and biomanufacture of active Au-nanornaterial. *Advanced Materials Research*. https://doi.org/10.4028/www.scientific.net/amr.20-21.647

Deplanche, K., Caldelari, I., Mikheenko, I. P., Sargent, F., & Macaskie, L. E. (2010). Involvement of hydrogenases in the formation of highly catalytic Pd(0)

nanoparticles by bioreduction of Pd(II) using Escherichia coli mutant strains. *Microbiology*, *156*(9), 2630–2640. https://doi.org/10.1099/mic.0.036681-0

Deplanche, K., Mikheenko, I. P., Bennett, J. A., Merroun, M., Mounzer, H., Wood, J., & MacAskie, L. E. (2011). Selective oxidation of benzyl-alcohol over biomass-supported Au/Pd bioinorganic catalysts. *Topics in Catalysis*, *54*(16–18), 1110–1114. https://doi.org/10.1007/s11244-011-9691-0

Deplanche, K., Bennett, J. A., Mikheenko, I. P., Omajali, J., Wells, A. S., Meadows, R. E., … Macaskie, L. E. (2014). Catalytic activity of biomass-supported Pd nanoparticles: Influence of the biological component in catalytic efficacy and potential application in "green" synthesis of fine chemicals and pharmaceuticals. *Applied Catalysis B: Environmental*, *147*, 651–665. https://doi.org/10.1016/j.apcatb.2013.09.045

De Windt, W., Aelterman, P., & Verstraete, W. (2005). Bioreductive deposition of palladium (0) nanoparticles on Shewanella oneidensis with catalytic activity towards reductive dechlorination of polychlorinated biphenyls. *Environmental Microbiology*, *7*(3), 314–325. https://doi.org/10.1111/j.1462-2920.2004.00696.x

Geboers, J., Van De Vyver, S., Carpentier, K., De Blochouse, K., Jacobs, P., & Sels, B. (2010). Efficient catalytic conversion of concentrated cellulose feeds to hexitols with heteropoly acids and Ru on carbon. *Chemical Communications*, *46*(20), 3577–3579. https://doi.org/10.1039/c001096k

Gomez-Bolivar, J., Mikheenko, I. P., Orozco, R. L., Sharma, S., Banerjee, D., Walker, M., … Macaskie, L. E. (2019). Synthesis of Pd/Ru bimetallic nanoparticles by Escherichia coli and potential as a catalyst for upgrading 5-hydroxymethyl furfural into liquid fuel precursors. *Frontiers in Microbiology*, *10*(JUN), 1–17. https://doi.org/10.3389/fmicb.2019.01276

Jae, J., Zheng, W., Karim, A. M., Guo, W., Lobo, R. F., & Vlachos, D. G. (2014). The role of Ru and RuO2 in the catalytic transfer hydrogenation of 5-hydroxymethylfurfural for the production of 2,5-dimethylfuran. *ChemCatChem*, *6*(3), 848–856. https://doi.org/10.1002/cctc.201300945

Kuzmin, A., & Chaboy, J. (2014). EXAFS and XANES analysis of oxides at the nanoscale. *IUCrJ*, *1*, 571–589. https://doi.org/10.1107/S2052252514021101

MacAskie, L. E., Humphries, A. C., Mikheenko, I. P., Baxter-Plant, V. S., Deplanche, K., Redwood, M. D., … Wood, J. (2012). Use of Desulfovibrio and Escherichia coli Pd-nanocatalysts in reduction of Cr(VI) and hydrogenolytic dehalogenation of polychlorinated biphenyls and used transformer oil. *Journal of Chemical Technology and Biotechnology*, *87*(10), 1430–1435. https://doi.org/10.1002/jctb.3763

Nagpure, A. S., Lucas, N., & Chilukuri, S. V. (2015). Efficient Preparation of Liquid Fuel 2,5-Dimethylfuran from Biomass-Derived 5-Hydroxymethylfurfural over Ru-NaY Catalyst. *ACS Sustainable Chemistry and Engineering*, *3*(11), 2909–2916. https://doi.org/10.1021/acssuschemeng.5b00857

Omajali, J. B., Mikheenko, I. P., Merroun, M. L., Wood, J., & Macaskie, L. E. (2015). Characterization of intracellular palladium nanoparticles synthesized by Desulfovibrio desulfuricans and Bacillus benzeovorans. *Journal of Nanoparticle Research*, *17*(6). https://doi.org/10.1007/s11051-015-3067-5

Omajali, J. B., Gomez-Bolivar, J., Mikheenko, I. P., Sharma, S., Kayode, B., Al-Duri, B., … Macaskie, L. E. (2019). Novel catalytically active Pd/Ru bimetallic nanoparticles synthesized by Bacillus benzeovorans. *Scientific Reports*, *9*(1). https://doi.org/10.1038/s41598-019-40312-3

Pillai, C. K., and Nandi, U. S. (1977). Interactions of palladium (II) with DNA. Biochim. *Biophys. Acta 474*, 11–16. https://doi.org/10.1016/0005-2787(77)90209-X

Santos, A. L., and Johnson, D. B. (2017). The effects of temperature and pH on the kinetics of an acidophilic sulfidogenic bioreactor and indigenous microbial communities. *Hydrometall 168*, 116–120. doi: 10.1016/j.hydromet.2016.07.018

Shamis, Y., Taube, A., Mitik-Dineva, N., Croft, R., Crawford, R. J., & Ivanova, E. P. (2011). Specific Electromagnetic Effects of Microwave Radiation on Escherichia

coli. *Applied and Environmental Microbiology*, *77*(9), 3017–3022. https://doi.org/10.1128/aem.01899-10

Shimizu, K. I., Furukawa, H., Kobayashi, N., Itaya, Y., & Satsuma, A. (2009). Effects of Brønsted and Lewis acidities on activity and selectivity of heteropolyacid-based catalysts for hydrolysis of cellobiose and cellulose. *Green Chemistry*, *11*(10), 1627–1632. https://doi.org/10.1039/b913737h

Zaritsky, A., Rabinovitch, A., Liu, C., & Woldringh, C. L. (2017). Does the eclipse limit bacterial nucleoid complexity and cell width? *Synthetic and Systems Biotechnology*, *2*(4), 267–275. https://doi.org/10.1016/j.synbio.2017.11.004

Zhu, J., Wood, J., Deplanche, K., Mikheenko, I., & Macaskie, L. E. (2016). Selective hydrogenation using palladium bioinorganic catalyst. *Applied Catalysis B: Environmental*, *199*, 108–122. https://doi.org/10.1016/j.apcatb.2016.05.060

CONCLUSIONS

1. The potential application of bio-Pd/Ru NPs synthesized by cells of *E. coli* for the conversion of 2,5-DMF from 5-HMF from hydrolyzates was proved.

2. The formation of Pd/Ru core/shell structures was reported in an analogous way to those reported previously with Pd/Au.

3. The use of sulfidogenic waste biomass and a "classical" sulfidogenic bacterium for the synthesis of Pd/Ru bimetallic NPs was proved.

4. The superior catalytic activity of the waste sulfidogenic bacteria from an unrelated biotechnology process over the classical sulfidogenic *D. desulfuricans* was reported and attributed (at least in part) to a sulfided form of the metallic catalyst

5. The higher dispersity of the Pd NPs synthesized by microwave irradiated cells of *D. desulfuricans* and *E. coli* prior to the exposure of Pd(II) solution over the untreated cells was proved.

6. The response to MW-radiation of *E. coli* and *D. desulfuricans* in the synthesis of NPs was different. With an increase in homogeneity of the Pd NPs in the cytoplasm of *E. coli* in about 32% compared with untreated cells. The main differences in *D. desulfuricans* were observed at the surface with an increase of 39% in homogeneity of the Pd NPs compared to untreated cells.

7. The higher catalytic activity of the RF treated cells of *D. desulfuricans* was proved for the hydrogenation reaction of 2-pentyne.